



**PFS for Mars Express**  
December 2002

**PFS**  
INTERNAL NOTE  
CALIBRATION II

**P.I. Vittorio Formisano**  
**CNR IFSI**

# **MARS EXPRESS**

## **PLANETARY FOURIER SPECTROMETER INSTRUMENT CALIBRATION REPORT**

### **VOLUME II**

V. FORMISANO, M. GIURANNA, D. GRASSI, A. MATURILLI, G. PICCIONI,  
B. SAGGIN, S. FONTI, H. HIRSH, L. ZASOVA, N. IGNATIEV  
AND  
A. MATTANA, D. BIONDI, E. MENCARELLI, F. NESPOLI, M. ROSSI.

**IFSI – IASF – UNIVPAD – UNIVLE – DLR BERLIN**



## TABLE OF CONTENT

1 - INTRODUCTION.....	3
2 - PROCEDURES FOR DATA ANALYSIS.....	3
3 - THEORETICAL CONSIDERATIONS.....	4
3.1 - LWC RESPONSIVITY AND NER IN LABORATORY.....	4
3.2 - EMISSIVITY OF IKI BLACK BODY FROM LABORATORY DATA.....	6
3.3 - EMISSIVITY OF INTERNAL BLACK BODY FROM LABORATORY DATA.....	7
3.4 - DETERMINATION OF FOV.....	7
3.5 - SWC RESPONSIVITY AND NER IN LABORATORY.....	7
3.6 - THERMAL PART.....	8
3.7 - SOLAR PART.....	8
3.8 - EFFECT OF TEMPERATURE ON SWC RESPONSIVITY.....	10
3.9 - DATA ACQUISITION FAILURE.....	10
3.10 - WAVENUMBER GRID CALIBRATION.....	12
3.11 - REFERENCE SOURCES.....	12
3.12 - THEORETICAL PFS PERFORMANCE .....	13
3.12.1 - SW CHANNEL.....	13
3.12.2 - LW CHANNEL.....	20
4 - LW CHANNEL CALIBRATIONS.....	25
4.1 - RESPONSIVITY AND NER.....	27
4.2 - RESPONSIVITY AND NER FROM IKI BB.....	30
4.3 - LINEARITY.....	40
4.4 - CHANGING TEMPERATURE (MEMORY EFFECT).....	40
4.5 - FORWARD VERSUS REVERSE MOTION.....	41
4.6 - IFSI BB- INTERNAL BB – RUSSIAN BB.....	42
4.7 - MODELLING DETECTOR-INSTRUMENT-SOURCE INTERACTION.....	42
4.8 - THE SNR IN TYPICAL CASES.....	43
4.9 - PERFORMANCE AT MARS.....	47
4.10 - THERMOMETERS INTERCALIBRATION.....	48
4.11 - THE LW CHANNEL CALIBRATION IN SPACE.....	49
5 - THE SW CHANNEL.....	50
5.1 - LINEARITY.....	50
5.2 - FORWARD VERSUS REVERSE MOTION.....	50
5.3 - THE SOLAR PART RESPONSIVITY.....	51
5.4 - THE THERMAL PART RESPONSIVITY.....	64
5.5 - RESPONSIVITY AND NER OF THE SW CHANNEL DETECTOR: ROOM TEMPERATURE.....	71
5.6 - IFSI BB- INTERNAL BB – RUSSIAN BB.....	75
5.7 - MODELLING DETECTOR-INSTRUMENT-SOURCE INTERACTION.....	76
5.8 - CERAMIC ELEMENT AND INTERNAL CALIBRATION LAMP.....	77
5.9 - GAIN FACTORS AND SNR.....	82
5.10 - RESPONSIVITY AS FUNCTION OF TEMPERATURE.....	82

		<b>PFS for Mars Express</b> December 2002	<b>PFS</b> INTERNAL NOTE CALIBRATION II Page 2	<b>P.I. Vittorio Formisano</b> <b>CNR IFSI</b>
--	---	--	---	---

5.11 - SNR AS FUNCTION OF TEMPERATURE.....	91
5.12 - SW CHANNEL FILTER SHAPE.....	94
5.13 - SUMMARY OF THE THERMAL/ GAIN BEHAVIOUR.....	95
6 - MONOCHROMATIC TRANSFER FUNCTION.....	99
7 - LASER DIODE TEMPERATURE CALIBRATION.....	101
8 - FOV MEASUREMENTS.....	103
9 - MEASUREMENTS IN THE EARTH'S ATMOSPHERE.....	110
10 - MINERALS.....	116
11 - DTM MODES.....	118
12 - CALIBRATIONS IN SPACE.....	119
13 - CONCLUSIONS.....	125

		<p><b>PFS for Mars Express</b> December 2002</p>	<p><b>PFS</b> INTERNAL NOTE CALIBRATION II Page 3</p>	<p><b>P.I. Vittorio Formisano</b> <b>CNR IFSI</b></p>
---	---	--	---	---

## 1-INTRODUCTION

In the first volume of the Instrument Calibration Report we have seen how all the calibration measurements were taken, and we have studied several raw data in order to discover the instrumental features that characterize PFS FM model. We have found the ghost, the non linearity and the jumping of the laser diode. It is clear that in computing the main calibration results like responsivity and NER we shall take into account these instrumental effects.

## 2-PROCEDURES FOR DATA ANALYSIS

In general many measurements have been taken in the same conditions in order to average them and increase the signal to noise ratio. Before averaging, however, the following procedure must be followed:

- Do not consider interferograms with spikes.  
It is an indication of bad motion.
- Plot all the spectra together in order to evidentiare, by looking at narrow features, if the laser diode behaviour is OK or not in the set of measurements considered.
- Average as many measurements as possible (made in consistent conditions) separating forward from reverse motion.
- Smoothing of the resulting data may be very useful sometimes, to eliminate at least partially the effects due to the terrestrial atmosphere.
- Correct the SW channel interferogram for the non linearity of the detector.
- Consider separately the forward or the reverse motion. From spectral point of view the effect we have found is present only in the SW channel, but is better not to mix the two sets of data before deeper study.

It should always be kept in mind that these are not the calibrations to be used for the computation of the radiance in space.

We add here the following considerations : there are some effects that will disappear in space, while others will be kept. Forward and reverse motion effect is really upward or downward motion, depending on the accuracy of horizontal assembling of the instrument. Gravity is acting in a way that speed is increased or decreased and the electronic filter will cut or not the highest frequencies.

Another very important effect that should be absent in space is the laser diode jumping. In all the lab measurements the laser diode temperature was not really controlled being the ambient temperature higher than the set temperature. When the laser diode temperature is not controlled, the normal heating prevails, and the temperature of the laser diode will drift independently from the set temperature. In this way the laser diode temperatures will explore all the allowed and not allowed temperatures. In doing so the multiple wavelength conditions may appear and disappear generating spiky data, or jumping of the laser diode wavelength. In space full control and stabilization of the laser diode temperature should be possible. To study this we have implemented test 6, which increases in a controlled way the laser diode temperature, so that we can select the best temperature to be used.

Up to now we have had no full control of the responsivity of the SW channel detector in cooled space conditions, also because we have no experience yet of the real detector working temperature. It is foreseen an increase of detector responsivity by a factor of 6-7. This should imply better SNR, also if the noise appears to increase with decreasing temperature. Taking into account the increase of responsivity, the increase of noise, and the increase of SNR with gain, we foresee an increase of global SNR using gain 4-6 of a factor  $(3-4) \times (5-6) = 15-24$  with respect to lab measurements at room temperature. This means that for Mars we should expect a SNR larger than 100 over a wide range of wavenumbers.

### 3 – THEORETICAL CONSIDERATIONS

#### 3.1 - LWC RESPONSIVITY AND NER IN LABORATORY

Results presented here are based on observations of IFSI and IKI black bodies. Emissivity of 0.97 has been adopted also for spectral range outside the certified one for the IFSI BB.

The interpretation of the results becomes difficult when we consider the very different conditions at which the measurements have been acquired respect to those actually expected for PFS around Mars:

- LWC detector looks at sources in some cases WARMER and in other cases colder than at Mars, and an identical behaviour in the two cases is not trivial to demonstrate,
- The whole instrument operates in the air. The gas lines are well visible in the measurements and represent a severe source of error, especially in spectral region affected by water vapour. Moreover the thermal behaviour of the instrument, with special regard to LWC detector, should be very different when operating in vacuum. The presence of air in the instrument ensures efficient thermal exchange between different parts due to convection; this phenomenon tends to smooth any thermal gradient that may generate while operating in space.
- It is important to keep in mind that the work done in the Lab is not calibration of the instrument for the LW channel, while it may be for the SW channel. For the LW channel we perform essentially an exercise aiming mostly to characterise the interferometer and the internal BB.

In general, a measurement with the LWC gives

$$1 \quad A_1 = \int r(n)\{I(n) - B(n, T_{eff})\}dn$$

by taking 3 measurements, we add :

$$2 \quad A_2 = \int r(n)\{B(n, T_2) - B(n, T_{eff})\}dn$$

$$3 \quad A_3 = \int r(n)\{B(n, T_3) - B(n, T_{eff})\}dn$$

Teff is the effective temperature of the instrument. PFS in the LWC measures the difference in temperature between the source and the instrument/detector. r(n) is the responsivity, and B(n, Teff) is the Planckian with temperature Teff. We have

$$4 \quad \frac{A_1 - A_3}{A_2 - A_3} = \int \frac{r(n)\{I(n) - B(n, T_3)\}dn}{r(n)\{B(n, T_2) - B(n, T_3)\}dn}$$

If the third measurement is at deep space then T3 = 0 and

$$5 \quad I(n) = B(n, T_2) \frac{A_1 - A_3}{A_2 - A_3}$$

		<b>PFS for Mars Express</b> December 2002	<b>PFS</b> INTERNAL NOTE CALIBRATION II Page 5	<b>P.I. Vittorio Formisano</b> <b>CNR IFSI</b>
---	---	--	---	---

$n$  is the wavenumber. With the previous expression we have calibrated data at Mars. The responsivity of the instrument is obtained in the following way, if we use two BB at temperature  $T_2$  and  $T_3$  :

$$6 \quad \text{Re } s = \frac{A_2 - A_3}{\{B(n, T_2) - B(n, T_{\text{eff}2})\} - \{B(n, T_3) - B(n, T_{\text{eff}3})\}}$$

In space,  $T_3=0$  and assuming that the instrument temperature does not change, we have :

$$7 \quad \text{Re } s = \frac{A_2 - A_3}{B(n, T_2)}$$

A crucial point is what description of the experiment are we going to use? Formula 6 includes a temperature of the instrument that we have to define or obtain from the data.

In all the computations of the LWC we have followed Hanel approach and we have used the approximation :

$$8 \quad B(T_{\text{eff}}) = \alpha B(T_i) + (1 - \alpha) B(T_d)$$

Where we have  $T_i$  as temperature of instrument and  $T_d$  is the temperature of the detector. This description has given reasonable results, with  $\alpha$  of the order 0.6. When we tried a more complex description, we were not able to achieve reasonable results. It is interesting to add that also  $\alpha$  can be measured :

$$9 \quad \alpha = \frac{A_3 \{B(T_2) - B(T_d)\}}{A_3 - A_2} \frac{1}{\{B(T_i) - B(T_d)\}}$$

A very important quantity to compute is the noise equivalent radiance characterising the instrument. In a general case, like the laboratory measurements we have made, the NER can be computed as :

$$10 \quad \text{NER} = \frac{\sigma(\text{Re } s)}{\text{Re } s} * B(T_{\text{eff}}) = \frac{\sigma(\text{Re } s)}{\text{Re } s} * (\alpha B(T_i) + (1 - \alpha) B(T_d))$$

In theory one could assume that the instrument is isothermal, and the formula could be simplified, but the conditions in laboratory measurements were such that the temperatures were not constant. Indeed housekeeping data show (fig. 1) that:

- during each observative session the temperature of LWC detector increases slowly (variation is in the order of 1.5 up to 4 K)
- average temperature of LWC detector between different sessions differs of 2-4 K

Thermal changes in OTHER parts of the instrument can affect the measurements too, because of emission of optical elements before the beamsplitter, reflected emission of the LWC detector and so on .

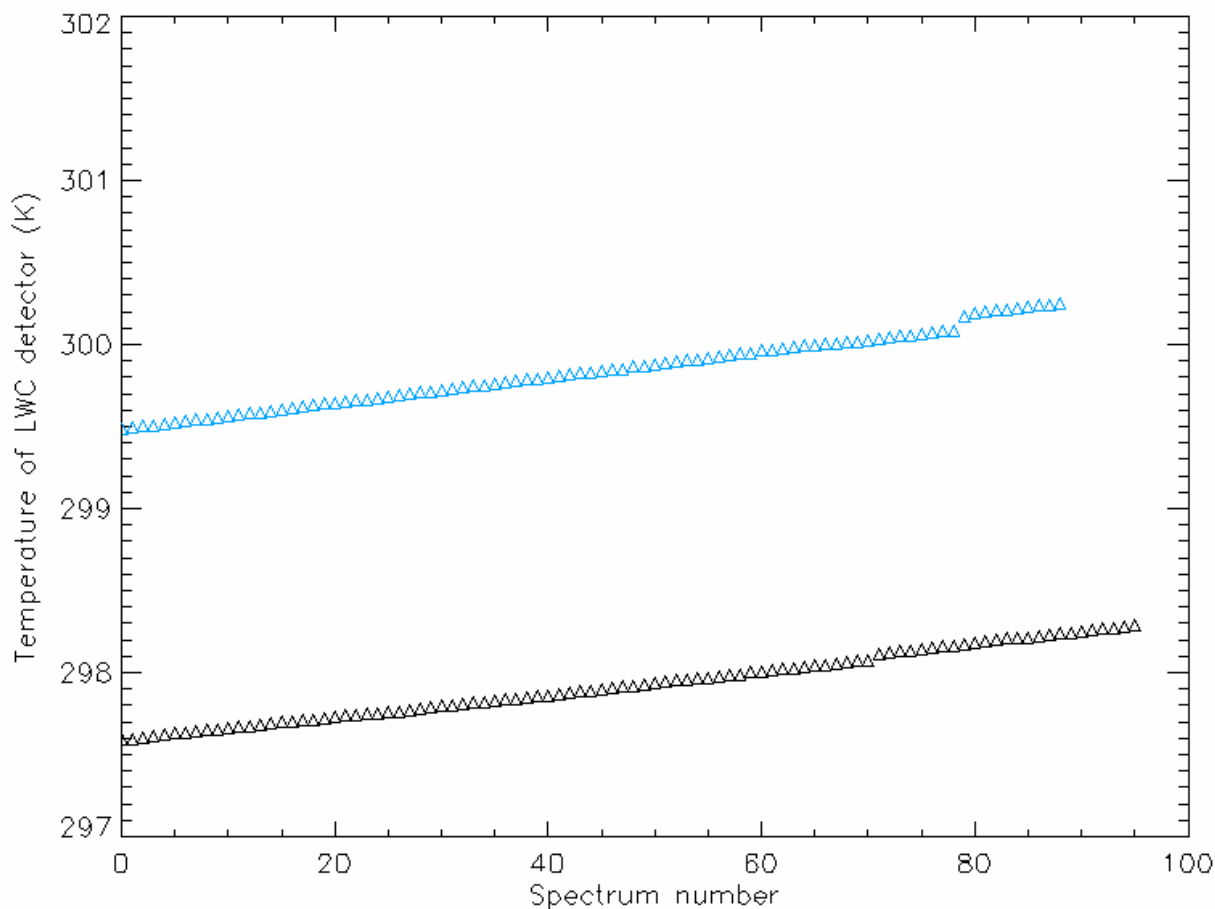


Fig-1

Temperature variations of the LWC detector during measurements.

Black diamonds: BB30\_011227\_100440

Blue diamonds: BB50\_011227\_113148

### 3.2 - EMISSIVITY OF IKI BLACK BODY FROM LABORATORY DATA

The emissivity  $\varepsilon_{v, BB}$  of a body at uniform temperature  $T_{BB}$  is defined as:

$$(11) \varepsilon_{v, BB} = \frac{I_{v, X}}{B(T_{BB})}$$

where  $I_{v, X}$  can be measured using PFS. Temperature of IKI BB showed during observative sessions temperature fluctuations in the order of some degrees, but it was possible to record continuously these data and relate each PFS spectrum with the instantaneous temperature of the source. More problematic is the assessment of its temperature uniformity, because small portion of external baffles may be in the FOV of PFS.

### 3.3 - EMISSIVITY OF INTERNAL BLACK BODY FROM LABORATORY DATA

The temperature of internal black body is provided directly, for each spectrum, by the housekeeping data. Formula 11 holds valid also in this context. Main problem for the determination of its emissivity is the small temperature difference between LWC detector and BB source. This produces a very low level of the power spectrum.

### 3.4 - DETERMINATION OF FOV

The field of view of an optical instrument can be defined as the ensemble of directions of light rays that can be detected by the sensor.

FOV consist usually of a well-defined solid angle (referred here as main cone<sup>1</sup>), but presents very often lobes around the main cone and spikes. In a well-designed optical instrument the sensor represents the field stop and the main cone is simply the dimension of the sensor in the focal plane. The response of the instrument to a unit light source inside of main cone can present variations due to:

- residual vignetting
- non uniform detectivity of the sensor over its surface (lacking a filed lens systems such as in PFS)

Lobes are usually related to diffraction of optics and, as well as spikes, internal anomalous reflections.

A rigorous study of FOV would require a very fine probing of instrument's response to a constant source at different directions of incoming rays.

In the conditions of planetary observation, each point on the planet's surface emits light in every direction BUT, needless to say, the instrument should detect only those emitted in the direction of the satellite. Due to great distance between probe and surface, these rays falls inside a very narrow cone, with a negligible width. Consequently, the instrument should see each single point on the surface only through rays incoming with a particular direction. If the instrument will see radiation from other directions, possibly at reduced intensity, then we shall have the stray light effects. It is obviously very important to know if these effects are present and what is their intensity. A point source emitting in half hemisphere at a distance from the instrument, which is moved over a space much wider than the FOV expected will be a good simulation of martian conditions.

This approach allows to determine the FOV modulated by the actual instrument responsivity in different directions (referred hereafter simply as FOV,  $F(\phi, \varphi)$  where angles axis are centered on optical axis).

### 3.5 - SWC RESPONSIVITY AND NER IN LABORATORY

The SW channel has been calibrated both at room temperature and with cooled detector. While the calibration at room temperature have been rather complete with measurements of different source intensity taken at different gains, at low temperature the measurements are not complete and only some temperatures and some gains have been effectively explored. The reason essentially is in the time needed to perform all the operations (the instrument could not work with the vacuum chamber switched on) and in the effective possibility to reach the needed temperatures (and keep them for a long time). The actual performance in space can only be obtained as extrapolation of the results obtained at higher temperatures to the predicted thermal conditions.

The whole SW channel is affected by non linearity effects. We shall describe later the results of the study of the non linearity. Essentially there are two non linearity, one due to the detector, which is non

---

<sup>1</sup> The intersection of the main cone with the planet's surface is usually refereed as footprint. Instruments (such as PFS) that do not use a motion compensation system have actually a smeared footprint, given by the translation of this intersection during the acquisition time.

linear at high light intensities. The second non linearity is generated by the strong cutoff of the Bessel filter imposed to the electronic signal : this filter is sensitive to the pendulum speed, therefore to presence of gravity (forward or reverse motion occur in different gravity conditions – uphill or downhill – with consequent different speed which influence the spectrum by means of the non linearity of the Bessel filter).

Corrective procedure described in the solar region paragraph point must be applied to SWC interferograms *before* computation of power spectra, regardless the considered spectral range.

### 3.6 - THERMAL PART

A procedure identical to the one adopted for LWC can be used on the range of SWC sensitive to thermal radiation from reference black bodies. This range extends approximately [ 2000 – 3500 ]  $\text{cm}^{-1}$ .

The small amount of energy absorbed by the sensor (now we work in the far Wien wing of Planck function) should lead to temperature variations of this device much reduced compared to those experienced in LWC. The amplitude of thermal waves should also be much reduced by the good thermal contact between SWC detector and cold finger. Anyway, the room temperature variations from different observative sessions are not negligible and the classical calibration approach, which assumes constant instrument emission, represents only a crude estimation of actual instrument's characteristics.

### 3.7 - SOLAR PART

In regions where the emission of the sensor and of the instruments can be neglected and formula 6 reduces, in the ideal case, simply to

$$(12) R_v = \frac{P_{v,x}}{I_{v,x}}$$

Here we used, as reference known sources ( $I_{v,x}$ ), the integrating sphere; the use of this device limits our study to the [4000;8200]  $\text{cm}^{-1}$  range.

The wide dataset acquired from January 3<sup>rd</sup> to January 5<sup>th</sup> for different luminances of the integrating sphere and different gains of SWC detector demonstrates however, for room temperatures, a non-linear response of the instrument. In particular, responsivity computed from equation 12 seems to decrease for high signal levels.

This effects can be explained considering the structure of SWC detector.

The interferogram signal is proportional to the variable component of:

$$(13) V_{signal} = V_{ref} \left( 1 - \frac{R_{pd}}{R_{pd} + R_L} \right)$$

The resistance of photodiode is inversely proportional to the incoming energy from the source; this means that, once the spectral shape of the source is fixed (as it happens in the case of integrating sphere), the relationship

 Planetary Fourier Spectrometer PFS		<b>PFS for Mars Express</b> December 2002	<b>PFS</b> INTERNAL NOTE CALIBRATION II Page 9	<b>P.I. Vittorio Formisano</b> <b>CNR IFSI</b>
---	---	--	---	---

$$V_{signal} = V_{ref} \left( 1 - \frac{\frac{C_2}{L_{sphere}}}{\frac{C_2}{L_{sphere}} + R_L} \right) = V_{ref} \left( 1 - \frac{C_2}{C_1 + R_L L_{sphere}} \right)$$

(14)

holds true, where  $L_{sphere}$  indicates the sphere's luminance.  $C_2$  contains all the multiplicative factors involved, including the spectral distribution of the sphere and the optical path differences.

Observe how the non linearity of SWC detector rises directly from interferogram and affects in different ways different Fourier components of the spectra. Consequently, recover action must be performed on interferograms, not on spectra.

Consequently, the interferogram peak value  $In_0$ , as a function of sphere luminance, should follow a relationship such as:

$$In_0 = A_1 \left( 1 - \frac{C_2}{C_2 + R_L L_{sphere}} \right) = A_1 \left( 1 - \frac{1}{A_2 L_{sphere} + 1} \right) \quad (15)$$

Factor  $A_1$  represent the multiplicative term between voltages and ADUs read in the interferograms and is expected to be directly proportional to SWC gain. Observe also that

$$\lim_{L_{sphere} \rightarrow \infty} \frac{In_0}{L_{sphere}} = A_1$$

We called this phenomena "saturation of the detector" and should not be confused with saturated interferograms, that occurs when  $In_0$  exceeds the digitalization limit of  $2^{15}$ .

In the limit for low luminances eq. 15 reduces to

$$In_0 = A_1 \cdot A_2 \cdot L_{sphere} \quad (16)$$

A responsivity retrieved for low values of sphere luminances may be used also at high signal levels when, (retrieving  $L_{sphere}$  form 15 and substituting in 16), each point in the interferogram is corrected according the equation

$$In_{corrected} = A_1 \left( \frac{In_{observed}}{A_1 - In_{observed}} \right)$$

This formalism is valid until the continue component of the signal is negligible respect to the fluctuations related to the changes in optical path difference.

In more realistic cases, continue component may shift the whole interferogram toward saturation levels and the behavior of the negative part of interferogram differs from that of positive side, closest to the saturation region.

Once the interferogram has been corrected computation of responsivity and NER may be carried on using the standard approaches of equations 9 and 12.

		<b>PFS for Mars Express</b> December 2002	<b>PFS</b> INTERNAL NOTE CALIBRATION II Page 10	<b>P.I. Vittorio Formisano</b> <b>CNR IFSI</b>
--	---	--	--	---

### 3.8 - EFFECT OF TEMPERATURE ON SWC RESPONSIVITY

It is expected that the SWC responsivity increases with decreasing of detector temperature. There are, however, a number of important questions to be investigated with the data collected.

Is the non linearity of the detector the same with low temperature?

Is the gain factors the same at low temperature?

Is the ghost feature depending somehow from the temperature?

Is the noise of the detector and of the instrument depending on the detector temperature?

What are the effects of a detector temperature being lower or higher than the source temperature?

In the following we shall try to answer to these questions.

### 3.9 - DATA ACQUISITION FAILURE

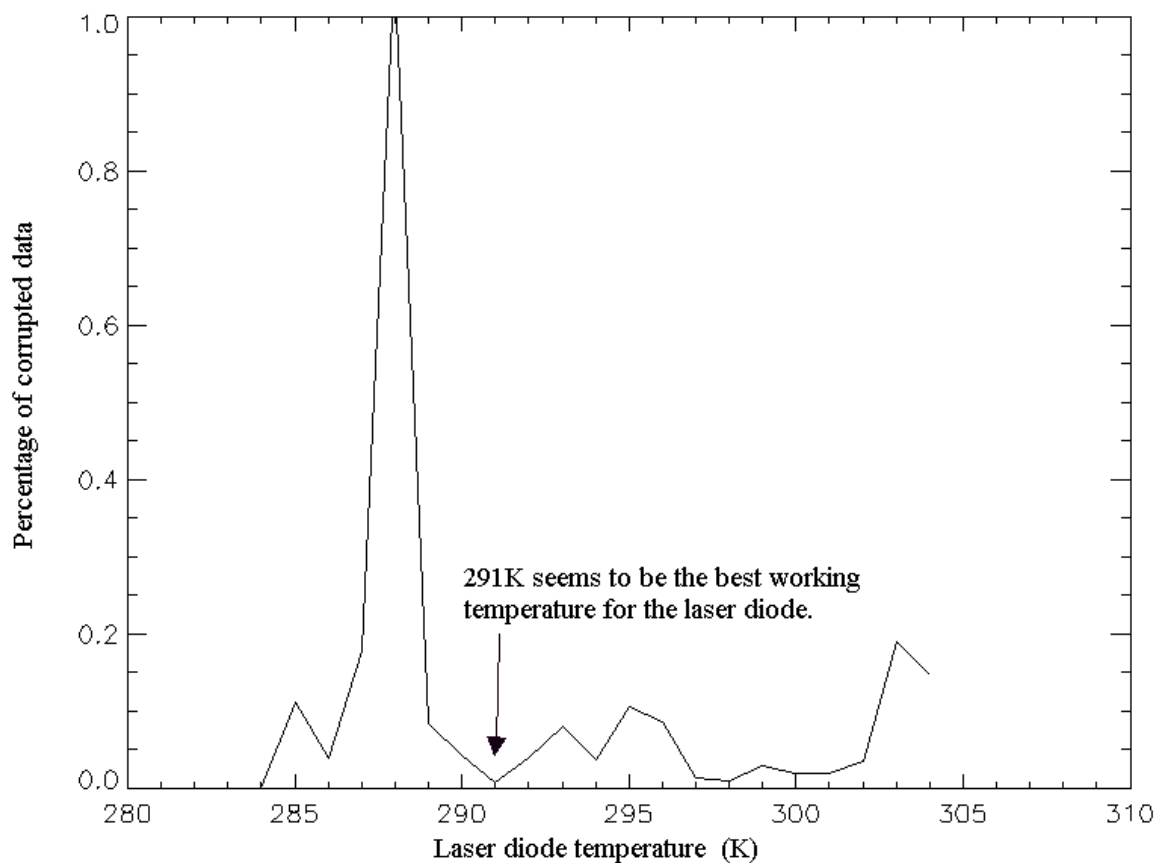
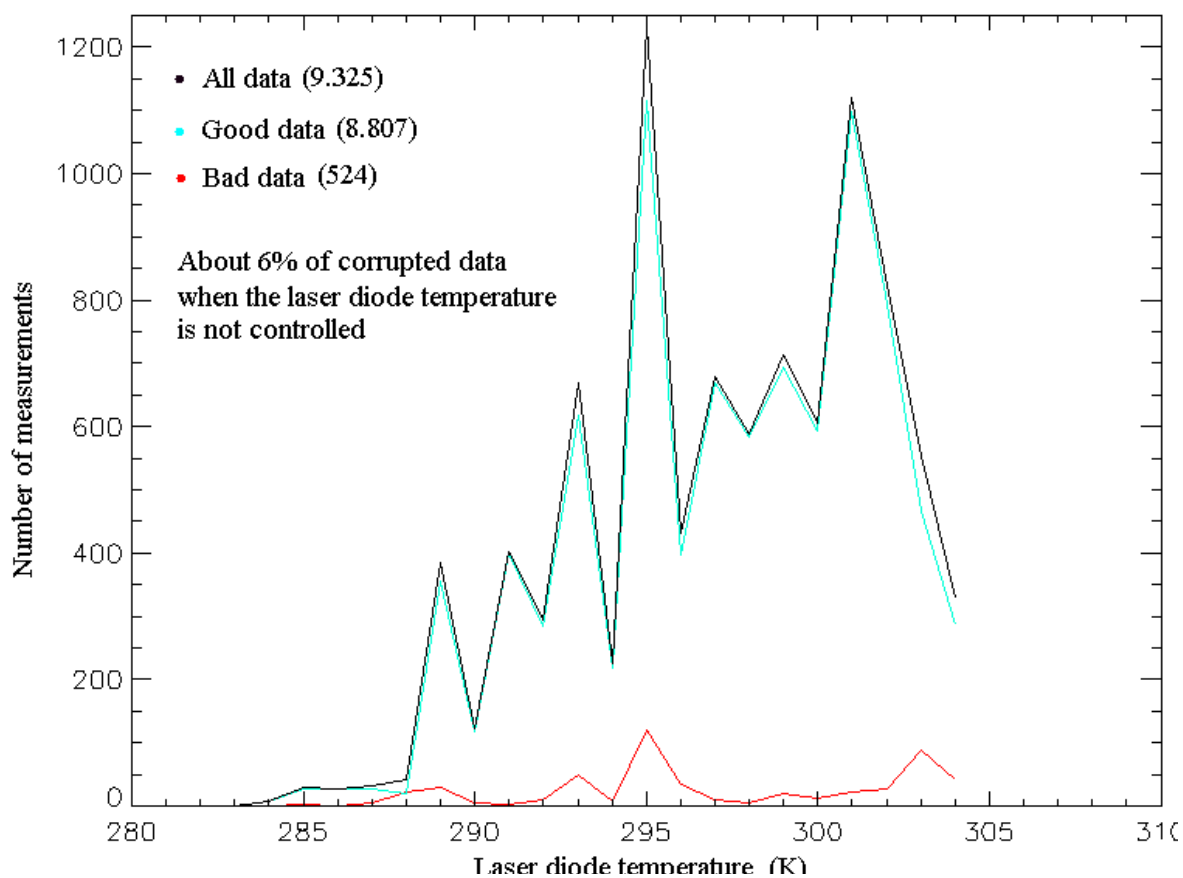
A number of data acquired by PFS can not be used due to corruption. The corruption causes fall in three class:

- saturation: occurs when a signal is too high and is not compatible with the dynamical range of the detector, as fixed by the required gain. Can be considered usually as an improper use of the instrument, not a real failure
- presence of spike: is the most serious cause of errors and consists in spikes in the interferogram. They occur as isolated spikes or as compact groups when the motion is not OK (depending on laser diode temperature and power to the motor). Other disturbances can be due to :
  1. microphonic disturbances (voices, vibrations due to machines)
  2. sudden changes (due to temperature) of  $\lambda_{\text{emitted}}$  of laser diode, with consequent bad sampling
  3. improper setting of signal electronic filter.

It is interesting to note that in all the calibration activity we had 6 % of bad data, due mostly to bad motion control as the temperature of the laser diode was almost never really controlled, and therefore the laser was not well monochromatic and the motion was not good.

There are some temperatures of the laser diode in which bad motion = bad data seems more likely : these are 285, 288, 293, 295, 299, 303 kelvin.

From the percentage of bad data seems that the worst temperature at all is 288 Kelvin.



### 3.10 - WAVENUMBER GRID CALIBRATION

Assuming that the position of spectral sampling points in an interferogram may be described in the form

$$\nu_i = i \cdot \Delta \nu$$

where index  $i$  denotes element index in sampling grid, the dependence of sampling step  $\Delta \nu$  on temperature of laser diode may be investigated in easy way.

If the sampling position  $i$  (in the wavenumber grid) corresponding to a fixed and stable spectral feature can be described empirically as a function of laser temperature by a form  $i=f(T)$ , we have:

$$\Delta \nu = \frac{\nu_{feature}}{i} = \frac{\nu_{feature}}{f(T)}$$

We have found that in order to have the best results, all the spectra must be calibrated in wavenumber using the laser diode temperature and the linear fit given in the figures below.

### 3.11. REFERENCE SOURCES

Reference sources used are:

1. "IFSI" black body (MIKRON M345X4 UDC): it has a certified emission of  $0.97 \pm 0.005$  in the range [8; 15]  $\mu\text{m}$  and [3; 5]  $\mu\text{m}$

Other non-certified sources are:

1. IKI black bodies: a value of emissivity of  $1. \pm 0.1$  has been estimated in Lecce laboratories
2. Ceramic element: stable source, able to provide intense signal in the whole PFS spectral range
3. Mercury lamp: (Oriel 6035) very stable against temperature variations, presents lines at 9862.13 8859.44 7369.09 7313.42 6537.74 5923.64 5910.10 5902.49 5857.27 5844.57 5770.54 5515.60 and 5076.09  $\text{cm}^{-1}$ . The line at 6537.74 is the strongest and the only actually reliable for our purposes. The width of these lines are declared as "negligible" by the manufacturer but any precise figure in this sense is provided.

Moreover, the PFS scanner hosts a calibration lamp and internal black bodies. The characterization of these sources is one of the most important tasks for the whole calibration program. A first order evaluation of black body paint emissivity and bare lamp intensity are provided by the manufacturer.

### 3.12 - THEORETICAL PFS PERFORMANCE .

#### 3.12.1 SW CHANNEL.

##### Signal-to-Noise Ratio

### SNR SWC

Minimum detectable radiance (SNR = 1):

$$\rho = \left[ \eta \sqrt{\varepsilon} D^* \delta\sigma \sqrt{\Lambda \Omega T} \right]^{-1} \left[ \frac{W}{\text{cm}^2 \text{sr cm}^{-1}} \right]$$

optical efficiency, $\eta$	0.3	
apodisation factor	2.25	
$D^*$ , $\Delta f = 2$ kHz, 225 K	$1 \cdot 10^{10}$	$\text{cm} \sqrt{\text{Hz}} / \text{W}$
spectral resolution, $\delta\sigma$	1.5	$\text{cm}^{-1}$
max. opt. path diff. $x$	0.5	cm
FOV, $\gamma$	14	mrad (0.8°)
throughput, $\Lambda$	0.004	$\text{cm}^2 \text{sr}$
solid angle, detector $\Omega$	3.4	sr
acquisition time, 1-sided Interferogram, $t$	2.048	s
$\rho$	$9.2 \cdot 10^{-10}$	$\text{W}/(\text{cm}^2 \text{sr cm}^{-1})$

##### Modulation factor due to the aperture effect

$$m_1 = \left| \text{sinc} \left( \frac{\pi}{2} x \gamma^2 \sigma \right) \right|$$

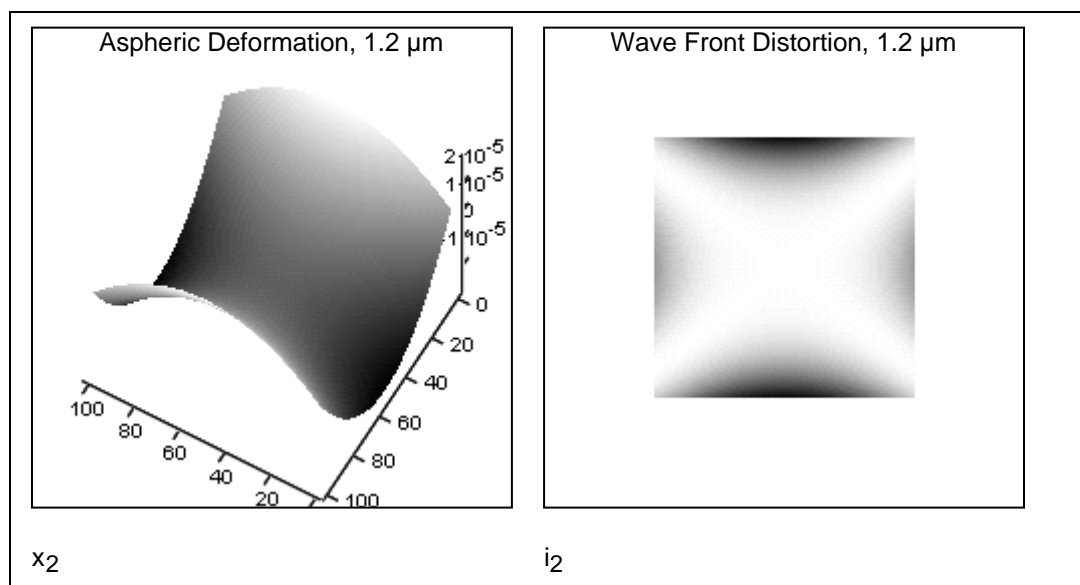
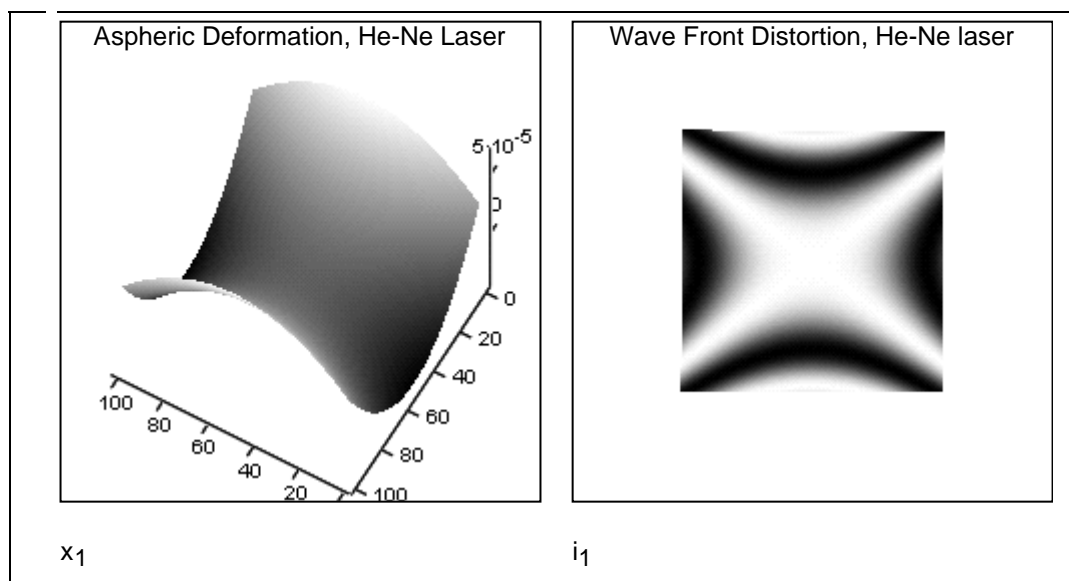
##### Modulation factor due to curvature of beamsplitter and cube corners

$$m_2 = \left| \frac{1}{\pi} \int_0^{2\pi} \int_0^1 \exp \left\{ 4\pi j \varepsilon \sigma r^2 [1 - \kappa - \kappa \cos(2\theta)] \right\} r dr d\theta \right|$$

spherical curvature  $\varepsilon = 150$  nm

aspheric parameter  $\kappa = 0.8$

This results in a curvature peak-to-valley of 480 nm.



**modulation factor due to misalignment**

$$m_3 = 2 \left| \frac{J_1(4\pi q\gamma\sigma)}{4\pi q\gamma\sigma} \right|$$

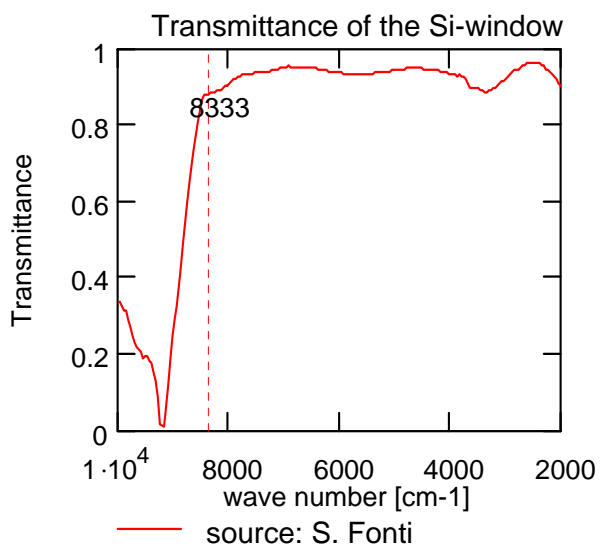
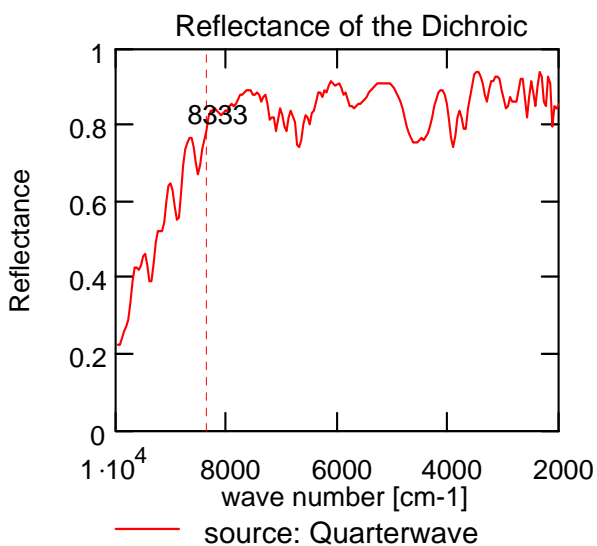
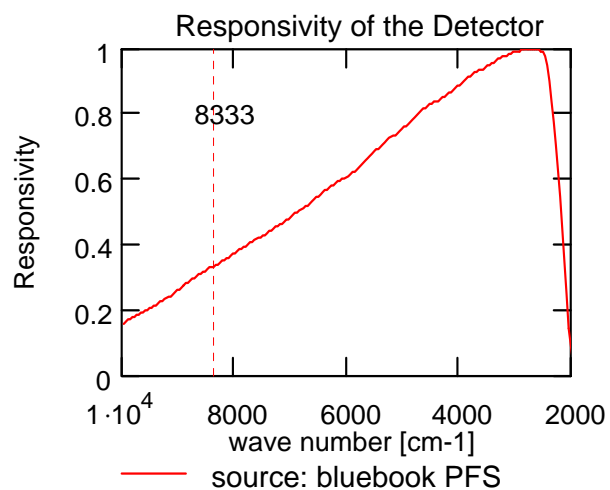
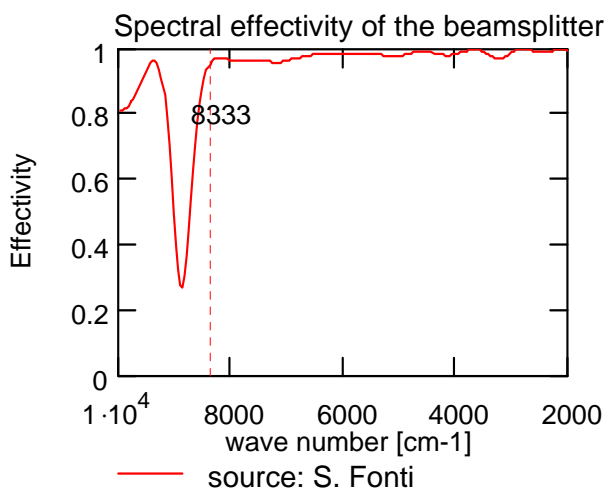
q = 5 μm, halve a strip

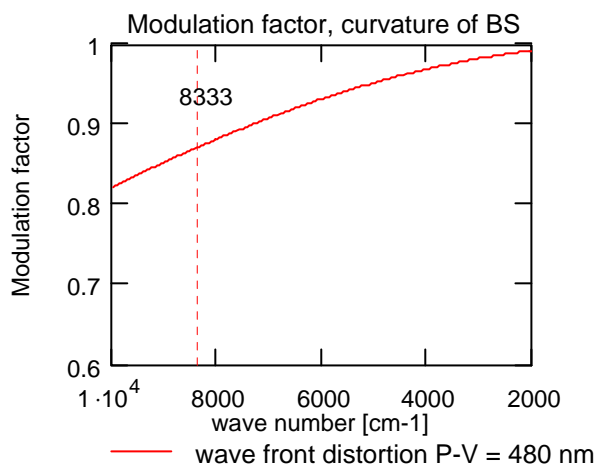
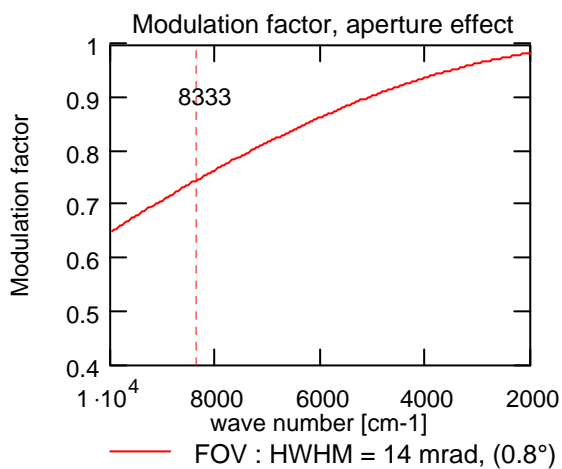
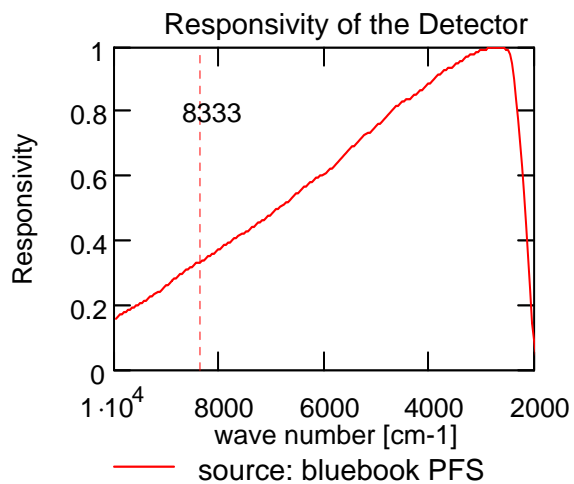
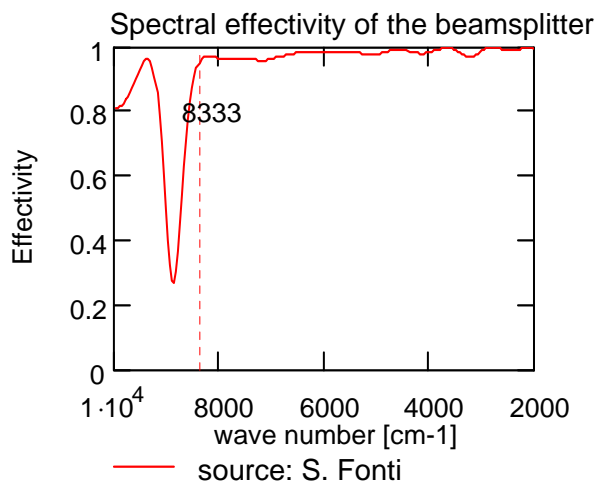
**total modulation coefficient**  $m_\sigma = m_1 m_2 m_3$

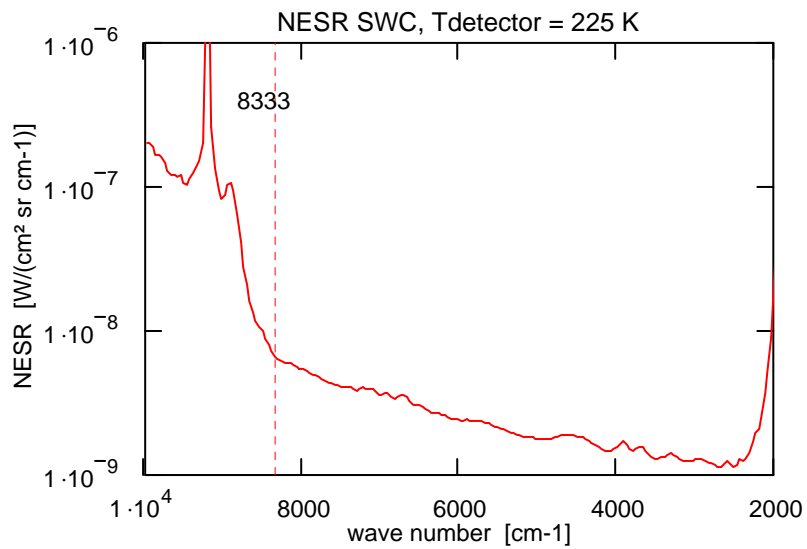
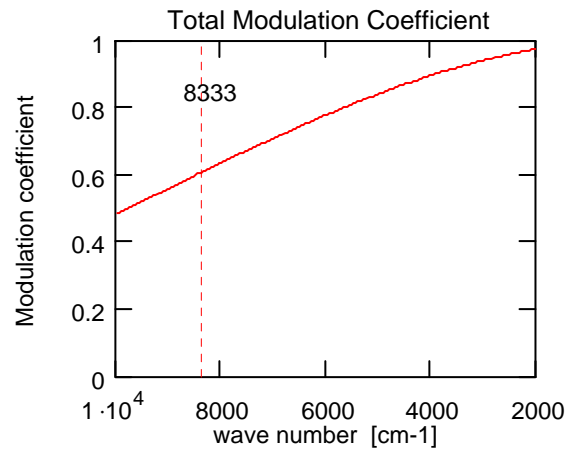
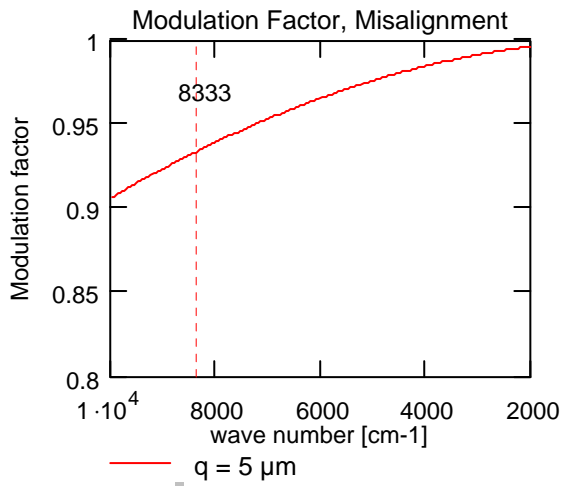
$$\text{NESR} = \frac{\rho}{R_\sigma T_\sigma B_\sigma F_\sigma m_\sigma}$$



reflectance of the dichroic	$R_{\sigma}$	transmittance of the Si-window	$T_{\sigma}$
effectivity of the beamsplitter	$B_{\sigma}$	detector response	$F_{\sigma}$



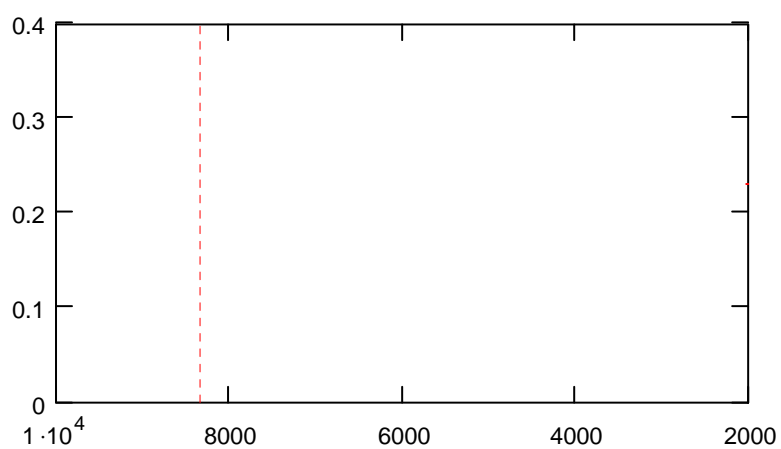


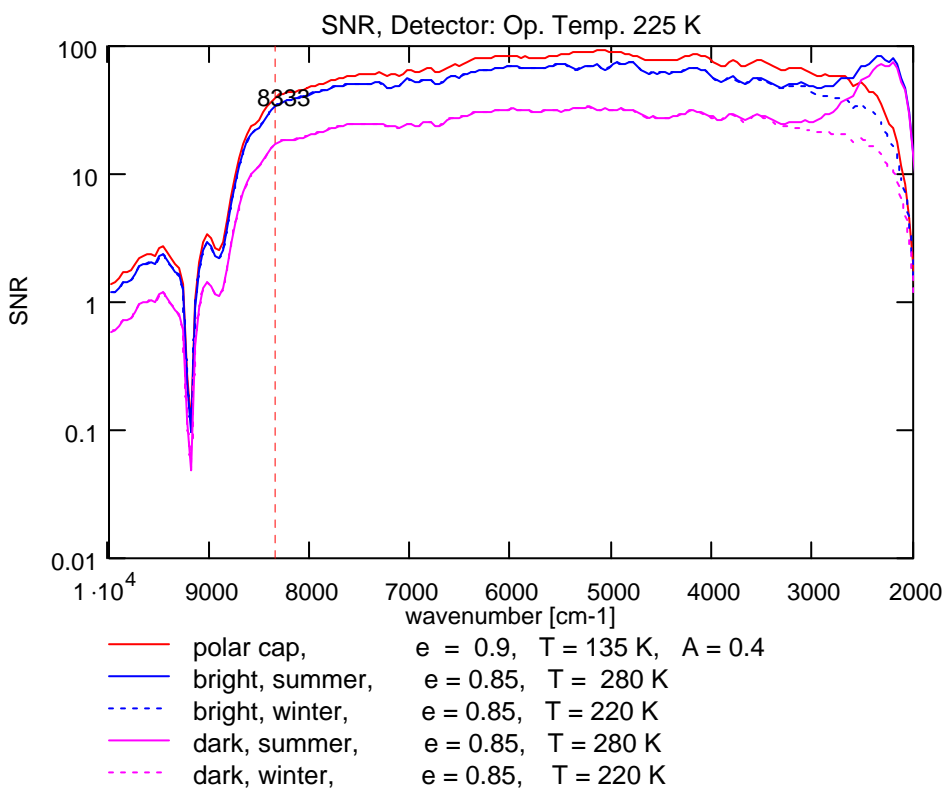
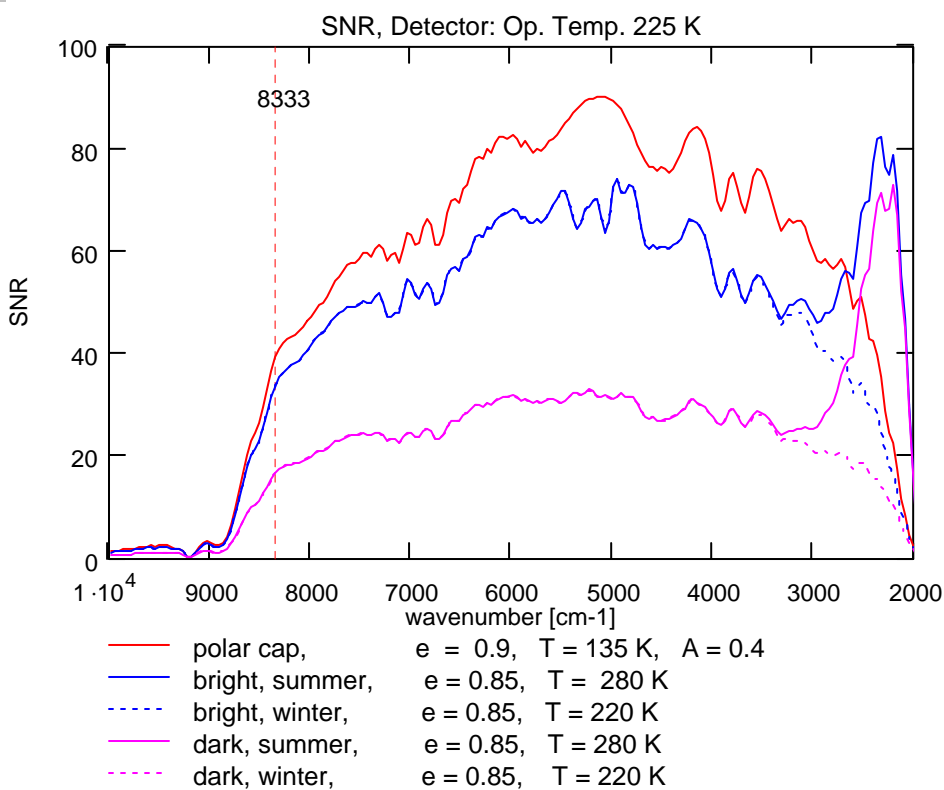


Martian spectral radiance

$$L_{\sigma} = \frac{A}{\pi} \frac{r^2}{R^2} \frac{c_1 \sigma^3}{\exp\left(\frac{c_2 \sigma}{T_s}\right) - 1} \cos \varphi + \frac{\varepsilon}{\pi} \frac{c_1 \sigma^3}{\exp\left(\frac{c_2 \sigma}{T_s}\right) - 1}$$

$$\text{SNR}_{\sigma} = \frac{L_{\sigma}}{\text{NESR}_{\sigma}}$$





### 3.12.2 - LW CHANNEL

#### SNR LWC

Minimum detectable radiance (SNR = 1):

$$\rho = \left[ \eta \sqrt{\varepsilon} D^* \delta\sigma \sqrt{\Lambda \Omega T} \right]^{-1} \left[ \frac{W}{\text{cm}^2 \text{sr cm}^{-1}} \right]$$

optical efficiency,	$\eta$	0.18	
apodisation factor		1.69	
$D^*$ , $\Delta f = 500$ Hz,		$3.2 \cdot 10^8$	$\text{cm}\sqrt{\text{Hz}} / W$
spectral resolution,	$\delta\sigma$	1.3	$\text{cm}^{-1}$
max. opt. path diff.	$x$	0.5	cm
FOV,	$\gamma$	24	mrad (1.37°)
throughput,	$\Lambda$	0.02	$\text{cm}^2 \text{sr}$
solid angle, detector	$\Omega$	2.3	sr
aquisition time, 1-sided Interferogram,	$t$	2.048	s
	$\rho$	$3.3 \cdot 10^{-8}$	$W/(\text{cm}^2 \text{sr cm}^{-1})$

Modulation factor due to aperture effect

$$m_1 = \left| \text{sinc} \left( \frac{\pi}{2} x \gamma^2 \sigma \right) \right|$$

Modulation factor due to nonplanarity of the beamsplitter

$$m_2 = \left| \text{sinc}(2\pi\varepsilon\sigma) \right|$$

$\varepsilon = 500$  nm – spherical nonplanarity

Modulation factor due to misalignment

$$m_3 = 2 \left| \frac{J_1(4\pi q \gamma \sigma)}{4\pi q \gamma \sigma} \right|$$

$q = 10$   $\mu\text{m}$  – lateral displacement

**modulation factor due to retroreflectors**

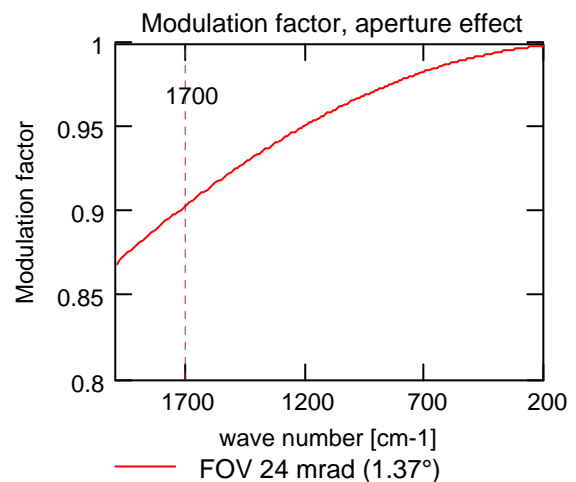
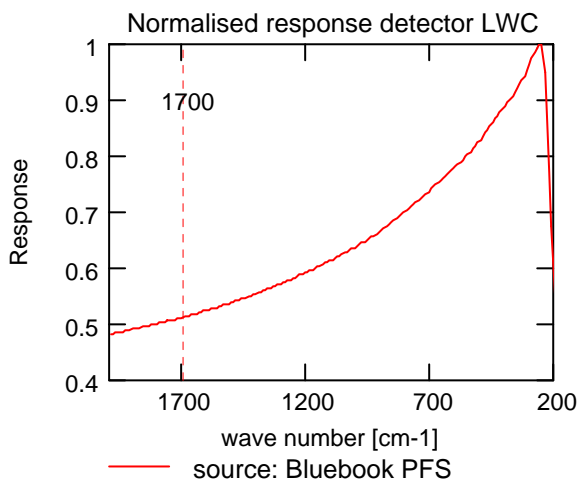
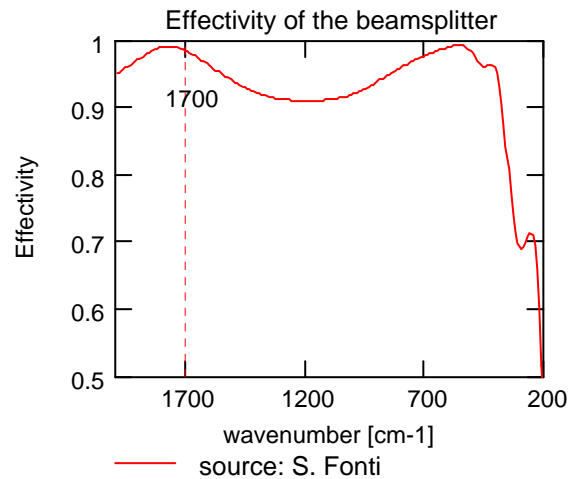
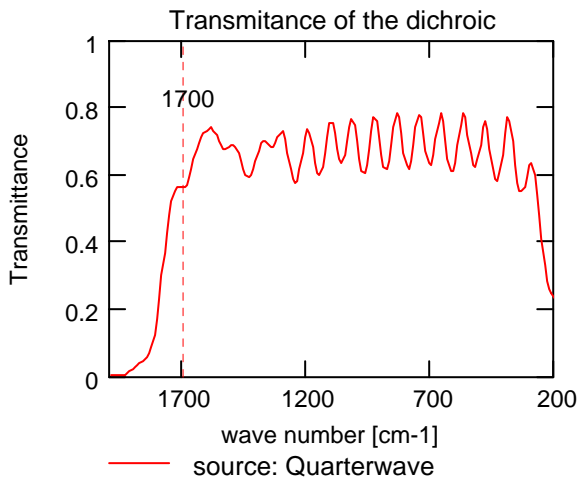
$$m_4 = 2 \left| \frac{J_1(4\pi\delta R\sigma)}{4\pi\delta R\sigma} \right|$$

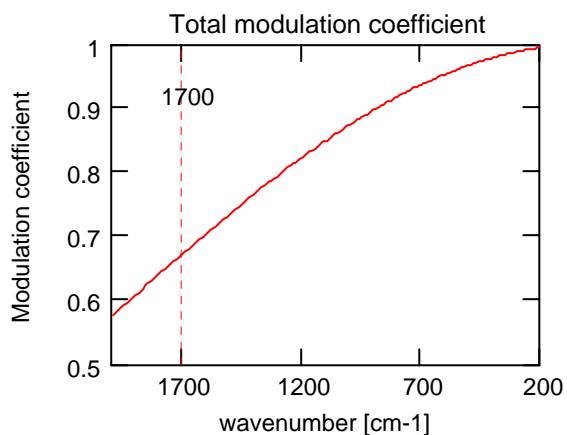
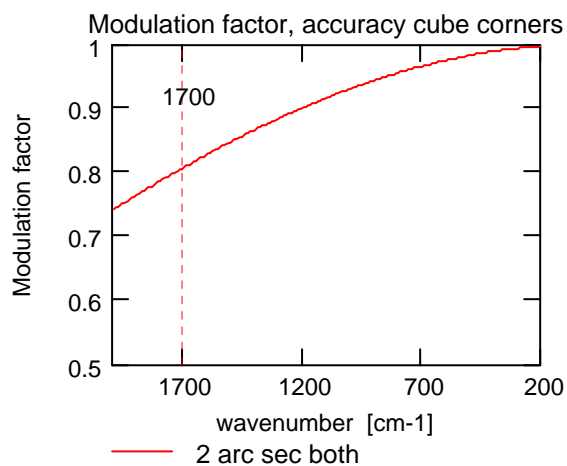
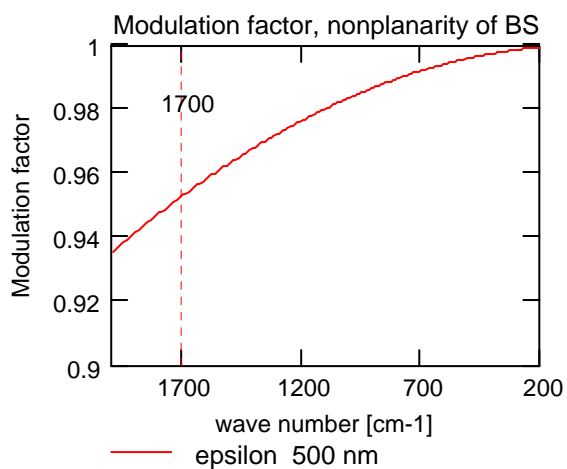
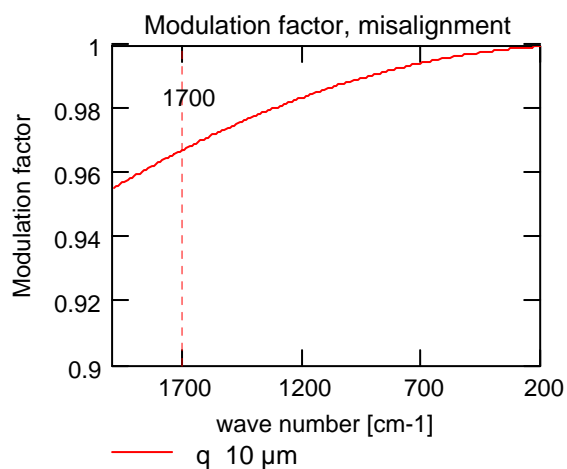
$\delta = 2 \cdot 10^{-5}$  – divergence angle, R – aperture radius of the retroreflectors

**total modulation coefficient**  $m_\sigma = m_1 m_2 m_3 m_4$

$$NESR = \frac{\rho}{T_\sigma B_\sigma F_\sigma m_\sigma}$$

transmittance dichroic	$T_\sigma$	effectivity beamsplitter	$B_\sigma$
detector response	$F_\sigma$		

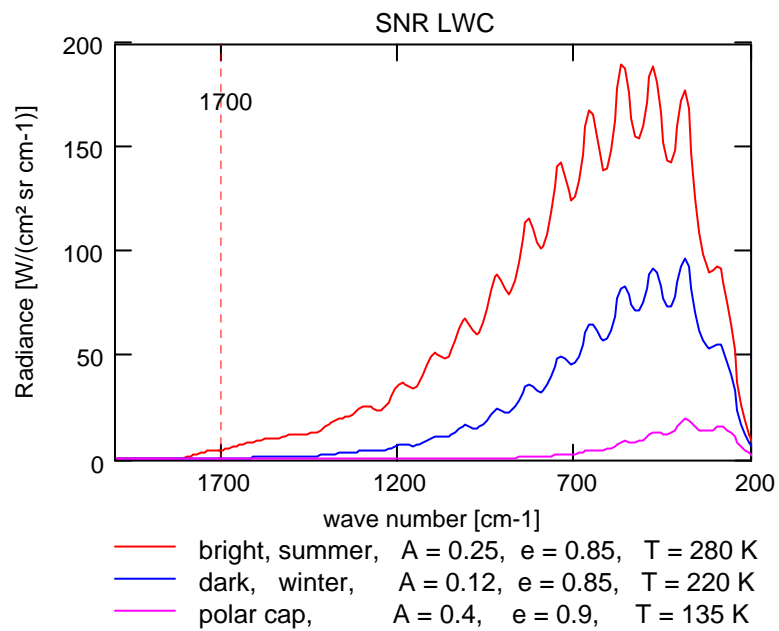
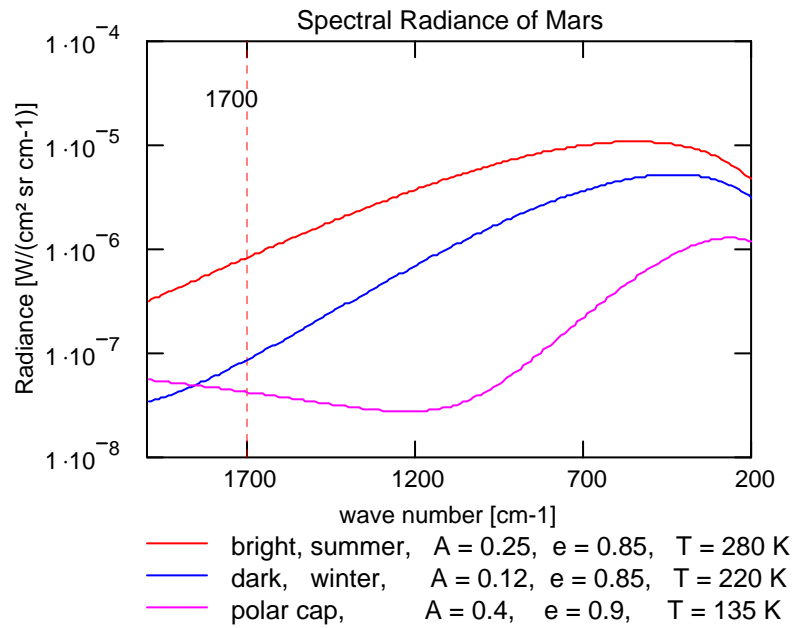


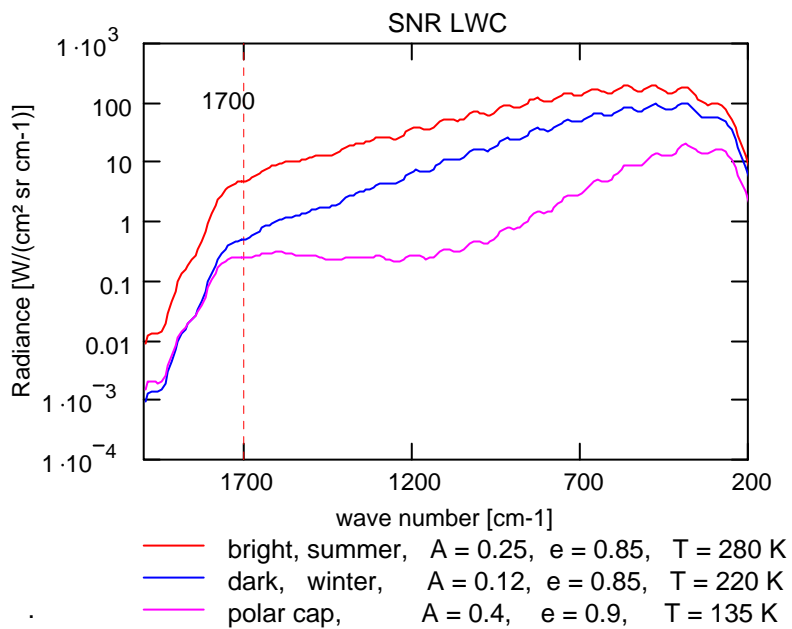


### Martian spectral radiance

$$L_{\sigma} = \frac{A}{\pi} \frac{r^2}{R^2} \frac{c_1 \sigma^3}{\exp\left(\frac{c_2 \sigma}{T_s}\right) - 1} \cos \varphi + \frac{\varepsilon}{\pi} \frac{c_1 \sigma^3}{\exp\left(\frac{c_2 \sigma}{T_s}\right) - 1}$$

$$\text{SNR}_{\sigma} = \frac{L_{\sigma}}{\text{NESR}_{\sigma}}$$





#### 4 – LW CHANNEL CALIBRATIONS

It is important to say here that we have used the laboratory measurements according to the indications given previously about the laser diode jumping.

Before the responsivity and the NER is computed, we note from the included figures that each spectrum seems to be 2.5 decades intense, although the noise level (sigma) is rather high .

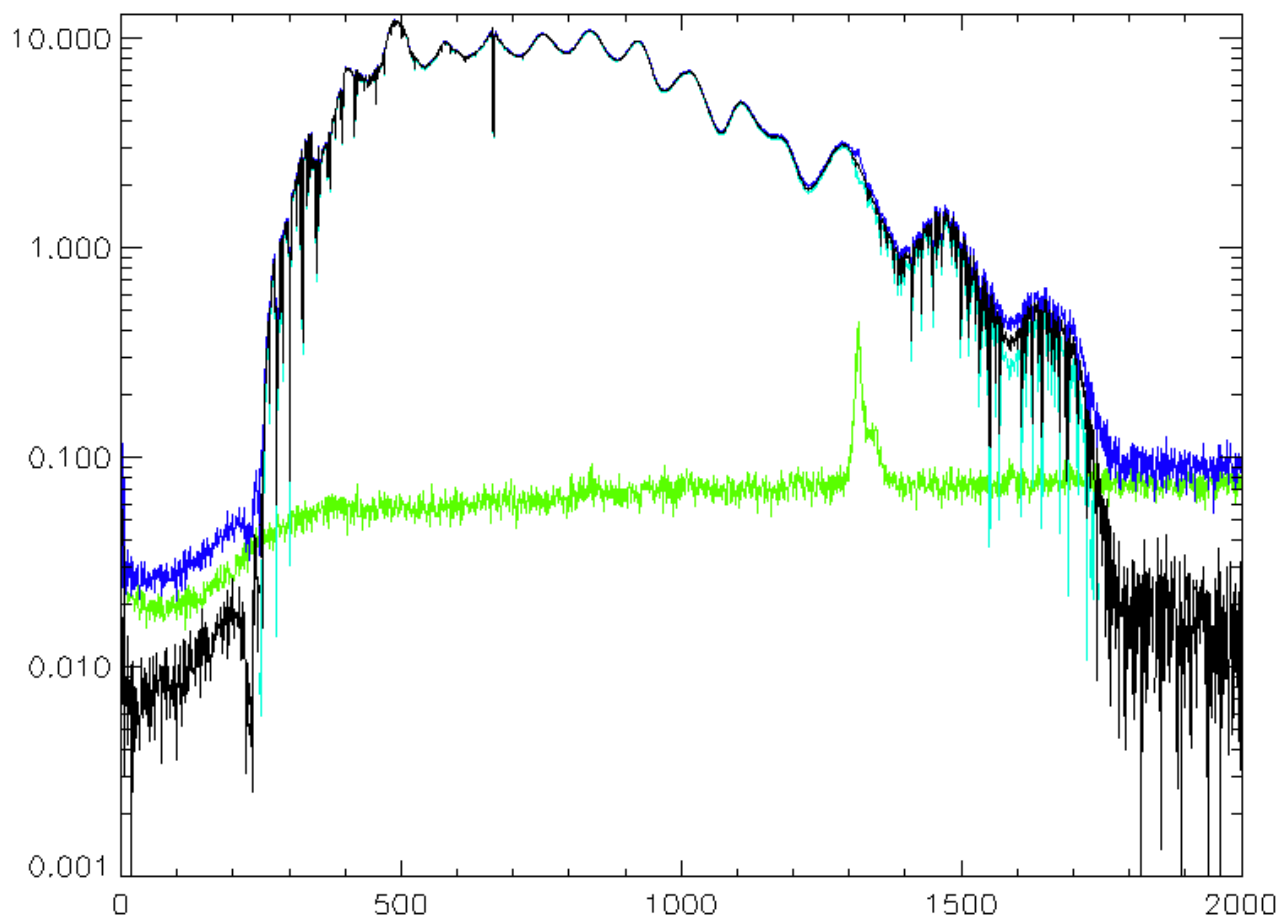
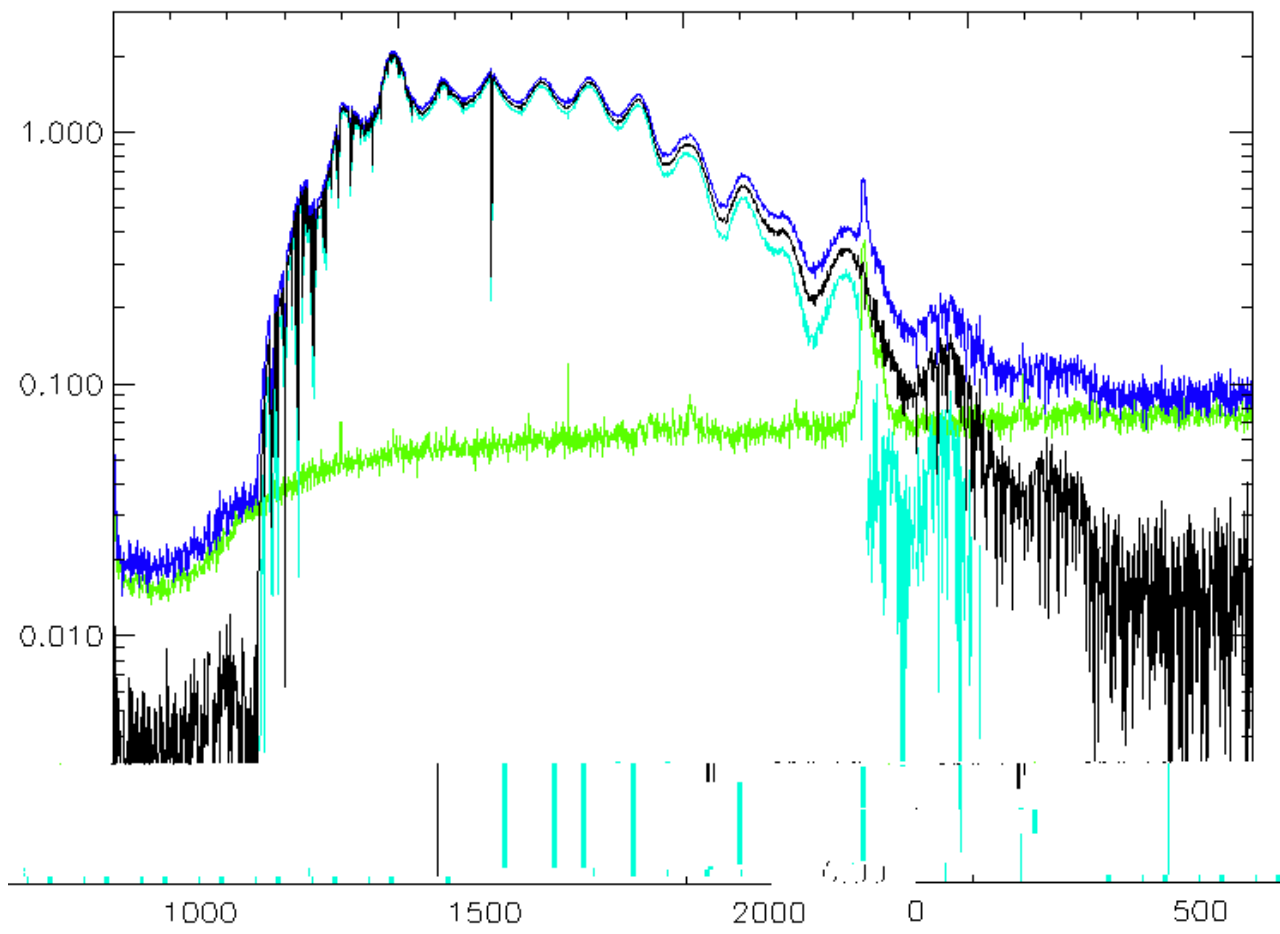


**Figure 2-** BBIFSI at 150 C, average over 100 measurements .

AVERAGE, SIGMA, AVERAGE+ - SIGMA.

NOTE ALMOST 3 DECADES RANGE FOR THE AVERAGE SPECTRUM.

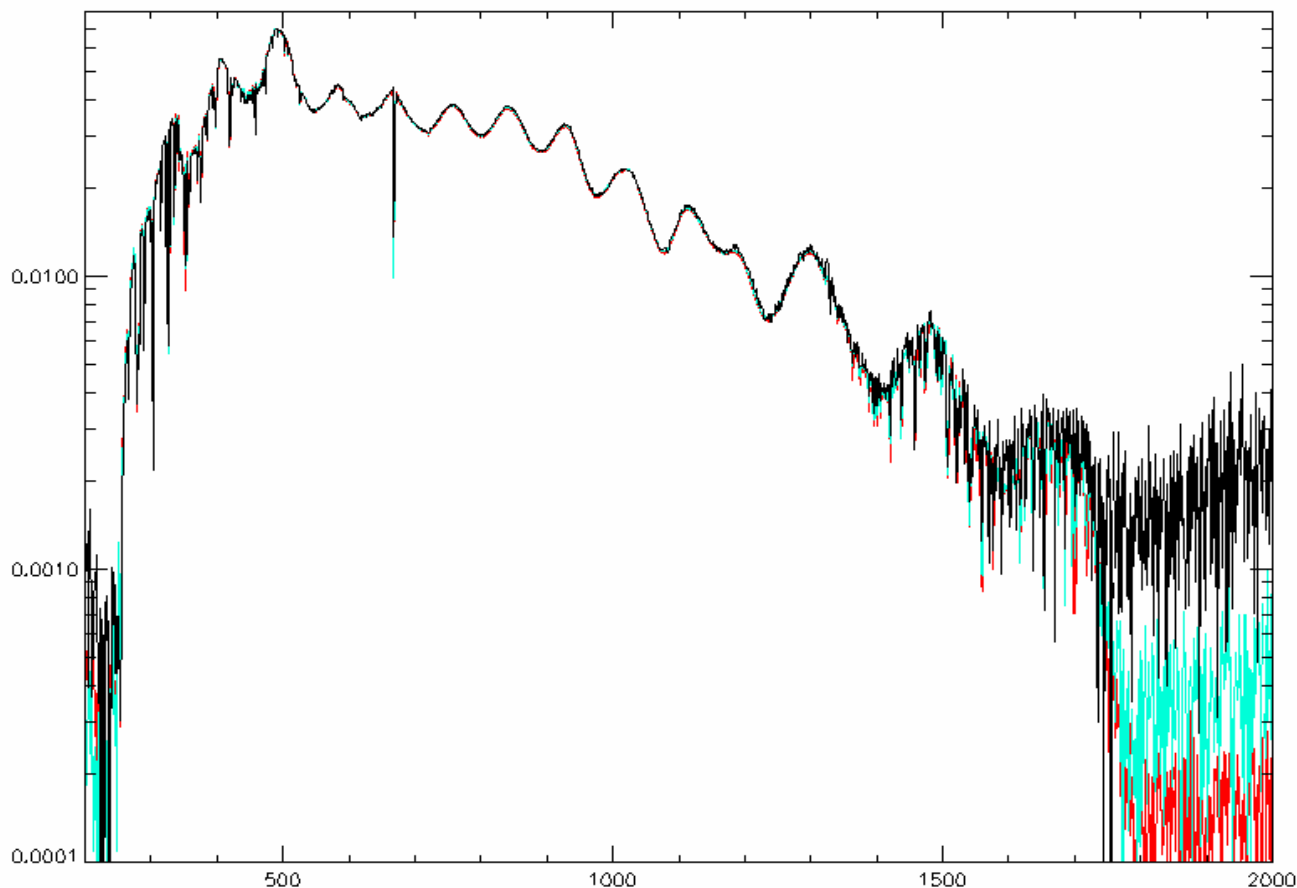
Figure 2 shows the average raw spectrum (black), the sigma value (green), and the spectrum plus and minus sigma. This is the spectrum used for the computation of responsivity and Ner. We note that the spectrum drops suddenly at noise level at 250 and at 1750  $\text{cm}^{-1}$  which are the limits of the instrument due to the characteristics of the dichroic mirror. Water lines are seen at both ends of the spectrum. Sigma has a peak at 1300  $\text{cm}^{-1}$ , which was caused, at the beginning, by the use of the wrong motor for the motion of the double pendulum. Note that from 400 to 900  $\text{cm}^{-1}$  the signal is about 10, while sigma is 0.06 : a SNR of 166. At 670  $\text{cm}^{-1}$  we have the narrow  $\text{CO}_2$  Q branch.



**Figure 3** - BBIFSI at 50 C, average over 100 measurements.  
AVERAGE, SIGMA, AVERAGE+ - SIGMA.  
NOTE 2.5 DECADES FOR THE AVERAGE SPECTRUM.

Figure 3 shows the average raw spectrum (black), the sigma value (green), and the spectrum plus and minus sigma. This is the spectrum used for the computation of responsivity and Ner. We note that the spectrum reaches noise level at 250 and at 1750  $\text{cm}^{-1}$ . Water lines are seen at both ends of the spectrum. Sigma has a peak at 1300  $\text{cm}^{-1}$ , which was caused, at the beginning, by the use of the wrong motor for the motion of the double pendulum. Note that from 400 to 900  $\text{cm}^{-1}$  the signal is about 1.5, while sigma is 0.06 : a SNR of 25. At 670  $\text{cm}^{-1}$  we have the narrow  $\text{CO}_2$  Q branch. Note the close similarity of the green curve in figures 2 and 3, demonstrating the stability of the instrument. It should be kept in mind that the instrument measures the temperature difference between the source and the detector: a source at 50 deg Celsius and the instrument at 25 celsius, make the signal relatively small.

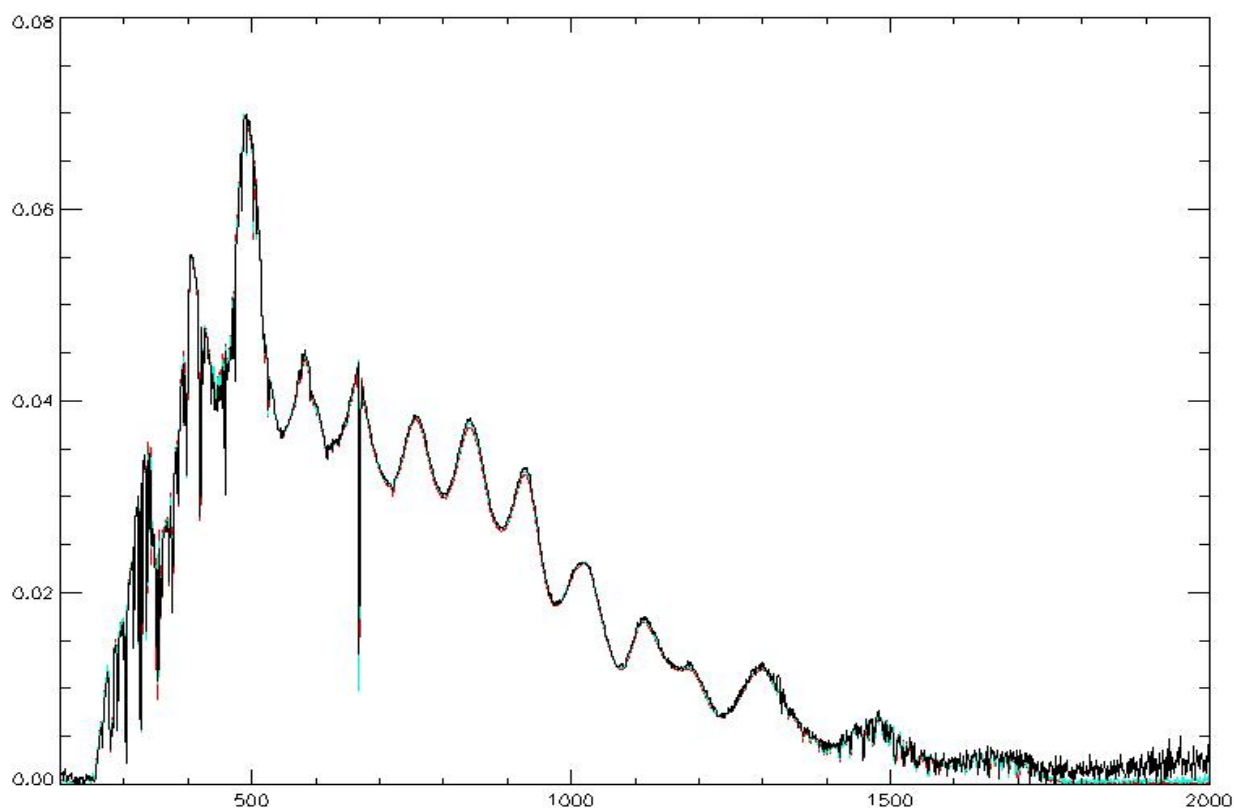
#### 4.1 – RESPONSIVITY AND NER



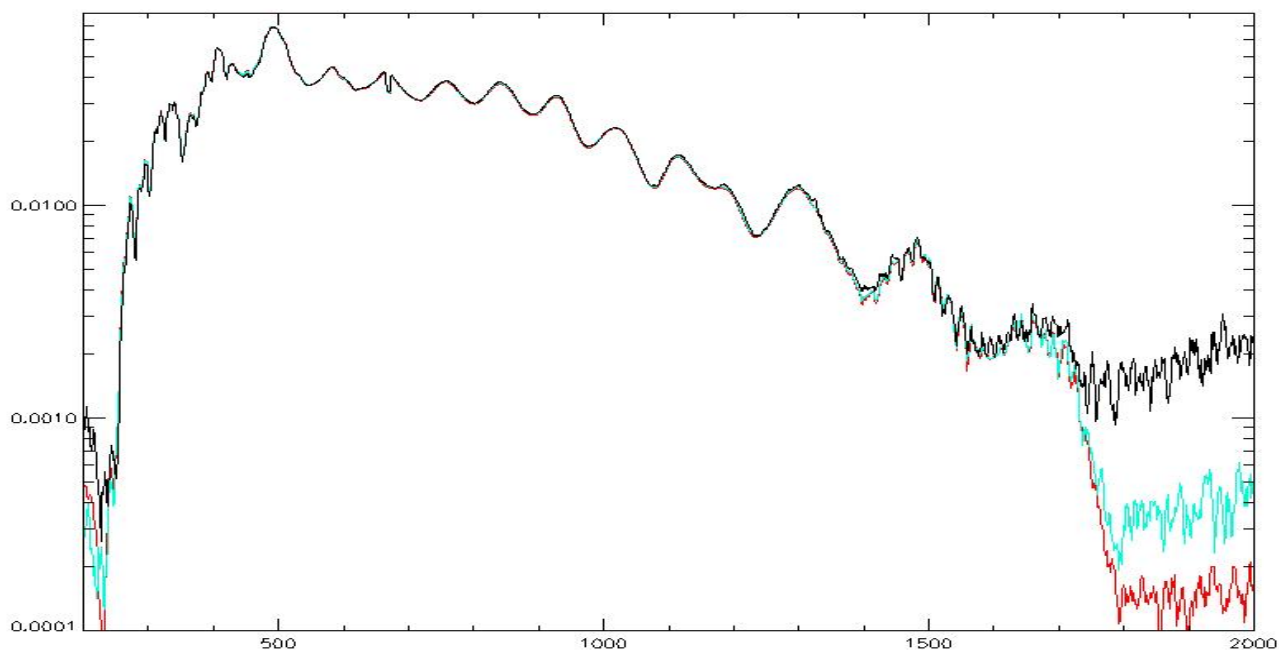
**Figure 4** - RESPONSIVITY FROM 150 – 50 C. Horizontal units are wavenumbers. Vertical units are  $\text{ergs/s cm}^{-2} \text{str cm}^{-1}$ .

Figure 4 shows the responsivity of the LW channel computed from the figures 2 and 3, and taking into account the emissivity of the detector and of the instrument. The instrument responds in the wavenumber range 250 – 1750  $\text{cm}^{-1}$ , and its responsivity spans over more than 2.5 decades. The same result is shown in figure 5, but smoothed over 7 points, in order to eliminate or decrease the atmospheric features.

This responsivity has been computed modelling the interaction between the source and the detector and the instrument. It results that the instrument counts for 97 % while the detector counts for 3 % in the interaction with the source : in other words the temperature of the detector is much less important in determining the  $T_{\text{eff}}$  of the detector in the differential measurements. The responsivity was also computed by taking the difference between 2 sources (or a BB at 2 different temperatures), but it results that the responsivity better cancel the instrumental features if computed from one BB at given temperature and using the detector-instrument interaction modelling. The 3 curves in the figure are responsivities computed as above, for BB at 50 C (black), 100 C (bleu), 150 C (red) .



**Figure 4bis** - RESPONSIVITY FROM 150 – 50 C on a linear scale. Atmospheric features are still visible .



**Figure 4 third** – Responsivity of the Lw channel smoothed on 7 points. Note the wavenumber range from 250 to 1800  $\text{cm}^{-1}$  for the red curve.

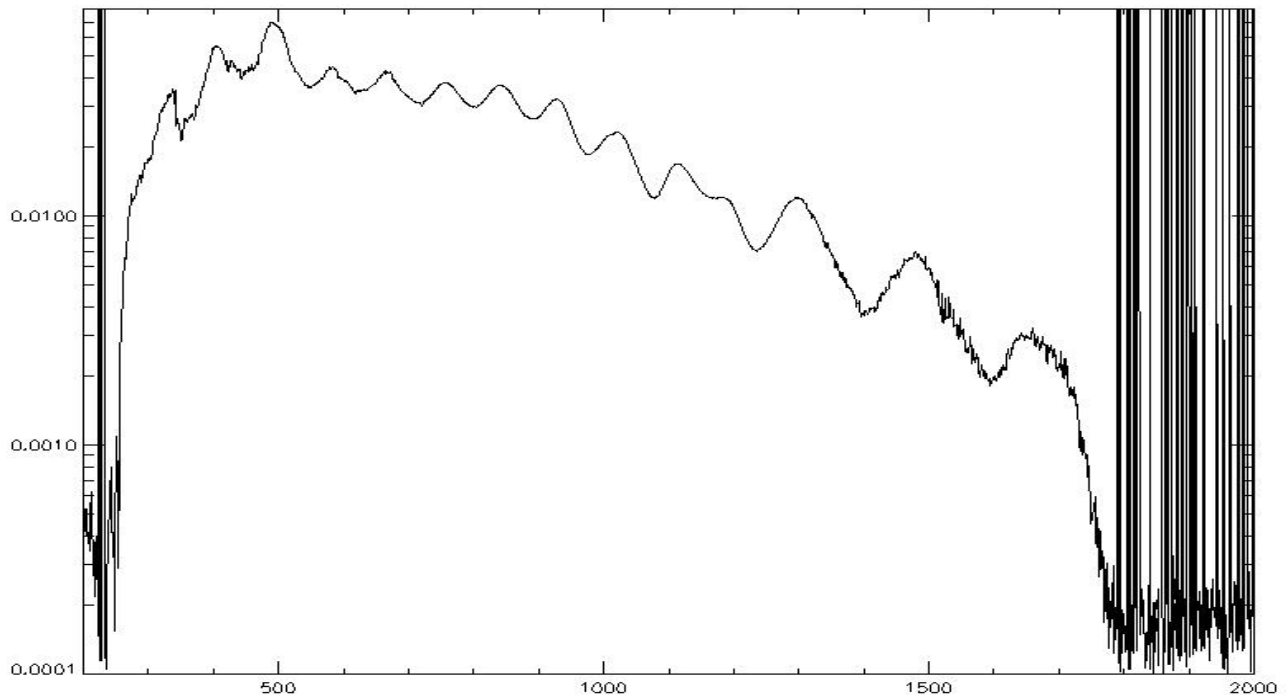


**Figure 5** – The same responsivity (150 C.) cleaned by hand of atmospheric features. The curve shown in figure 4 ter is close to the curve we expect to obtain in space, when we will calibrate using the deep space and the internal Black Body.

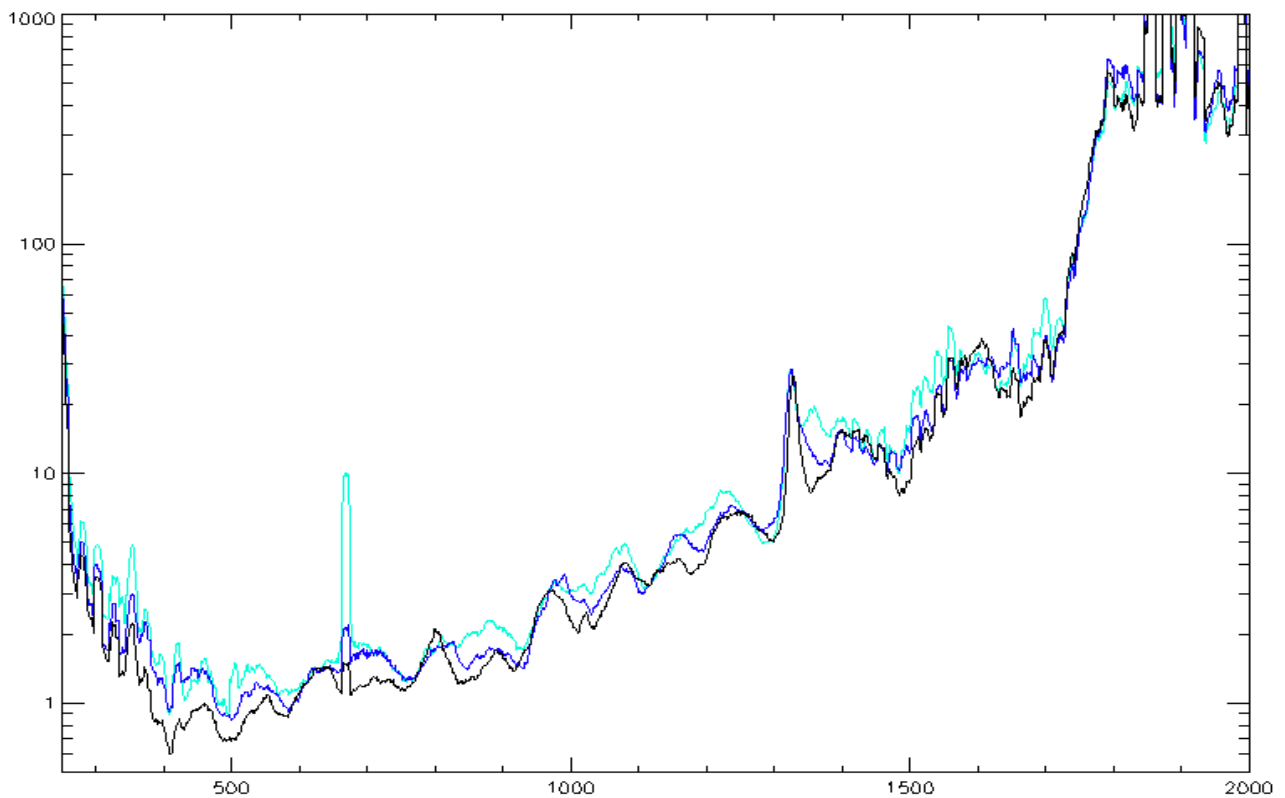
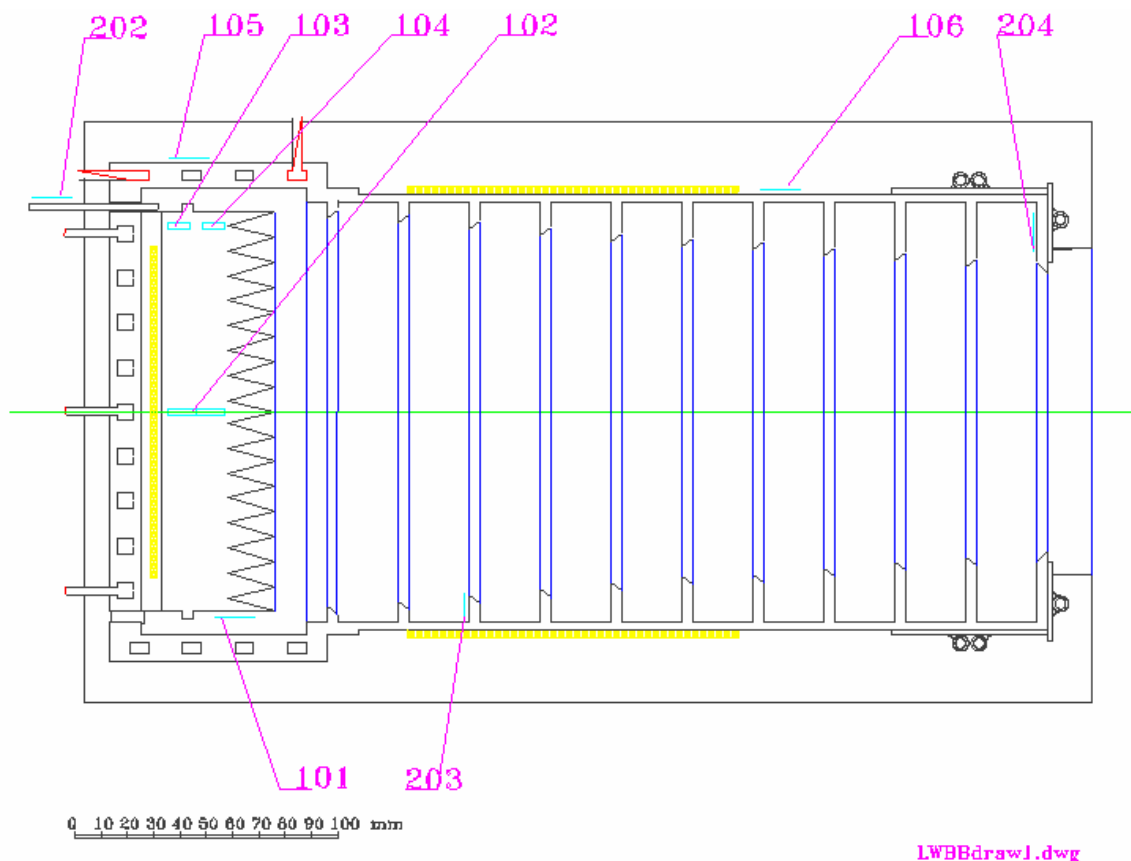


**Figure 6** - NER FROM 150, 100, 50 C .SMOOTHED OVER 11 POINTS.

Figures 4 bis and 4 ter give the responsivity again, but either on linear scale, or smoothed on 7 points in order to decrease the effects of the Earth's atmosphere. Figure 5 is again the responsivity, but now the water and CO<sub>2</sub> atmospheric lines have been eliminated interpolating the adjacent continuum. It should be noted that this does not necessarily eliminate the atmospheric contamination of the calibration because there is a continuum effect from water vapour which may still be present. Figure 6 gives the NER computed from the 3 measurements at 150, 100, 50 Celsius (100 measurements each). There are some significant differences, probably related to the different conditions in which the measurements were taken.

#### 4.2 – RESPONSIVITY AND NER FROM THE IKI BB

We have repeated the study of the responsivity and NER of the LW channel using the measurements made using the IKI BB cooled at very low temperatures. It should be noted that differently from the past, in this case also the baffle of the BB was cooled, and the temperatures were measured in several places.



LWBBdraw1.dwg

**Figure 8** - BB IKI and the location of the thermometers used for monitoring the BB temperature. Thermometer 102 was not working, so BB temperature is defined from T101, 103.

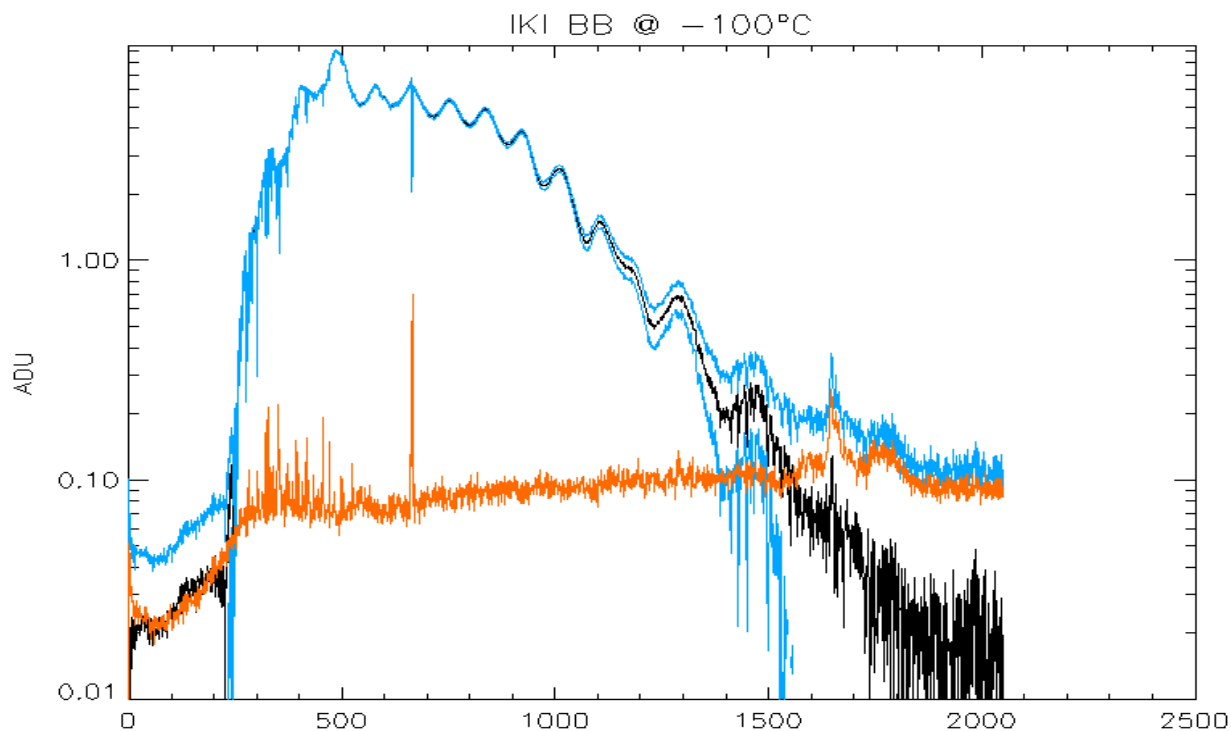


**Figure 9** - Spectrum of IKI BB at  $-100$  Celsius. The sigma computed is also shown together with the spectrum plus and minus sigma (blue curves).

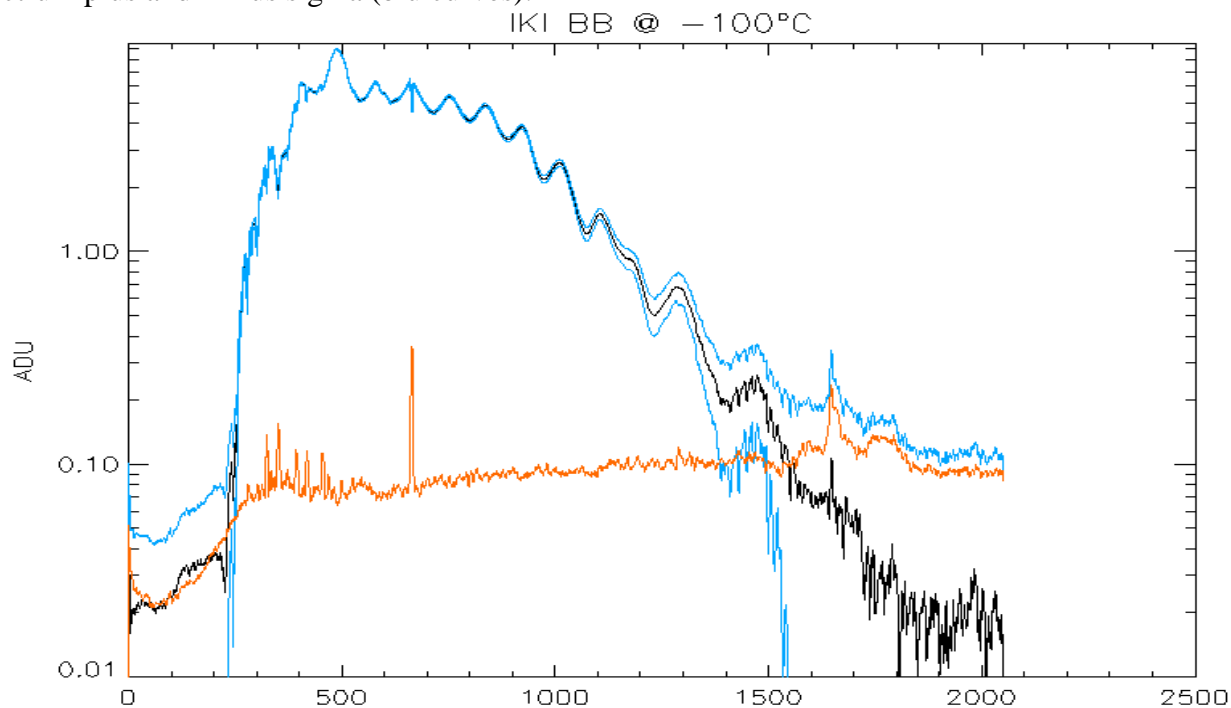


**Figure 10** - Spectrum of IKI BB at  $-100$  Celsius smoothed over 7 points. The sigma computed is also shown together with the spectrum plus and minus sigma (blue curves) also smoothed.

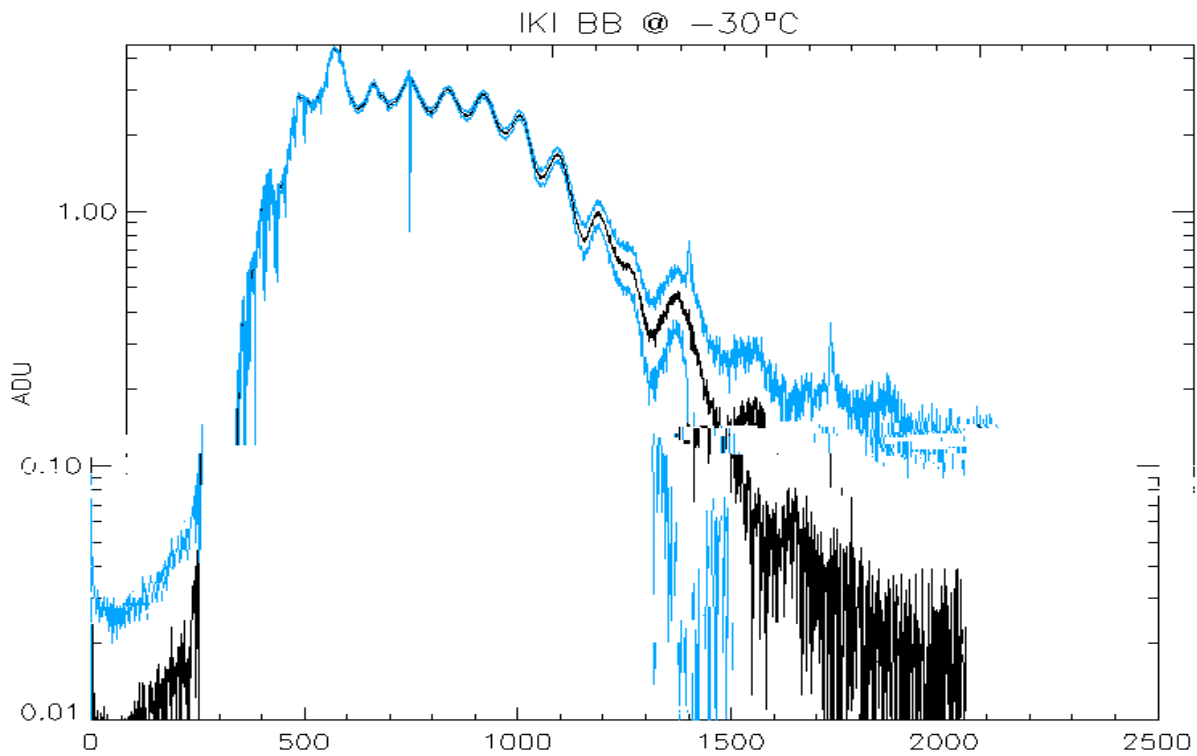


**Figure 11** - Spectrum of IKI BB at  $-30$  Celsius. It is also shown the spectrum plus and minus sigma (blue curves).

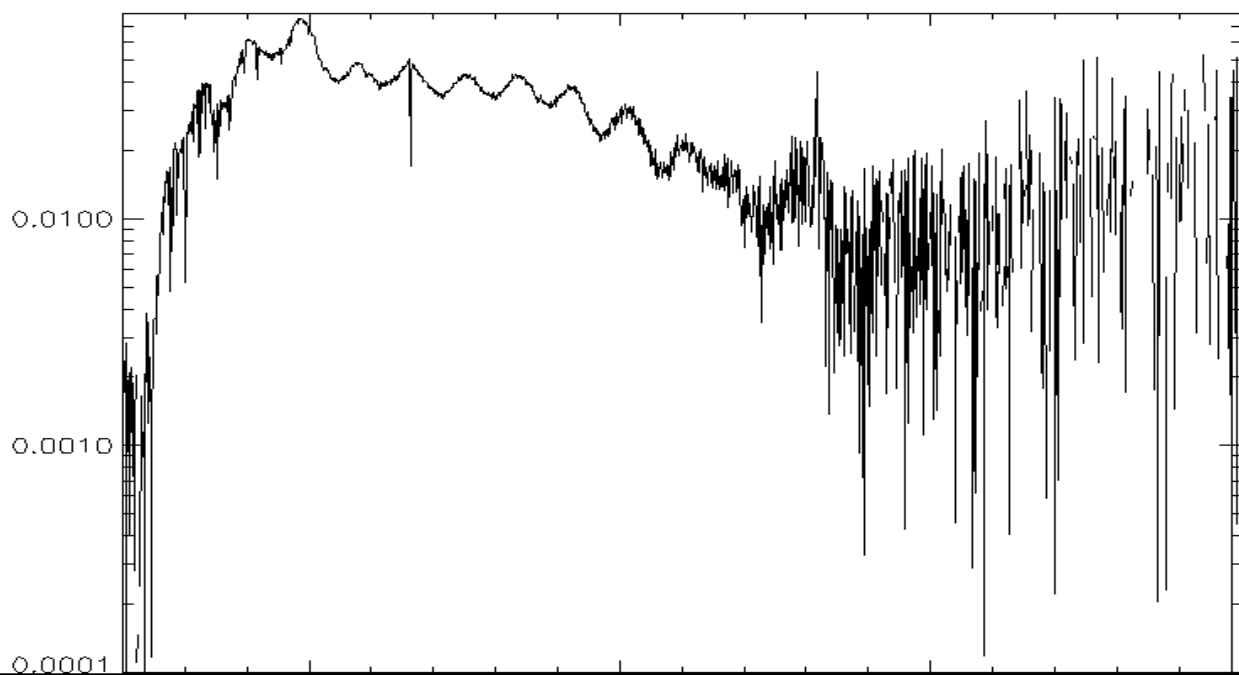


**Figure 12** - RESPONSIVITY FROM IKI BB. TEMPERATURE 0 AND  $-100$  have been used. Note the absence of information above  $1500$   $\text{cm}^{-1}$ .

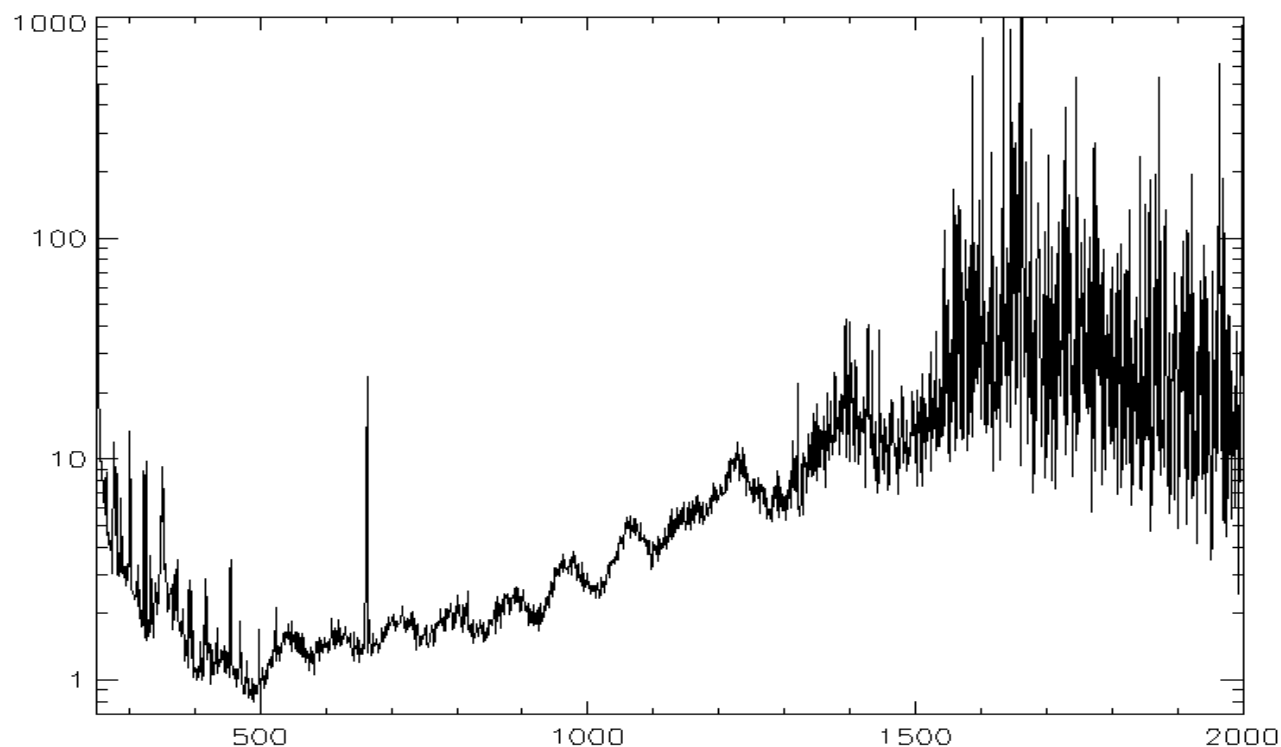


**Figure 13** - NER FROM IKI BB using the same data set as for the responsivity.

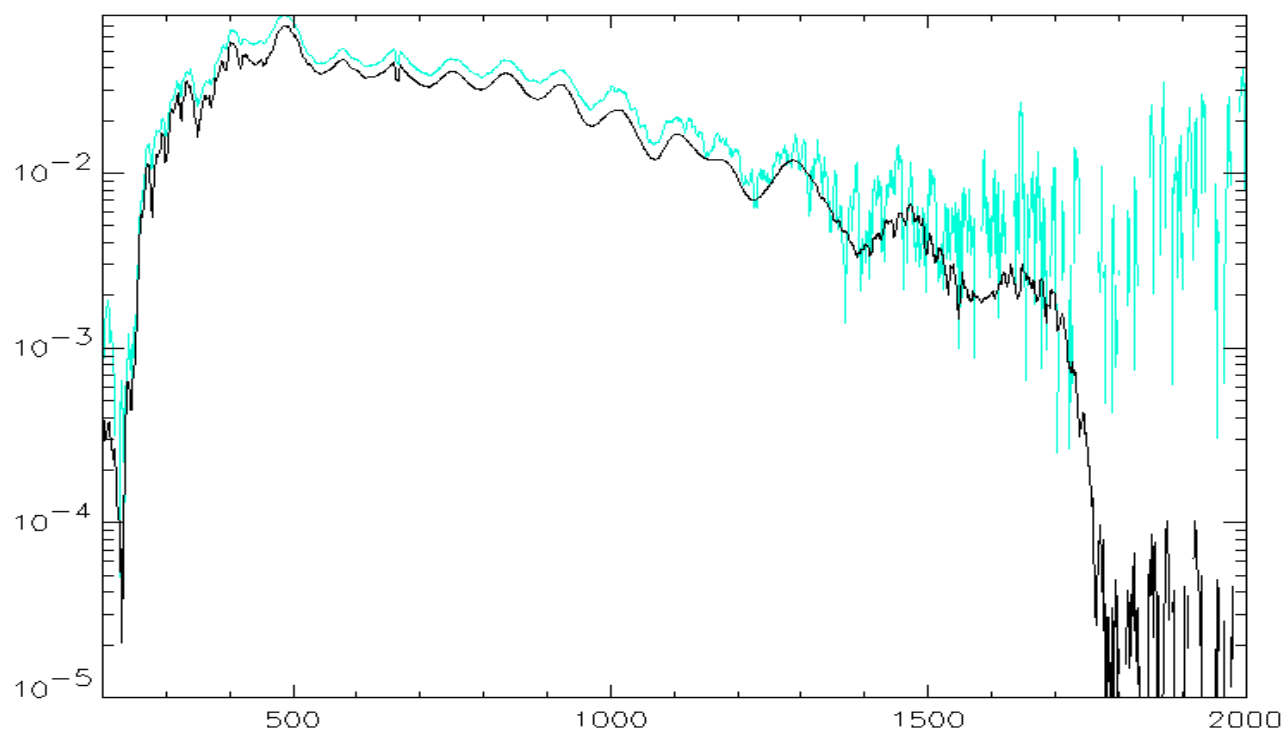


**Figure 14** - RESPONSIVITY FROM IFSI BB AND FROM IKI BB. The responsivity is better defined from IFSI BB, being the radiance larger, but for some reasons seems to be lower than with cold sources. This may be due to errors in the temperature readings.

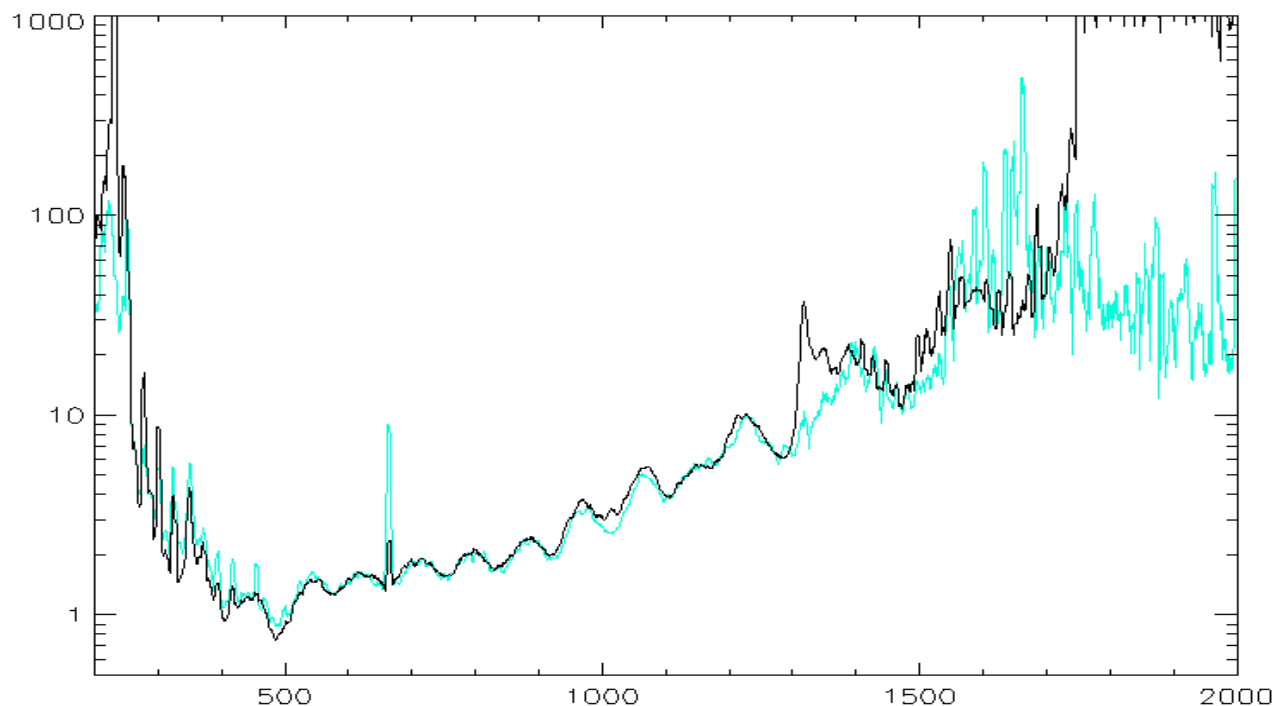
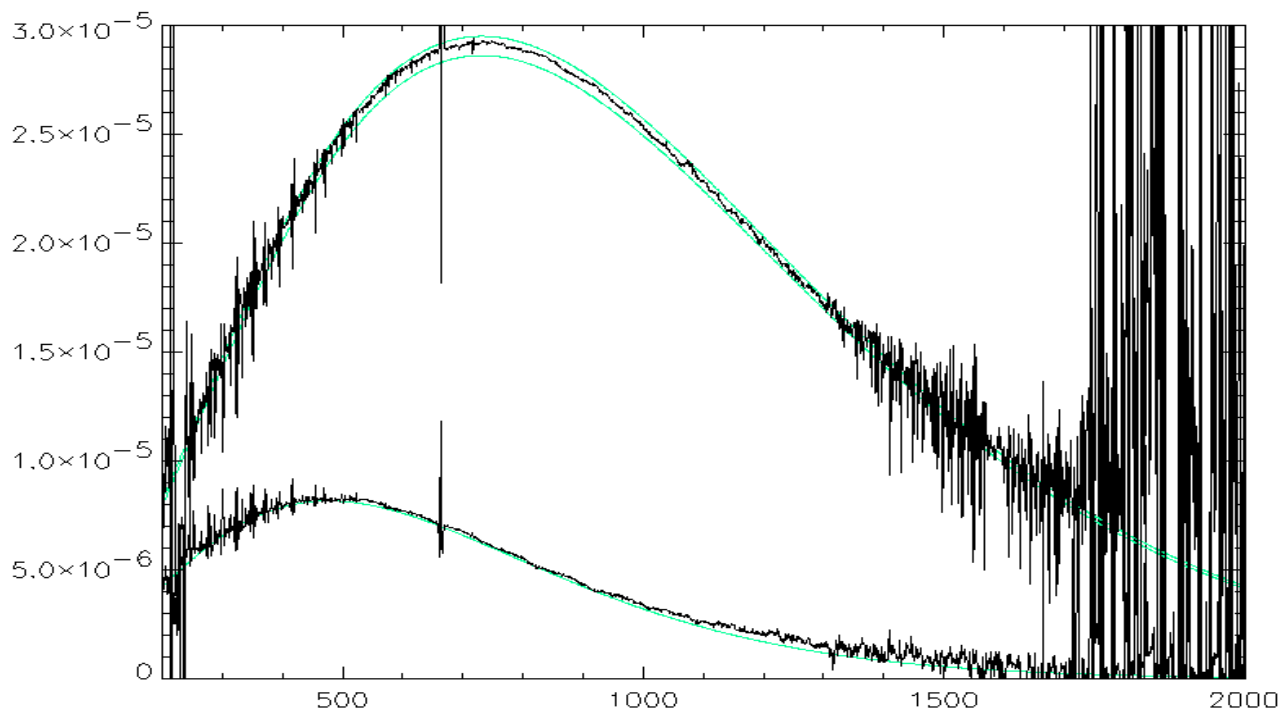


**Figure 15** – NER FROM IFSI BB AND FROM IKI BB. The NER is better defined from IFSI BB, being the radiance larger, but for some reasons seems to be occasionally higher than with cold sources.

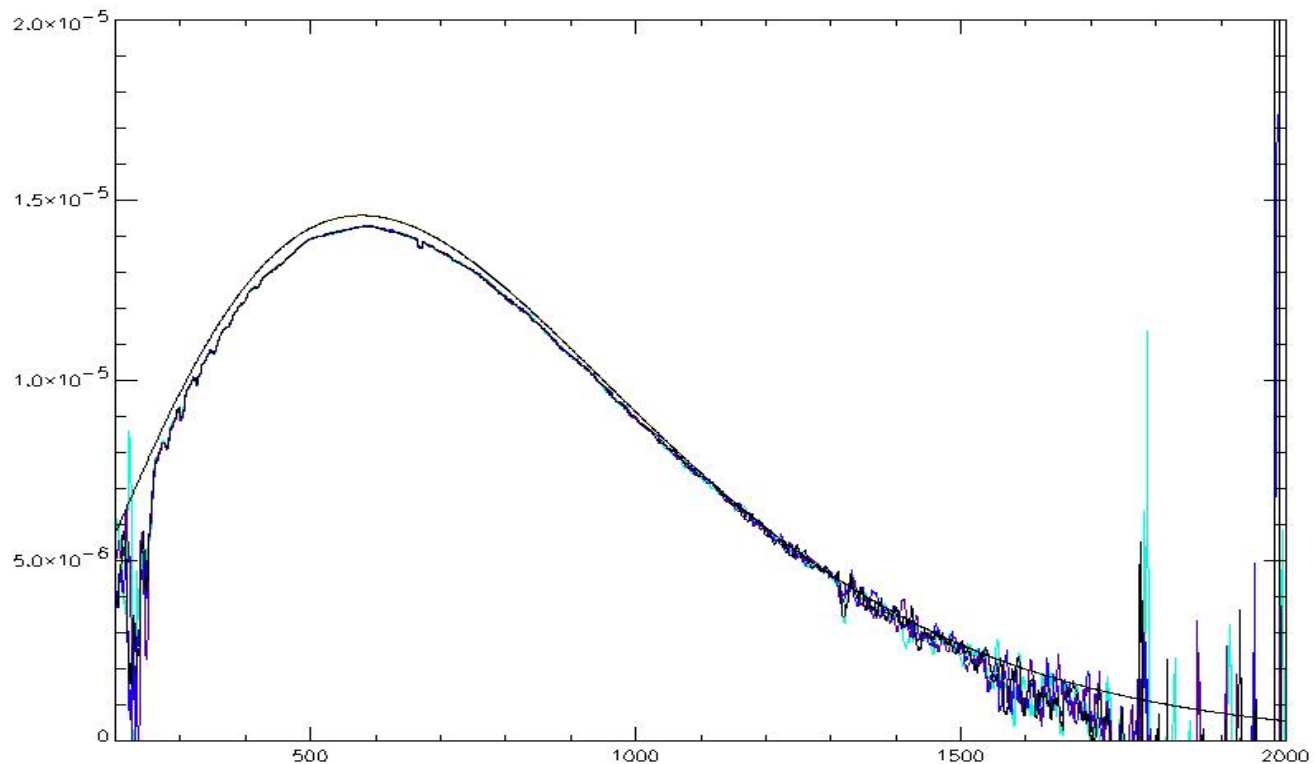
Figures 9 and 10 show the measured spectrum for an IKI BB at  $-100$  deg : raw data and smoothed over 7 points. Figure 11 shows the same kind of spectrum for the BB at  $-30$  celsius. Figure 12 is the responsivity computed from these data. Figure 13 gives the NER from these measurements. Figure 14 gives a comparison between the 2 responsivity obtained with IFSI and IKI BB. The responsivity using a cold BB seems to be a little higher. Fig 15 compares the NER obtained in the 2 ways. There are small differences but not significant.

Figure 16 shows how the use of the measured responsivity can produce calibrated data : Planckian in this case .

Figure 17, and figure18 finally provide very important results : first we have the sovrapposition of 4 spectra taken in atmosphere at different gain factors for the LW channel, and calibrated with the responsivity given above. The 4 spectra overlap completely. They give the characteristic of the internal BB for calibrations : emissivity seems to be 0.98 %.



**Figure 16** - PLANKIAN RADIANCES FOR 100 CELSIUS AND -30 CELSIUS using IFSI BB responsivity. Note the small deviation from the planckian when temperature is -30 celsius. This difference may be due to the difference already noted between IFSI BB responsivity and IKI BB responsivity.



**Figure 17** – The internal BB observed at gain 0,1,2,3. The 4 observations overlap. Gain factors were 1,2,4,8.

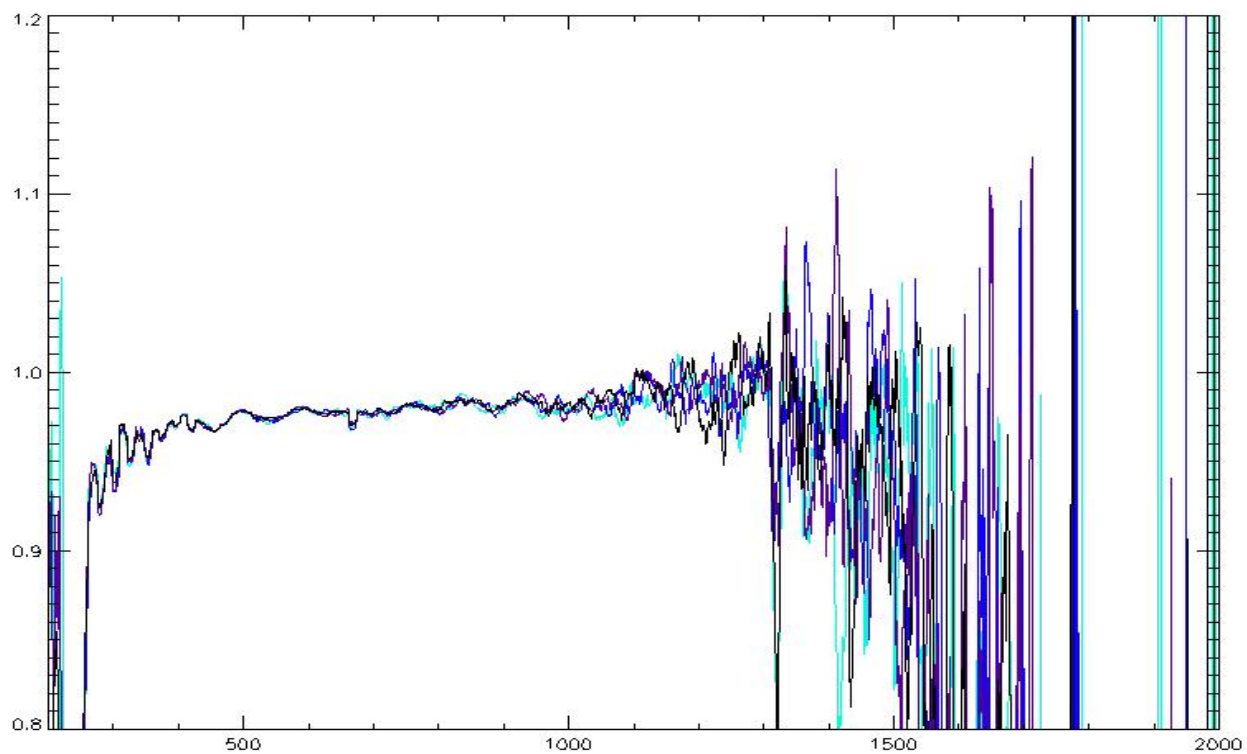


**Figure 18** - Internal black body emissivity: 0.98. measurements in air. Again 4 curves are plotted from the 4 gains.

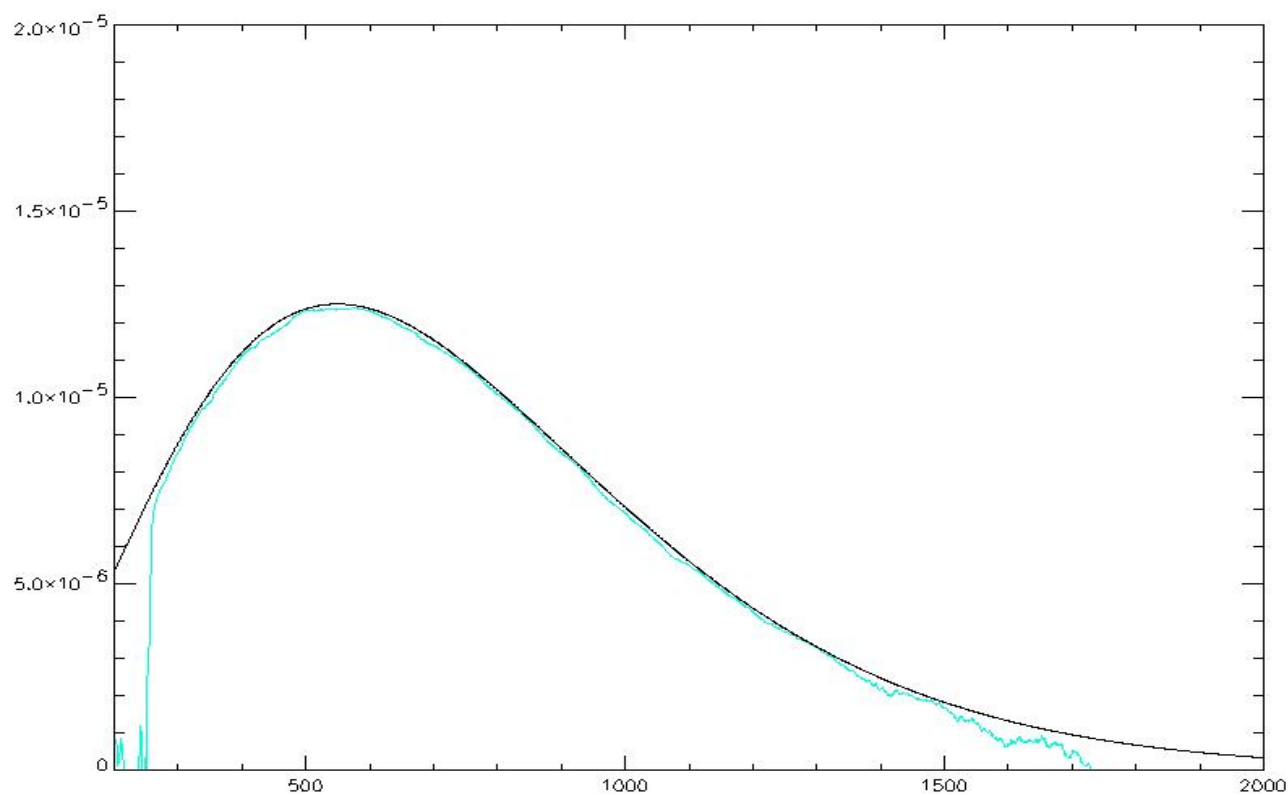


**Figure 19** – Internal BB measured in vacuum, and elaborated with a responsivity cleaned from atmospheric features. Note that the internal thermometers of the BB gave a temperature of 284.6 K, while the detector was at 296.4 K. The Planckian shown has a temperature of 4 deg lower than read by the thermometers. The emissivity of the BB is 0.99 .

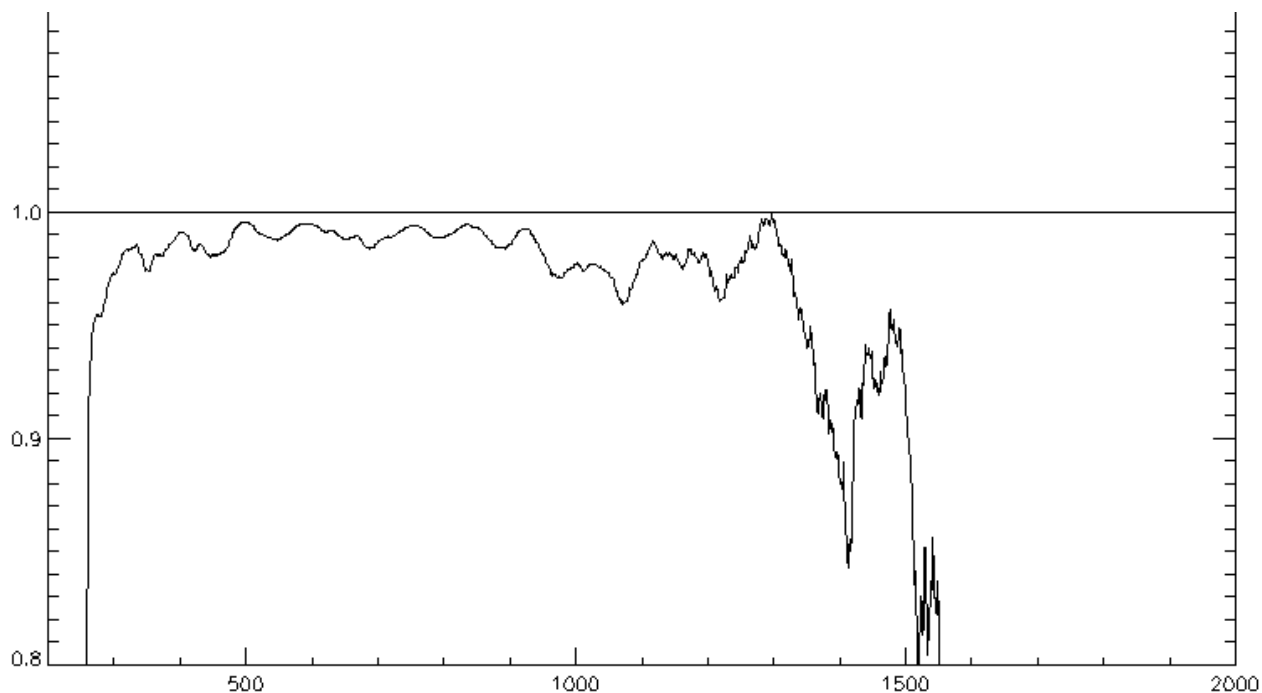


**Figure 20** - Emissivity of the internal BB from the measurement in vacuum shown in figure 17b .

The same results have been obtained from measurements taken in vacuum : figure 19 shows the planckian of the internal BB measured in vacuum and calibrated with the responsivity cleaned from atmosphere. The Planckian has been selected to be close to the measurements and “best fitting” them, in the sense that emissivity be slopeless. Figure 20 shows the emissivity to be 0.99%. This is actually the value measured in the Lab before integration in module S. It is important to note that the temperature of the planckian is 4 deg lower than the temperature we read in the housekeeping data or in the MH1 block.

The results shown in figure 17 and 18 are of crucial importance, as in space the two sources available will be deep space (at zero temperature, and zero radiance emitted) and our internal BB at measured temperature, with emissivity 0.99 and known gain factors.

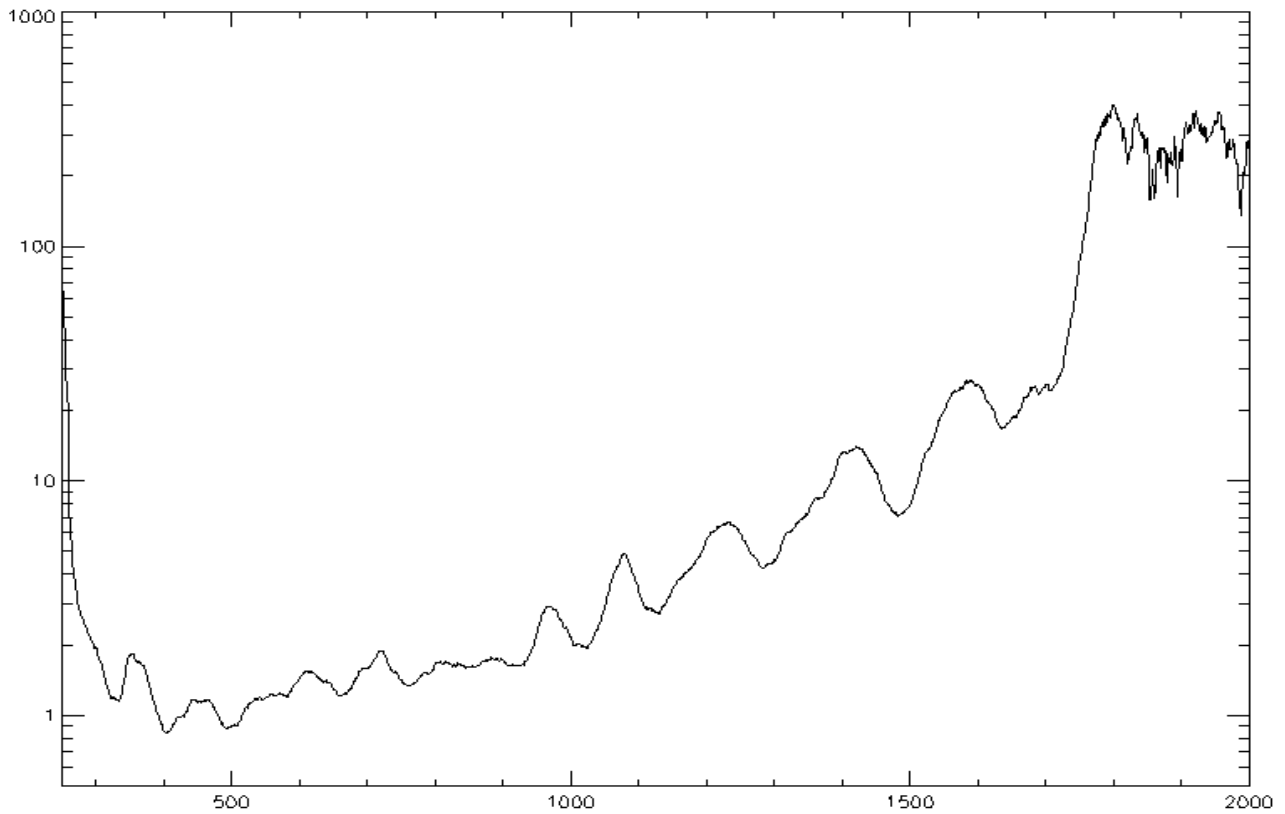


**Figure 21** - NER FROM Internal BB in vacuum measurements .

Figure 21 shows the NER computed from 150 measurements taken in the thermovacuum chamber looking at the internal BB. The figure shows that will be difficult to measure radiances lower than 1 erg, without averaging a number of spectra. Note the absence of atmospheric features ..

### 4.3 – LINEARITY

Essentially no linearity measurement has been made for the LW channel, but this fact should not be of importance as when we calibrate a BB spectrum and we obtain a reasonable Planckian curve which extends from low to high radiance intensity, we automatically perform also the linearity check.

### 4.4 – CHANGING TEMPERATURE (MEMORY EFFECT)

An essential check for the LW channel is the capability to follow the temperature of a BB which is changing. At Mars the planet surface temperature will be changing continuously along the orbit, and if a “memory effect” is present in the instrument, then many difficulties arise and becomes difficult almost any study. Figure 19 and figure 20 show that PFS is able to follow correctly a BB with changing temperature. The two figures show data from the same experiment : we have used the IKI BB in changing conditions, and we have compared the measured BB temperature with the PFS derived planckian temperature. Also the detector temperature is given. Note the detector is not cooled by the cold source. PFS follows rather well the BB temperature : there is no memory effect.

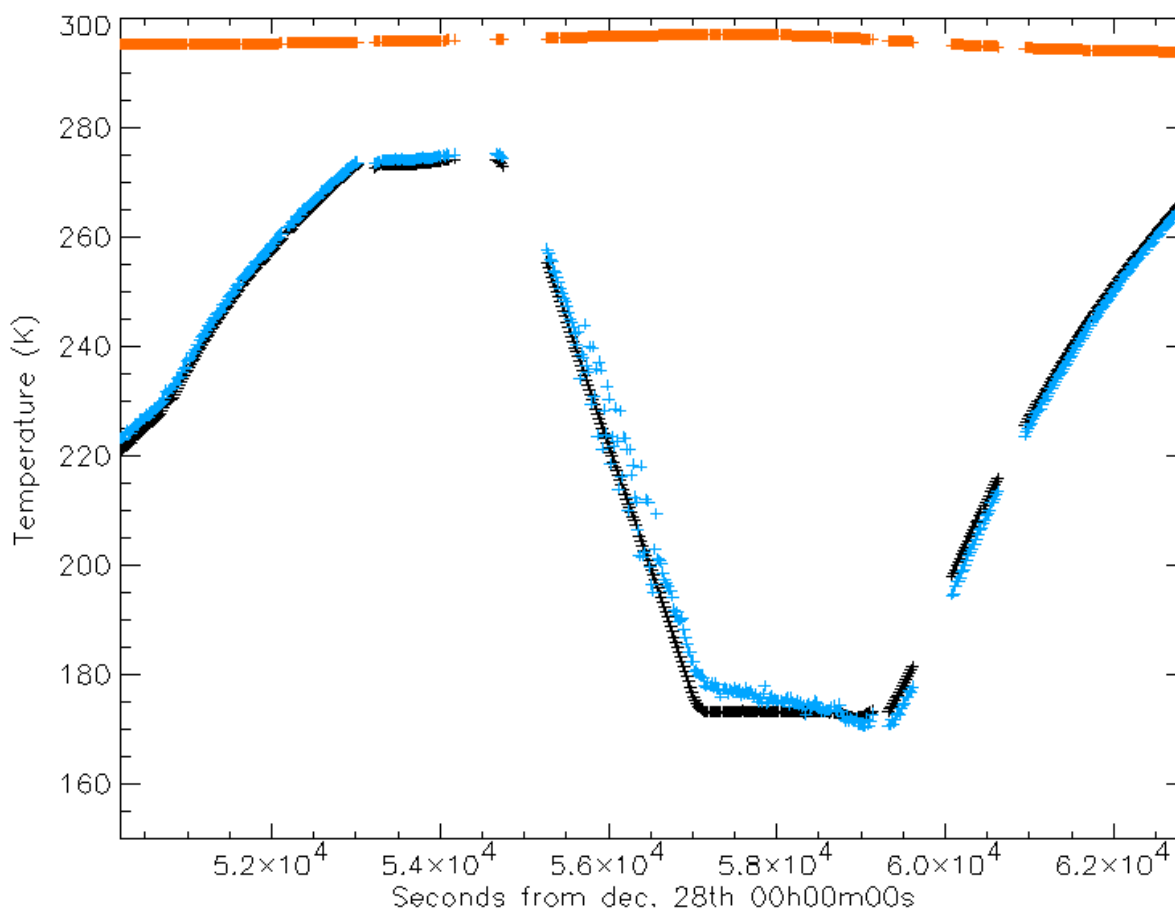


**Figure 19** - Temperature variations of IKI BB. Black measurements of thermometer 101. Bleu as measured by the PFS planckian, orange LWC detector temperature. In the descending temperature part some bad double pendulum motion occurred.

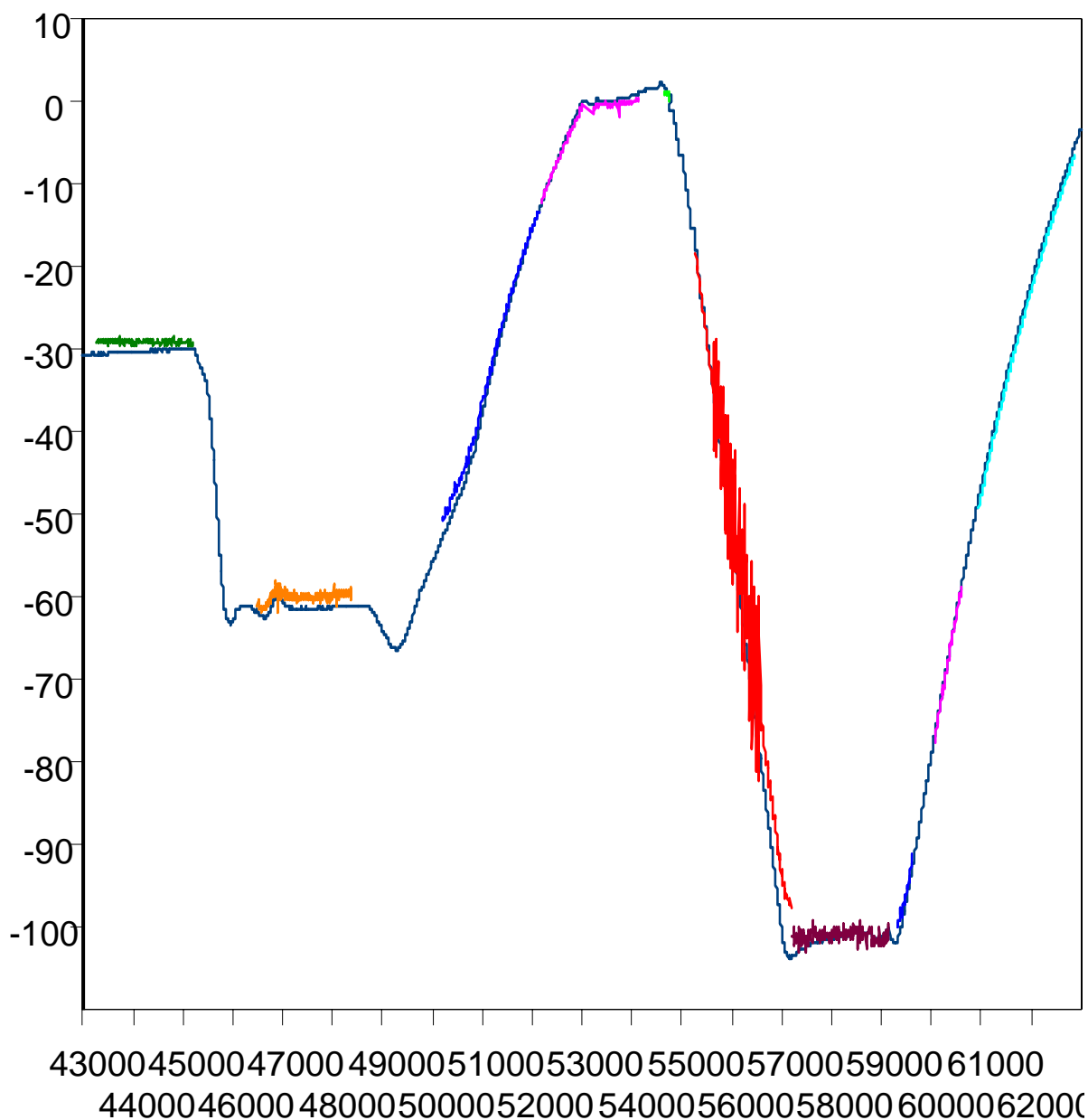


**Figure 20** - The same as for figure 19, but for a longer time period. Dark bleu is thermometer 101, colors, different periods, PFS planckian.

#### 4.5 – FORWARD VERSUS REVERSE MOTION

We have always separated forward from reverse motion measurements. Usually they are not very different, but, as it was already reported in volume 1 of calibrations, one has to be careful in keeping the two sets of data separated because the influence of motion uphill or downhill may be very strong. We shall come back on this point for the SWC, as for the LWC we have not seen a major effect.

#### 4.6 – IFSI BB- INTERNAL BB – RUSSIAN BB

Some comments here on the comparison between the 3 BB. The really important point is that we can state we know very well the internal BB and its emissivity (0.99). If the temperature difference between the BB and the detector can be of the order of 5-10 degrees also in space, as we expect, then we will be able to make good calibrations also in space.

#### 4.7– MODELLING DETECTOR-INSTRUMENT-SOURCE INTERACTION

Concluding the LWC study we would like to stress that some modelling of the source – instrument – detector interaction it is necessary in order not to have false results, namely responsivity depending on the detector temperature or similar effects. We have adopted the description given by Hanel, and it seems to work reasonably well. It is evident, however, that emissivity of the 2 BB (instrument and detector) a priori could be different from 1, in which case the approach given is not correct. We have tried a more complex description, but no reasonable results were obtained.

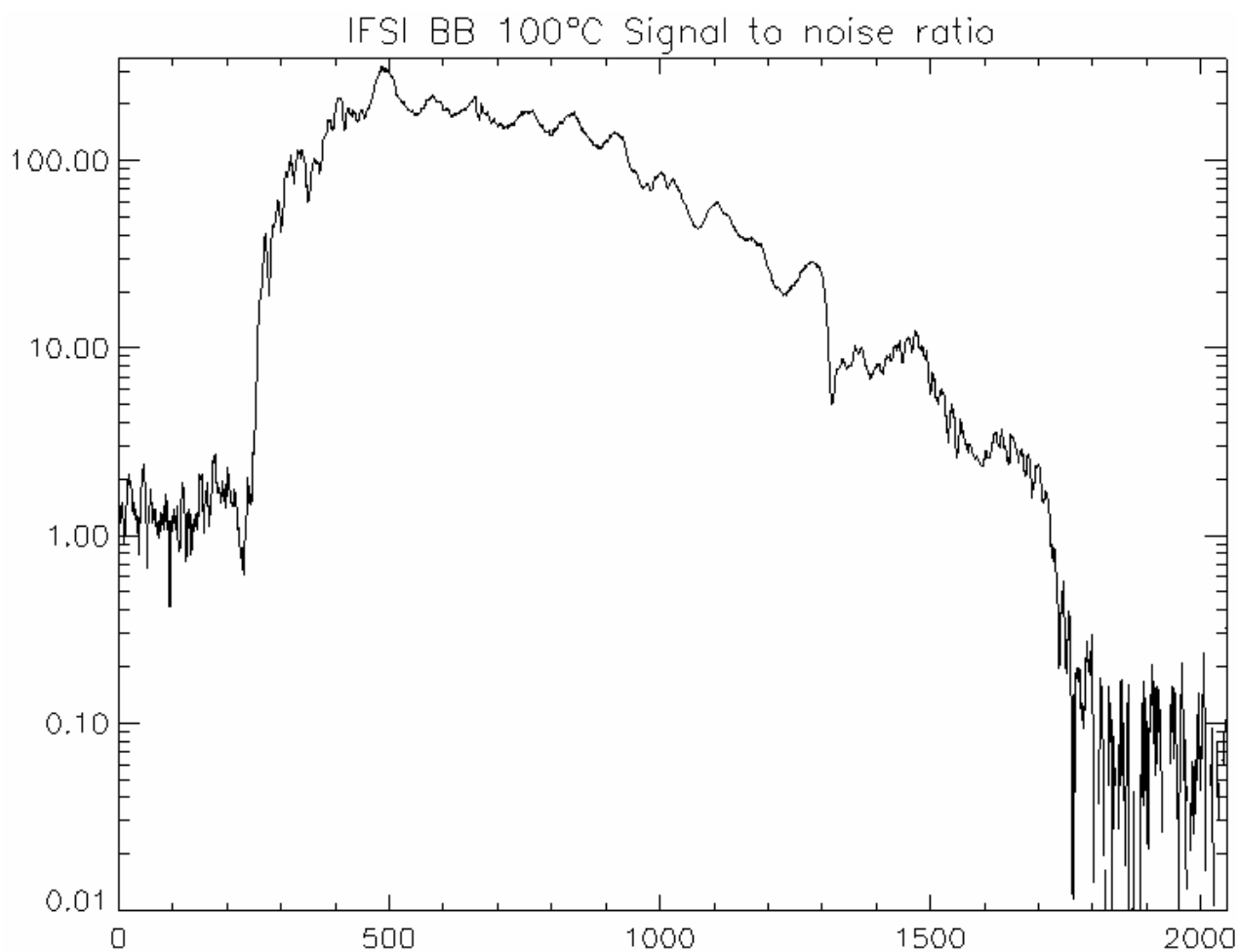


**Figure 21** – SNR for IFSI BB at 100 celsius measurements.

#### 4.8 – SIGNAL TO NOISE RATIO FOR TYPICAL CASES

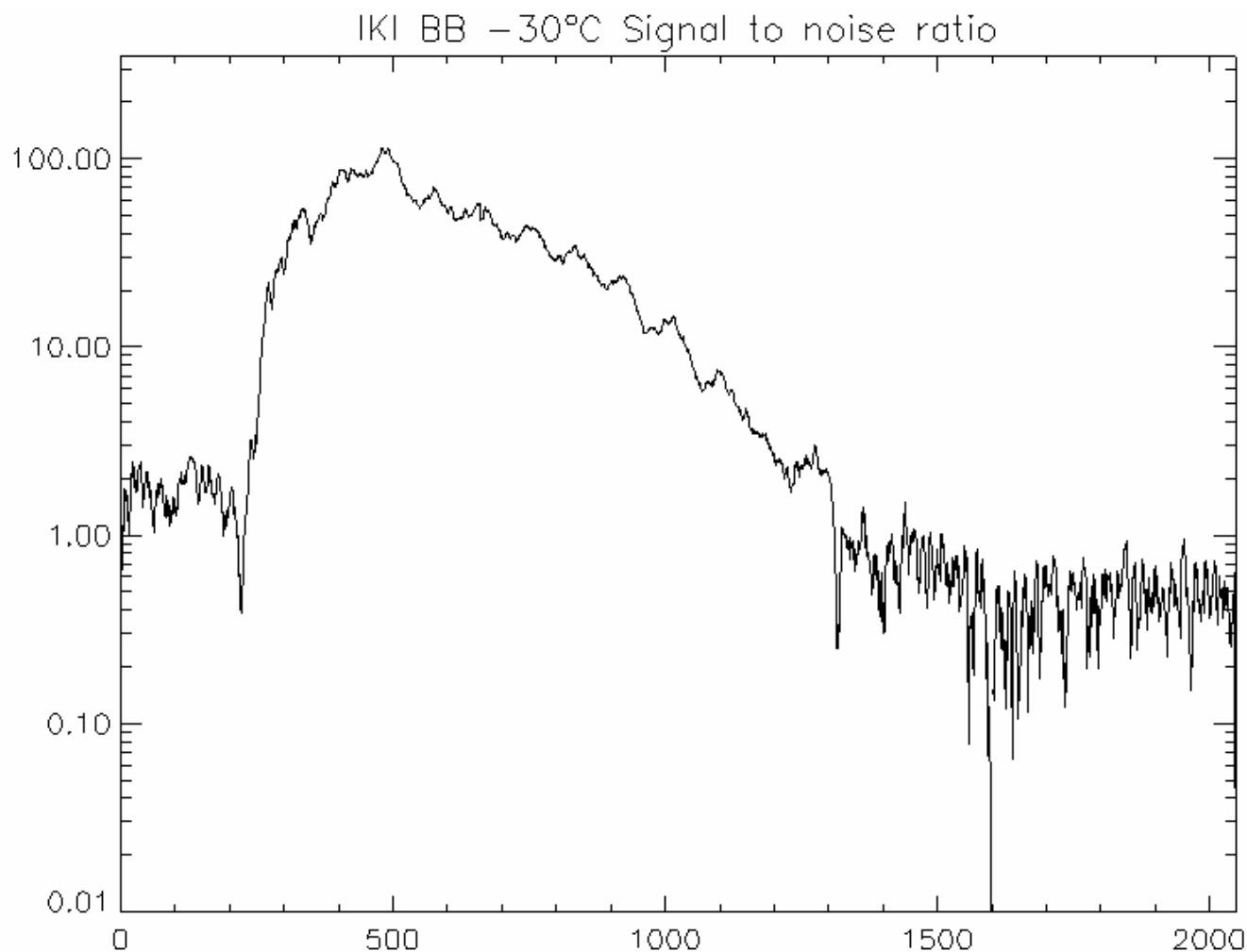


**Figure 22** – SNR for IKI BB at -30 celsius measurements.

We show here the SNR for typical cases, from real measurements. Figure 21 shows that SNR for IFSI BB at 100 celsius goes up to 300. Figure 22, shows measurements from IKI BB : this is a situation similar to Mars : the SNR goes up to 100. Figure 23 shows the SNR for the internal BB : the SNR can go up to 150 – 200.

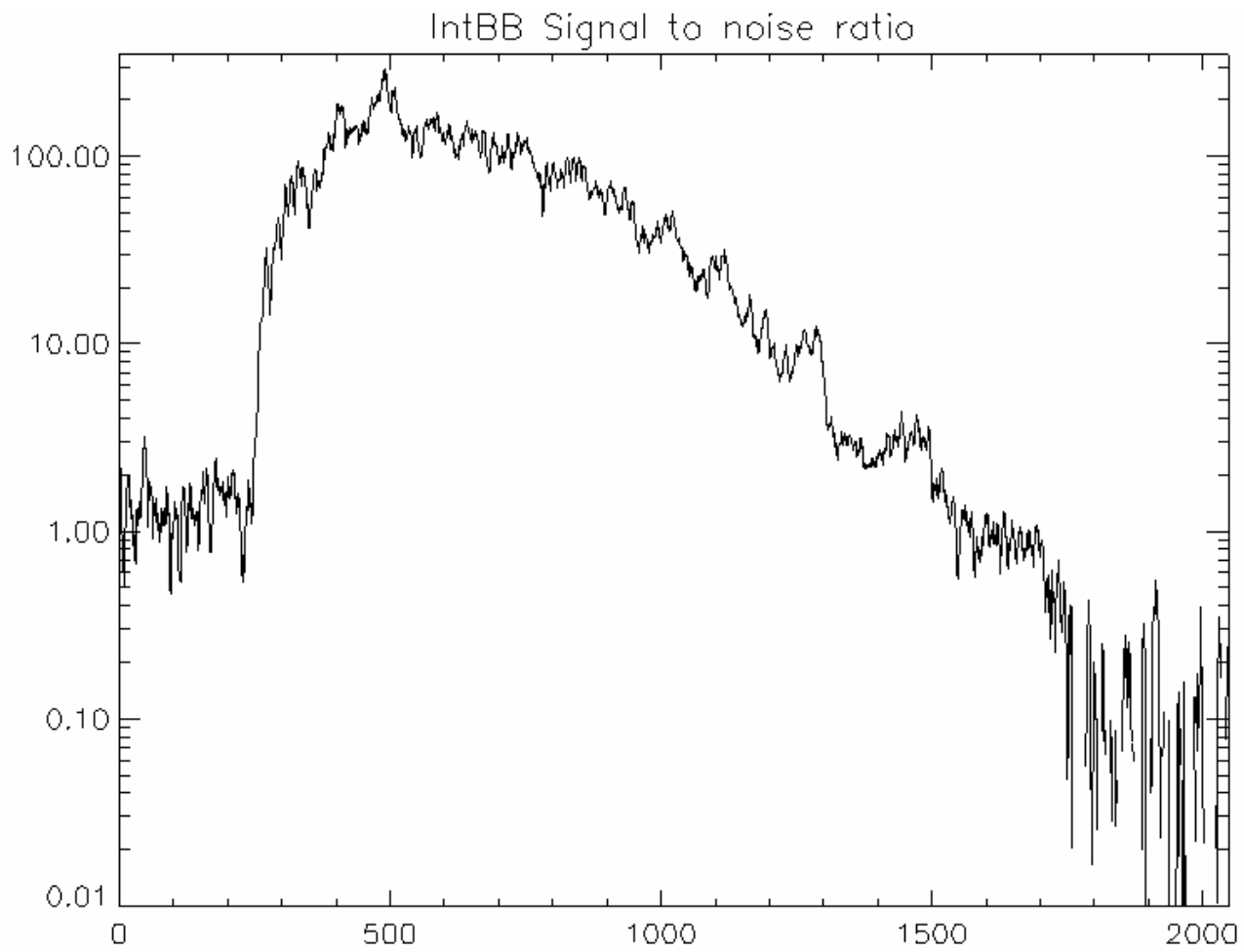


**Figure 23** – SNR for the internal BB.

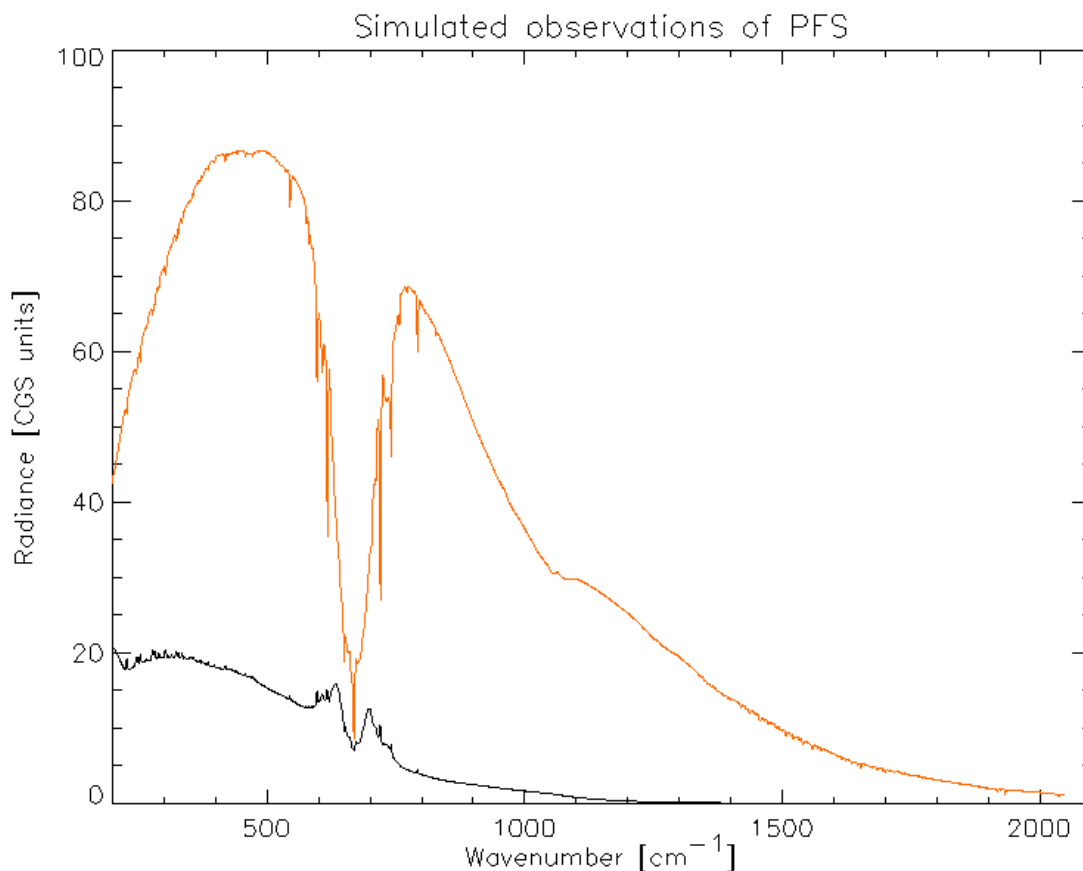


**Figure 24** – Simulated spectrum for equator and polar regions at Mars .

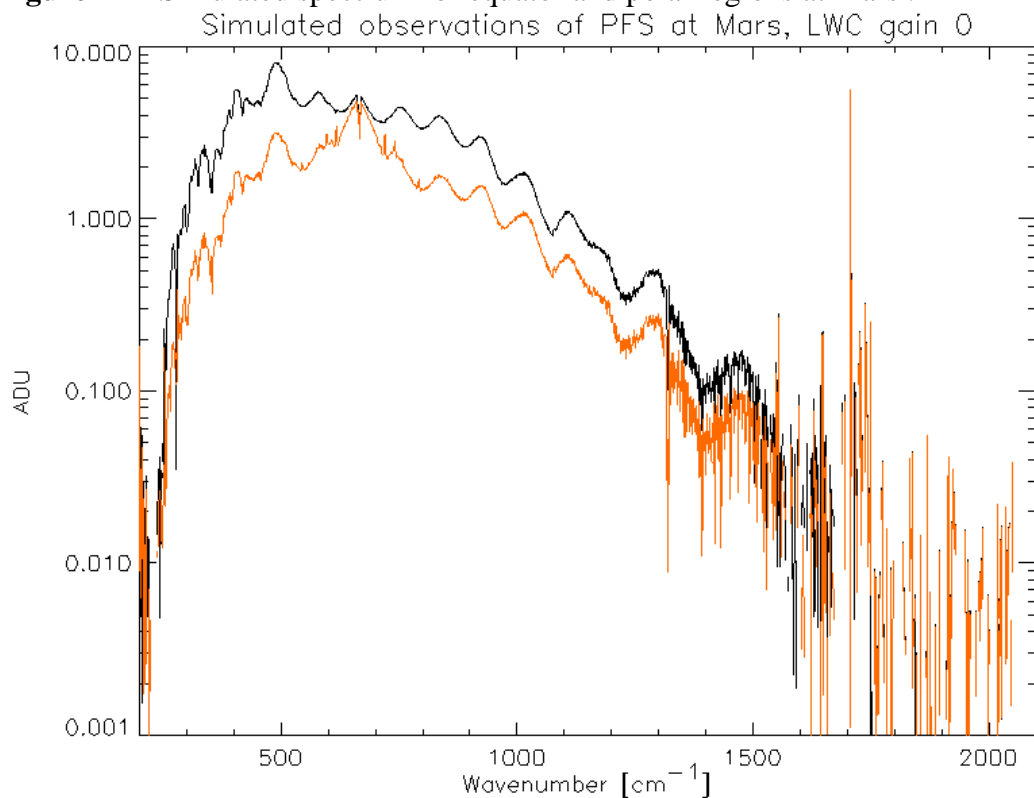


**Figure 25** - Simulated raw data of Martian spectra: responsivity has been applied to the spectra of fig.24

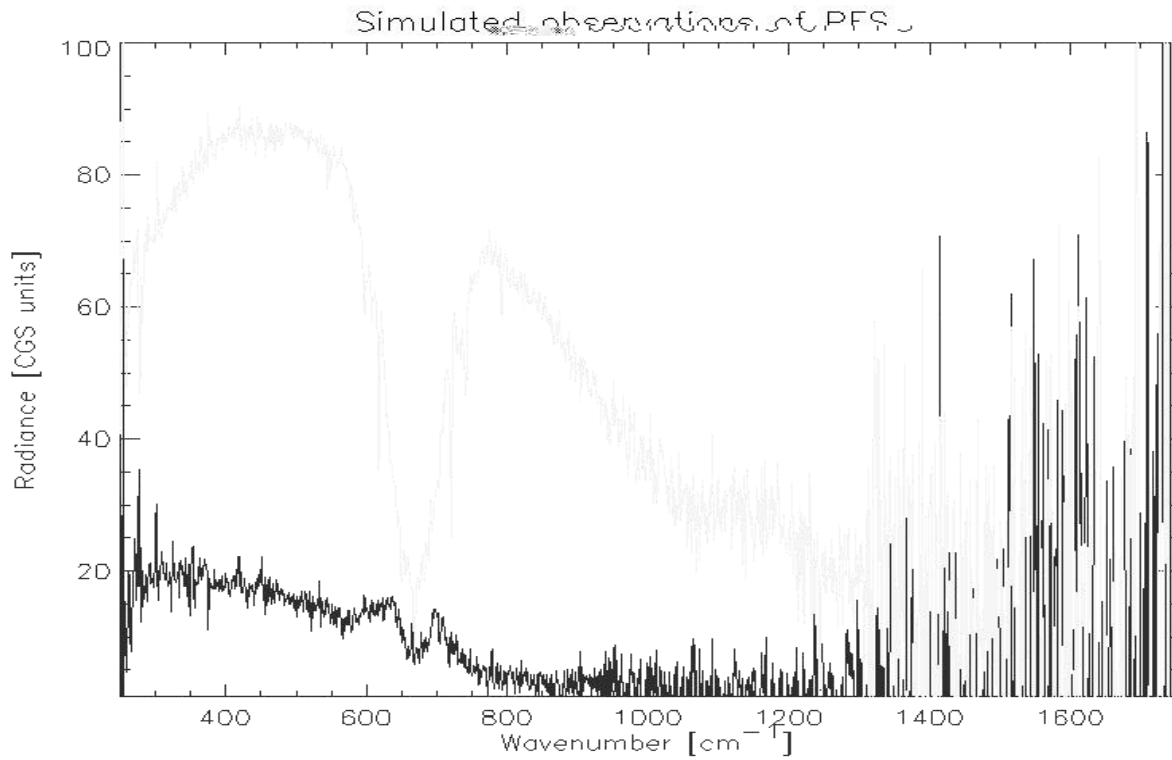
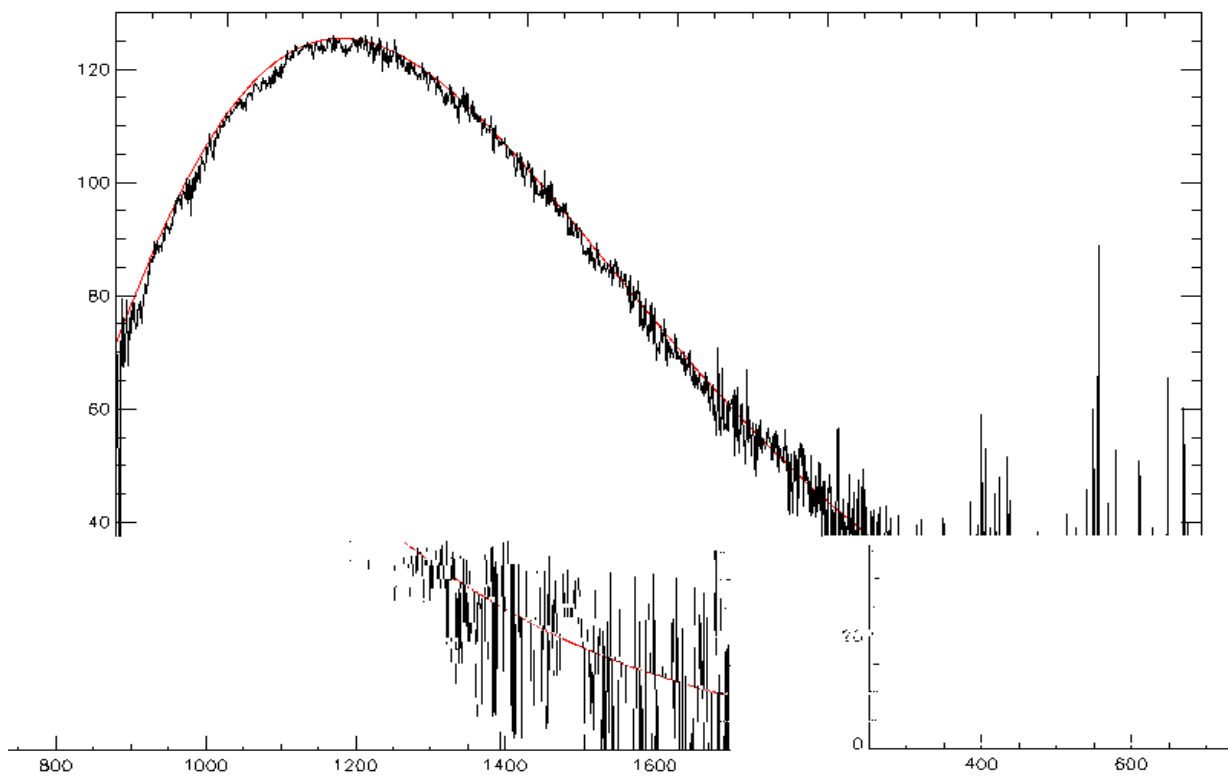


**Figure 26** - Radiance spectra as derived from the raw data: Ner is also included .



Single measurement of internal BB with a temperature difference of 10 degrees.

**PFS for Mars Express**  
December 2002

**PFS**

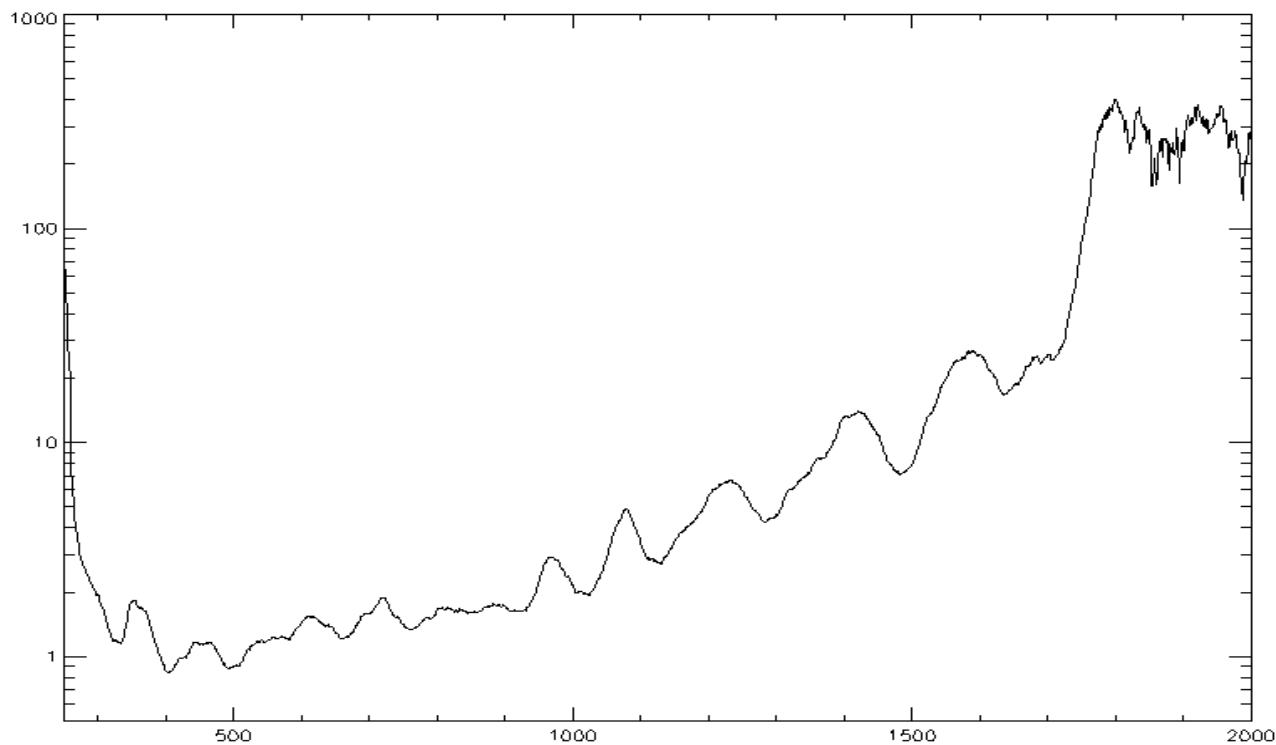


Figure 28 – LWC official NER.

#### 4.10 - THERMOMETERS INTERCALIBRATION

The first column of the following table shows the discrepancies between chamber temperature 24.5 celsius and the ones provided by probes (file Tvbalance\_011215\_165646.ifg).

Temperature point	T <sub>chamber</sub> <sup>-</sup> T <sub>measured</sub> (K)	T <sub>module</sub> T <sub>measured</sub> (K) °-
LWD	2.3	1.3
SWD	1.0	2.6
Laser LWD	4.1	-0.5
Laser SWD	3.4	0.3
T1	4.3	-0.7
T2	3.7	-0.1
T3	3.9	-0.3
T4	3.8	-0.2
T5	5.0	-1.4
T6	3.1	0.5
T7	4.0	-0.4
T8	4.7	-1.1
Internal BB 1	1.54	-
Internal BB 2	1.425	-

The diagram of calibrated temperature probes inside the chamber shows anyway temperature differences in the order of 1.-1.5 K between different probing points even in the last phases of the experience, indicating that the chamber probably had still not reached its thermal equilibrium during the measurements. This fact does not allow to rule out a real thermal gradient between the instrument and the chamber of the same order of magnitude of those reported in the table.

Assuming the module O as isothermal, the average difference between outputs of probes inside its body (first 12 points) and 24.5°C has a value of 3.6°C. It is reasonable therefore considering as the real value of temperature of module O as 28.1°C. The third column of previous table reports consequently the suggested values of temperature offset for PFS temperatures to be used during data analysis. It is important to note that the internal BB real temperature is 1.4, 1.5 degrees lower than what we read, as there is no reason to claim that the scanner temperature is different from the chamber.

#### 4.11 – THE LW CHANNEL CALIBRATION IN SPACE

In space we shall repeat many times the LW calibrations. In particular in the Near Earth Verification phase we shall take many measurements at deep space and at the internal BB. Assuming that deep space generates zero radiance, and using the measured emissivity of the internal BB of 0.99, we can measure the responsivity and NER

$$Re_s = \frac{A_2 - A_3}{\epsilon B(n, T_2)}$$

$$NER = \frac{\sigma(Re_s)}{Re_s} * B(T_{eff}) = \frac{\sigma(Re_s)}{Re_s} * (\alpha B(T_i) + (1 - \alpha)B(T_d))$$

In the NEV (Near Earth Verification) we shall have several hundreds of measurements, while in orbit around Mars we shall have only 10+10+10 \* 2 measurements. In the last case the measurements are taken as an indication of constant conditions, not really as new calibrations. Possible interpolation of internal BB temperature, and therefore of Res, may be needed if the internal BB temperature is going to change along the orbit during the data taking phase.

## 5 – THE SW CHANNEL

### 5.1 – LINEARITY

We know from the volume I of the calibration report that the SW channel is non linear. This implies that the responsivity we compute for different source intensities are not going to be identical. Furthermore, as the central part of the interferogram gives information on all the frequencies, in particular the low frequencies, the shape of the spectrum is deformed (low frequencies) by non linear effects. This means that we have to correct the non linearity effect on the interferogram before computing the spectrum. There are 3 studies on which we report here : first we study the statistical behaviour of the peak of the interferogram. Figure 29 shows the behaviour of the peak of the interferogram as function of the integrating sphere light intensity. The behaviour is linear until 500 FootLamberts. For intensity higher than that the non linearity is evident. The point is that the non linearity is different for Forward and for Reverse motion. To understand this fact, as the non linearity of the detector should be the same in the two cases, we have performed another study to understand the reason of this difference. Figure 30 shows the behaviour of the integral of the spectrum between 4000 cm-1 and 6500 cm-1 for both motions. The two non linearities are identical. This is the non linearity of the detector.

### 5.2 – FORWARD VERSUS REVERSE MOTION

Figure 31 shows the behaviour of the integral of the spectrum between 6500 and 8200 cm-1. The two non linearities are strongly different in the two motions. This is understood in terms of Bessel filters applied to the electronic signal with a strong non linear cut at the edge of the bandpass (8200 cm-1). The motion uphill or downhill changes a bit the speed of the double pendulum, therefore the frequencies of the signal with respect to the Bessel filter. The spectral shape close to the edge of the range covered is therefore changed depending if the Bessel filter acts or not on the spectrum.

It is clear that the difference Forward or reverse (better uphill or downhill) shall disappear in space, as it is due mostly to the presence of gravity in the Laboratory measurements.

The correction of the interferograms is not an easy task. After several studies and tries, we have come up with the following procedure :

- 1 - First the corrections to the central part of the interferograms should be done not according to the Figure 29, but according to the figure 32. Here we again plot the peak of the interferogram as function of the integrating sphere luminosity. However we are now considering the SIMMETRIZED INTERFEROGRAMS. The simmetrization process is changing the value of the peak of the interferogram. We are correcting the interferograms for the non linearities, after simmetrization.
- 2 – Only hinterferograms peak values above 1600 are corrected. This is the value for which the non linearity starts.
  - The non linearity data in figure 32 (33) have been fitted with a curve of second order which is :

#### **Forward**

$$Y = AX^2 + BX + C \quad A = -0.000115313, B = 1.96436, C = 706.254$$

#### **Reverse**

$$Y = AX^2 + BX + C \quad A = -0.0000833814, B = 1.86040, C = 72.069$$

		<b>PFS for Mars Express</b> December 2002	<b>PFS</b> INTERNAL NOTE CALIBRATION II Page 51	<b>P.I. Vittorio Formisano</b> <b>CNR IFSI</b>
--	---	--	--	---

- 3 to correct the data above 1600 means to replace a value which is on this curve with a value which is on the line fitting the linear part, and that is given by the equation:

$$Y = aX + b$$

**forward**

$$a=4.56359, b=0.0$$

**reverse**

$$a=4.45717, b=0.0$$

If we do not correct the interferogram before computing the spectrum, we obtain for the responsivity the values shown in figure 34 : the values for the linear part are noisy, but overlap well for different source intensity. The values for the non linear part give responsivities decreasing for increasing source intensity.

### 5.3 - THE SOLAR PART RESPONSIVITY

After the correction of the central part of the interferogram (both the peak and the 2 minima should be corrected) the computed responsivity for the many different source intensities, are reasonably close that an average can be computed and used. Figure 35 shows the responsivities obtained for the forward motion after correction of the interferograms.

The responsivity average for the linear behaviour part of the detector is given in figure 36 : clearly there are many atmospheric features (water lines) disturbing. Smoothing over 11 points produces a more clean responsivity, although water features are still present (see figure 37).

The responsivity forward and reverse, smoothed on 7 points are shown in figure 38 for the part solar (integrating sphere). Note that the two curves coincide everywhere except at wavenumber higher than 7500, where the effect of the Bessel filter may become important.

The responsivity has been used to generate calibrated spectra of the integrated sphere spectra at different intensities. Figure 39 shows the 400 footlamberts spectrum (the red curve is the integrating sphere spectrum), while the figure 40 shows the 2000 footlamberts. The agreement is not perfect, but is the best we have been able to achieve.

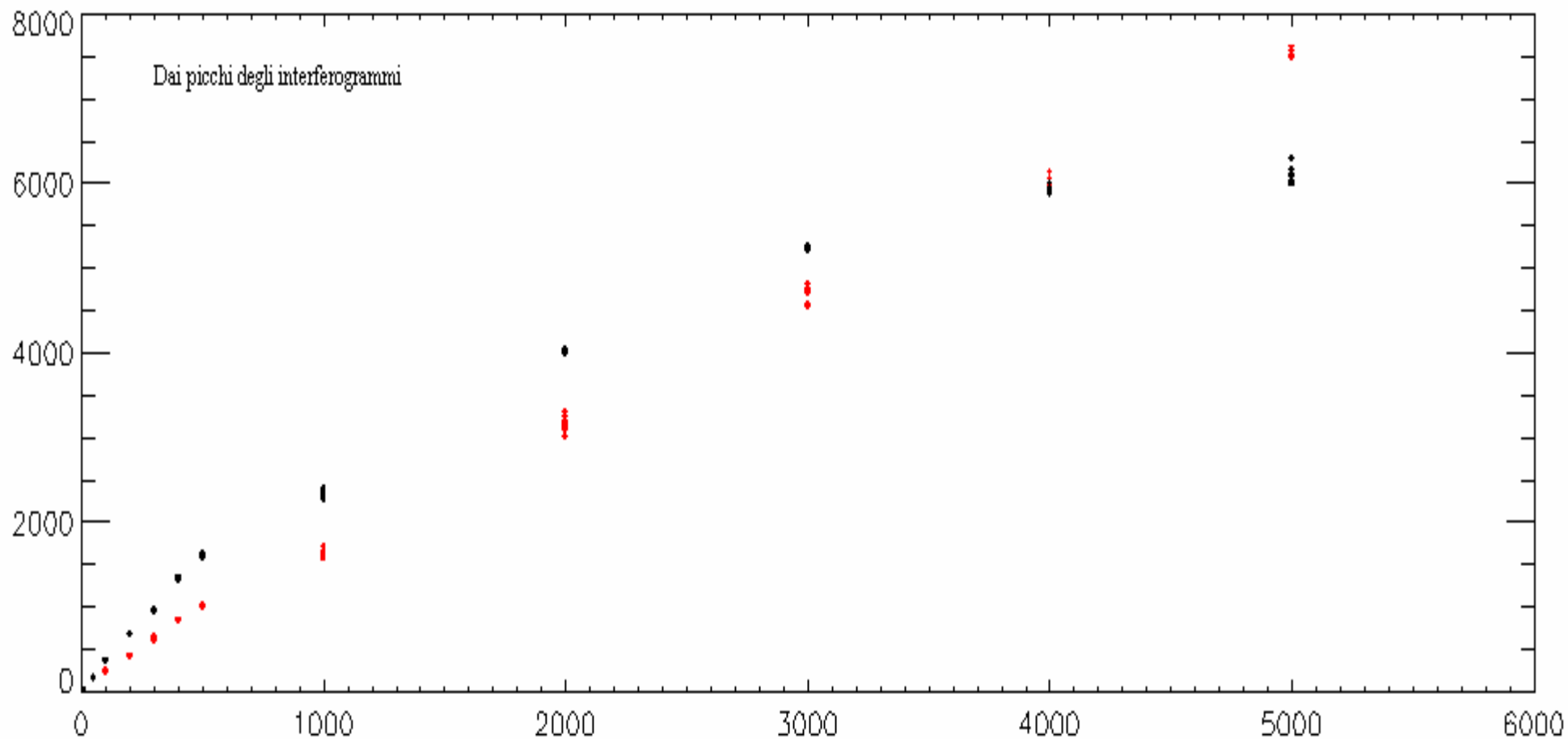


**Figure 29** - Horizontal scale: footlamberts in the integrating sphere used as source. Vertical scale: peak of the interferograms. Note the linear behaviour until 500 feetlamberts and then the non linear increase of the signal. Forward and reverse motion are considered separately.

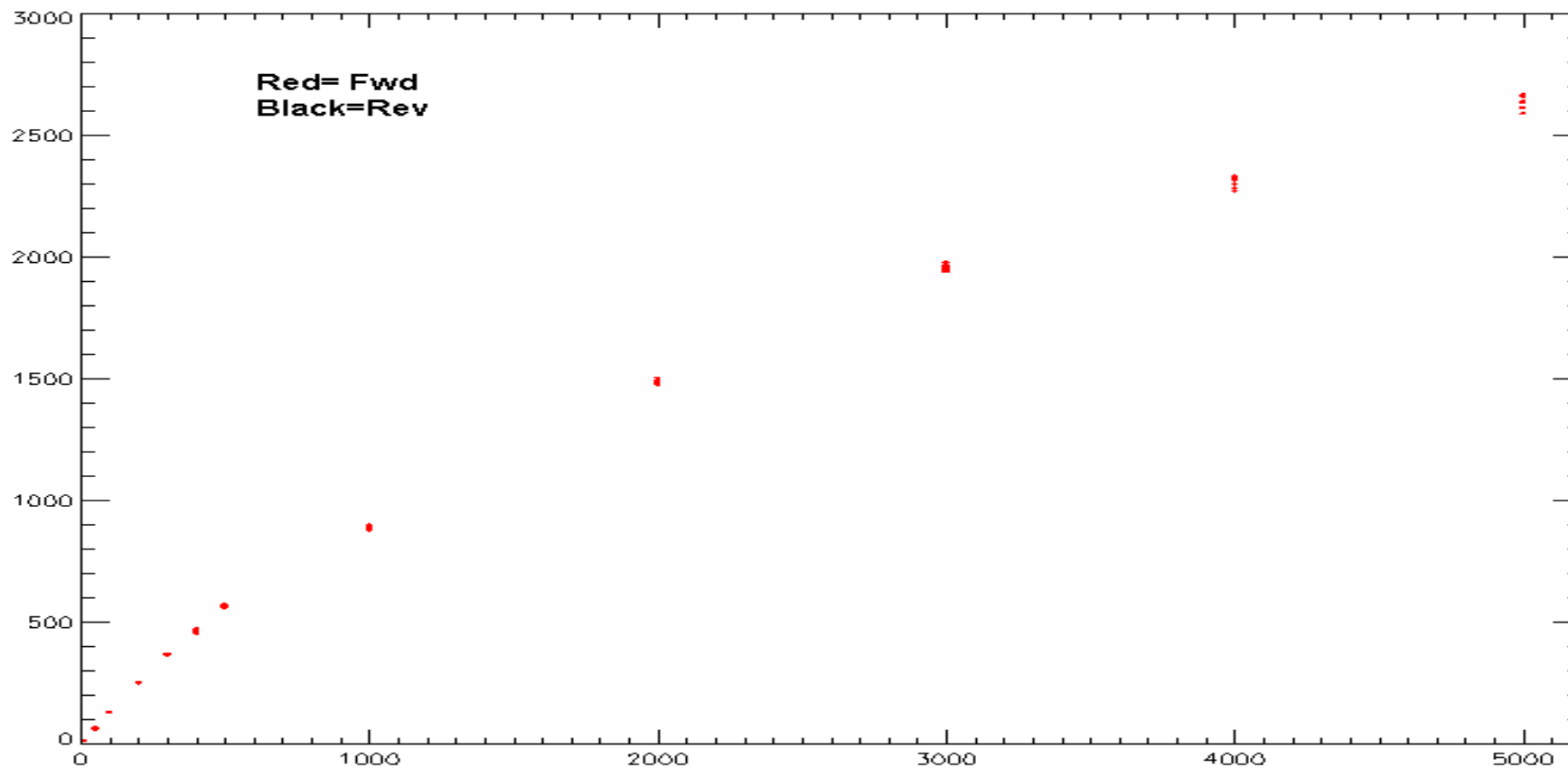


**Figure 30** - Horizontal scale : footlamberts in the integrating sphere used as source. Vertical scale: integral of the spectrum in the 4000 to 6500  $\text{cm}^{-1}$  wavenumber range. Note the linear behaviour until 500 feetlamberts and then the non linear increase of the signal. The important point is that forward or reverse motion give exactly the same non linear behaviour (black is not visible).

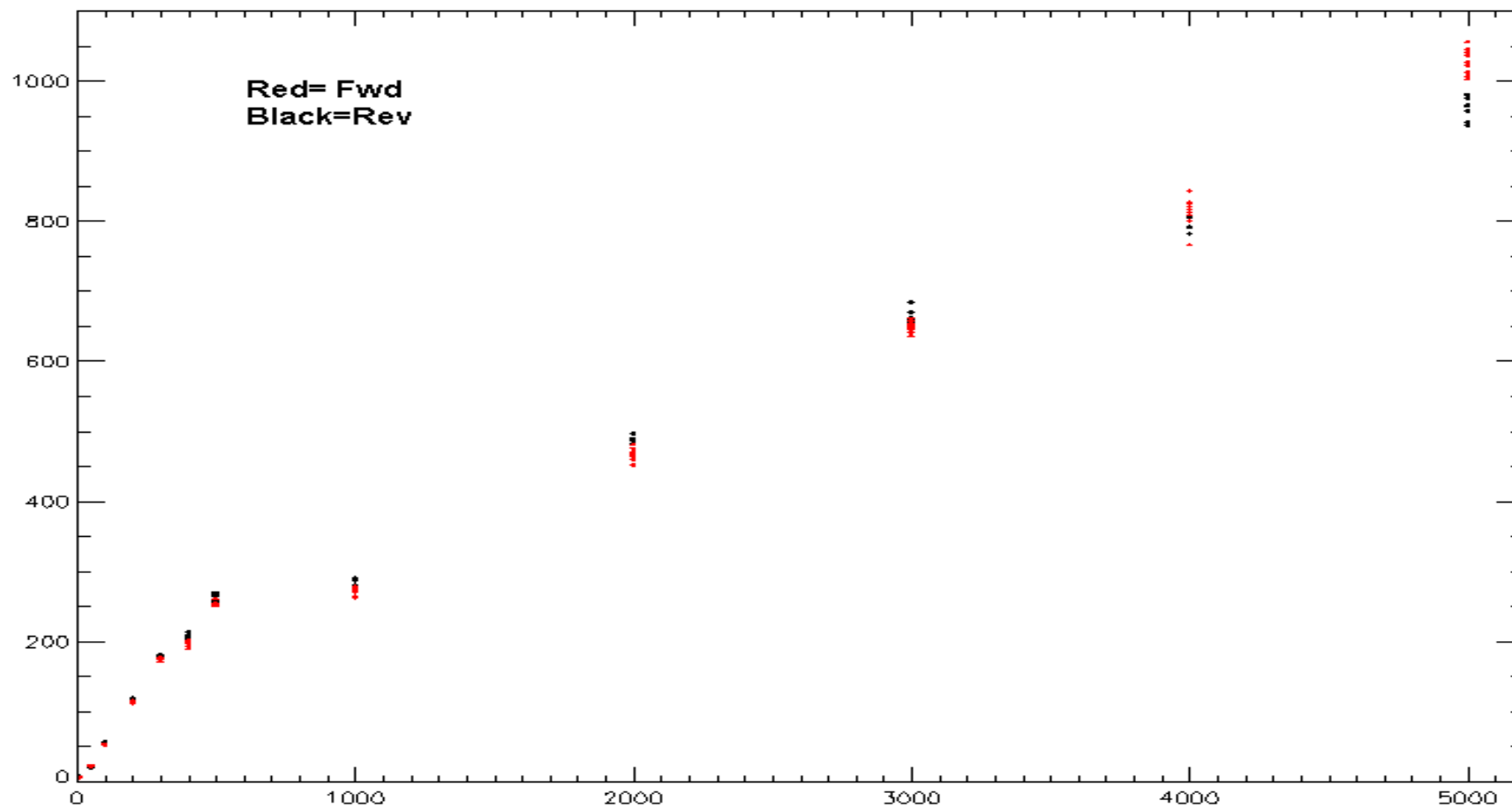


**Figure 31** - Horizontal scale : footlamberts in the integrating sphere used as source. Vertical scale: integral of the spectrum in the 6500 to 8200  $\text{cm}^{-1}$  wavenumber range. Note the linear behaviour until 500 feetlamberts and then the non linear increase of the signal. The important point is that forward or reverse motion do not give the same non linear behaviour, but somehow they are opposite.

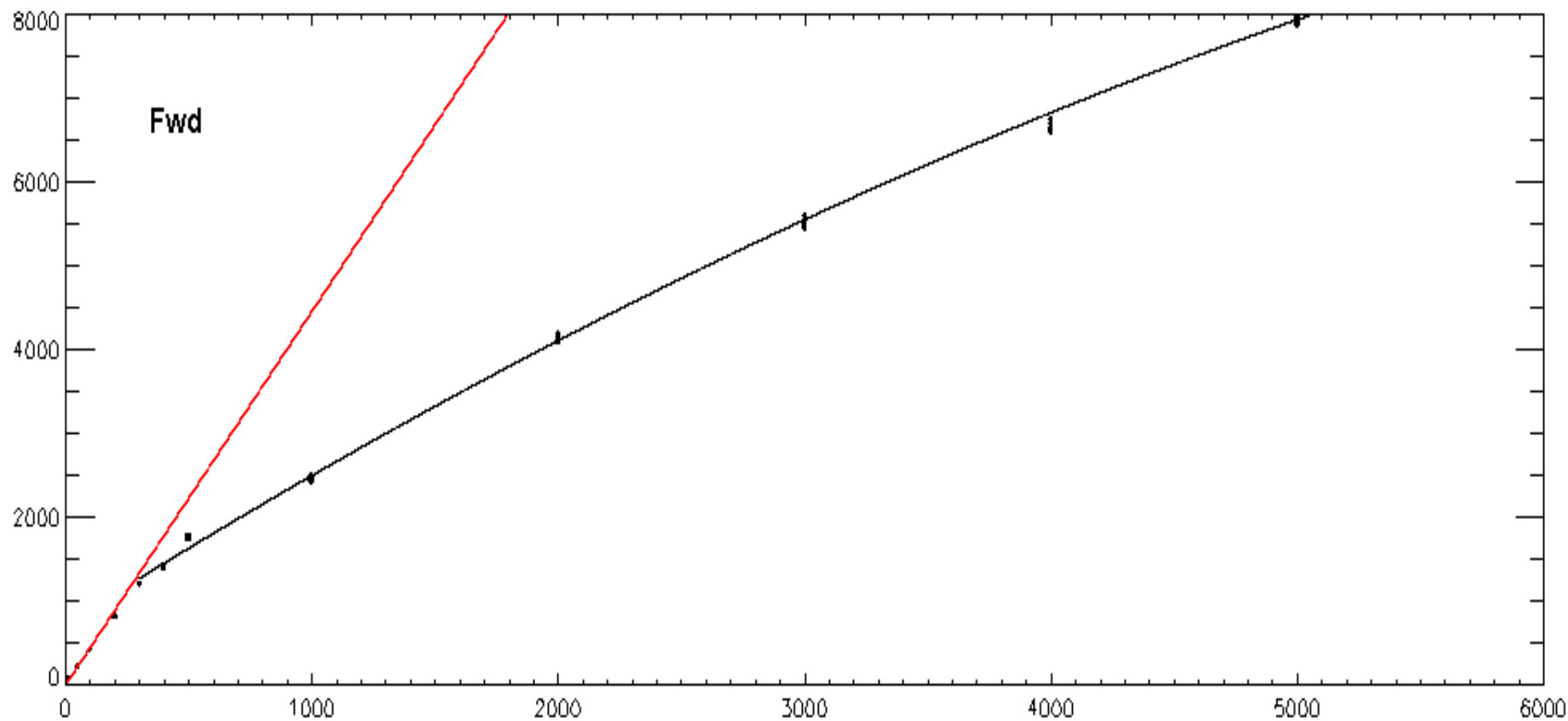


**Figure 32** - Peak of the symmetrized interferograms versus source intensity. Forward motion.

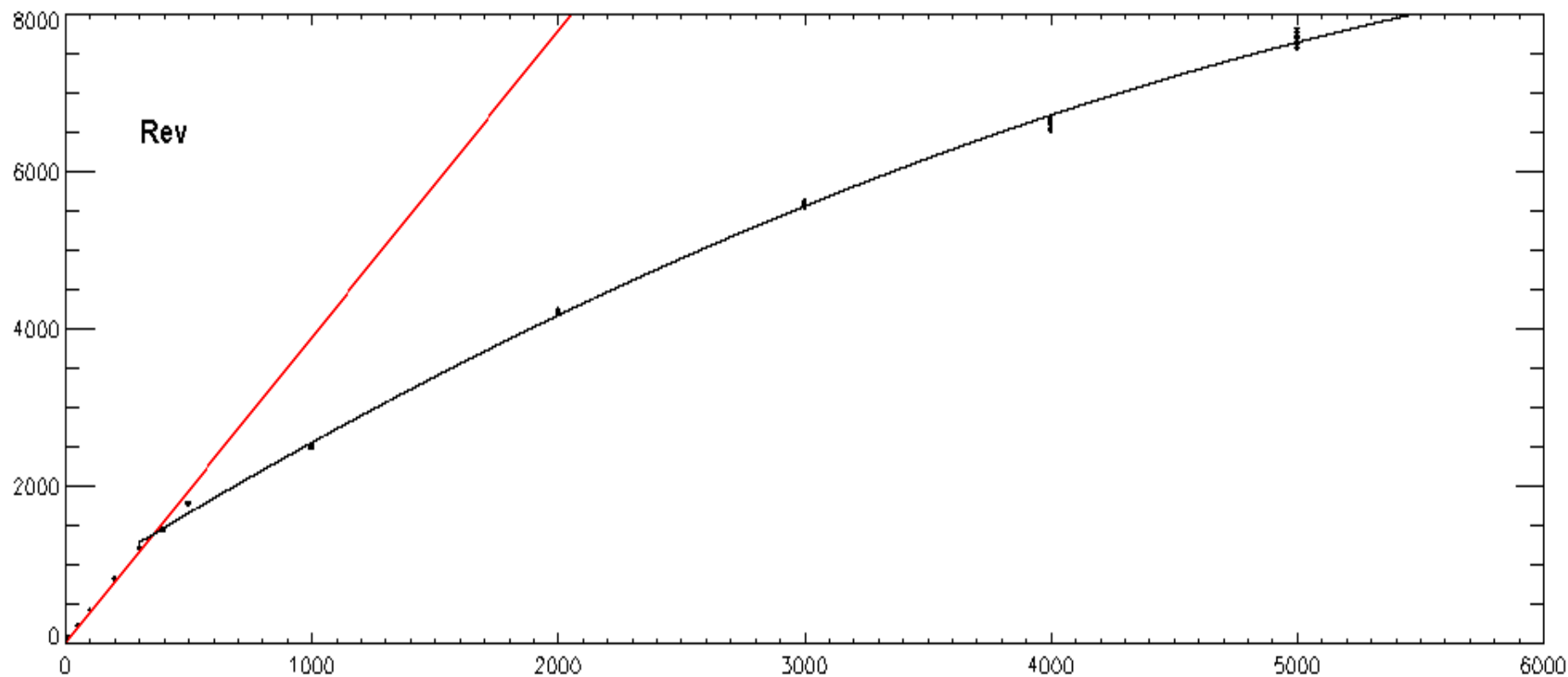


Figure 33 - Peak of the symmetrized interferograms versus source intensity. Reverse motion.

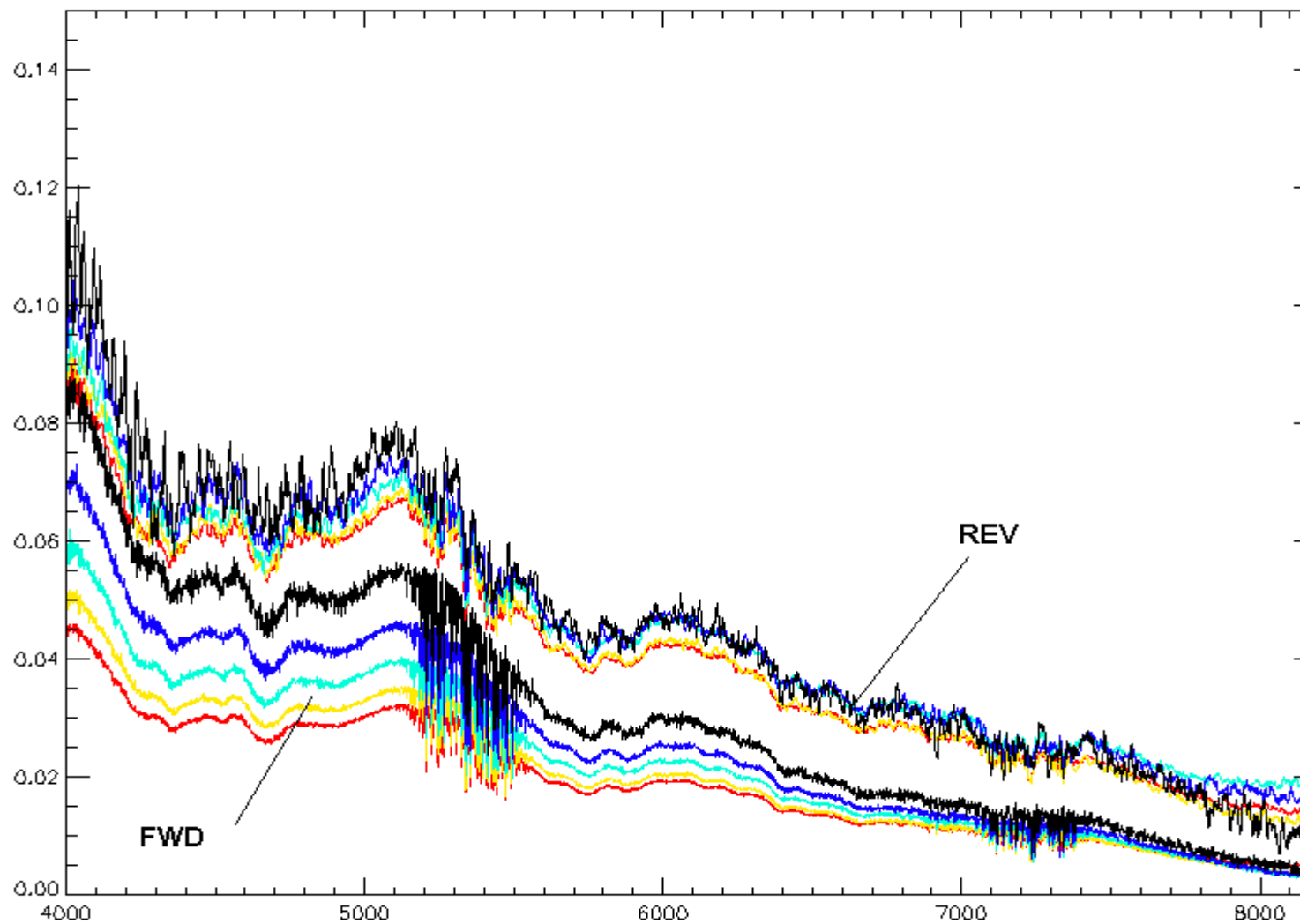
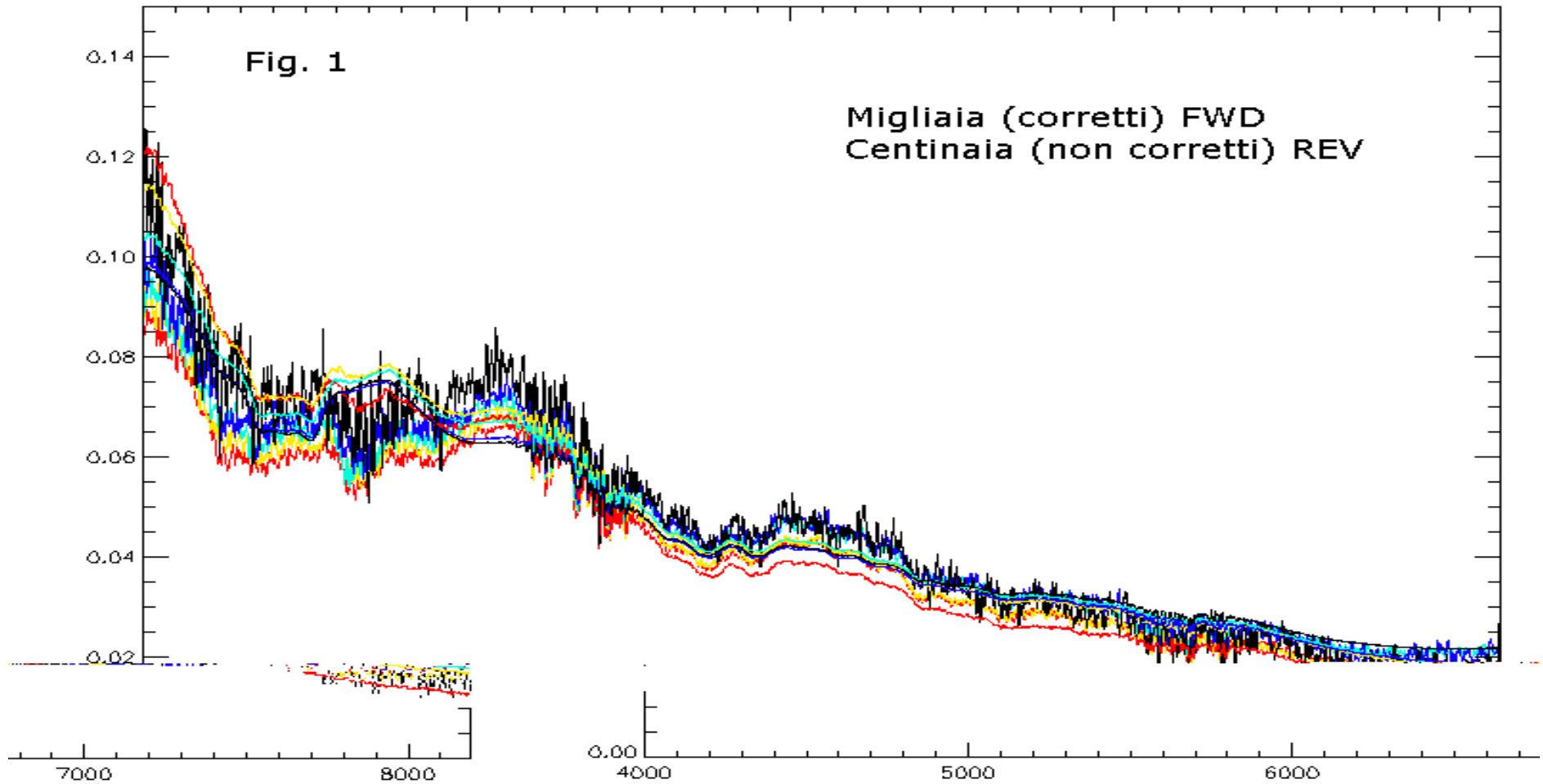
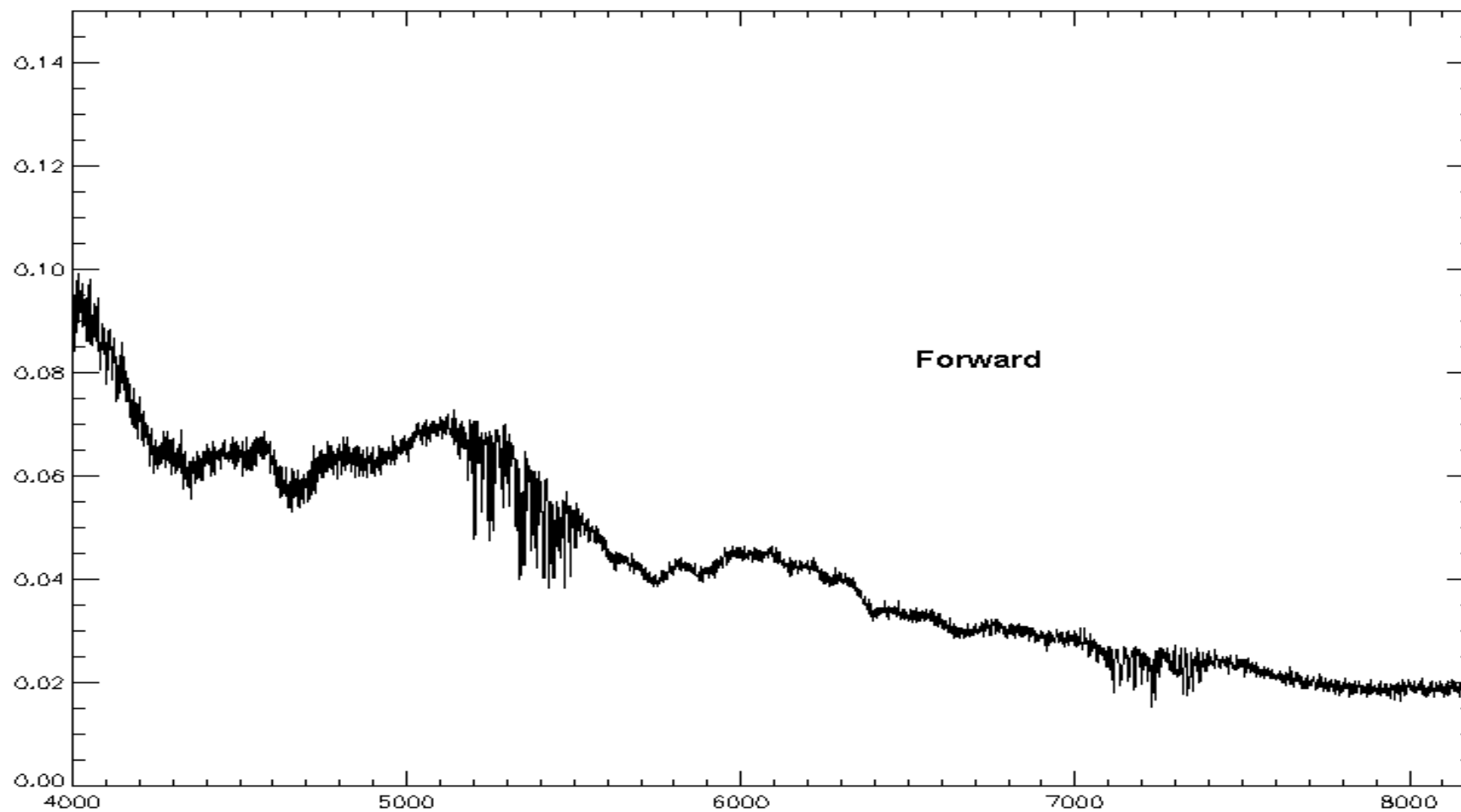


Figure 34 - responsivity of the SW channel in the interval 4000 - 8200 cm<sup>-1</sup> from the uncorrected interferograms.



**Figure 35** - responsivity of the sw channel for all the source intensities, corrected for the non linearity according to figure 27. the red curve (bottom), is the start of new set of measurements, the source may not be stabilised.



**Figure 36** – responsivity of the SW channel in the linear part.

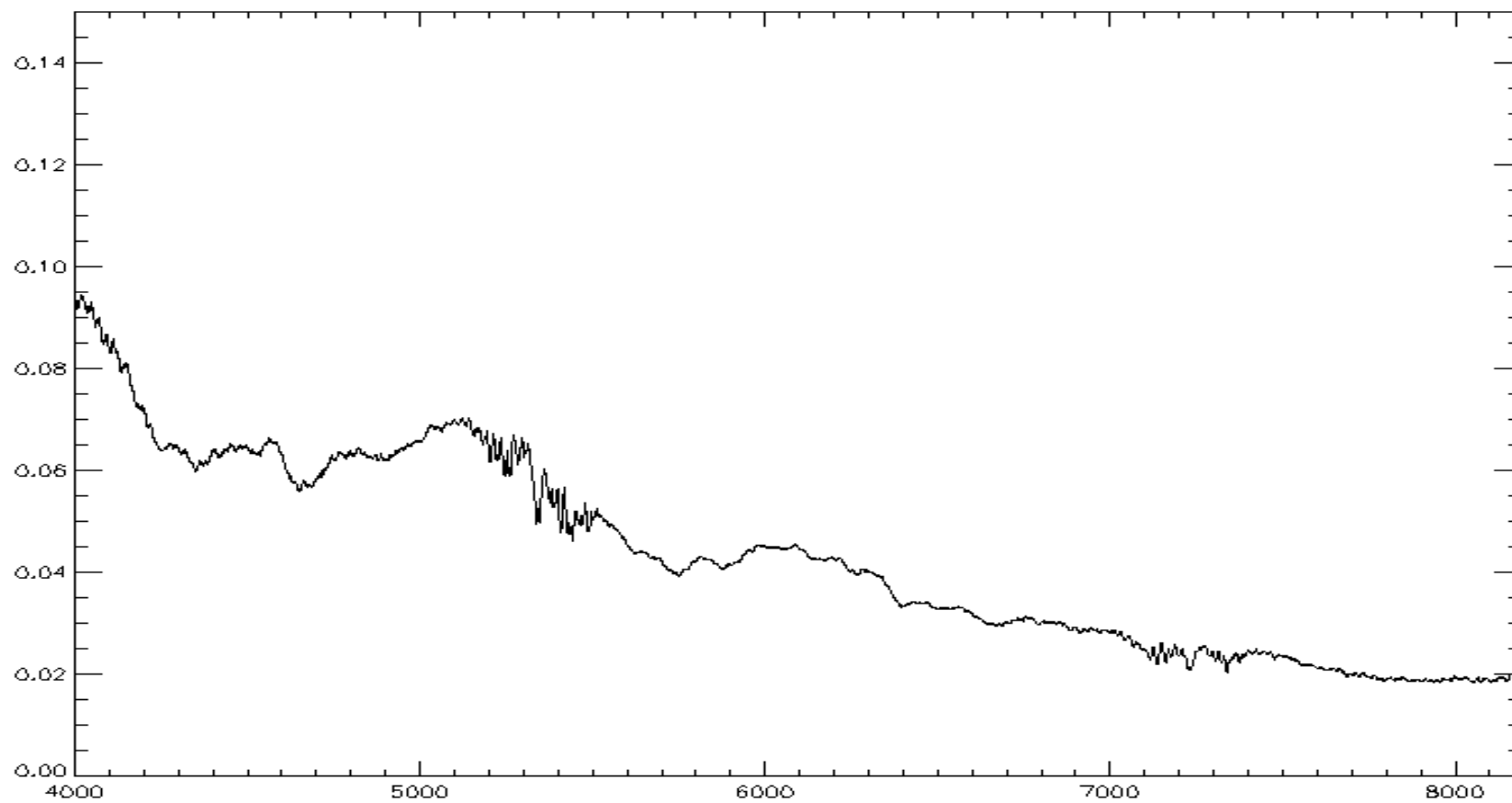


**Figure 37** – responsivity of the SW channel in the linear part, smoothed on 11 points, forward motion.

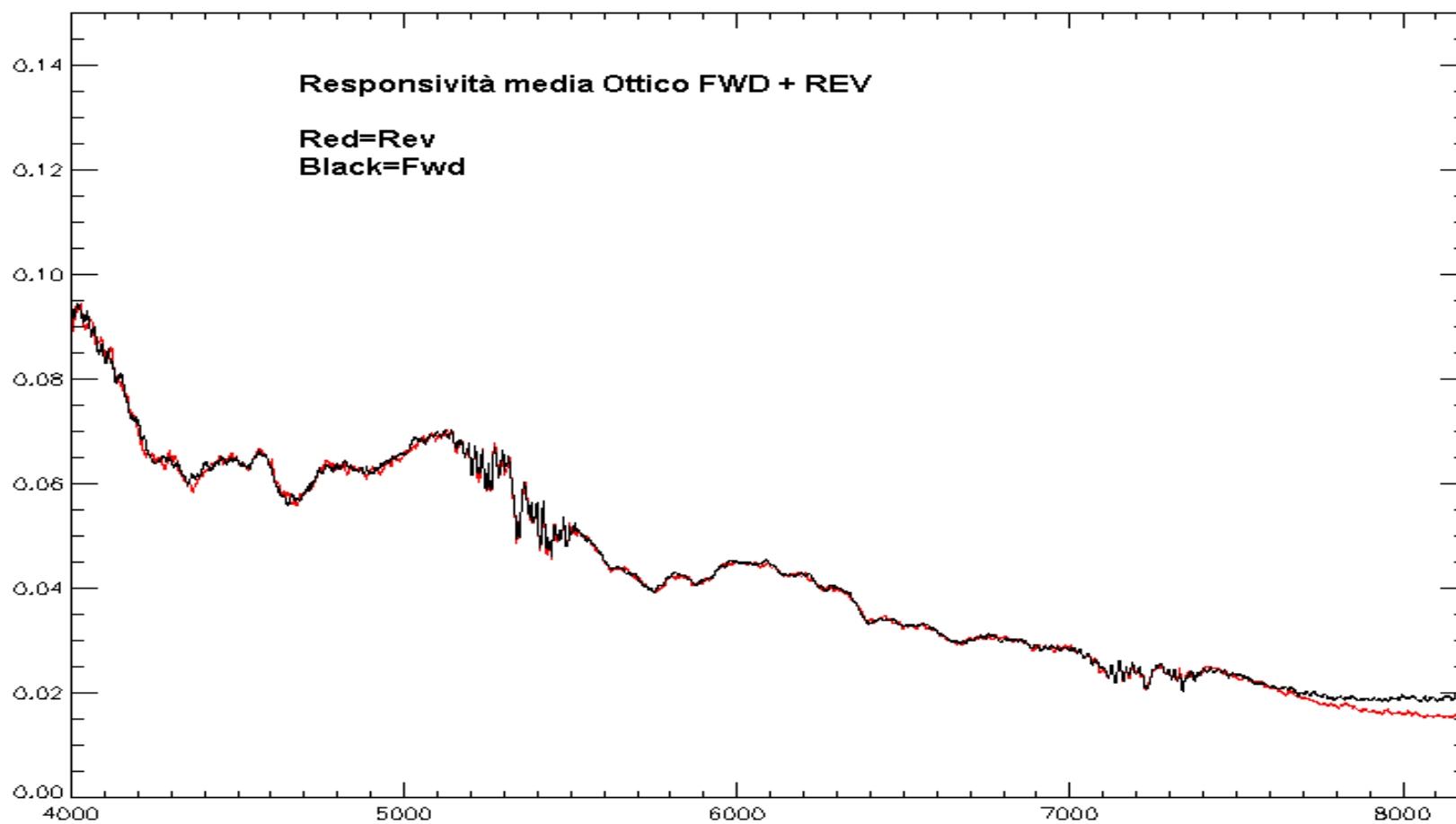


**Figure 38** – responsivity of the sw channel in the linear part. the curves are smoothed on 7 points. note the difference between forward and reverse motion above 7500 cm<sup>-1</sup> .

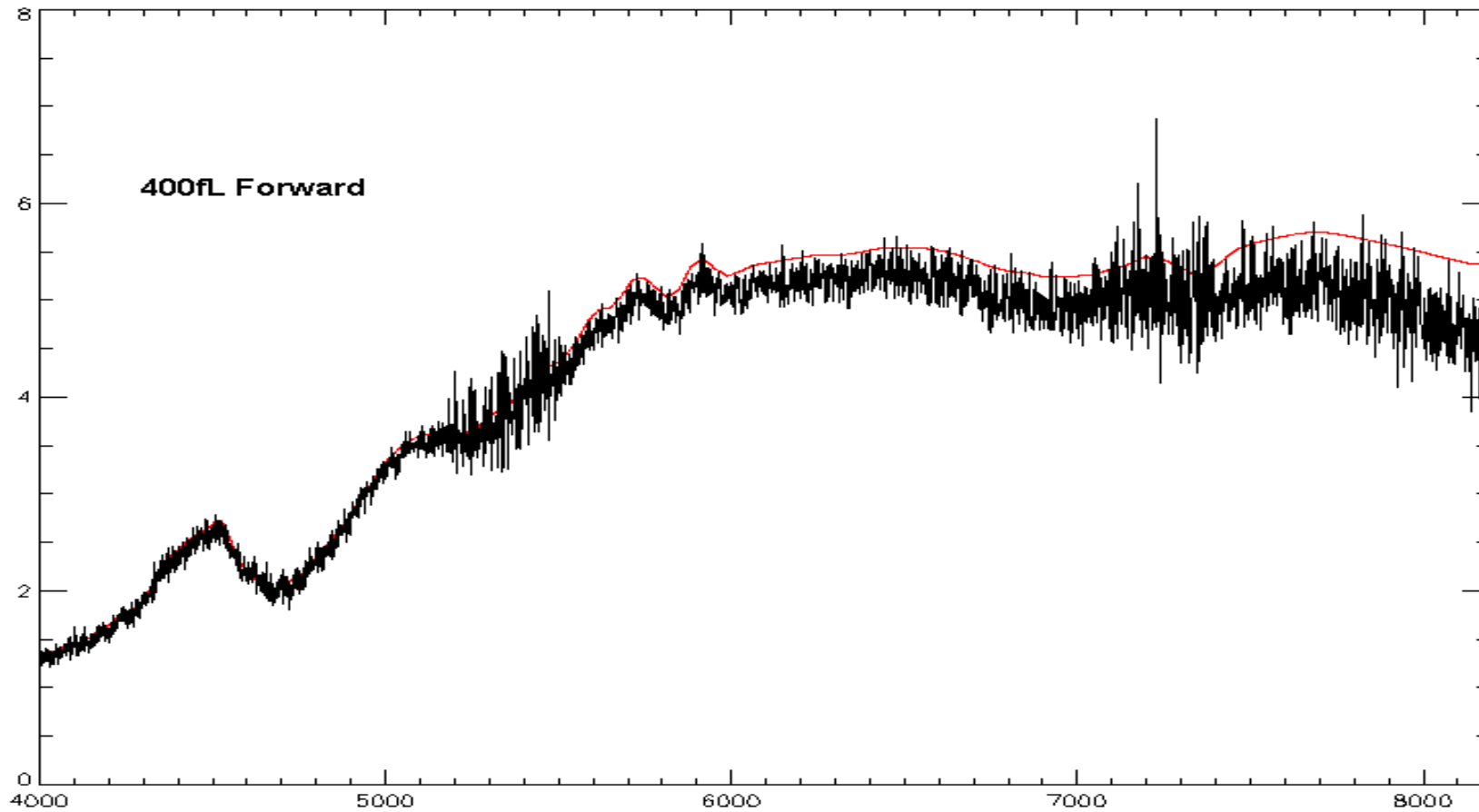


**Figure 39** - Calibrated integrating sphere spectrum : black measured, red given.

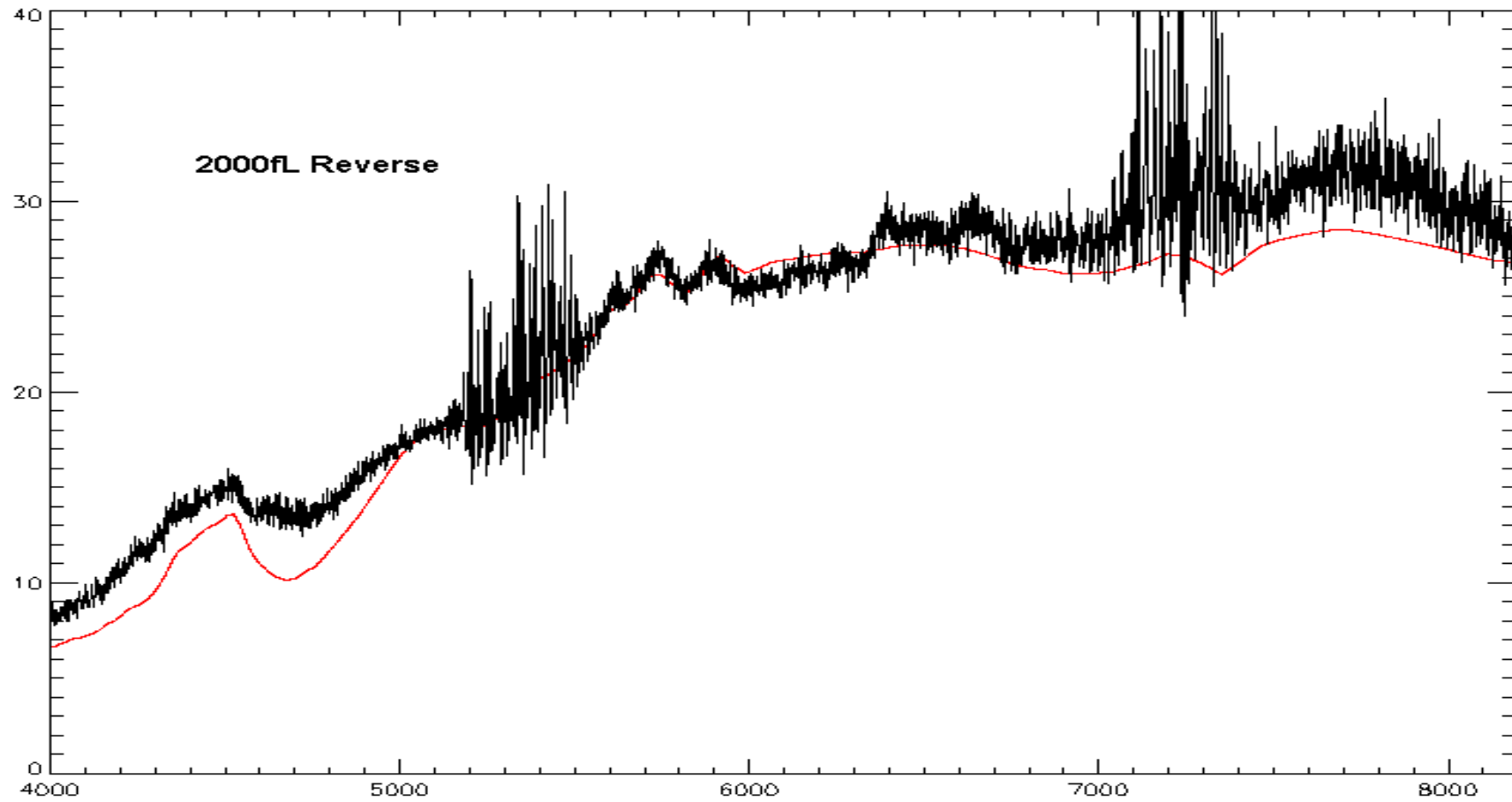


**Figure 40** – Calibrated integrating sphere spectrum: black measured, red given.

## 5.4 – THE THERMAL PART RESPONSIVITY

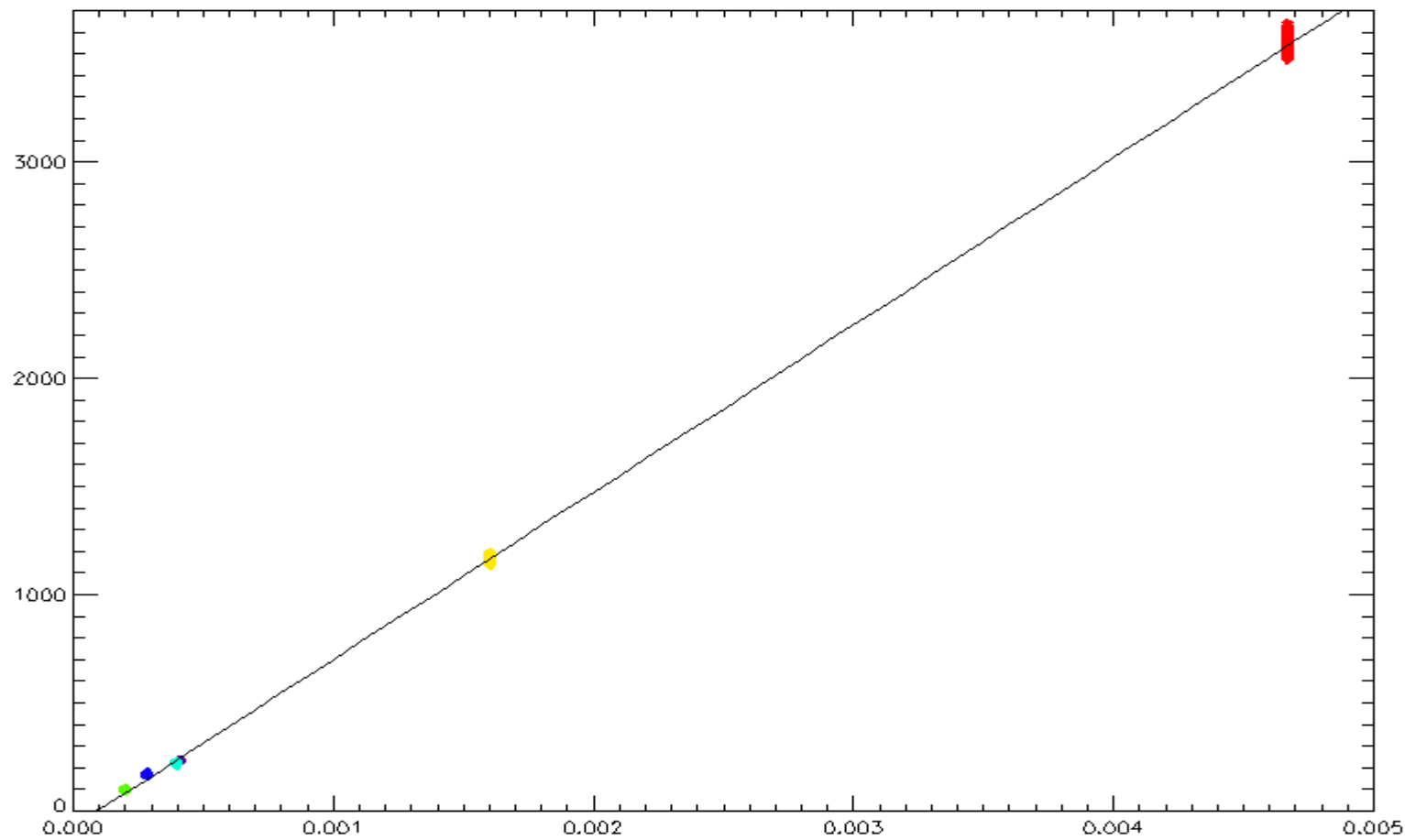


**Figure 41** – Apparent linearity of the SW channel detector in the thermal region.

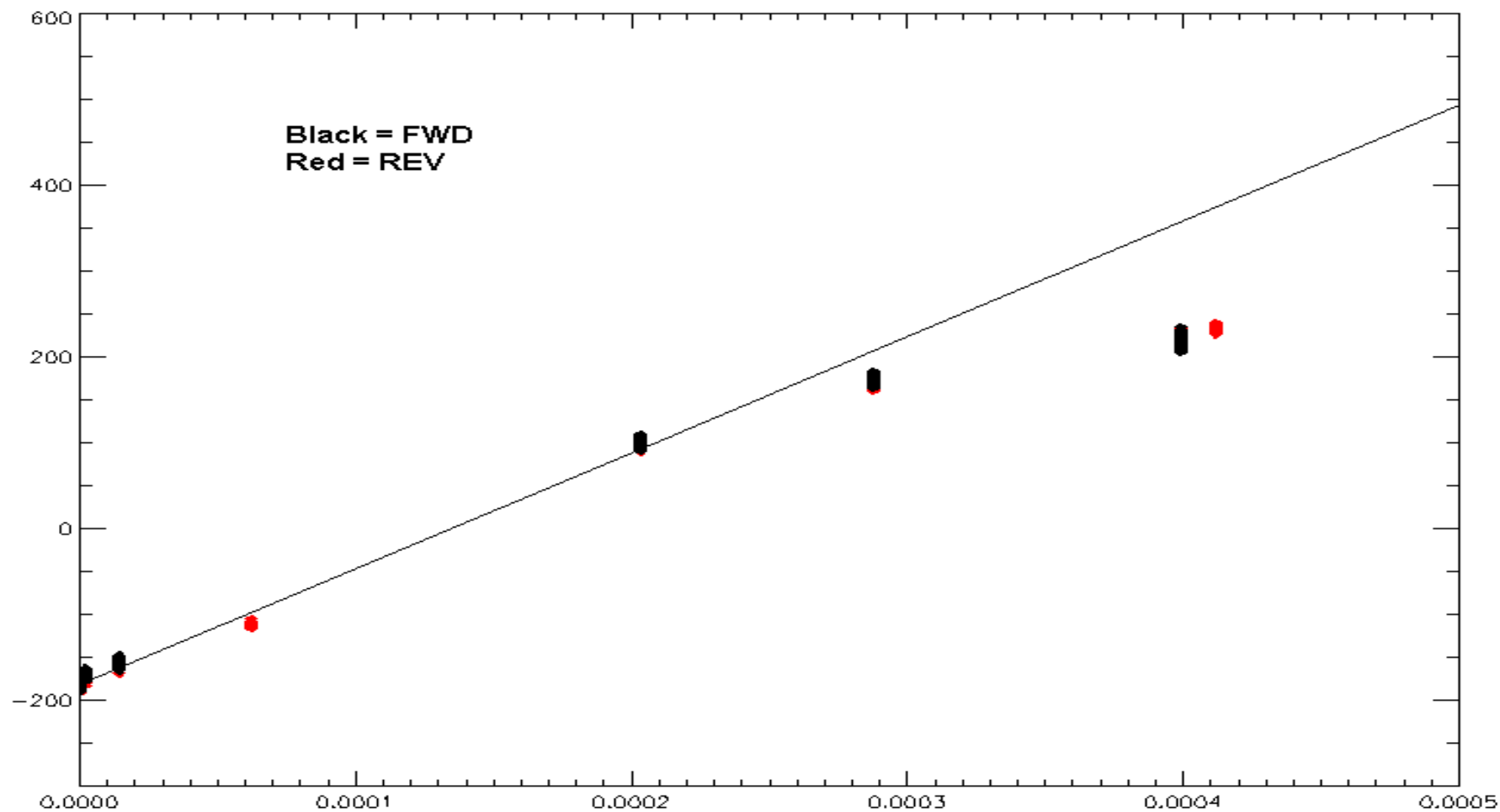
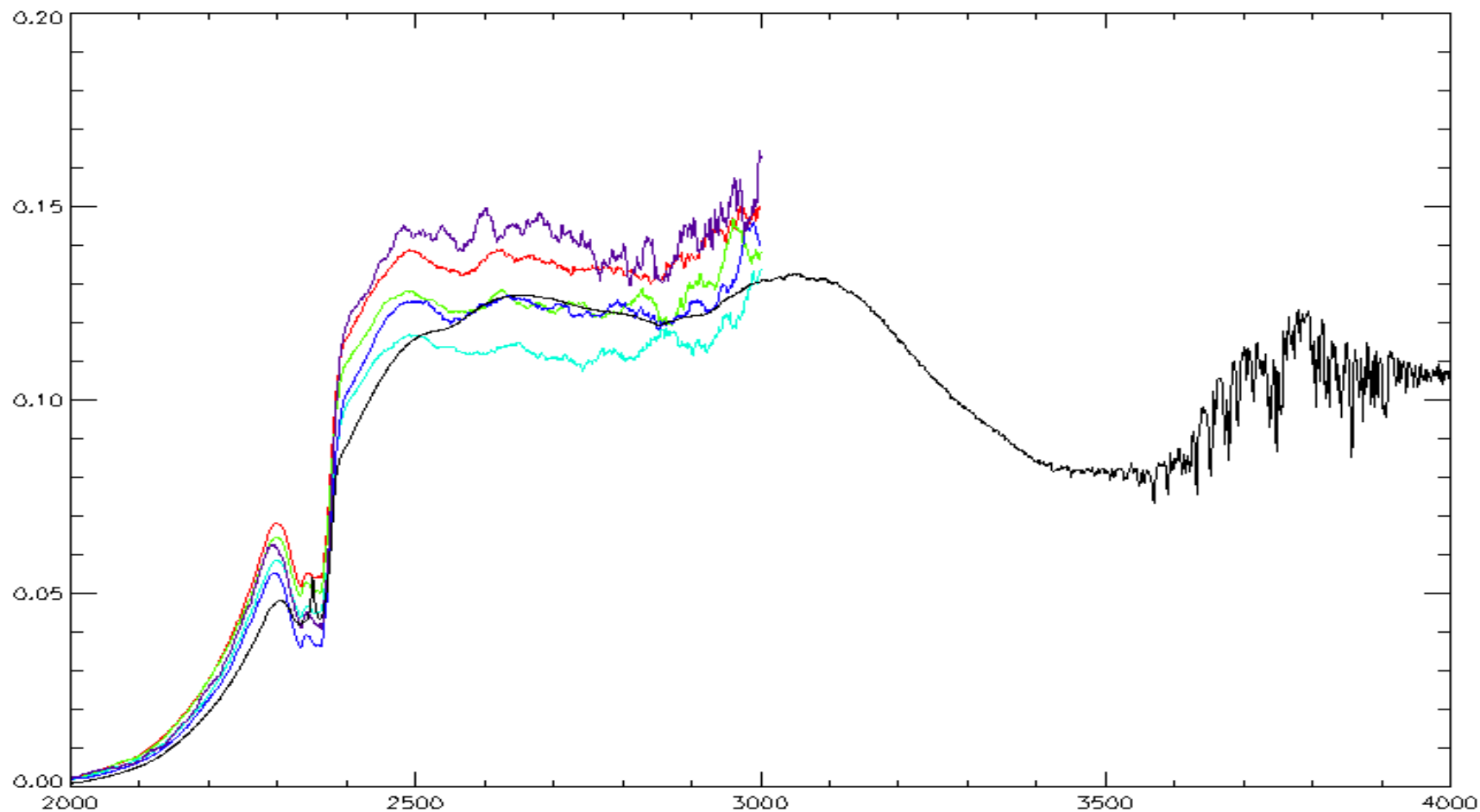


Figure 42 – Non linearity of the SW channel in the thermal region. The lowest points are for the -100, -60 and -30 C. with IKI BB.



**Figure 43** – Responsivity of the SW channel in the thermal part : in color are responsivity from the linear part, in black is responsivity from the BB at 150 celsius with the interferogram corrected for the non linearity.

 Planetary Fourier Spectrometer PFS		<b>PFS for Mars Express</b> December 2002	<b>PFS</b> INTERNAL NOTE CALIBRATION II Page 67	<b>P.I. Vittorio Formisano</b> <b>CNR IFSI</b>
--	--	--	--	---

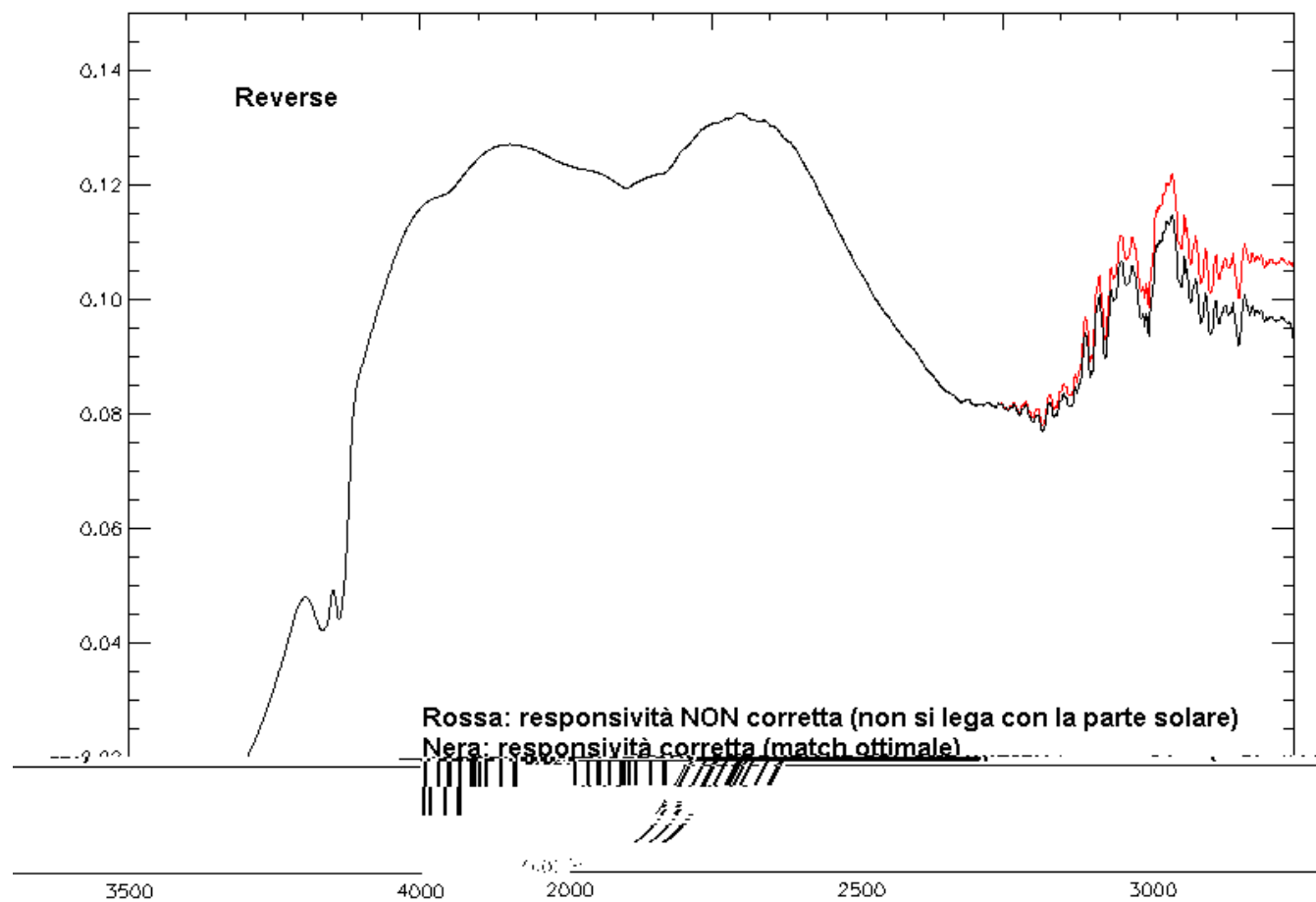
In order to proceed and obtain the responsivity and NER in the thermal part of the SW channel at room temperature, we have used the measurements obtained during the LW calibrations.

First we study the linearity of the measurements. We do not have now the intensity of the source, as we had for the integrating sphere, therefore we use the integral of the Planckian at the temperature of the source, over the wavenumber range 2000 – 4000  $\text{cm}^{-1}$ .

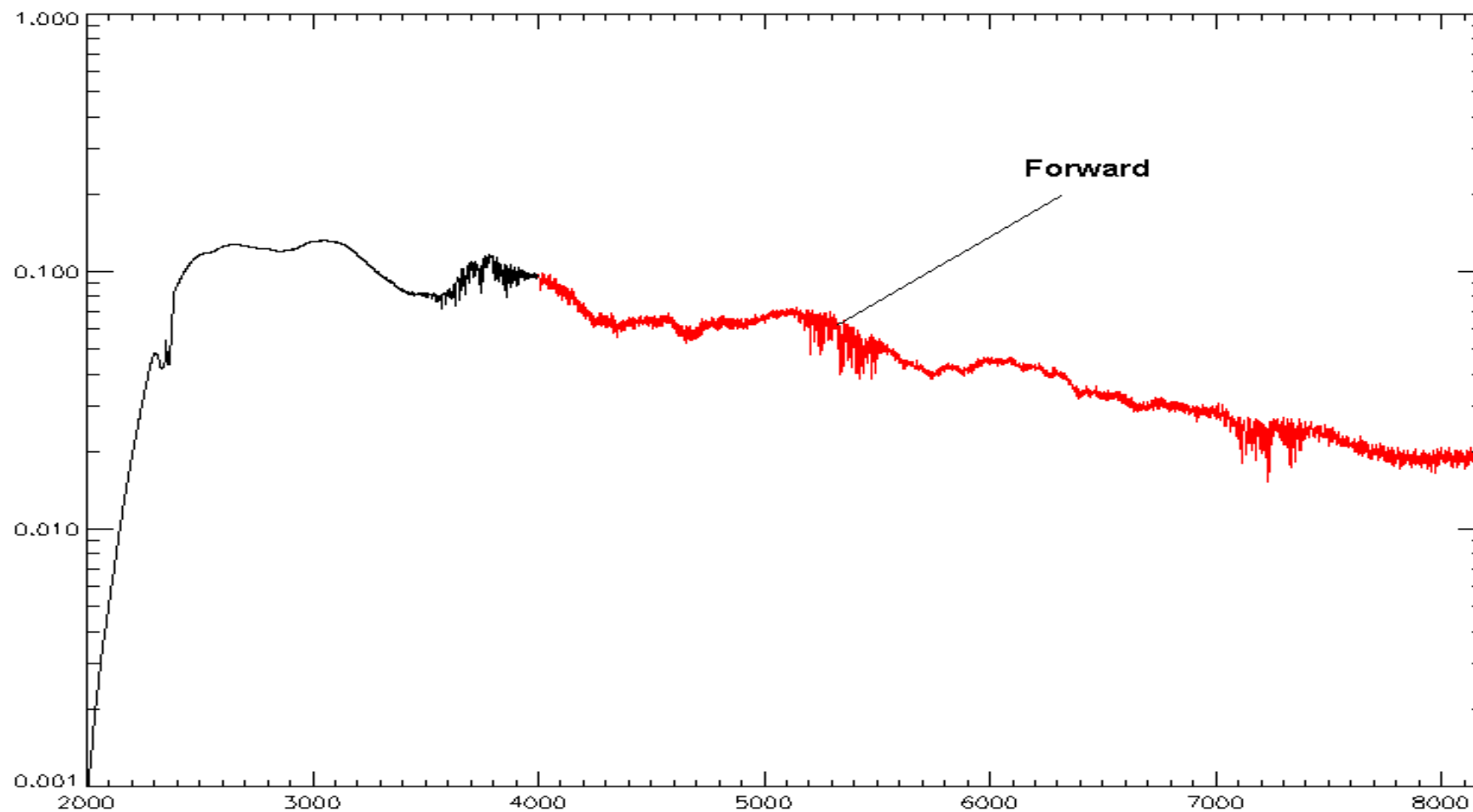
Figure 40 gives the behaviour of the interferogram peak versus the integral of the Planckian. The behaviour is apparently linear, generating a number of questions on the reliability of the work done.

Figure 41 shows that the SW channel is actually non linear also in the thermal part, when we consider the lowest fluxes measured : IKI BB at  $-100$ ,  $-60$ ,  $-30$  Celsius, plus  $0$ ,  $30$ ,  $40$  degrees Celsius. Around  $40$  deg the detector starts behaving as non linear.

Figure 42 gives the responsivity computed from the linear part of the measurements :  $-100$ ,  $-60$ ,  $-30$ ,  $0$ ,  $40$  Celsius are in color. These measurements do not give a good signal up to  $4000 \text{ cm}^{-1}$ , therefore we consider the  $150 \text{ C}$ , which, however is the non linear region. After correction for the non linearity, the responsivity obtained is the black curve shown. It is of the same order as the responsivity from the linear part, meaning that the correction is correct. The signal is, on the other hand good enough to be different from zero up to  $4000 \text{ cm}^{-1}$ .



**Figure 44** – SW channel responsivity in the thermal part: red is the curve from fig. 38, black it is the same curve corrected to match the responsivity from the solar part so there is no discontinuity at 4000 cm-1.



**Figure 45** – Total responsivity of the SW channel over the entire wavenumber range. Forward motion. Horizontal units are wavenumber, vertical units are DN/(ergs /s cm<sup>2</sup> sr cm<sup>-1</sup>).



 <p>Planetary Fourier Spectrometer PFS</p>		<p><b>PFS for Mars Express</b> December 2002</p>	<p><b>PFS</b> INTERNAL NOTE CALIBRATION II Page 71</p>	<p><b>P.I. Vittorio Formisano</b> <b>CNR IFSI</b></p>
--	--	--	--	---

### **5.5 – RESPONSIVITY AND NER OF THE SW CHANNEL DETECTOR: ROOM TEMPERATURE.**

It should be noted that the responsivity from the two sides solar and thermal part of the SW channel at 4000 cm<sup>-1</sup> do not match exactly, but there is a difference of the order of some percentage. After a small correction (see figure 44) the matching is very good and the total responsivity is given in figure 45 for a forward motion, and in figure 46 for a reverse motion.

Note that in the figures given there are 4 spectral regions contaminated by atmospheric features which should be removed. These are CO<sub>2</sub> absorption band and 3 water band regions.

The NER computed from the same data is shown in figure 47. There is a minimum of roughly 0.12 ergs /s cm<sup>2</sup> sr cm<sup>-1</sup>. At 8200 cm<sup>-1</sup> the NER is almost 10 times larger. It should be noted that this NER is for room temperature and gain factor zero.

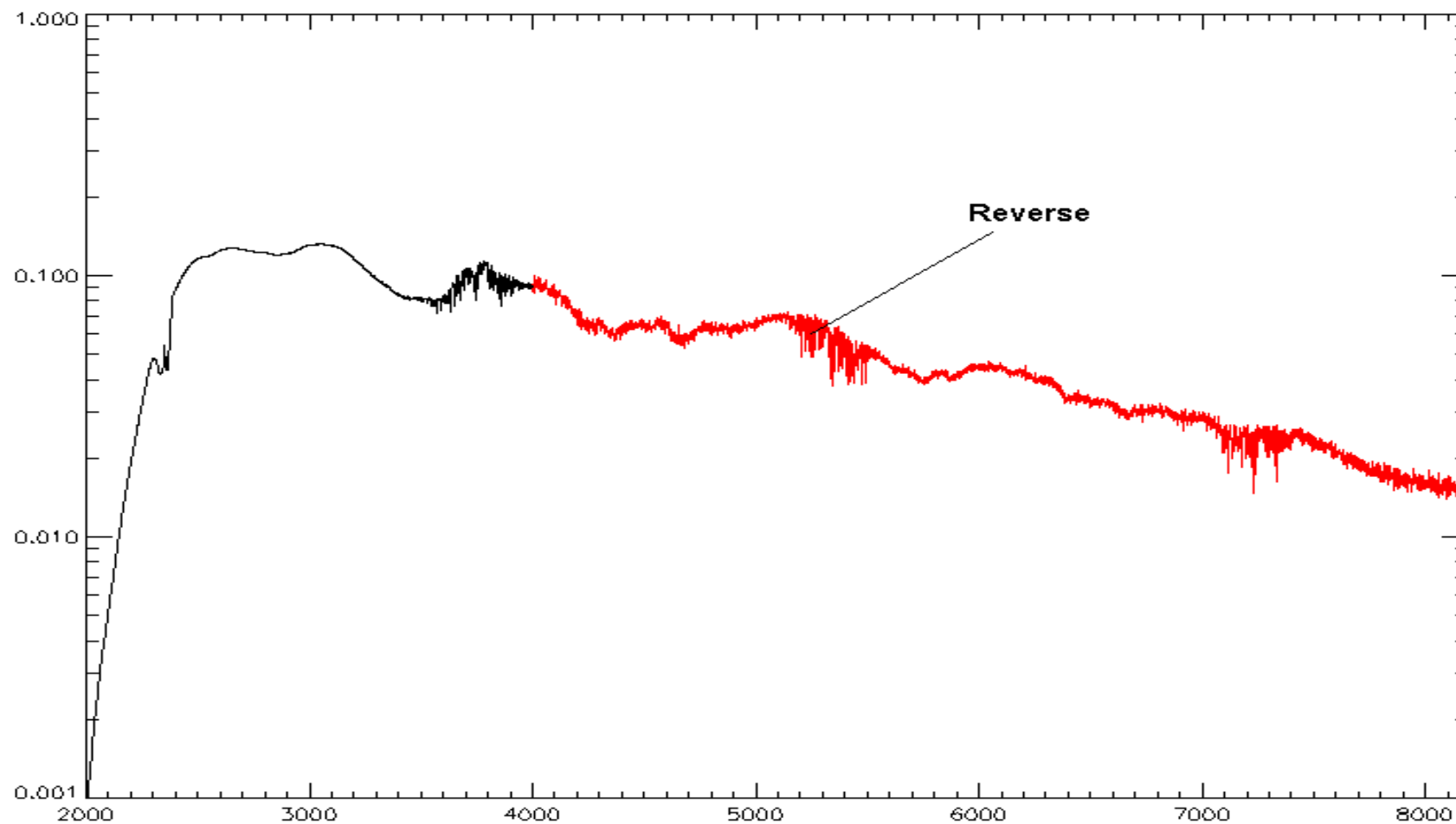


**Figure 46** – Total responsivity of the SW channel over the entire wavenumber range. Reverse motion.

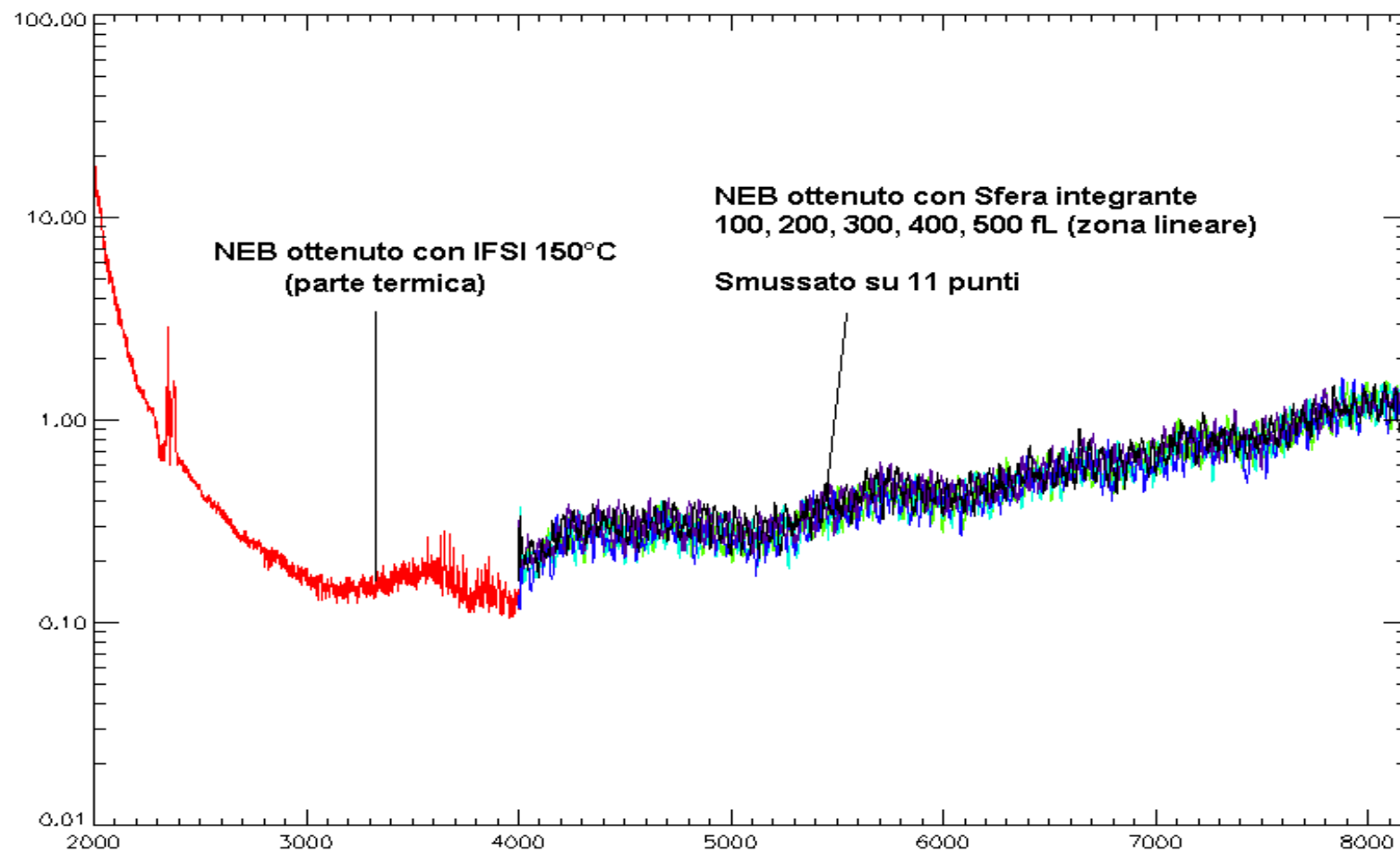


Figure 47 – NER for the SW channel from the measurements used to obtain the responsivity .



 Planetary Fourier Spectrometer <b>PFS</b>		<b>PFS for Mars Express</b> December 2002	<b>PFS</b> INTERNAL NOTE CALIBRATION II Page 75	<b>P.I. Vittorio Formisano</b> <b>CNR IFSI</b>
--	--	--	--	---

## 5.6 - IFSI BB- INTERNAL BB – RUSSIAN BB

It is important to note that in order to completely understand the SW channel we had to consider not only the Integrating sphere calibrations, and the IFSI BB, but also the IKI BB because the IFSI BB behaves as a source of intense radiation, while to see the linear behaviour of the detector we have to go to low enough signals, as those obtained from the IKI BB at low temperature.

Another very important point is the behaviour of the instrument in the 2 different aspects : solar part and thermal part of the SW channel. In the solar part the instrument is just a normal absolute instrument. In the thermal part the instrument is differential and the interaction with the source is not negligible. There are several consequences of this behaviour : in figure 42, in order to identify the linear behaviour of the instrument we had to take into consideration the temperature of the source AND THE PHASE SIGN. Being the phase negative the interferogram peak has been plotted in the negative semiplane when the source temperature is lower than the detector temperature, and in the positive semiplane when it was larger. The behaviour of the instrument with a source going from below to above the detector temperature has to be further investigated.

## 5.7 - MODELLING DETECTOR-INSTRUMENT-SOURCE INTERACTION

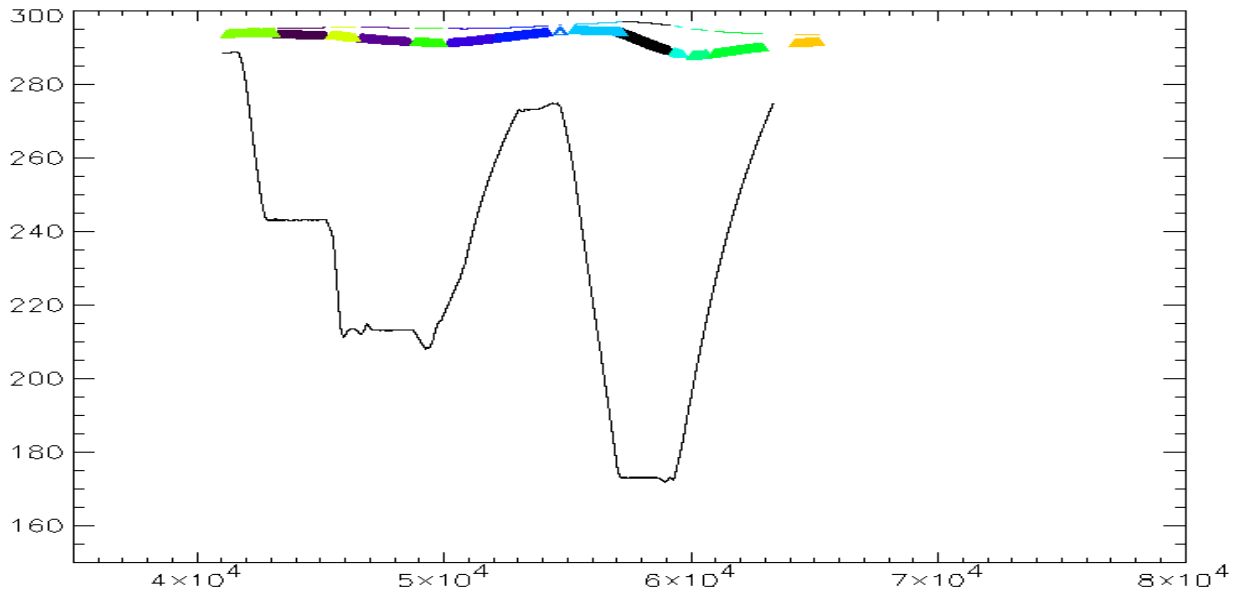


**Figure 48** – SW detector temperature and IKI BB temperature variation.

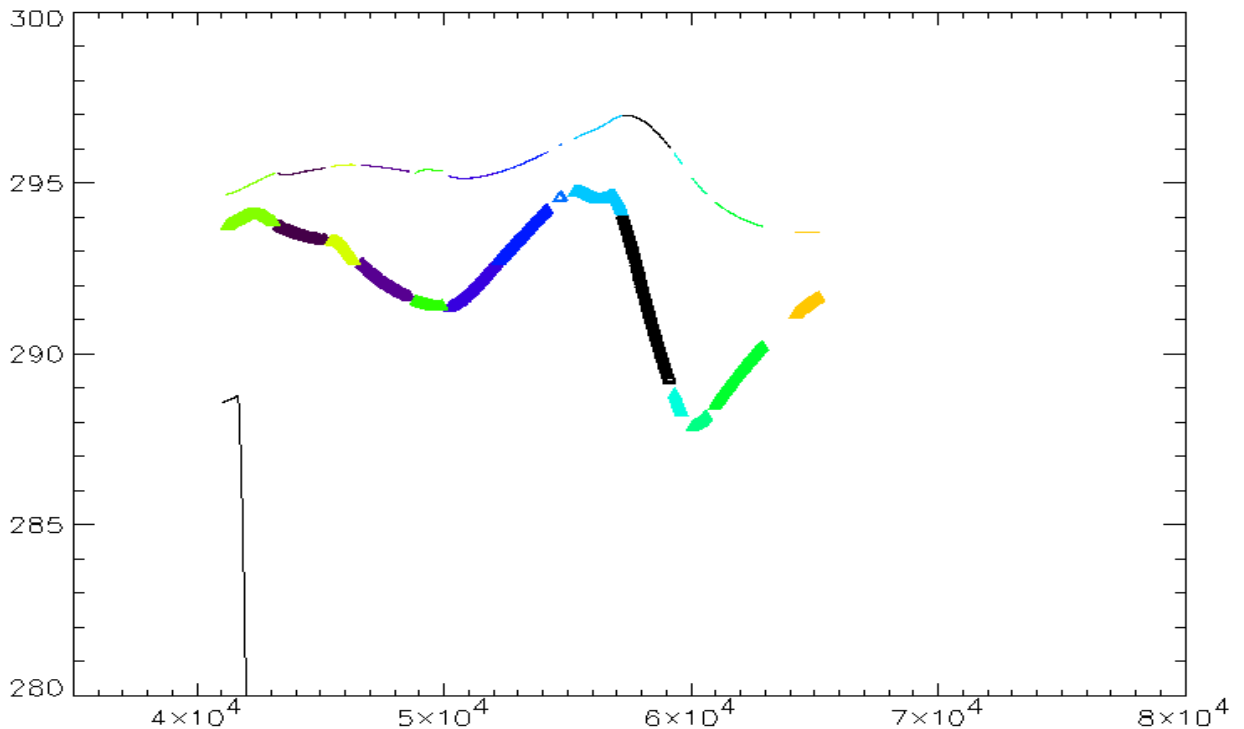


**Figure 49** - blow up of the vertical scale of figure 48. Note up to 7 degrees temperature variation of the detector (in colour).

It is important to remember that in order to have a good description of the instrument behaviour we have to introduce a modelling of the cross-talk between the source, the detector and the instrument. For the LW channel this was done using the approach suggested by Hanel, and we found that the

 Planetary Fourier Spectrometer PFS		<b>PFS for Mars Express</b> December 2002	<b>PFS</b> INTERNAL NOTE CALIBRATION II Page 77	<b>P.I. Vittorio Formisano</b> <b>CNR IFSI</b>
--	---	--	--	---

instrument contributed 97 %, while the detector contributed only 3% (see the parameter  $\alpha$  in the expressions given below). Most measurements were dealing with sources hotter than the instrument and the detector. For the SW detector we find that the detector is more important (if the source is colder than the detector) and it contributes 94 % against 6 % .

$$Re_s = \frac{A_2 - A_3}{\epsilon B(n, T_2)}$$

$$NER = \frac{\sigma(Re_s)}{Re_s} * B(T_{eff}) = \frac{\sigma(Re_s)}{Re_s} * (\alpha B(T_i) + (1 - \alpha) B(T_d))$$

It is likely that also for the LW channel there is a different behaviour when the source is colder than the detector. For the SW channel, when the source became hotter than the detector, we obtained the usual behaviour of the LW channel. This must be further investigated.

In any case it is important to keep in mind that the SW channel has a double characteristic : in the thermal part and in the solar part.

## 5.8 - CERAMIC ELEMENT AND INTERNAL CALIBRATION LAMP

The responsivity and NER given above can be used to give the characteristics of the ceramic element source and the internal calibration lamp, as they were measured in air. The radiance from the 2 sources are given in figure 45 and 46. Note that for the internal calibration source we have two curves as the current of the lamp was reduced from the original 16 mA to 12 mA (red curve) and then to 10 mA (black curve).

We note that the ceramic element reaches 15 at 4200 cm<sup>-1</sup>, i.e. a SNR of 50, the same is also true for the internal calibration lamp at the same wavenumber. The internal calibration lamp has a SNR of 100 at 3000 cm<sup>-1</sup> (black curve). It should be noted that this values are for room temperature and gain factor zero.

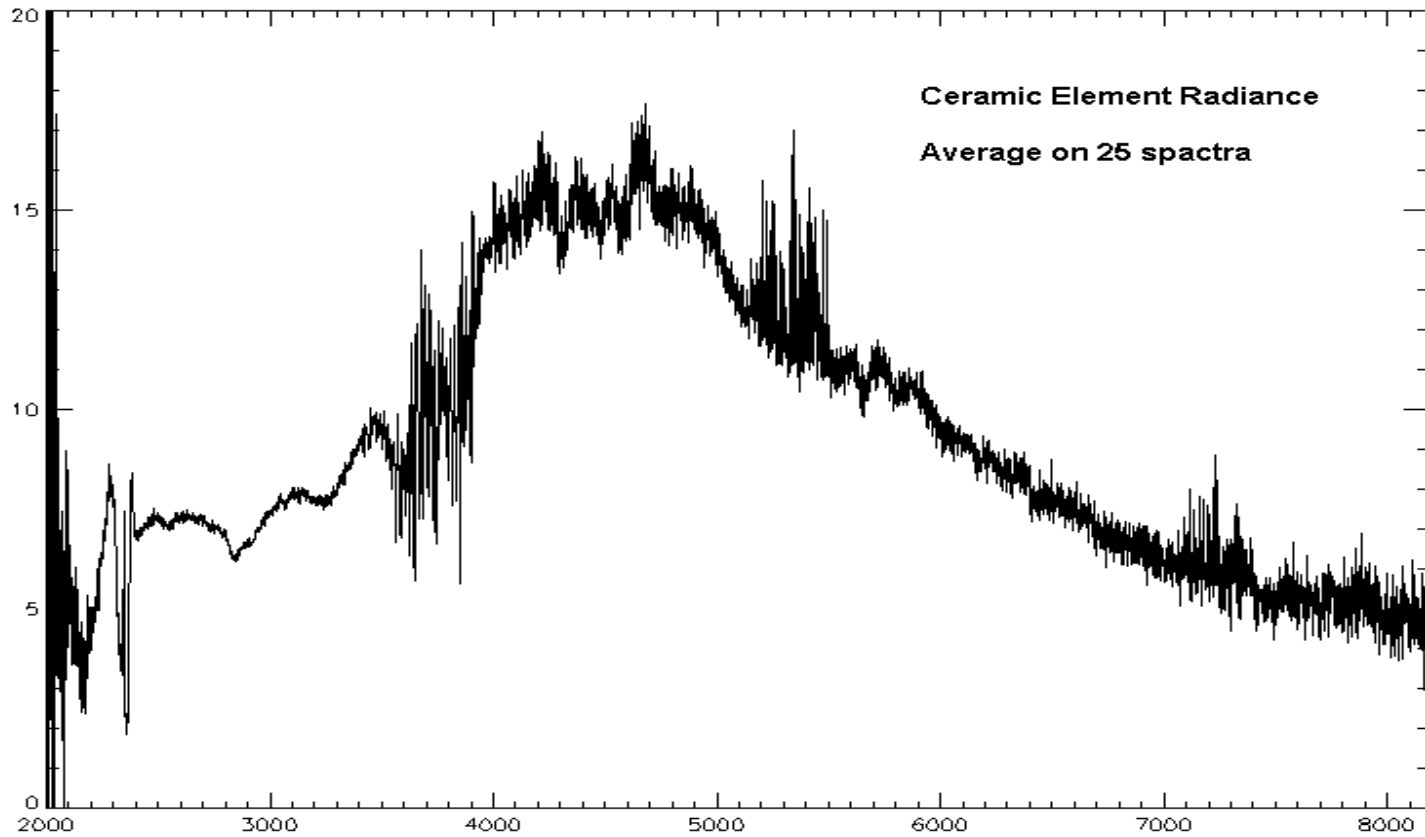


**Figure 50** – Radiance in the atmosphere of the ceramic element.

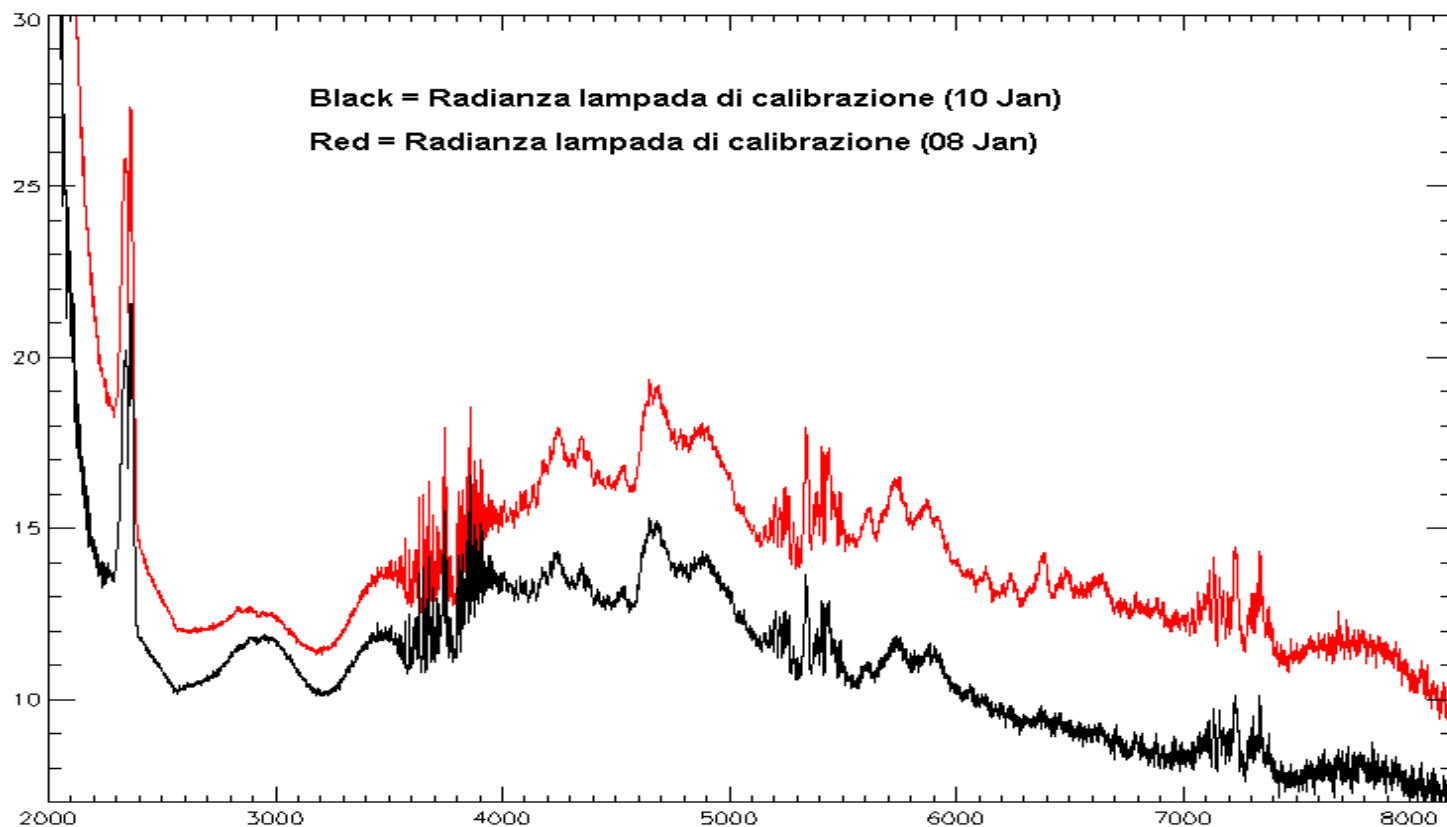


**Figure 51** – Radiance in air of the internal calibration lamp. The 2 curves are for 10 and 12 mA current. The black curve is reflecting the final Flight situation.

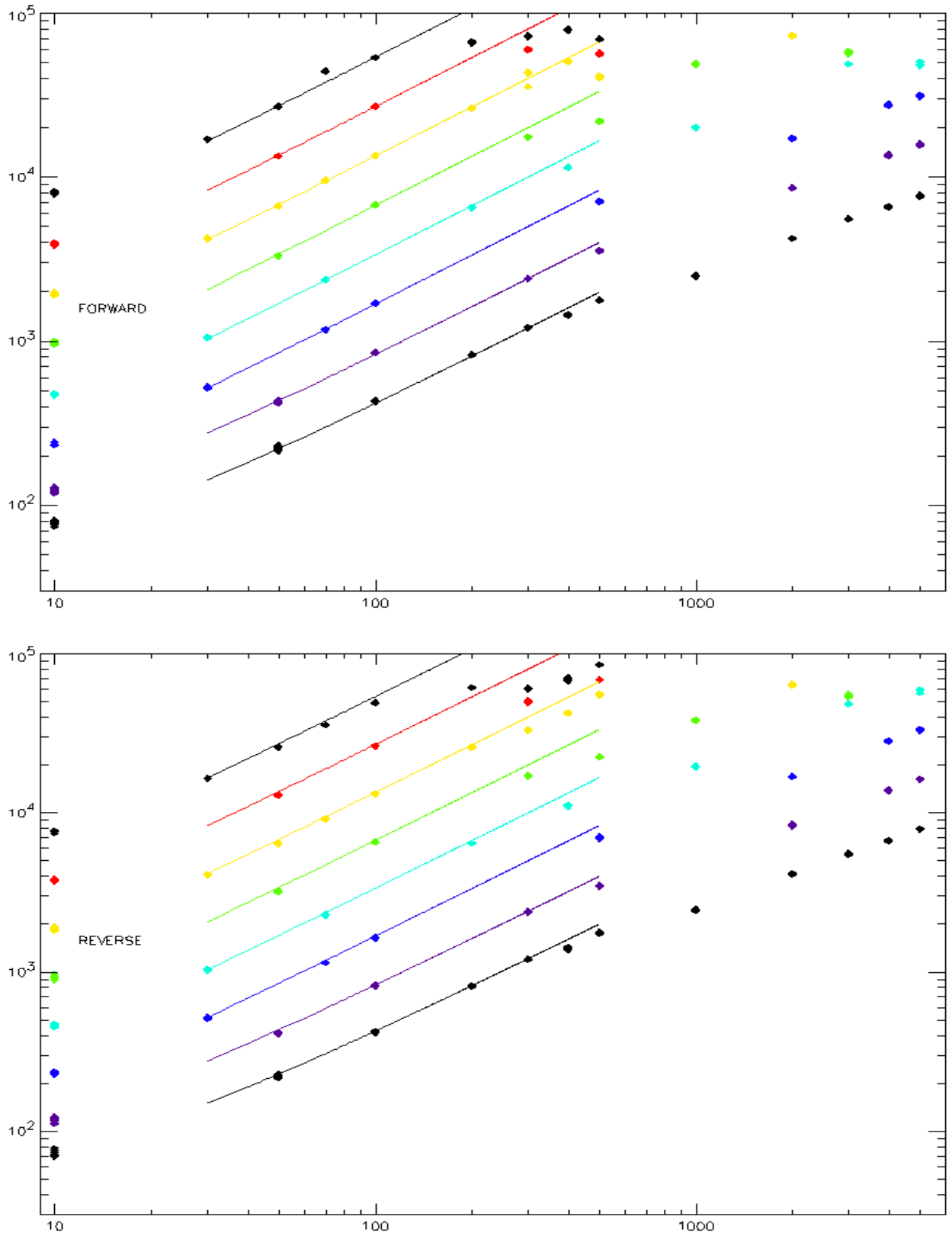


**Figure 52** – Linearity and gain factors : foot lamberts versus interferogram peak. Forward upper panel, reverse lower panel.

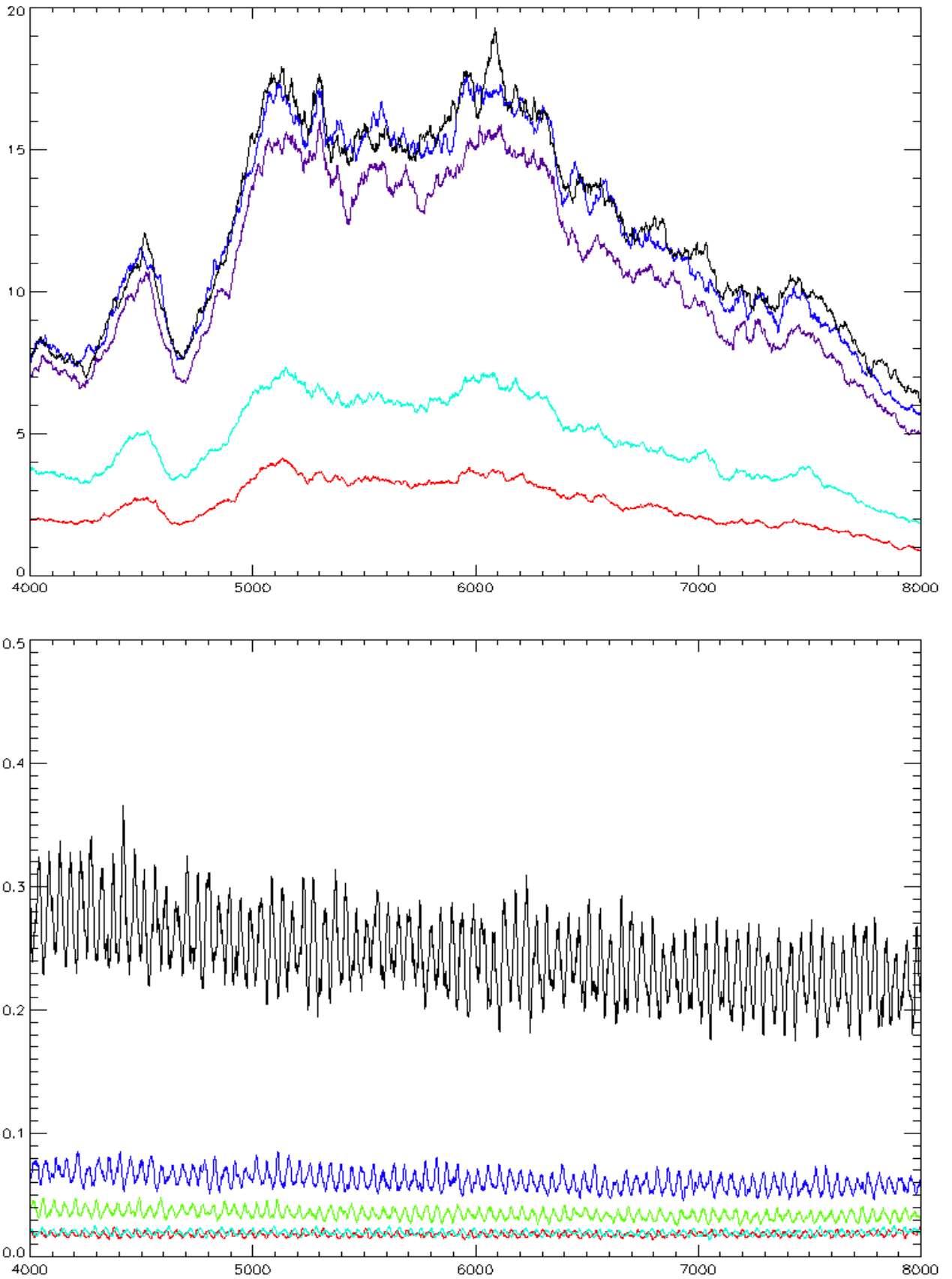


Figure 53 – SNR versus different gain factors (above), noise level lower panel.

## 5.9 – GAIN FACTORS AND SNR

The SW channel has 8 gain factors that can be used. Figure 52 shows the peak of the interferograms as function of the footlamberts of the integrating sphere. The two panels are for forward and reverse motion respectively. We note first of all that the linear regime is kept at all the gain values. The highest gain has saturation already in the linear regime. We are plotting the peak of the symmetrized interferograms, therefore the values can be higher than 32000. The linear segments plotted have been obtained by fitting the first data (gain 0) with a straight line, then plotting the same line shifted by a constant factor to fit the other points.

**THE GAIN FACTORS ARE (MEASURED FROM 100 FOOTLAMBERTS DATA):**

**GAIN 0 = 1**

**GAIN 1 = 2.0**

**GAIN 2 = 4.0 = 2.0 X 2**

**GAIN 3 = 8.0 = 2.0 X 2 X 2**

**GAIN 4 = 16.0 = 2.0 X 2 X 2 X 2**

**GAIN 5 = 32.0 = 2.0 X 2 X 2 X 2 X 2**

**GAIN 6 = 64.0 = 2.0 X 2 X 2 X 2 X 2 X 2**

**GAIN 7 = 128.0 = 2.0 X 2 X 2 X 2 X 2 X 2 X 2**

In the last gain the measured value was only 119.1 because of saturation of the interferograms.

A very important study is concerning the behaviour of the SNR with the gain. Indeed it was reported that the SNR was increasing with increasing gain factor.

Figure 53 top panel gives the SNR of SW channel measurements for 100 footlamberts source (similar to Mars) for gain factors 0, 1, 3, 4, 6. For gain factors 0,1,2,3 the SNR maximum increases from 3 (gain 0) to 15 (gain 3) : **THERE IS AN INCREASE OF A FACTOR 5.** Above gain 3, and for gains 4,5,6,7 the SNR does not increase any more .

**FOR THIS REASON GAIN 3 IS THE BEST TO BE USED AT room temperature.**

In figure 53 top panel the curve has been smoothed over 50 points because the net computed, which is shown in figure 53 bottom panel, shows a non realistic oscillations caused by the correction for the laser diode temperature correction of the wavenumber scale.

The reason for the increase of the SNR with increasing gain factors is in the fact that the noise of the detector SW channel is lower than the noise of the AD converter, therefore the signal increases with the amplification, while the dominant noise does not. At gains above 3 the noise of the detector dominates over the noise of the digital electronics, and the SNR does not increase substantially any more.

## 5.10 RESPONSIVITY AS FUNCTION OF TEMPERATURE

In order to study the behaviour of the SW channel responsivity as function of the detector temperature we have made a sequence of measurements over the internal calibration lamp while the detector was being cooled. In figure 54 we have the study of the central part of the interferogram for measurements of the internal calibration lamp. Note that we are in a region of strong non linearity of the detector, according to the previous study. The peak values, indeed, are almost always above 10 000 DN. The behaviour of the three lines is essentially linear, meaning that the responsivity of the SW channel detector increases linearly for a decreasing temperature of the detector. We shall now make some theoretical considerations, in order to simplify the study for decreasing temperature.

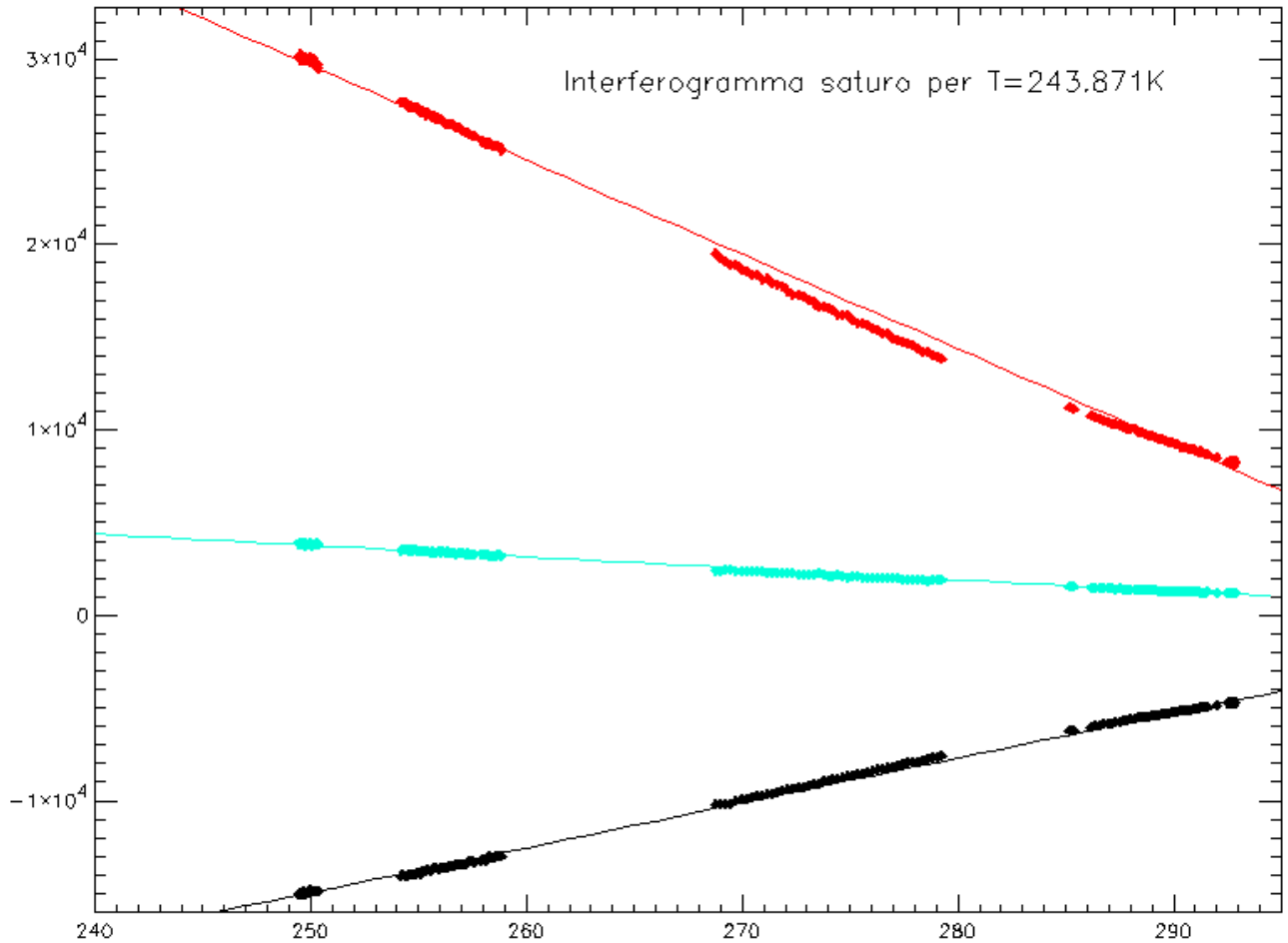


**Figure 54** – variation of the interferogram peak (red), two minima (black), and two maxima (light blue) with a decreasing temperature. Horizontal scale is T in Kelvin, Vertical scale is the peak of the symmetrized interferogram value.

Let  $I(\nu, T, \gamma) = \text{Re } s(\nu, T, \gamma) * S(\nu)$  be the measurement with  $\text{Re } s$  the responsivity of the instrument and  $S$  the source.  $\nu$  is the wavenumber  $T$  the temperature and  $\gamma$  the gain factor. We have seen that the gain factor is a multiplicative constant, therefore we have :

$$I(\nu, T, \gamma) = \text{Re } s(\nu, T, \gamma) * S(\nu) = \text{Re } s(\nu, T) * \gamma * S(\nu)$$

We assume that the responsivity  $\text{Re } s(\nu, T)$  can be written as  $F(T, T_0) * \text{Re } s(\nu, T_0)$ . This is justified by the linear behaviour seen in the figure above. The interferogram peak can be written as :

$$\Gamma(T, \gamma) = \int \gamma * F(T, T_0) * \text{Re } s(\nu, T_0) * N(S) * S(\nu) * d\nu$$

With  $N(S)$  we have indicated the non linearity function seen as a function of the source intensity : The source, as seen by the detector is lower than reality. The interferogram peak is function of temperature of the detector and of the gain factor. We can write:

$$\Gamma(T, \gamma) = \gamma * F(T, T_0) * \int \text{Re } s(\nu, T_0) * N(S) * S(\nu) d(\nu) = \gamma * F(T, T_0) * \Gamma(T_0)$$

Which gives :

$$\frac{\Gamma(T, \gamma)}{\gamma * \Gamma(T_0)} = F(T, T_0)$$

This function must be linear and at  $T_0$  for gain 1 must be 1. The function

$$\gamma * F(T, T_0)$$

describes the changing of the responsivity of the SW channel with gain and with temperature.

Note that the questions to be investigated are :

1 - is the non linearity behaviour of the detector the same at different temperatures?

2 - is the responsivity increase with decreasing temperature the same for the linear part and for the non linear regime ?

3 - is the spectral shape the same at different temperatures?

4 - is the gain factor the same at different temperatures?

5 - is the description given above for  $f(t, t_0)$  correct and can we predict the increase of the responsivity at different temperatures, in particular at 200 kelvin?

One of the measurements done in thermovacuum was to take the spectrum of the SW channel internal calibration lamp while the cold finger of the SW detector was being cooled. The observed spectra are plotted in figure 55. The spectra show that responsivity increases with decreasing temperature and that the spectral shape is essentially kept. Small changes are observed at the edge of the wavenumber range covered. This can be seen by taking the ratio of the last spectrum divided by the first spectrum, as shown in figure 56. Note that the ratio has an increase by a factor 10 toward the 2000  $\text{cm}^{-1}$ , this is due to the fact that the peak of the responsivity of the detector moves toward lower wavenumbers with decreasing temperatures, while it increases in value, therefore the ratio low temperature divided high temperature spectra, like fig 56, shows a larger values toward 2000  $\text{cm}^{-1}$ .

### **ANSWER 3 - THE SPECTRAL SHAPE IS THE SAME IN MOST WAVENUMBER RANGE, BUT MAY DEVIATE AT THE EXTREME EDGES.**

In figure 54 we have seen that the peak of the interferogram increases linearly at decreasing temperature of the detector. This can be seen also if we integrate the spectrum of the sequences of figure 55 from 3000 to 6000  $\text{cm}^{-1}$  and plot the value of the integral as function of temperature. We obtain figure 57 that gives the increase of the SW channel responsivity with decreasing temperature. In the figure the value of the increase has been fixed at 1 for temperature of 290 Kelvin. This figure gives essentially the function  $F(T, T_0)$  : we see it is linear and its best fit is :

$$F = a - b * T = 20.3 - 0.066666 T \quad \text{for } T=290, F= 1 \quad \text{for } T=200 \quad F= 6.968$$

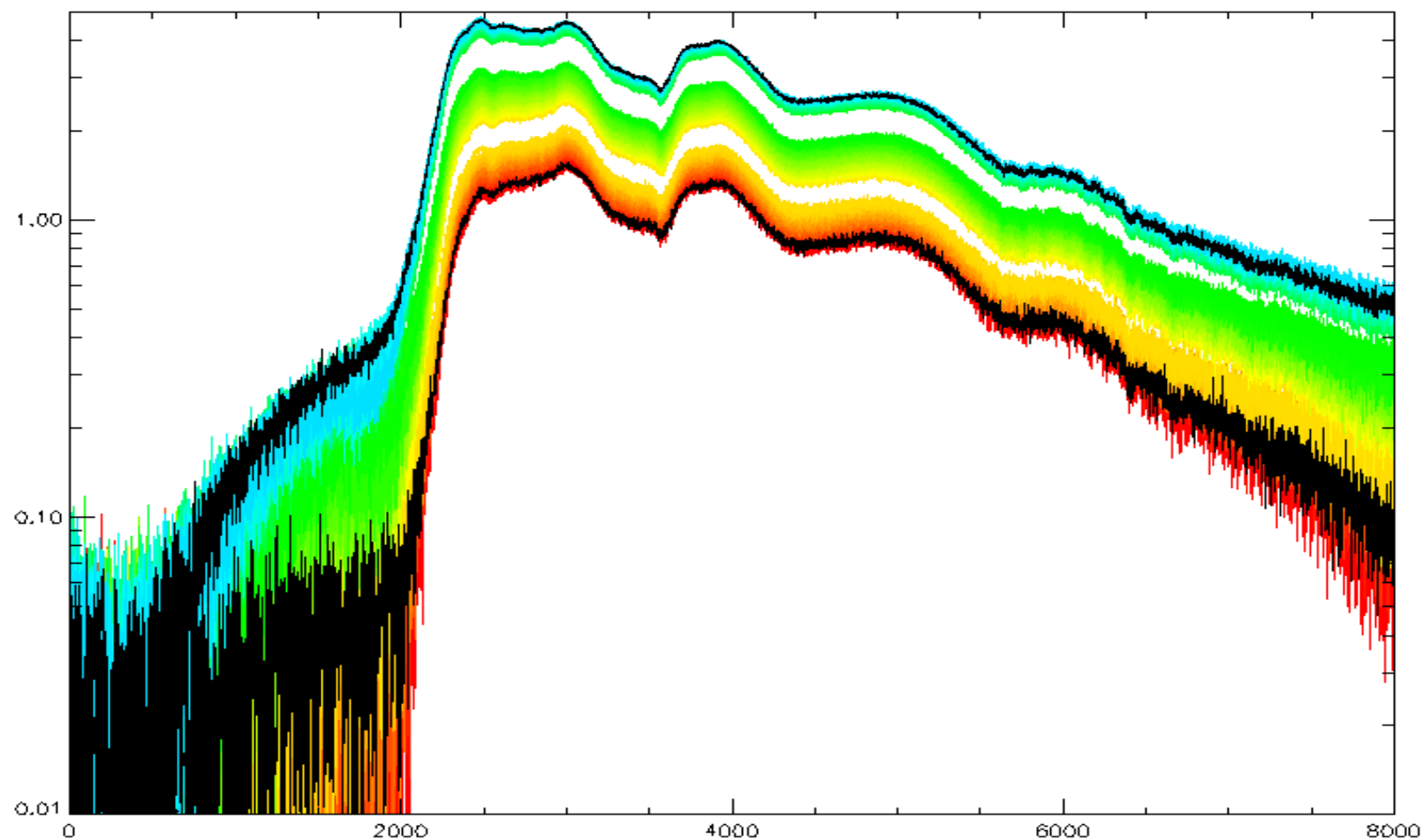


**Figure 55** – Sequence of spectra of the internal calibration lamp while the SW detector was being cooled. The temperature decreased from 293 down to 250 Kelvin. Data are from 3 files.

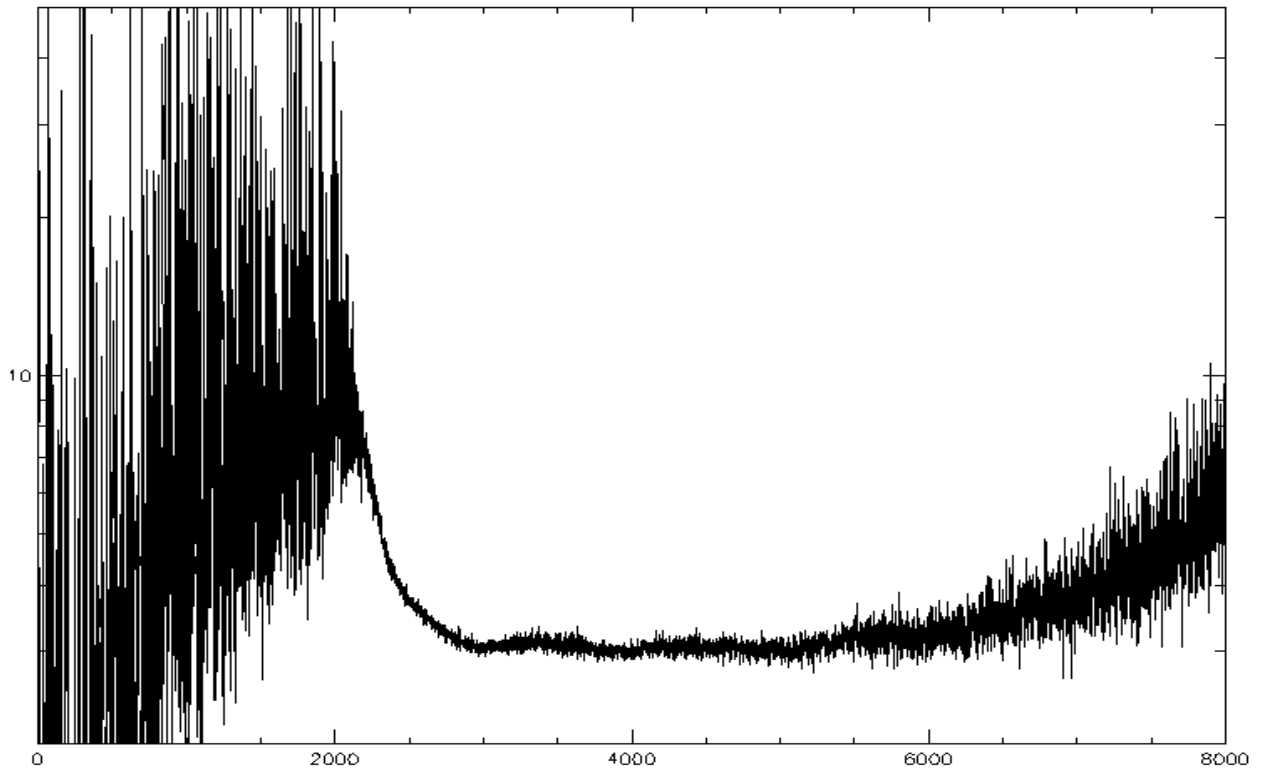


**Figure 56** – Ratio of the last spectrum of the sequences shown in figure 50, divided by the first spectrum of the first sequence. On average the ratio is constant at a value close to 3.

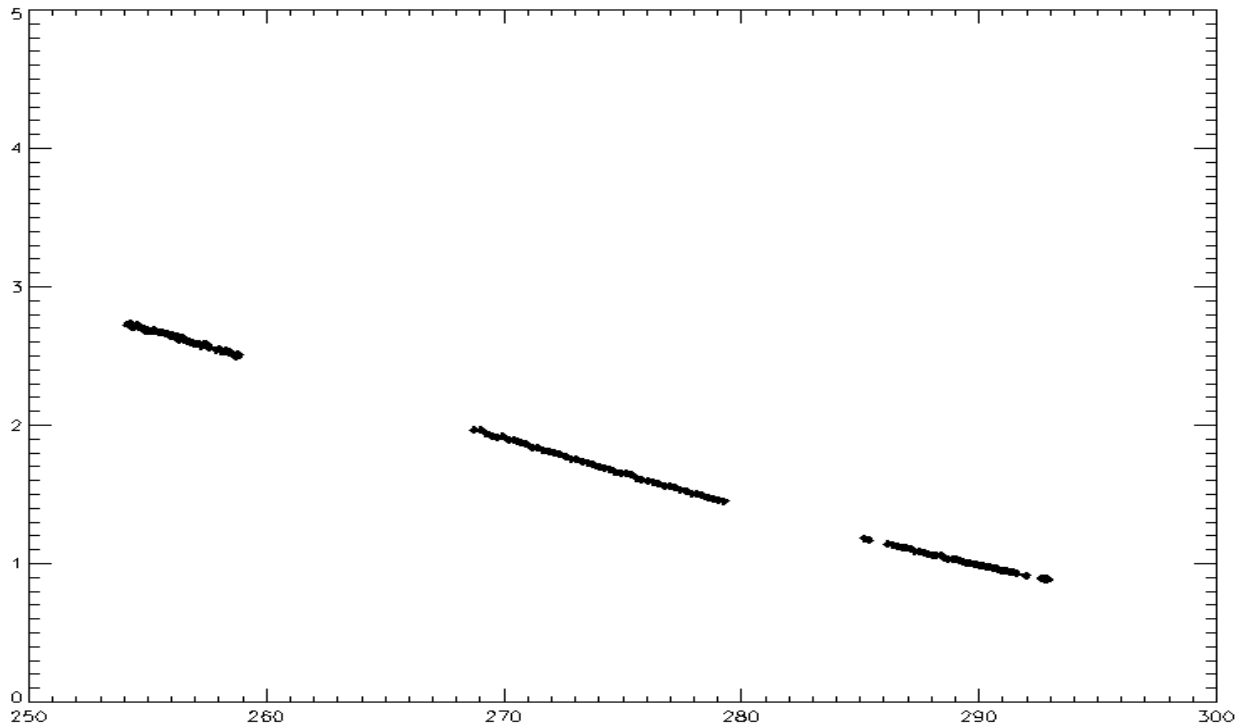


**Figure 57** – Increase of responsivity of the SW detector as function of temperature. It is plotted the ratio  $I(T)$  equivalent to interferogram peak at temperature  $T$  divided by  $I(T_0)$  equivalent to the interferogram peak at temperature  $T_0 = 290$  Kelvin, versus temperature.

Before making any conclusion, we remind that the previous study has been made using the internal calibration lamp which has a very intense interferogram peak, in other words it is not working in the linear regime of the detector.

Is the description given above for  $f(t, t_0)$  correct and can we predict the increase of the responsivity at different temperatures, in particular at 200 kelvin?

It seems that the  $f(t, t_0)$  has a linear form and that the description given above is partially correct. the responsivity increase at 200 kelvin is very close to 7 for the internal calibration lamp : this is a strongly non linear regime for the detector .

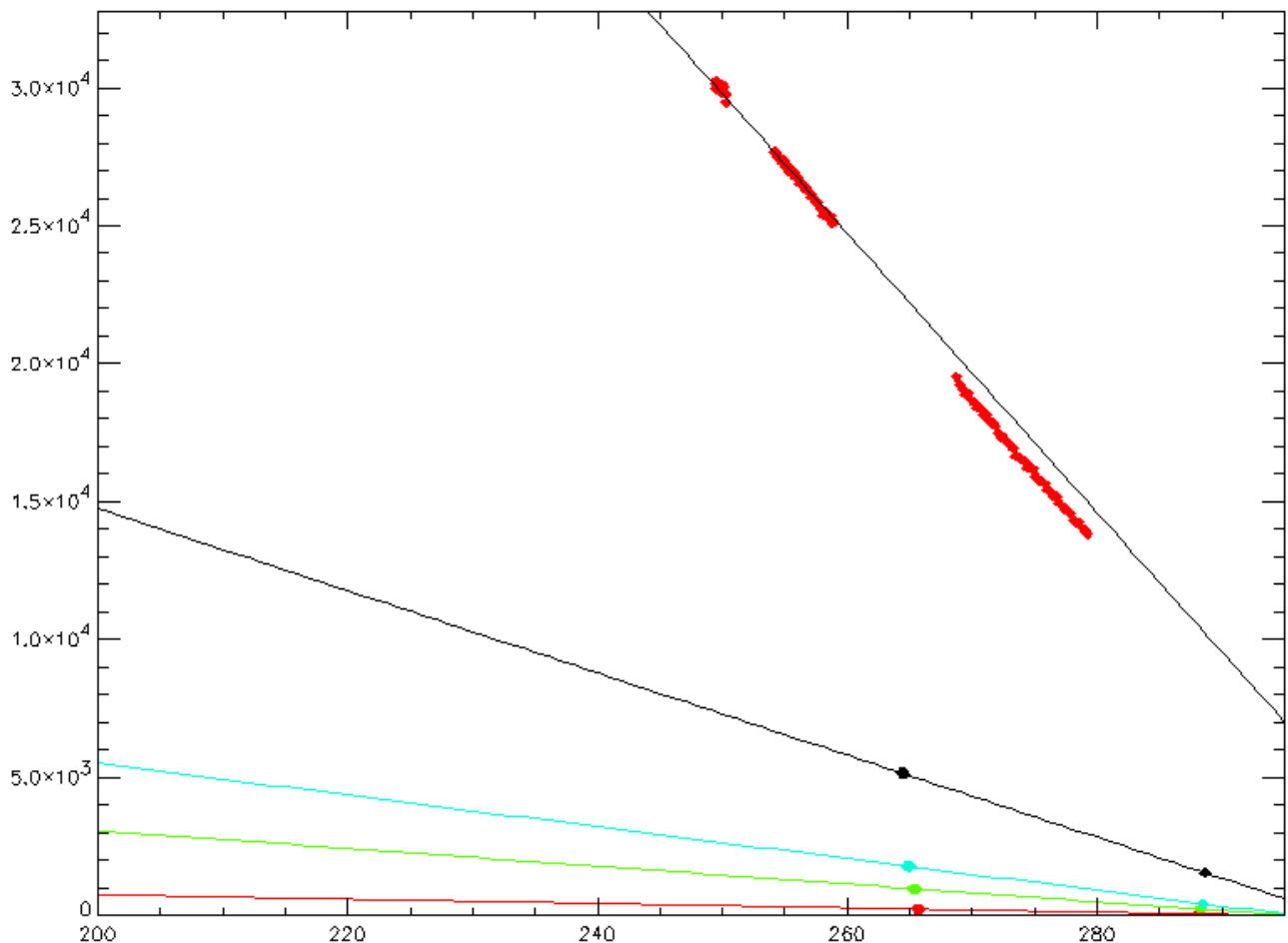


**Figure 58** - Responsivity increase at decreasing temperature. Internal calibration lamp measurements on top, integrating sphere measurements for intensities 100, 500, 1000, 5000 feetlamberts at temperatures 287 and 266 Kelvin. These are the observed interferogram peaks.

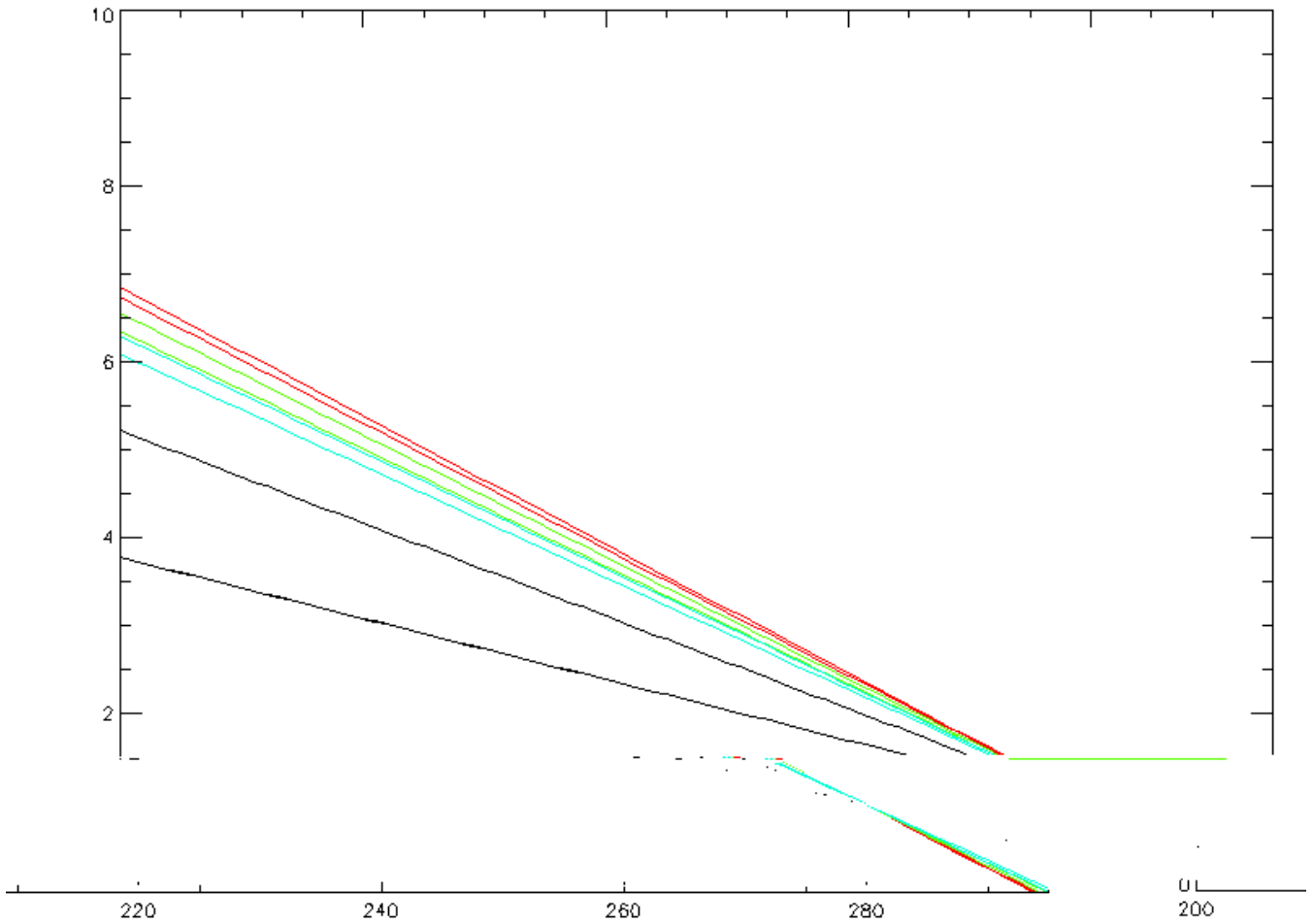


**Figure 59** - Responsivity increase at decreasing temperature. The linear best fits of the previous figure have been normalised at 1 for temperature of 280 Kelvin. Internal calibration lamp, integrating sphere measurements for intensities 100, 500, 1000, 5000 footlamberts at gain factors 2 and 4 are used. The black lines are for footlamberts 5000. One line is perfectly over the internal calibration lamp line.

To verify the behaviour of the responsivity as function of decreasing temperature we can use measurements made in thermovac on January 8, 10, and 21, 2002. Figure 58 shows the peaks of the observed interferograms for the linear and for the nonlinear part. Figure 59 shows the fitting lines but normalised at 1 at 280 Kelvin. The result show that indeed the responsivity in the linear part increases by a factor 7 going from 280 to 200 Kelvin.

**ANSWER 5:** The description given previously for the responsivity behaviour with temperature is in first approximation correct and we can predict the increase of responsivity with temperature decreasing below 280 kelvin

$$R = 22 - 0.075 * T$$

**ANSWER 2:** The responsivity increase with decreasing temperature is lower in the nonlinear part of the sw detector, but not substantially lower.



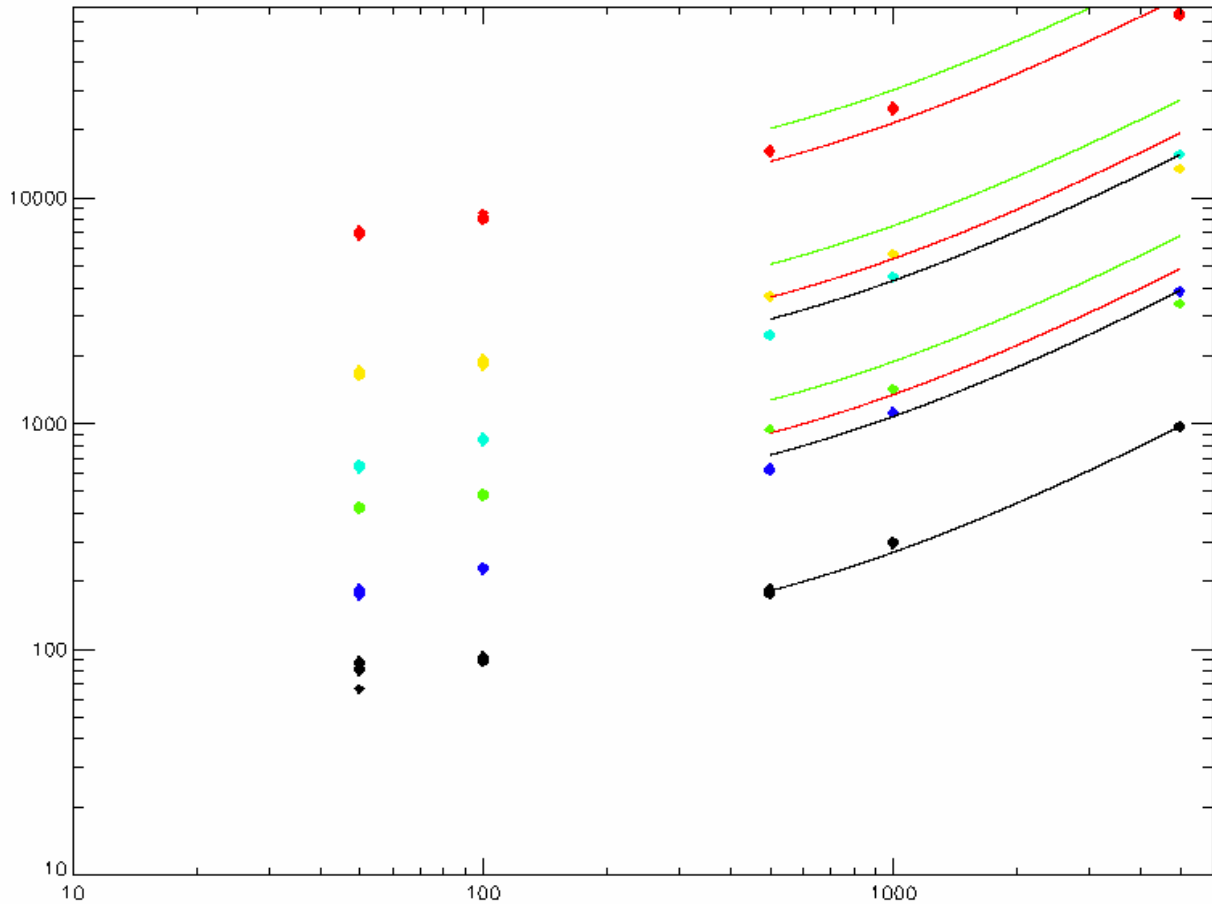


**Figure 61** - Linearity and gain factors : footlamberts versus interferogram peak : black, bleu and cyan (gain 0,2,4) at room temperature, green, yellow and red, (gain 0,2,4) at 260 kelvin. Note that 50 and 100 footlamberts are dominated by the thermal emissivity of the vacuum chamber window.

In order to study the gain factors at low temperature, we have plotted the interferogram peaks for different gains and for different temperatures in figure 61 as we have done in figure 52. The data are from the integrating sphere at thermovac. The contribution of the chamber window is dominating the measurements at 50 and 100 footlamberts, so we shall ignore these measurements. From the others we see that the gain 0,2,4 have gain factors 1, 4, and 16 both at room temperature (288) and at 266 kelvin.

**ANSWER 4:** The gain factor is the same at different temperatures.

This fact is better shown in figure 62, where the same data are plotted on a linear scale.



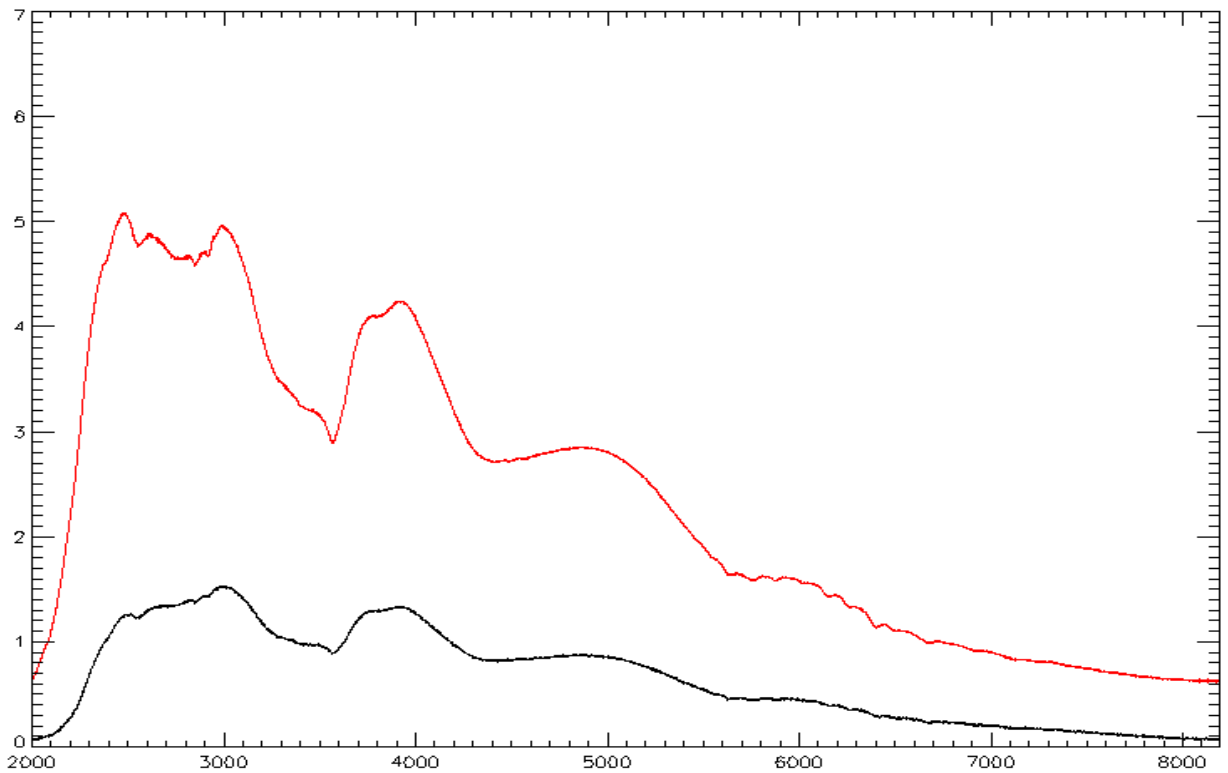


**Figure 63** – Average spectrum of the cold (red) and warm internal calibration lamp.

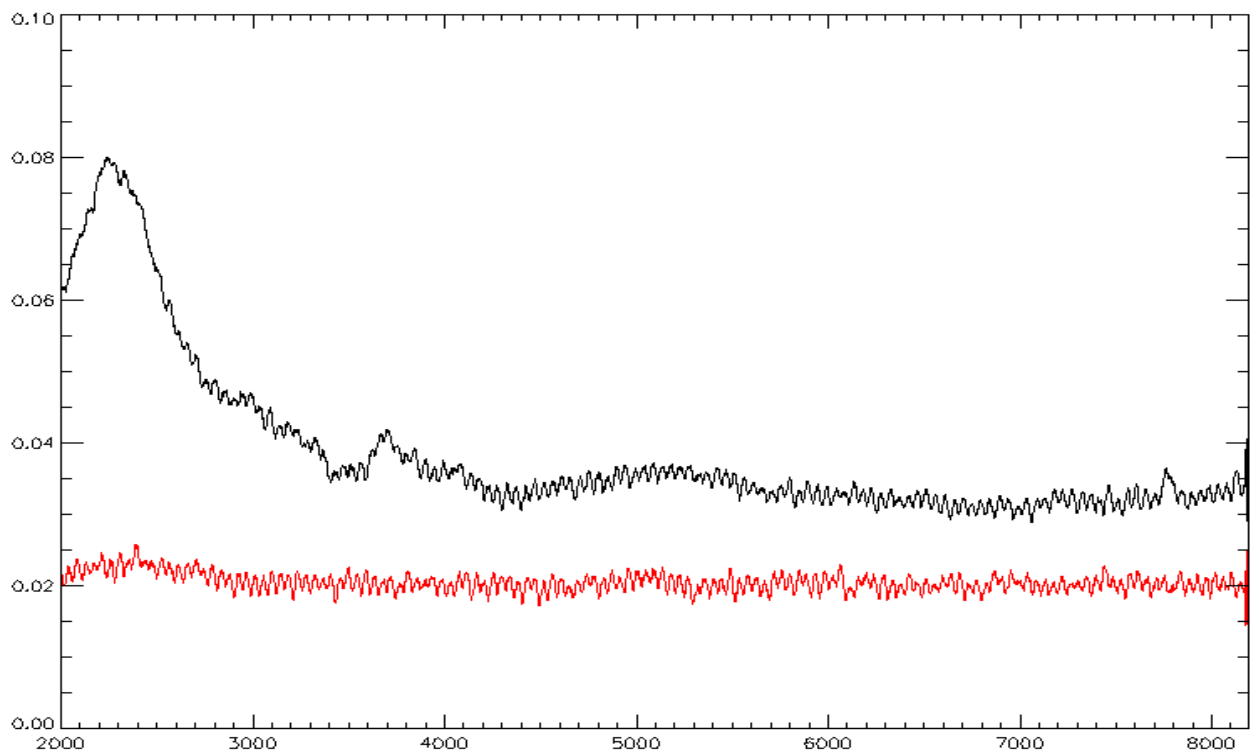


**Figure 64** – Standard deviation for the measurements of the previous figure.

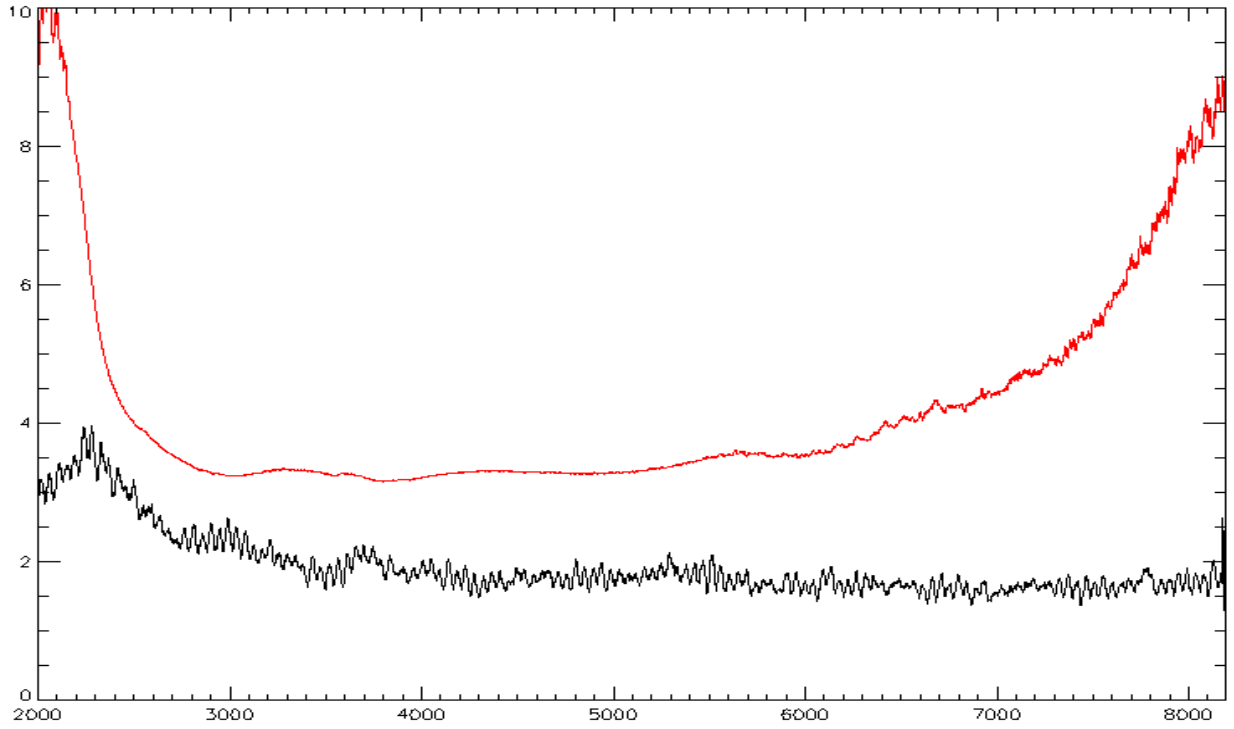


Figure 65 – Ratios between the signals (red curve) and between the noises (black).

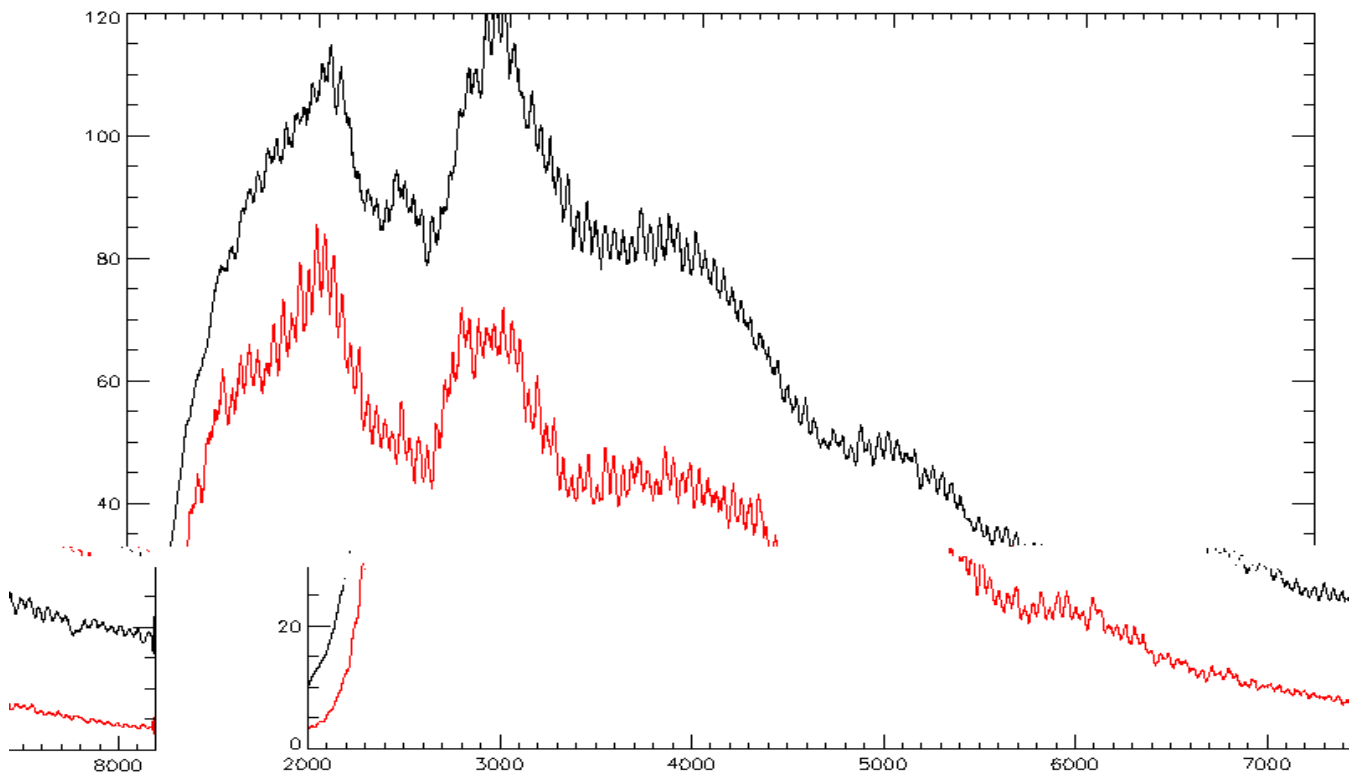
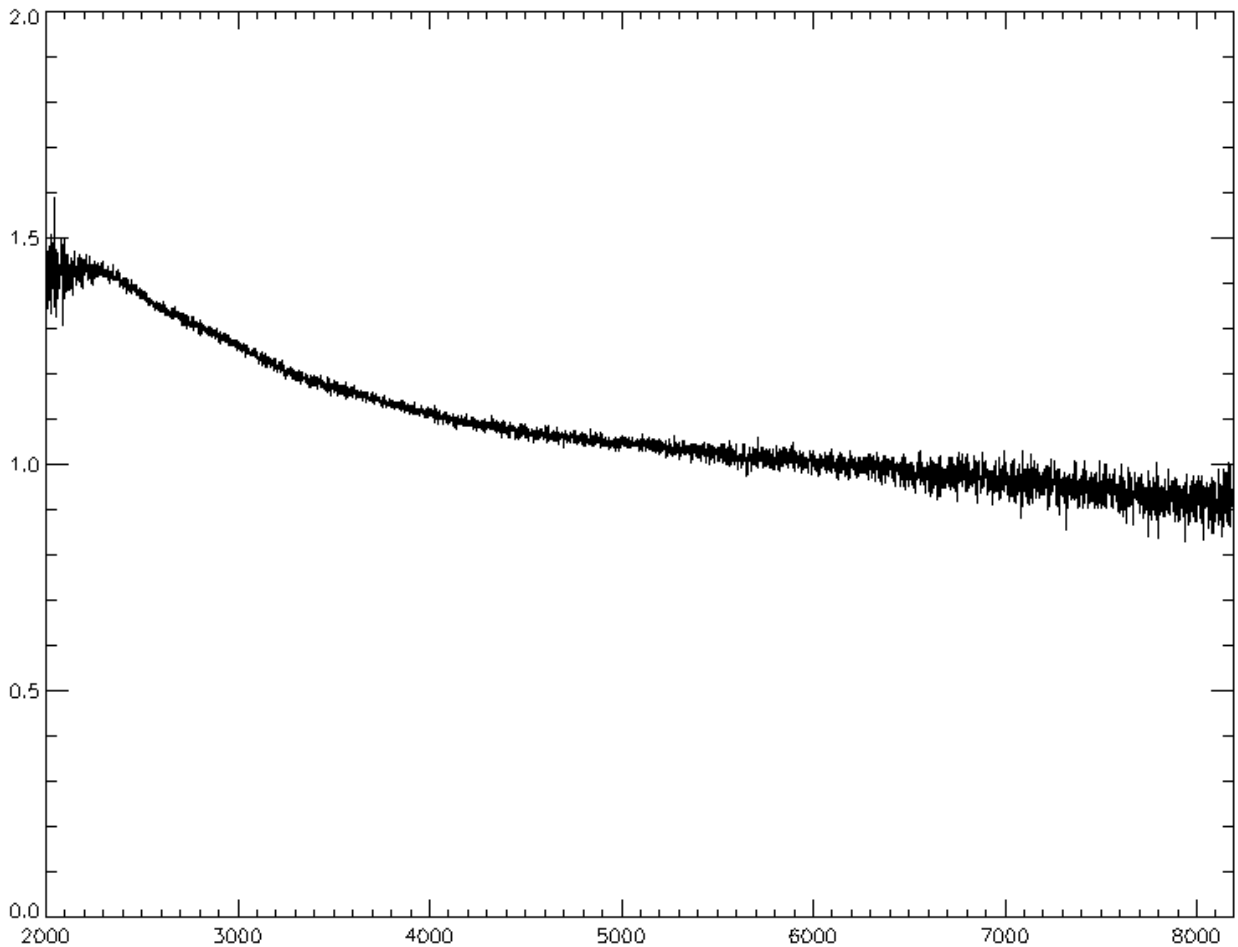


Figure 66 – SNR at room temperature (red curve) and at 250 Kelvin.

## 5.12 – SW CHANNEL FILTER SHAPE

The SW channel has the possibility to filter the spectral shape in order to attenuate the importance of the thermal contribution. This is tested with the so called Test 5, when we reoatte all the gain factors for the SW and LW channel. The gain rotation is done first without the filter, then with the filter. Test 5 was activated with the SW detector at temperature 250 Kelvin. There is no reason to believe that the filter shape should depend on the detector temperature. The filter shape is shown in figure 67 as ratio of gain 0 internal calibration lamp without the filter and with the filter. The spectrum is modified by 50 % only as the filter is a linear filter.



**Figure 67** – SW channel filter : Internal calibration lamp without filter divided the same spectrum with filter applied. Detector temperature 250 K.

### 5.13 SUMMARY OF THE TERMAL/GAIN BEHAVIOUR

In order to summarise the results found and described above, we shall make the following considerations :

Having defined and studied the Responsivity  $R_o$  and Noise  $N_o$  (not NER but noise) at room temperature and gain zero, we discover that increasing gain increases the signal by a known factor and also increases the noise, but by a smaller factor .In particular going from gain zero to gain 3 the SNR increases by a factor 5 (the signal increases by 8 and noise by 1.6). Linearity is kept with increasing gain : in other words if the instrument is in a linear region for gain zero (i.e. peak of the interferogram lower than 1600 DN), the amplification does not bring the experiment in the non linear regime .In different words we may say that the experiment is in the linear regime when the peak of the interferogram is:

<b>Gain</b>		<b>0</b>	<b>1</b>	<b>2</b>	<b>3</b>	<b>4</b>	<b>5</b>	<b>6</b>	<b>7</b>
<b>Peak of interferogram</b>									
<b>Below 1600 x</b>		<b>1</b>	<b>2</b>	<b>4</b>	<b>8</b>	<b>16</b>	<b>32</b>	<b>64</b>	<b>128</b>

On the contrary to decrease the temperature means to increase the responsivity ad therefore to get in the non linear regime. We have seen that at gain zero, to go from 290 Kelvin to 250 Kelvin means to increase responsivity by a factor 4. The non linearity will still start at 1600 DN, as before, so can be reached with sources of smaller intensity.

Extrapolating the measurements at room temperature and with the cooled detector to the conditions we will have in space at Mars, we can conclude that responsivity at 200K will be 7 times the  $R_o$ . At the same time the noise will be 3.7 times larger. If we are going to use gain 3, we shall have a signal  $8 \times 7$  times larger than the signal at room temperature gain zero, and a noise which is going to be  $3.7 \times 1.6$  times larger. The SNR at mars can be almost a factor 10 larger than at gain zero at room temperature. Obviously the problem will be to make sure we are not saturating the interferogram and that we are possibly in the linear regime or very close to it.

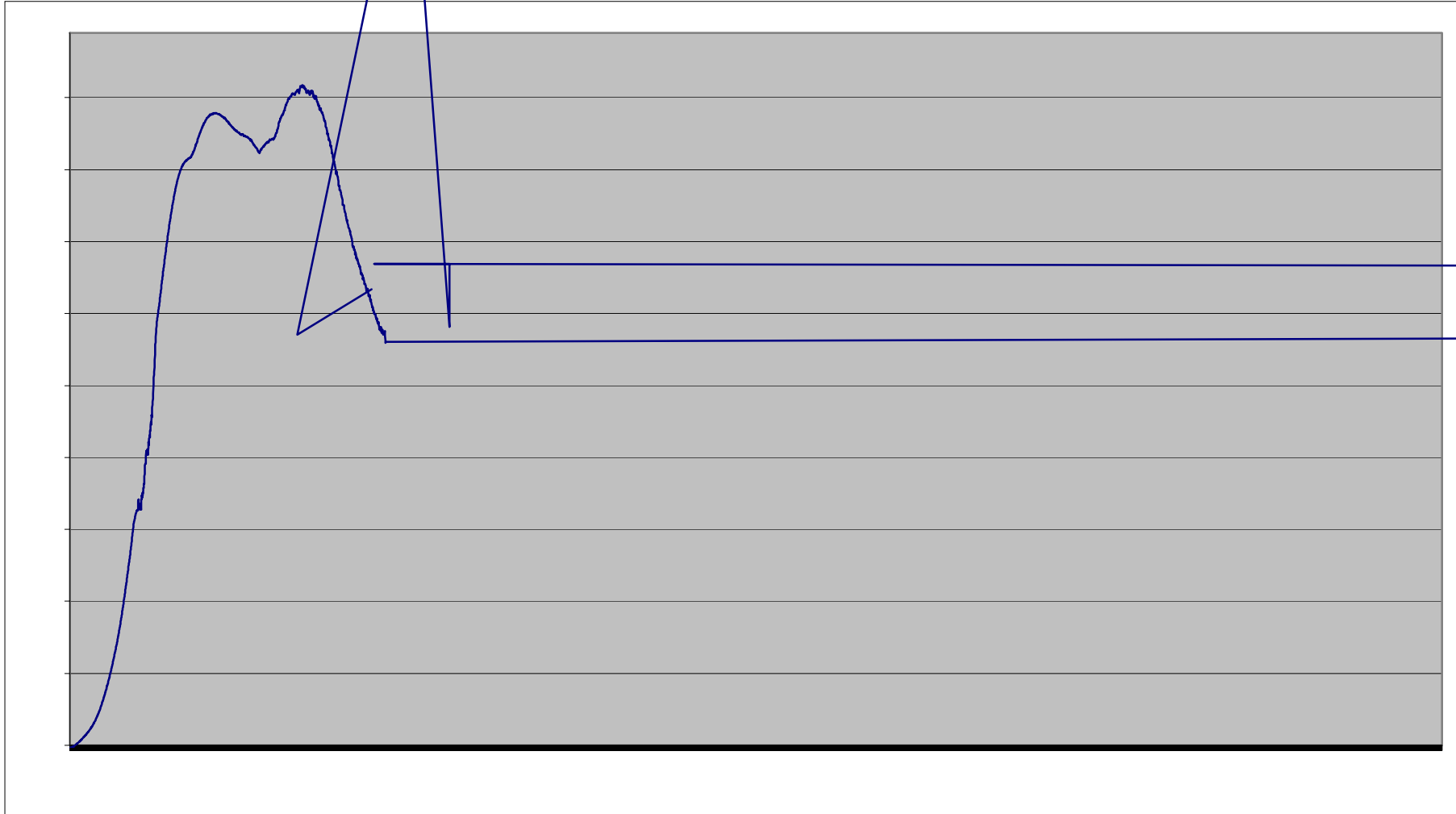
In figure 68 the responsivity of the SW channel for detector temperature of 200 K and corrected for the atmosphere.



**PFS for Mars Express**  
December 2002

**PFS**  
INTERNAL NOTE  
CALIBRATION II  
Page 96

**P.I. Vittorio Formisano**  
**CNR IFSI**



Responsivity of th



SECTION II  
Page 97

CNR IFSI

Summary of SV

det



## 6- MONOCHROMATIC TRANSFER FUNCTION

To study the monochromatic transfer function of PFS, information very important, needed for the apodization procedure, to avoid misleading details in the spectra, we have taken many measurements of the mercury lamp. This lamp has indeed some monochromatic lines in the near IR. The measurements, therefore are valid for the SW channel. Unfortunately no single line is present in the LW channel wavenumber range, so it is not possible to do the same study for the LW channel.

During a sequence of measurements the laser diode temperature was always varying slowly, until, suddenly, it would change state, changing, consequently the wavelength. The average wavelength variation with temperature of the laser diode, essential for the correct transformation of the spectral channel number into wavenumber (cm<sup>-1</sup>), will be studied in the following. Here we study a small variation of the wavelength of the laser diode which goes together with a small variation of the laser temperature (see figure 69).

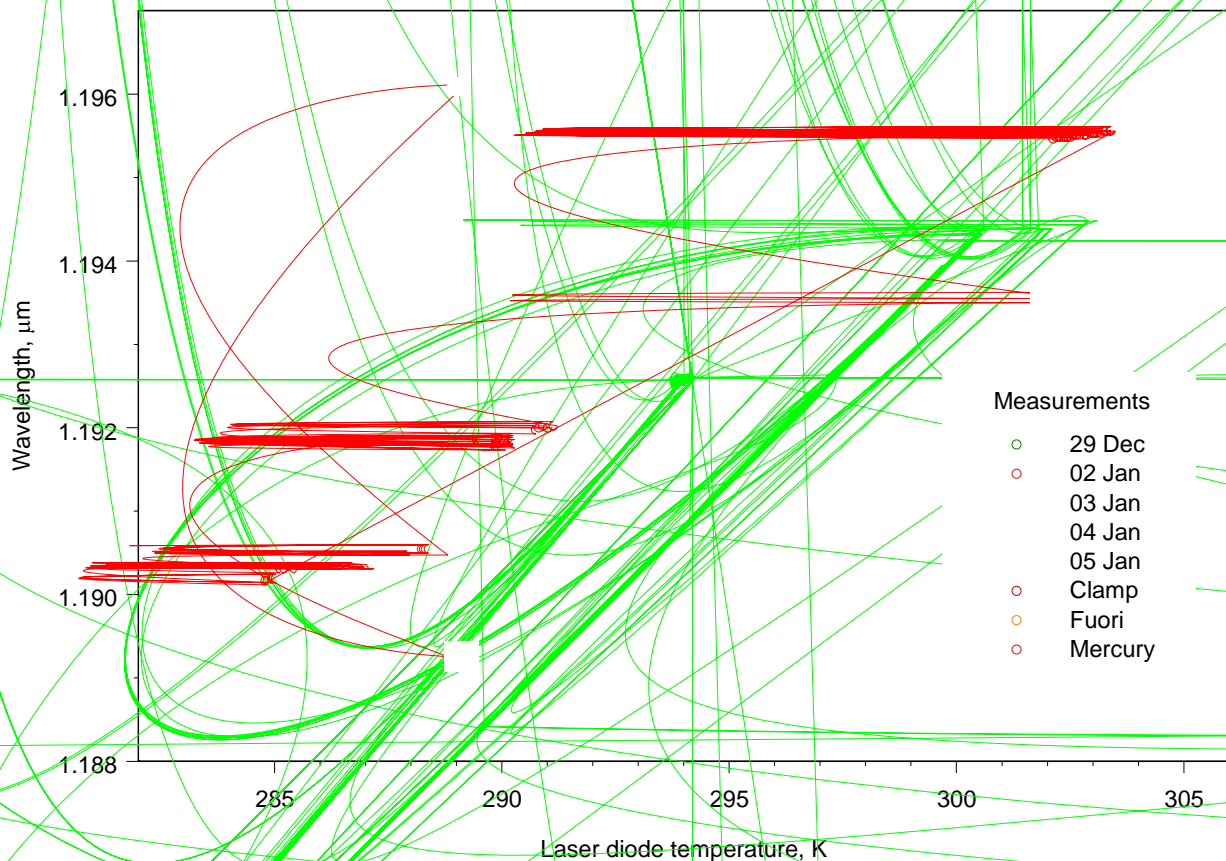


**Figure 69** – Laser diode wavelength variation with changing laser temperature.

The resulting monochromatic transfer function of the instrument, shown in figure 70, it appears to be almost the theoretical one, in the sense that goes to zero at slightly above  $\pm 1$ , namely at 1.2 cm<sup>-1</sup>. The apodised monochromatic transfer function of the instrument is shown in the bottom panel of figure 70.

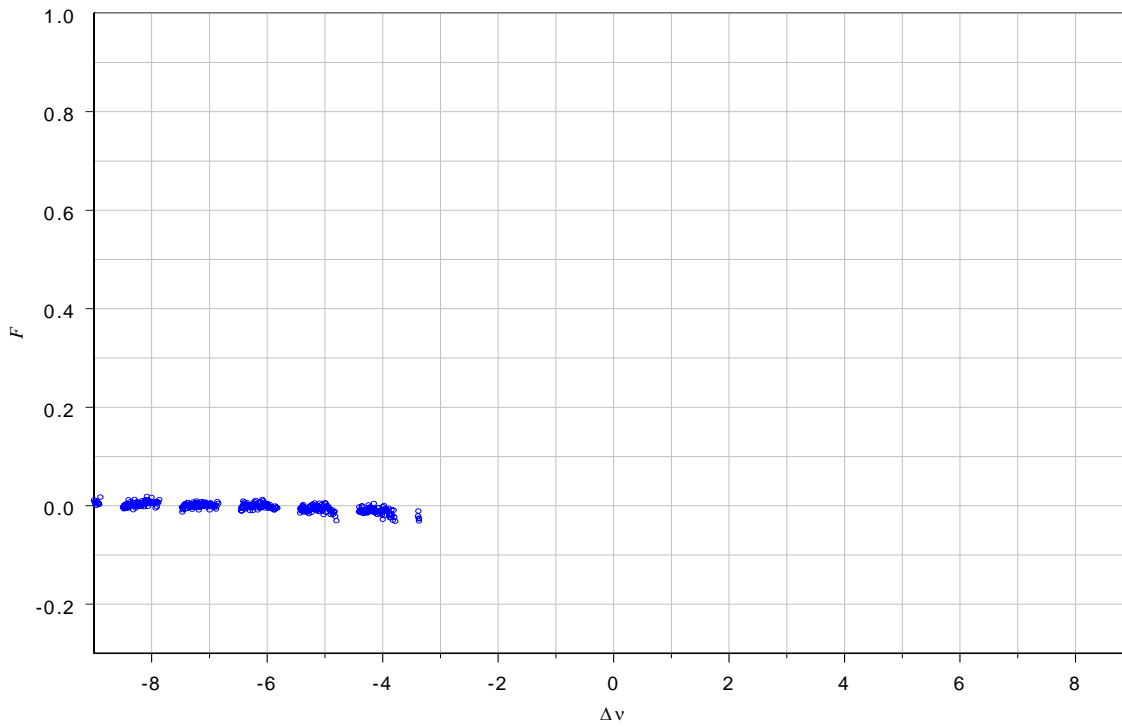
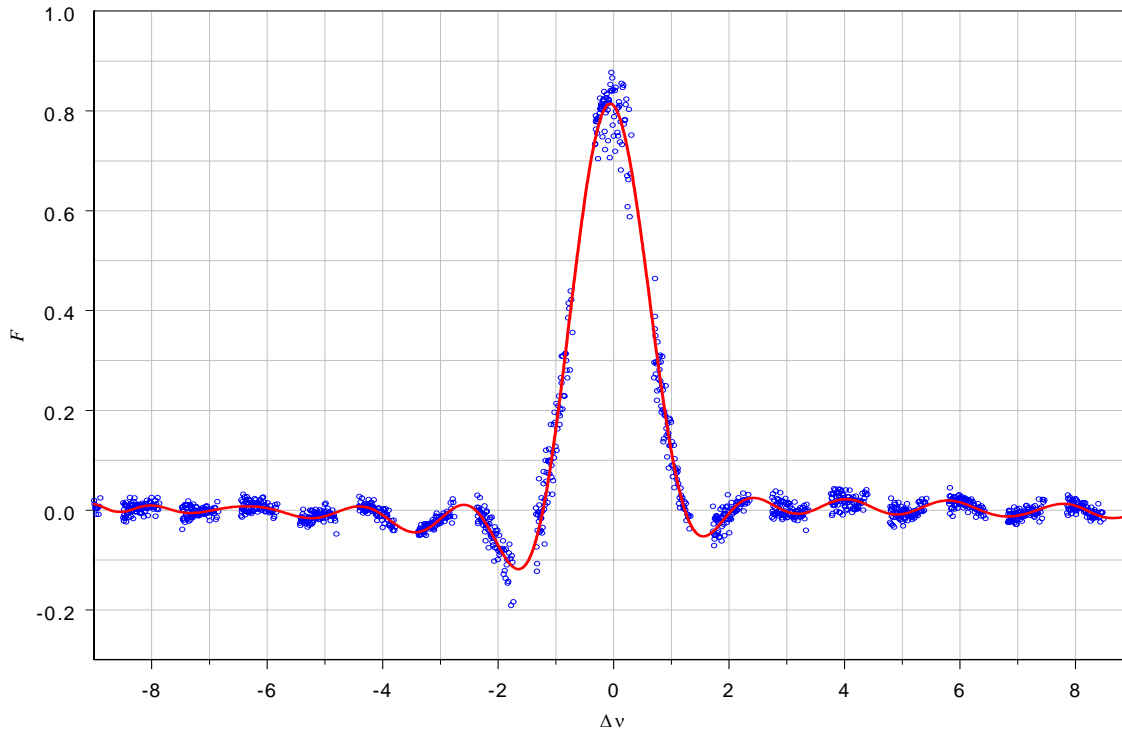


**Figure 70** - Top panel : monochromatic transfer function of the instrument. Bottom panel the same but apodised.

## 7 - LASER DIODE TEMPERATURE CALIBRATION

In order to compute the correct wavenumbers when computing FFT, we have to take into account the temperature of the laser diode. The two laser diodes have been calibrated and the temperature dependence is given below.

### SW CHANNEL LASER DIODE CALIBRATION

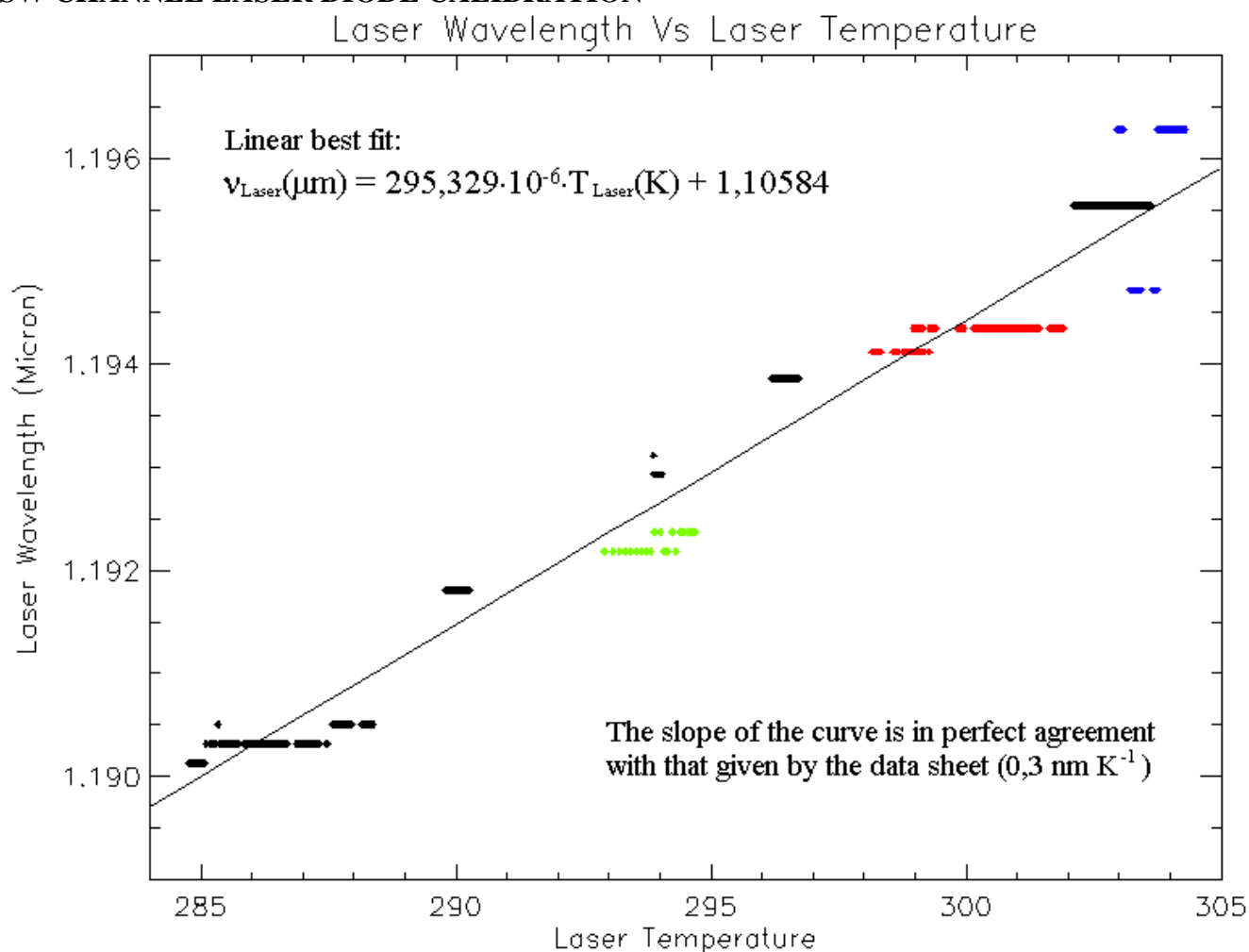


**Figure 71** - Wavelength of the laser diode as function of laser temperature, obtained by matching some real, well known line, either water or CO<sub>2</sub>. The linear best fit given in the figure has been used in all the calibration studies.

## LW CHANNEL LASER DIODE CALIBRATION

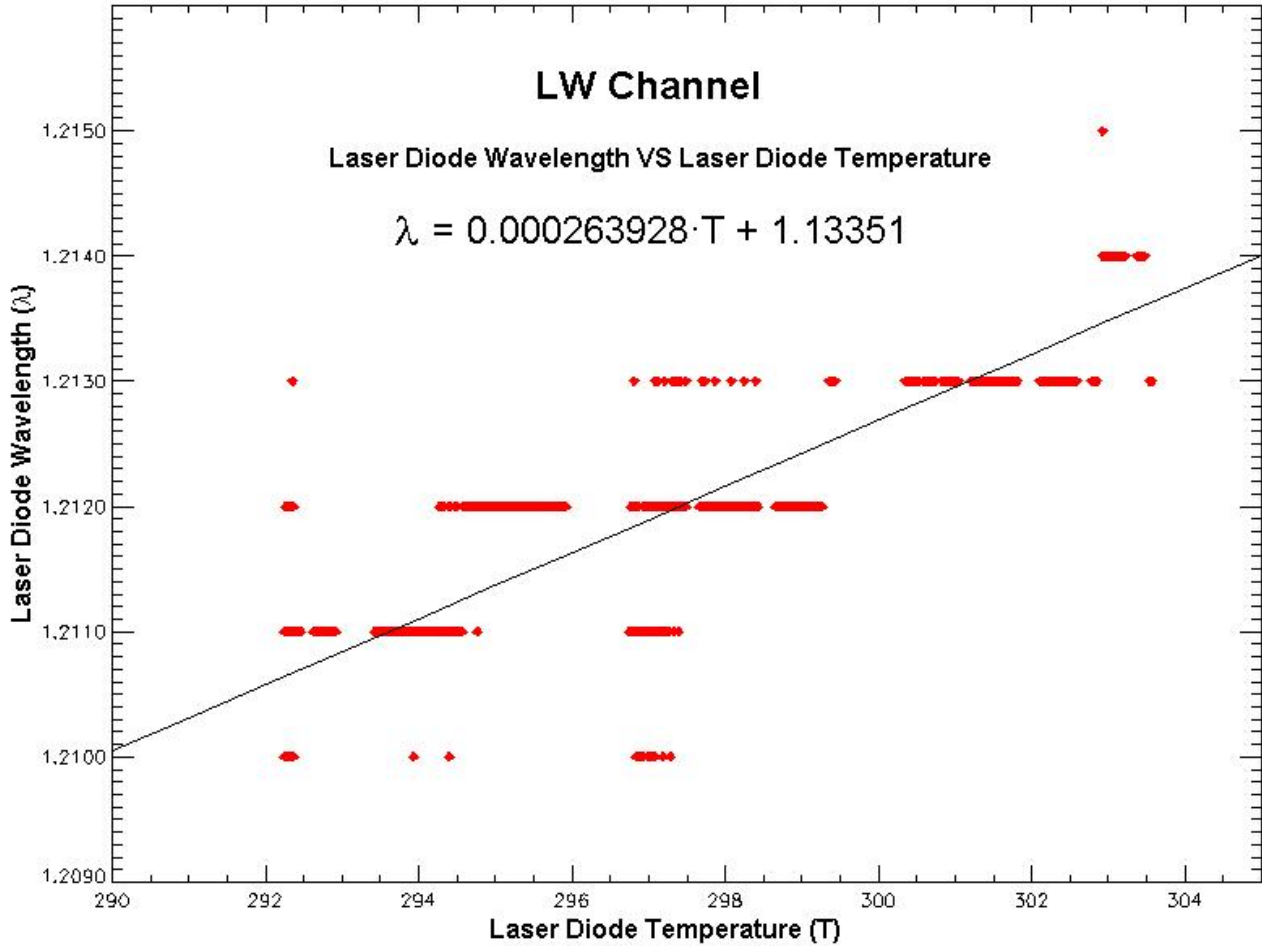


**Figure 72** – Wavelength of the LWC laser diode as function of laser temperature. The linear best fit given in the figure has been used in all the calibration studies .

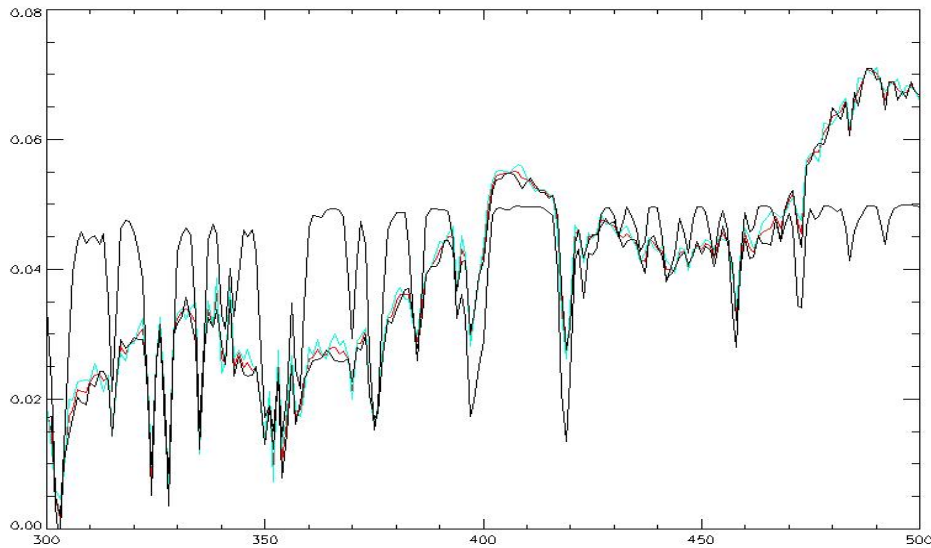


**Figure 73** - Water lines of LW channel demonstrating that the laser diode wavenumber calibration produces correct results. Black line is the synthetic spectrum, color lines are measurements. All the water lines are placed at the correct wavenumber.

## 8 - FIELD OF VIEW MEASUREMENTS

The Field of view of the instrument, as well as the orientations of optical axes of SWC and LWC, have been estimated observing the changes in the instrumental signal related to the motion of a stable point source in a plane parallel to module O wall. See Volume 1 for details of the experimental apparatus.

The ceramic element, an intense source covering the whole PFS wavenumber range, has been mounted on a computer controlled XY actuator. This device can move the source in a plane. The module O has been arranged in order to have the actuator's plane parallel to the instrument's wall hosting optical entrance, at a distance of 93 cm. The Scanner was removed for this set of measurements. All measurements have been acquired in laboratory at room temperature.

In Calibration Volume I it was reported how the measurements were taken.

The measurements have been studied from different point of view. First it was studied the FOV from the peak of the interferogram. This study, however can give non correct results. We show here, in figure 74 and 75, that the spectra observed were very different when the lamp was indeed in the FOV or when it was out of it. In theory we should see only noise when the lamp is not seen, but in practice, the walls of the laboratory room, with their temperature, different from the detector temperature, is also a source of radiation, and it is indeed seen by both the SW channel and the LW channel. It is evident also that it is relatively easy to clean the SW channel observations, so to get a clean FOV with high rejection factor (see figure 76). For the LW channel the situation is so that it is not possible to obtain a large rejection factor : see figure 77.

The measured FOV, as it results from the FWHM of the gaussians shown in figures 76 and 77 is : for the SW channel 1.6 degrees and for the LW channel 2.8 degrees. The two channels, however, are not completely overlapped, they overlap only partially. The displacement of the centres is of the order of 1.8 degrees. Note that these measurements are without the transfer function of the Scanner.

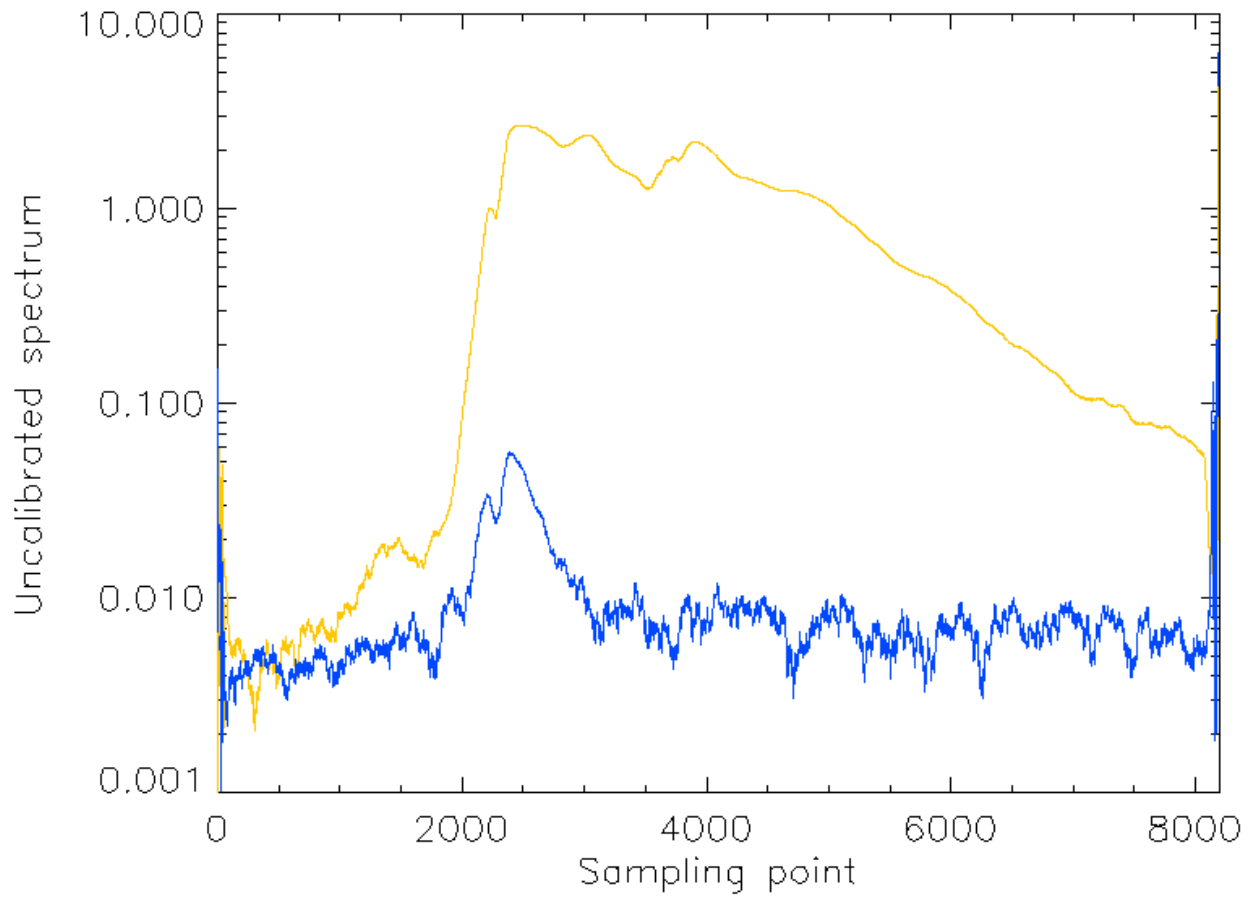


**Figure 74** – Observed spectrum for the SW channel FOV measurements. Yellow curve is observed when the ceramic element lamp is seen. blue spectrum is measured when the lamp is out of FOV.

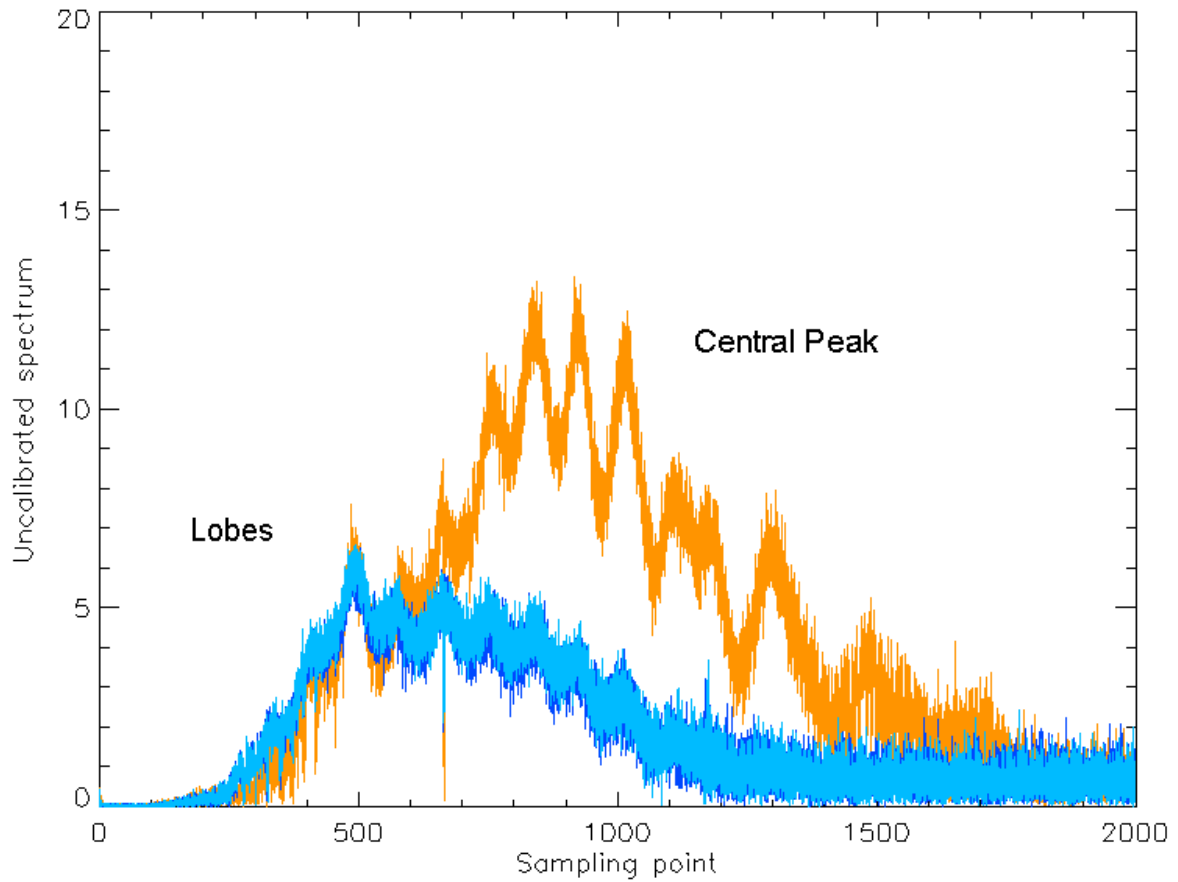


**Figure 75** – LW channel spectrum observed when the ceramic element lamp is in the FOV (yellow curve) and when it is out of the FOV (bleu curve). The ambient wall temperature is responsible for the observed BB spectrum (bleu) .

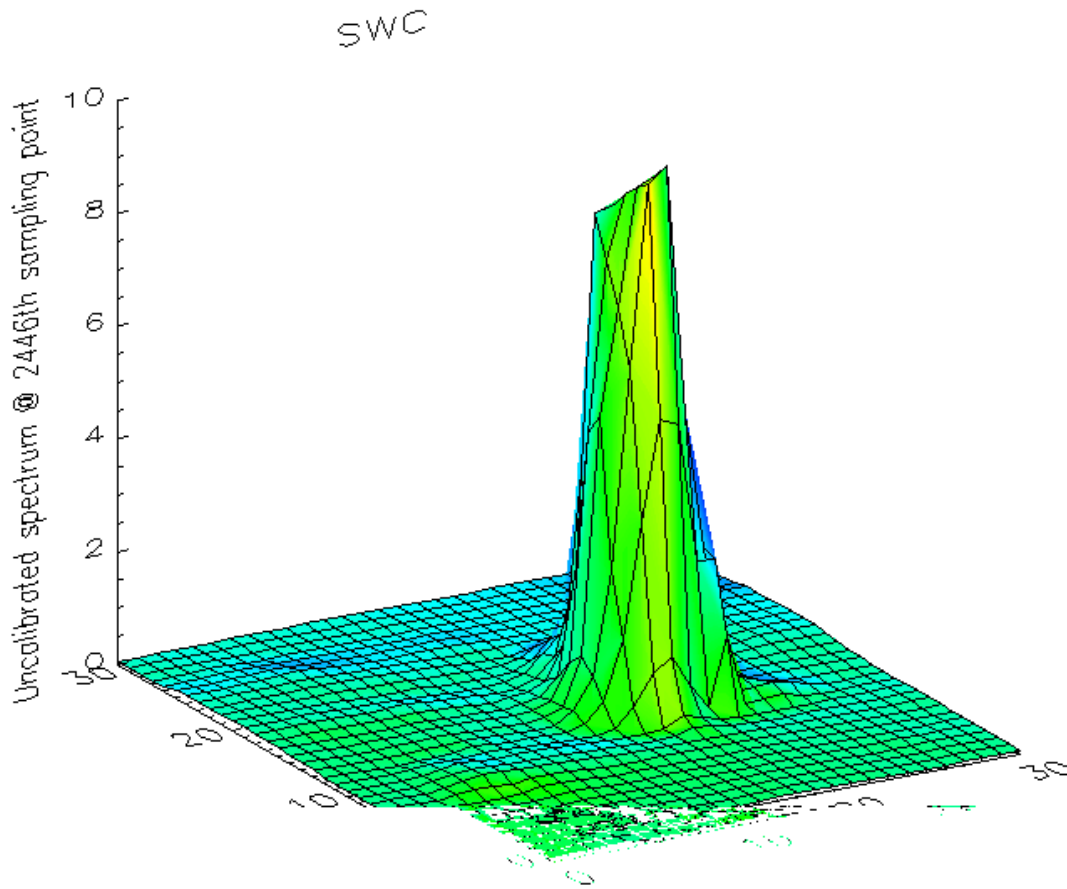


**Figure 76** – FOV measured of the SW channel.

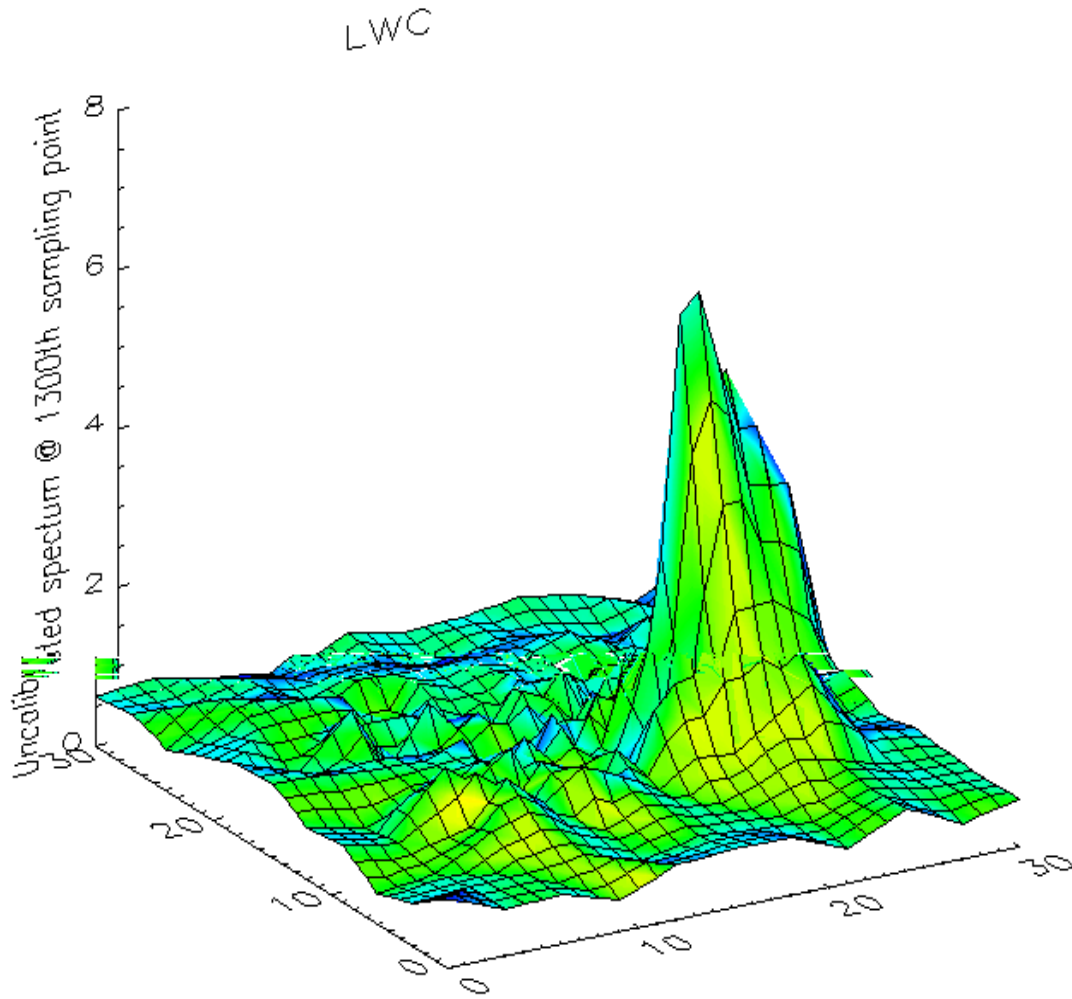
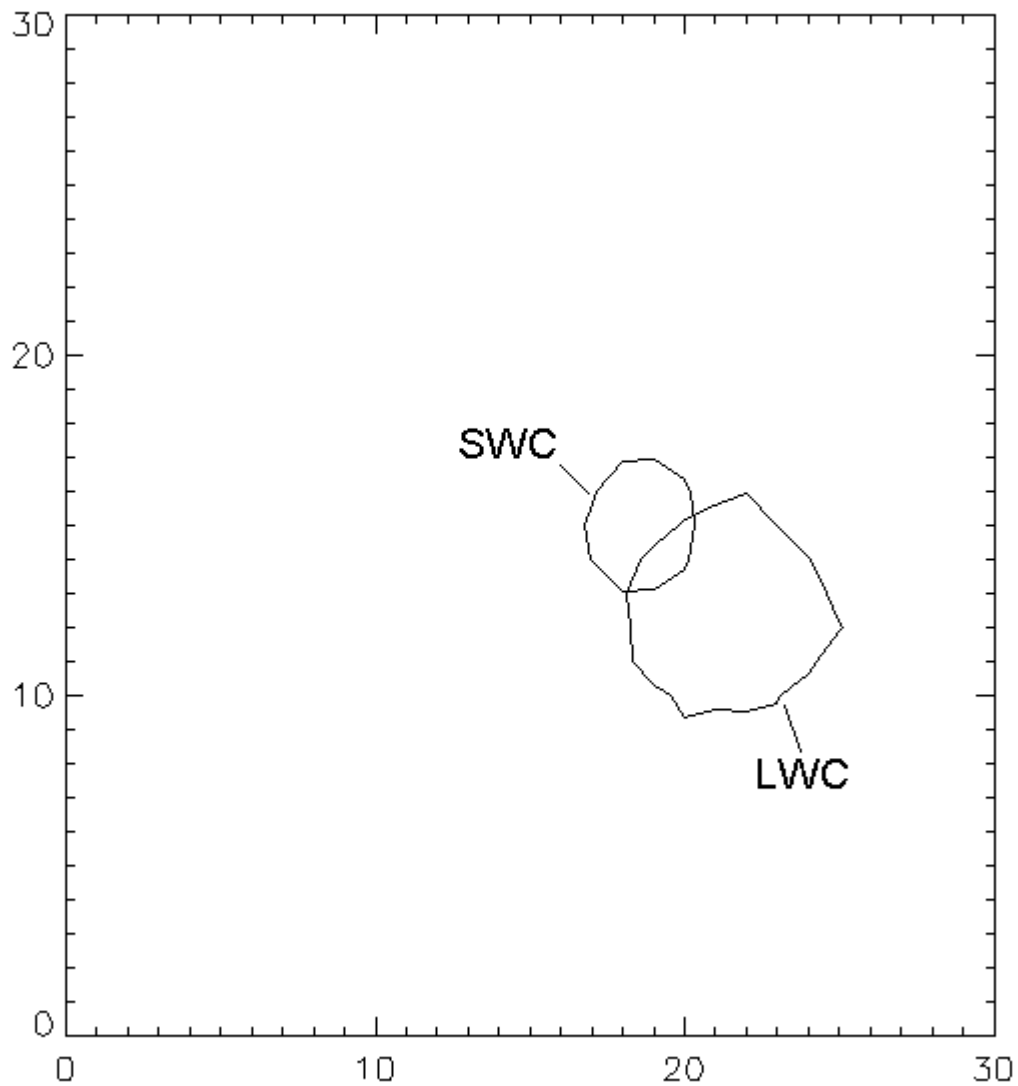
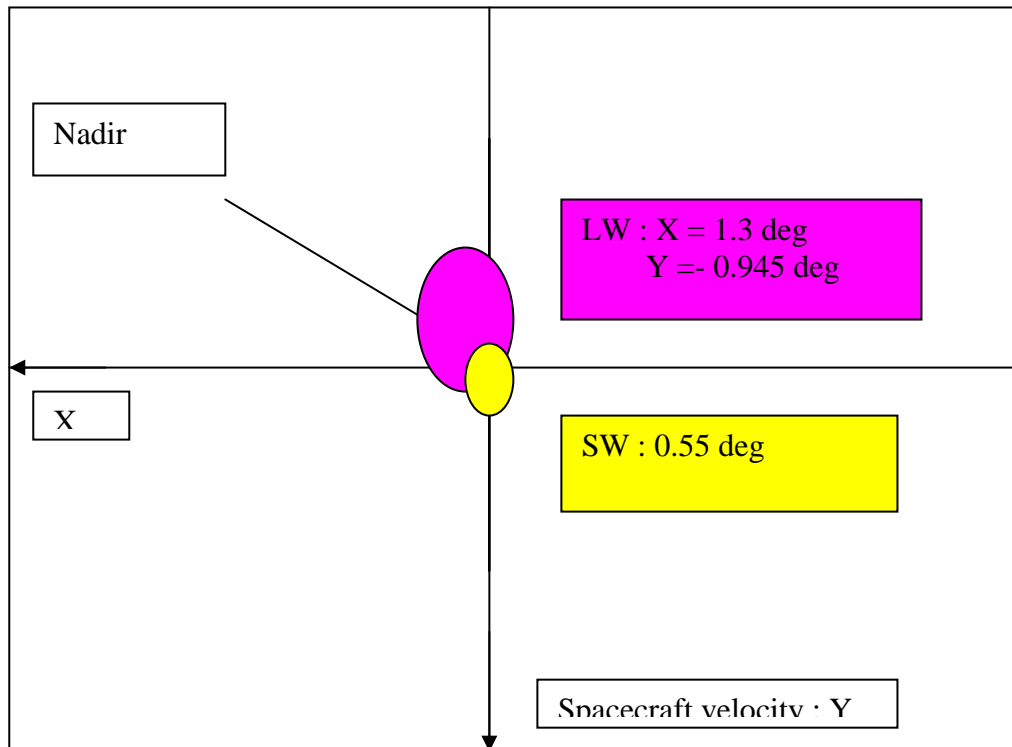


Figure 77 – LW channel FOV measured.



**Figure 78** – FWHM for both channels LW and SW channels: the SW is 1.7 degrees wide, while the LW is 2.8 degrees wide. Note the displacement of the two channels of 1.8 degrees. The two channels overlap only partially.



**Figure 79** – Location with respect to Nadir, of the FOV of the LW channel and of the SW channel.

The transfer function of the scanner has been measured and it results in a tilt of the FOV in the direction of motion of the spacecraft. The amount of this tilt is of 0.55 degrees.

It should be noted that there is also a cube mirror on the scanner and we have requested Astrium to measure the direction of the upper face of the mirror with respect to Nadir, but we do not have this measurement yet.

In figure 79 we have taken into account all the information available today, to see where PFS is looking with respect to the Nadir direction. Nadir happens to be in between the two channels : the SW is pointing in the direction of motion of the spacecraft by 0.5 degrees. The LW channel is pointing backward by 1.3, 0.9 degrees. In the figure the motion of the spacecraft during the measurement taking has been considered and the footprint has been elongated in the motion direction.

## 9 – MEASUREMENTS IN THE EARTH'S ATMOSPHERE

We show here some measurements taken in the Earth's atmosphere, in order to give an idea of the capabilities of PFS for atmospheric studies. All the measurements were done with the SW detector at room temperature.

### 9.1 - CO<sub>2</sub> AND WATER MAIN BANDS CHARACTERISTICS

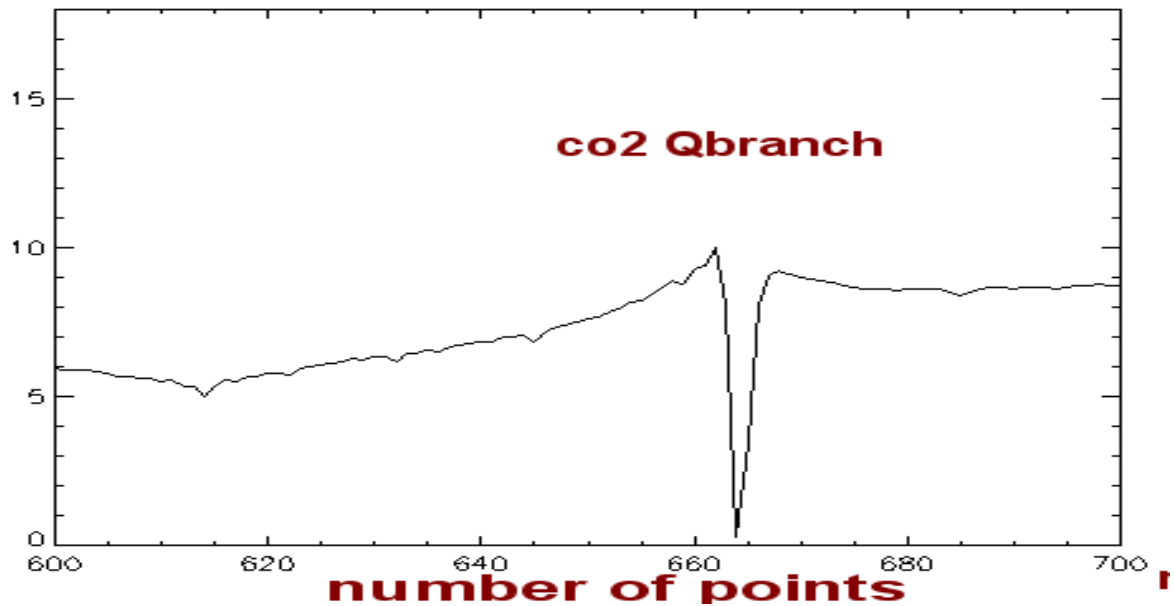


Figure 80 – CO<sub>2</sub> band at 15 microns : only the Q branch is seen.

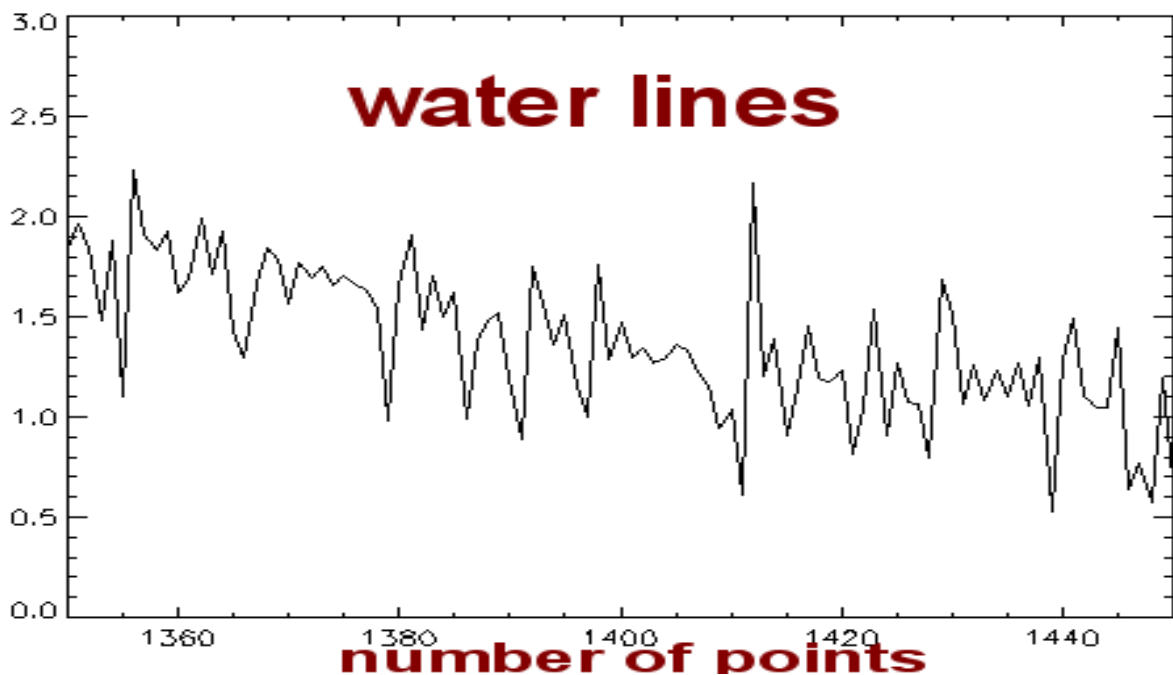
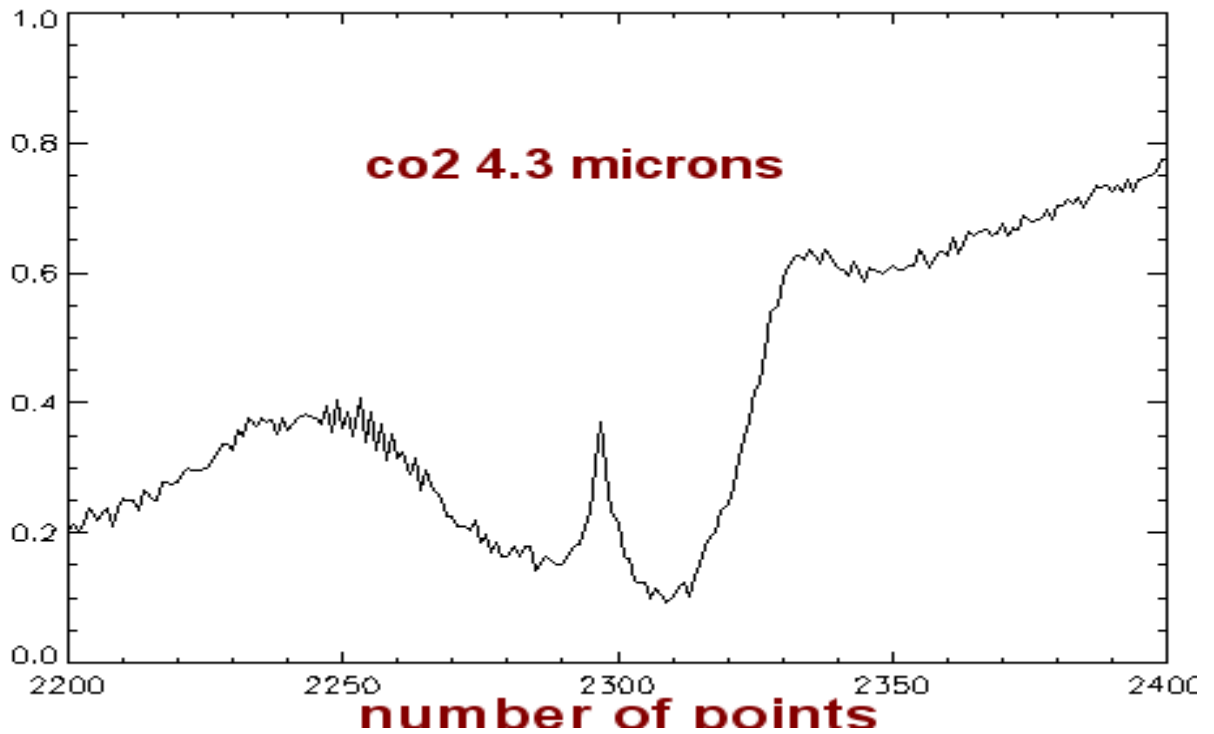
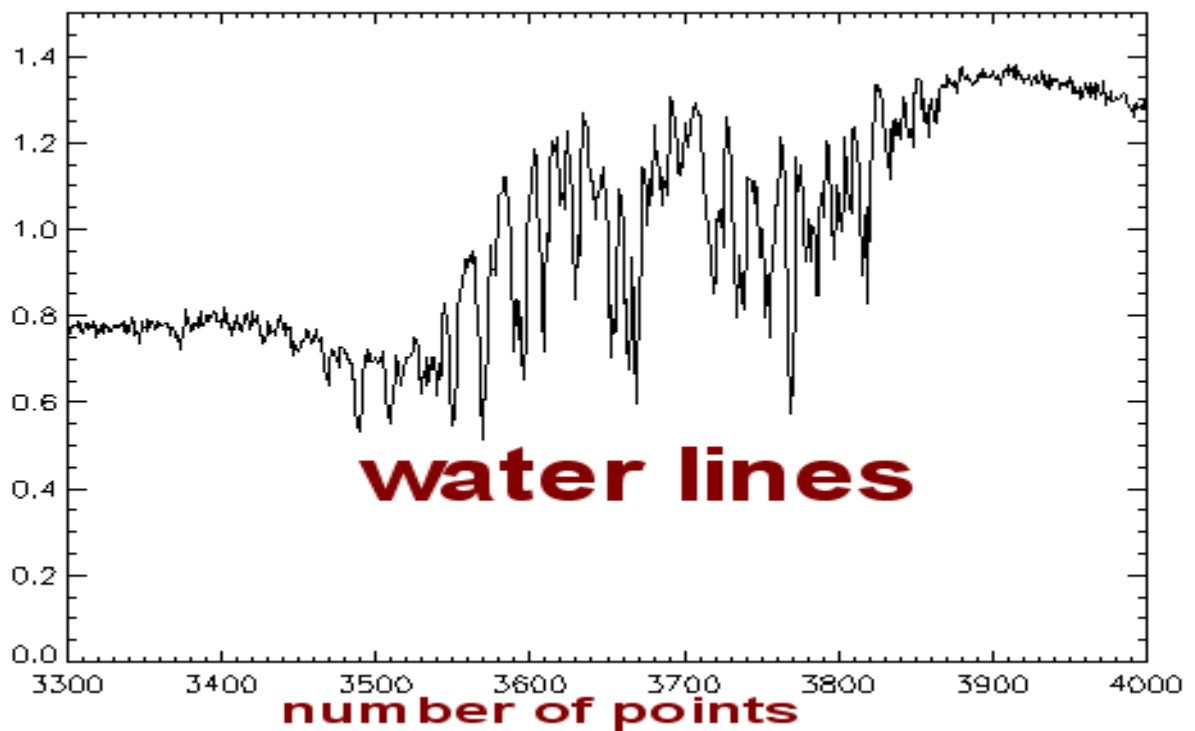


Figure 81 – Atmospheric Water vapour lines around 7 microns.



**Figure 82** - CO<sub>2</sub> band at 4.3 microns. Some rotovibrational features are seen on the left side of the band.



**Figure 83** - Atmospheric water lines near the 2.7 microns.

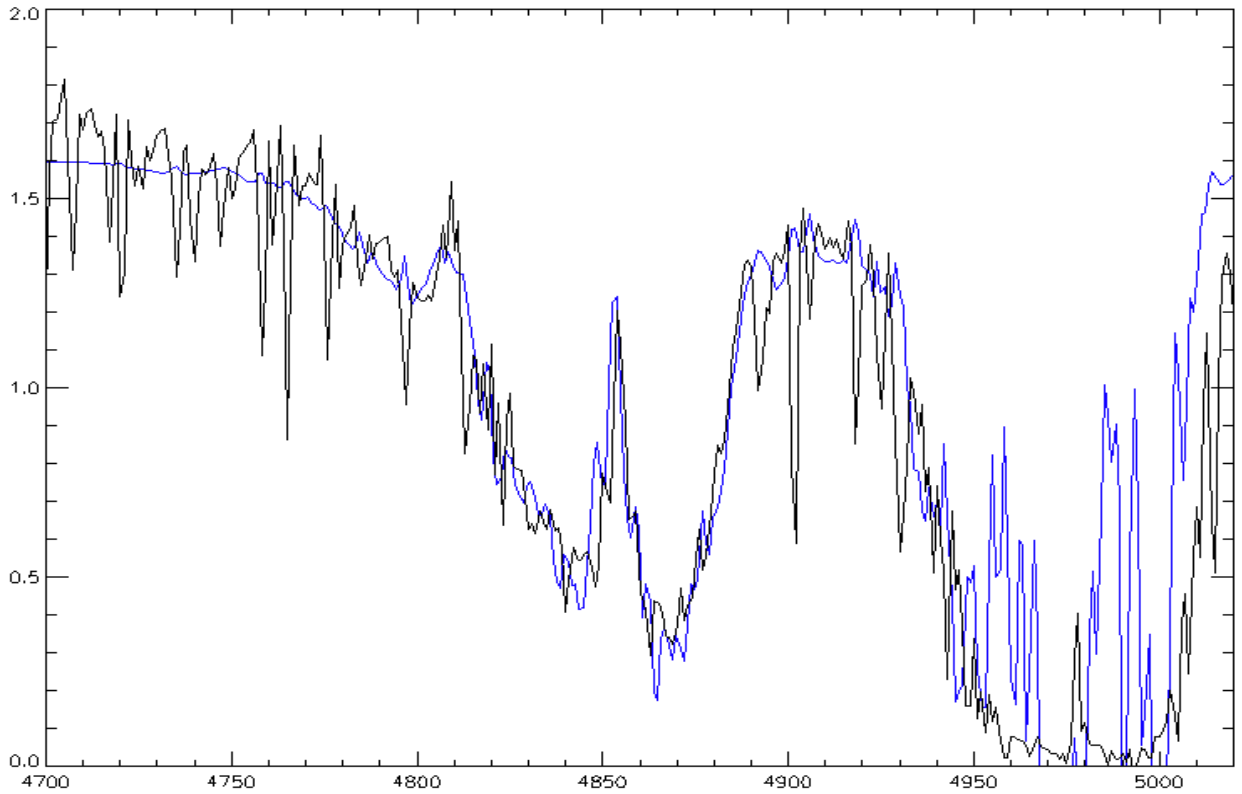


**Figure 84** – Two of the three CO<sub>2</sub> bands around 2 microns : measurements and synthetic spectrum fitting.

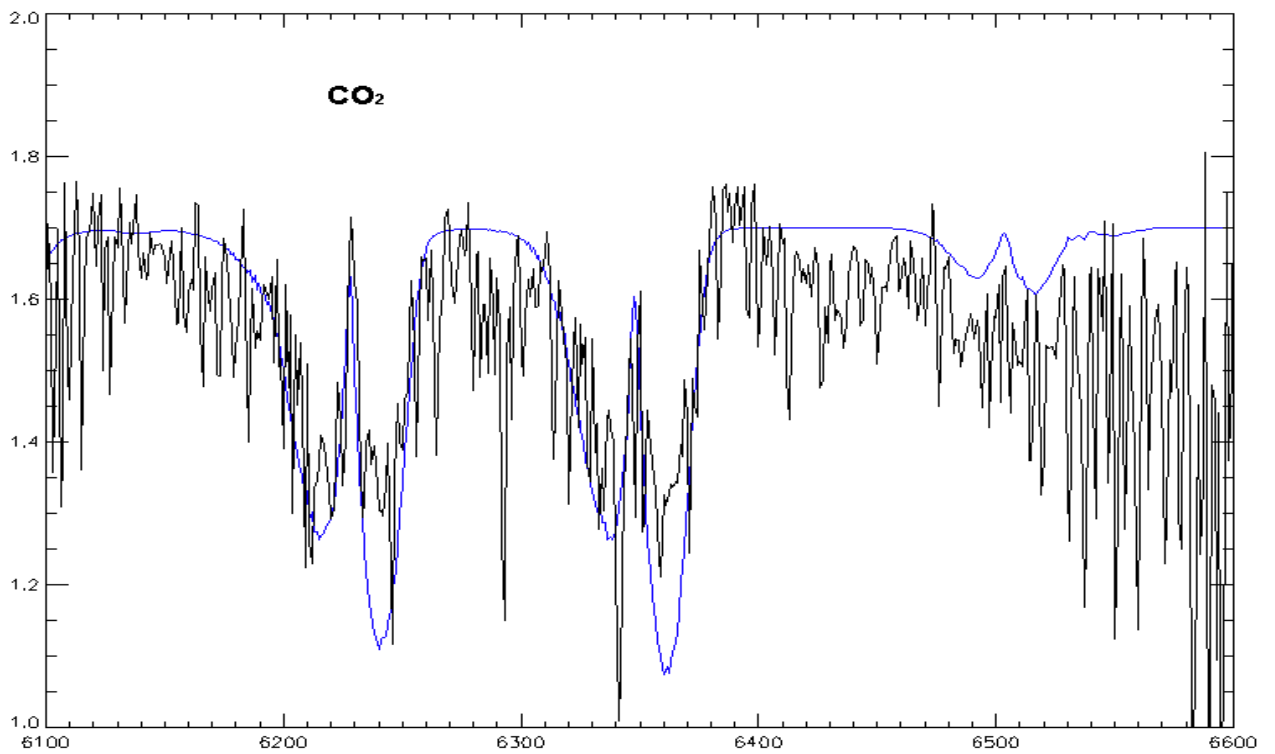


**Figure 85** – Minor CO<sub>2</sub> bands.

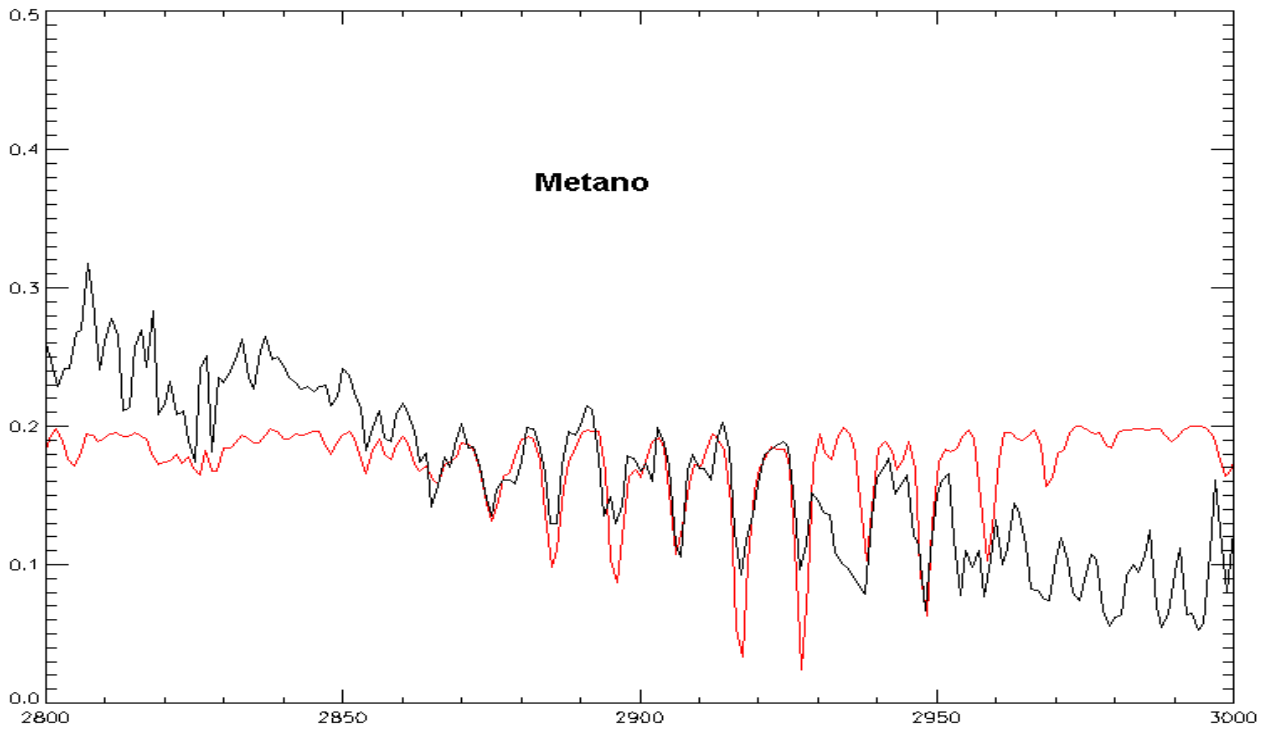


Figure 87 – Part of the 3000 cm<sup>-1</sup> methane band.

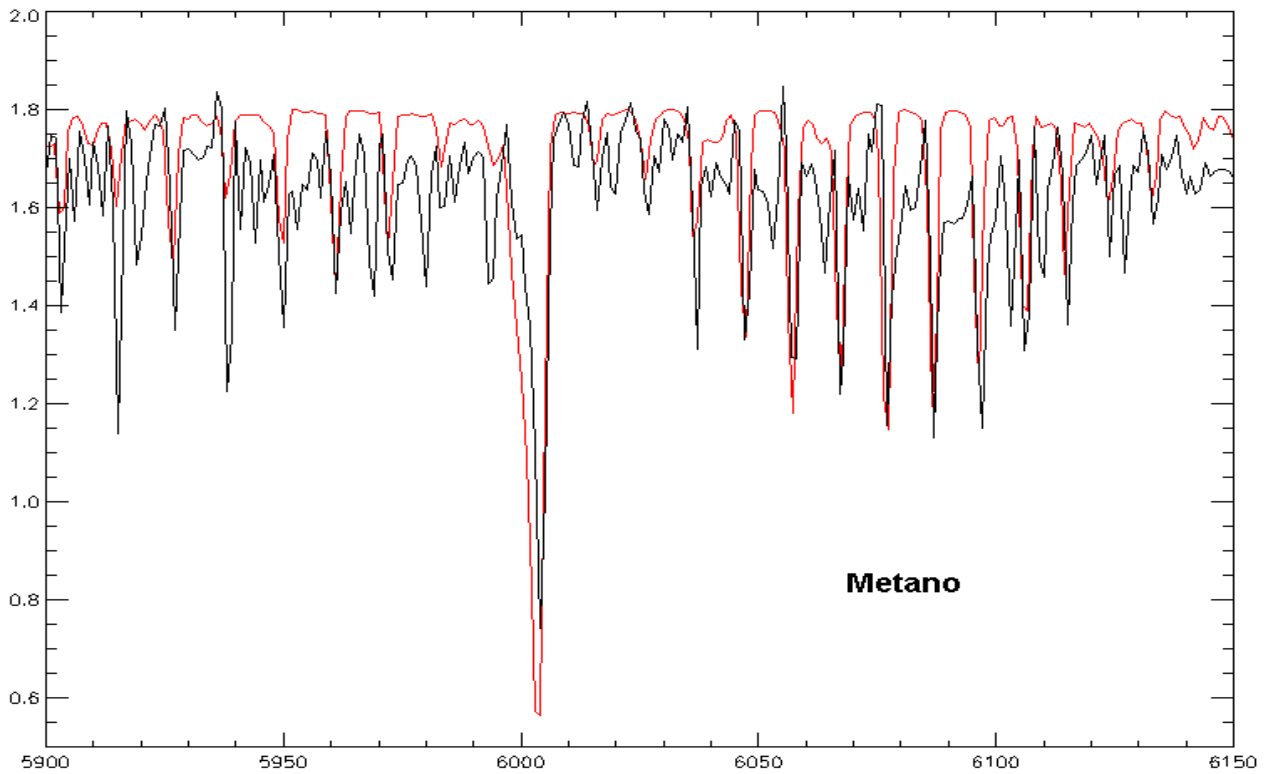


Figure 88 – Methane band at 6000 cm<sup>-1</sup>. Black curve measurements, red curve synthetic spectrum.

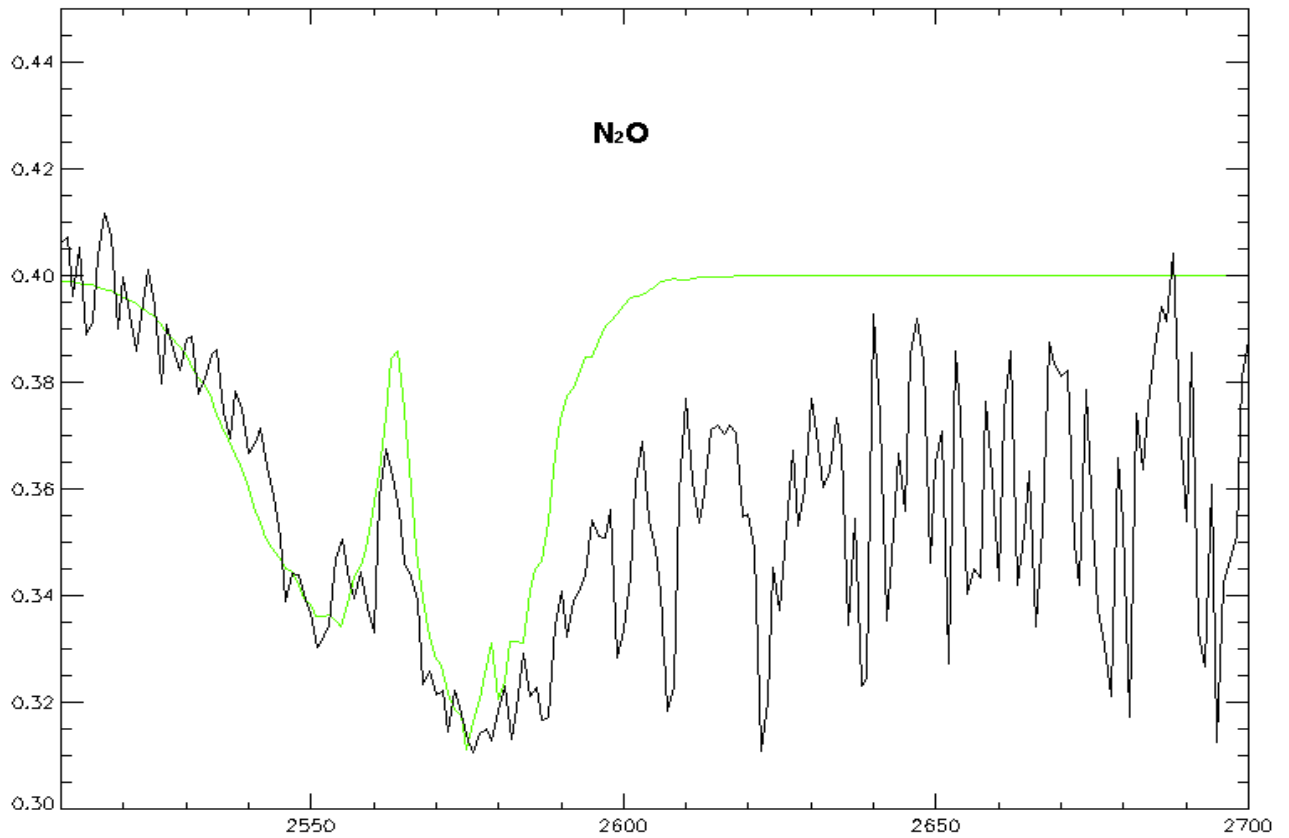


Figure 89 – N<sub>2</sub>O band. Black is measured spectrum, green is synthetic spectrum.

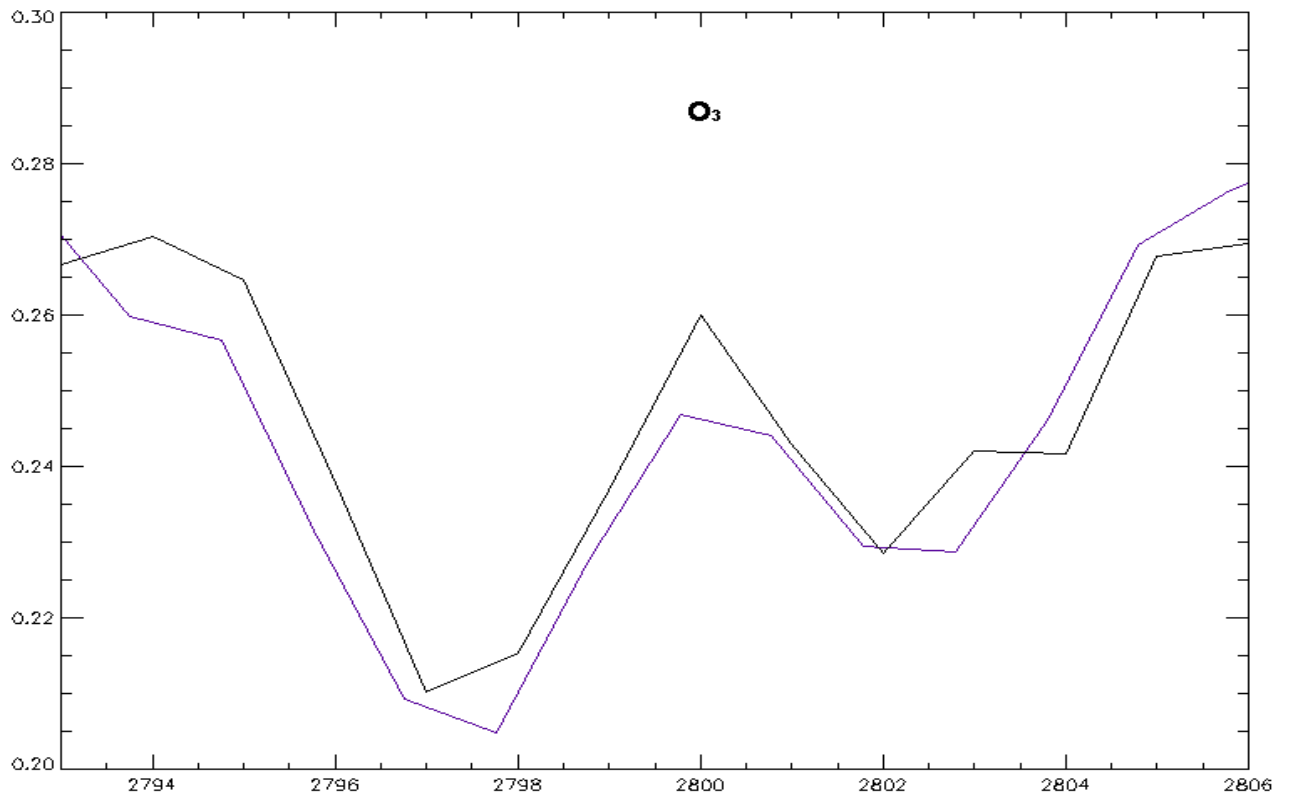
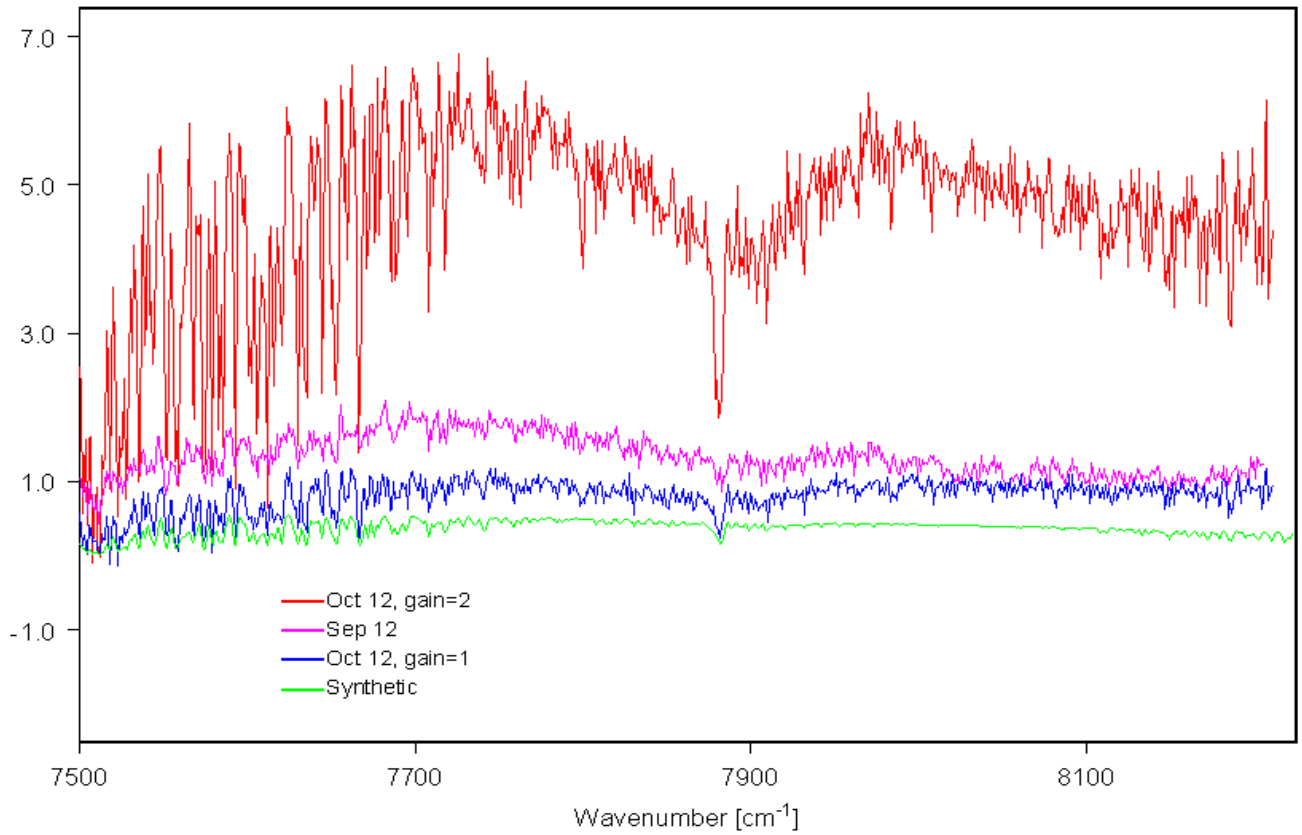
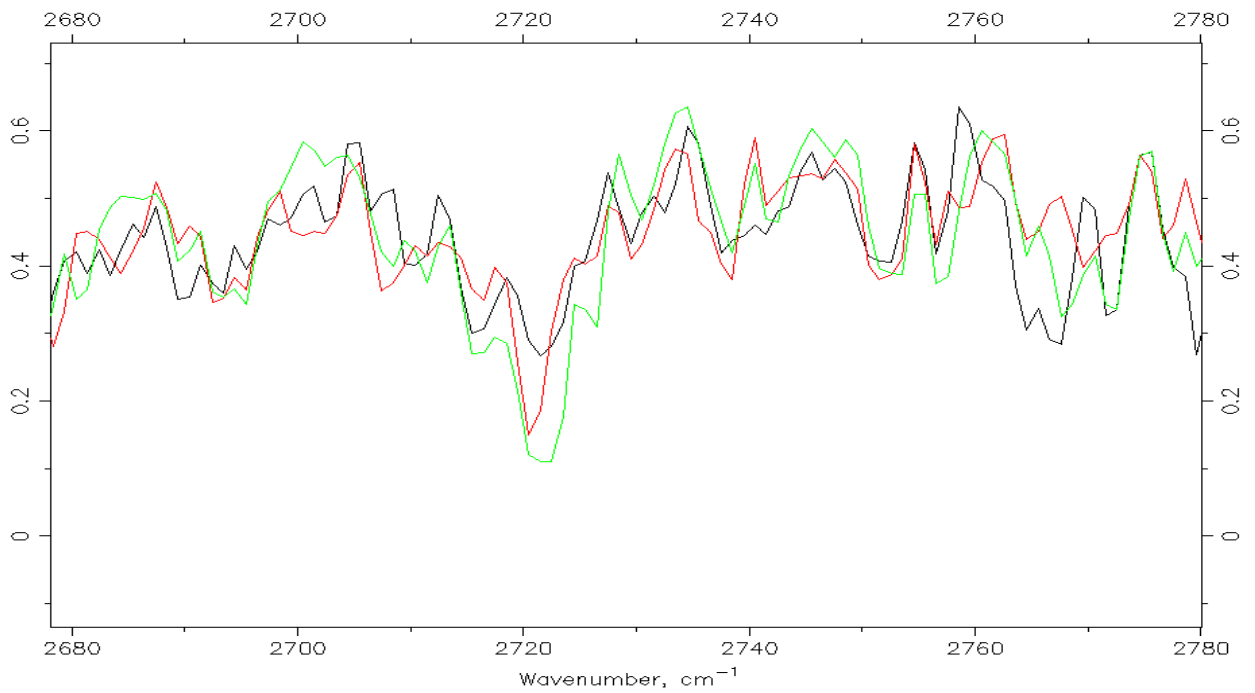


Figure 90 – Ozone band at 2800 cm<sup>-1</sup>.



**Figure 91** – O<sub>2</sub> band at 7900 cm<sup>-1</sup>. Different measurements and synthetic spectrum (green).



**Figure 92** – HDO band at 2720 cm<sup>-1</sup>. Different measurements and synthetic spectrum (green).

## 10 – MINERALS

Transmissivity of some minerals was measured by measuring first some KBr material clean, then by measuring some KBr with few dust particle included. The ratios are shown here. This should not be considered as a real study on the materials, but only as a test for PFS.

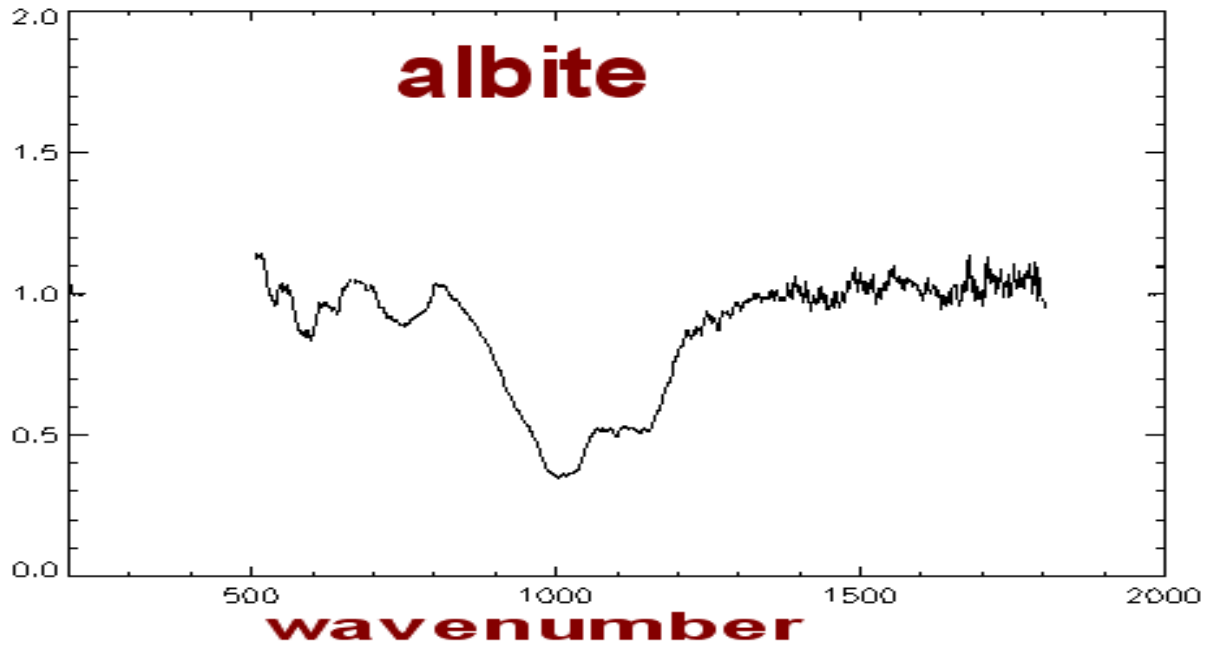


Figure 93 - Transmissivity in the LW channel of Albite dust.

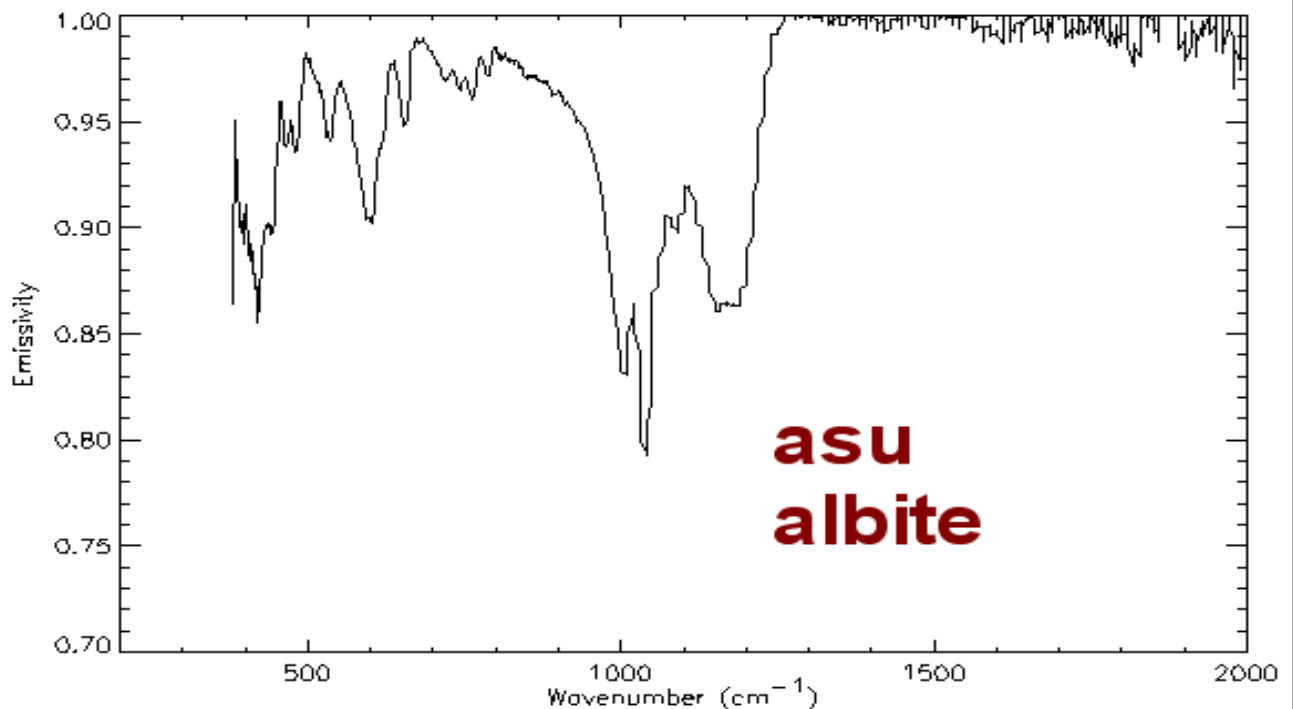


Figure 94 – Emissivity in the LW channel of Albite as measured by ASU people.

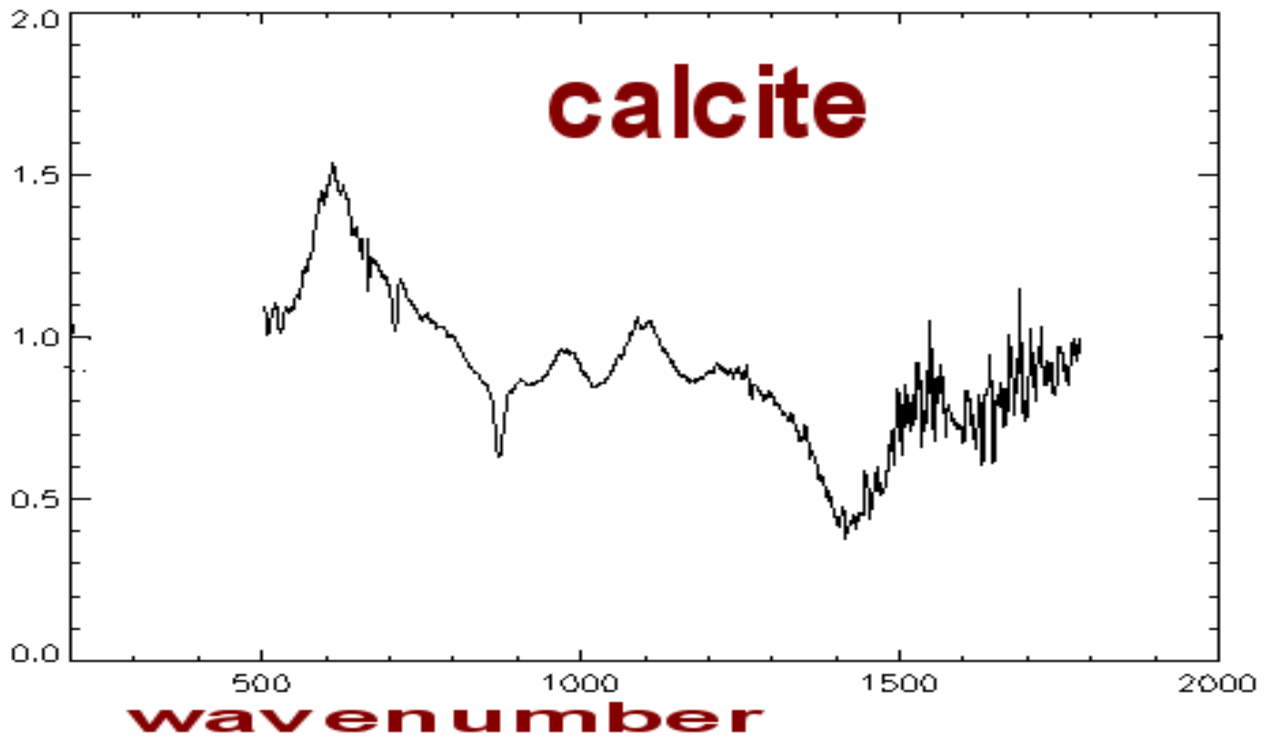


Figure 95 – Transmissivity of Calcite in the LW channel.

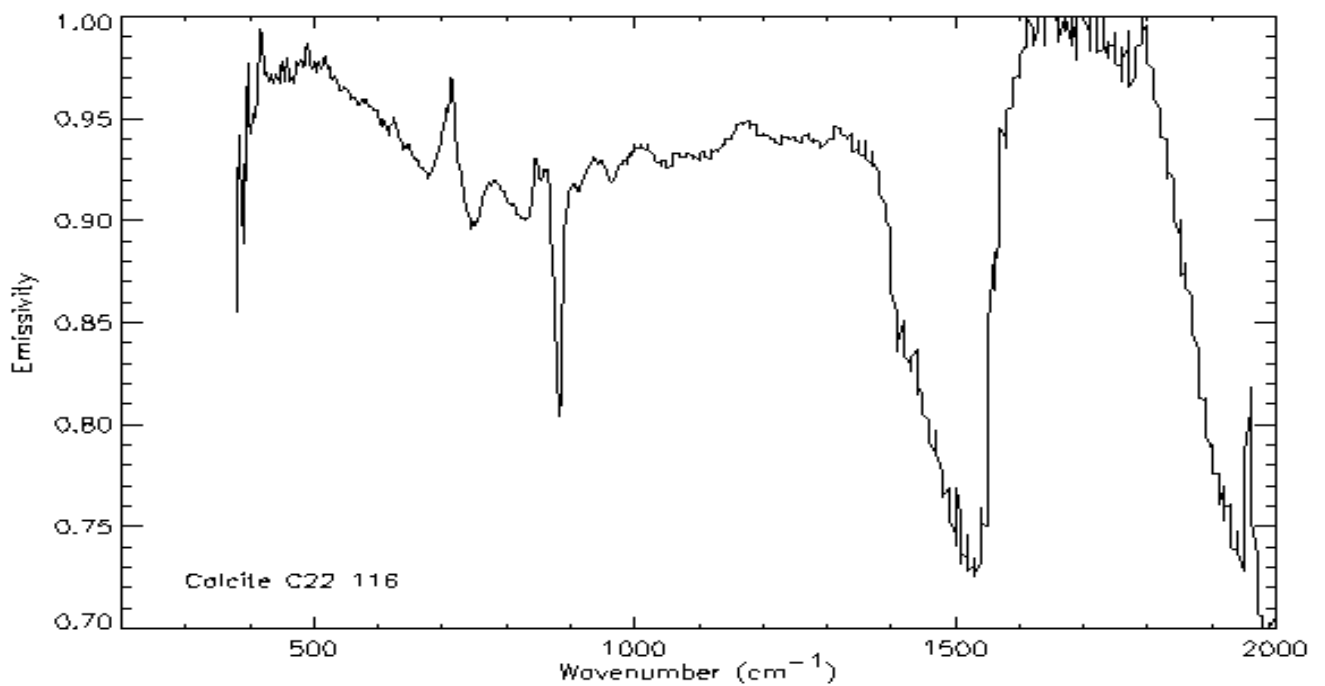


Figure 96 – Emissivity of Calcite in the LW channel measured by ASU people.

		<b>PFS for Mars Express</b> December 2002	<b>PFS</b> INTERNAL NOTE CALIBRATION II Page 118	<b>P.I. Vittorio Formisano</b> <b>CNR IFSI</b>
--	--	--	---	---

## 11 – DTM MODES.

### DATA TRANSMISSION MODES

For every measurement PFS sends measurement conditions and data. The measurement conditions contain an angle of the Scanner position, a state of the module O during the acquisition, a data transmission mode and other parameters to be used for the correct interpretation of the scientific data. The data transmission mode defines the kind of scientific data PFS must select and store in the Mass Memory to be sent to the Earth.

The data transmission modes are obtained with pfs operating in the science operating mode described later. only data transmission mode 0 is obtained in the pfs operating mode called autonomous test.

For any science data transmission mode PFS acquires both LW and SW interferograms. If spectra are required, PFS makes Fast Fourier transform of the interferograms. Then, depending on the data transmission mode, PFS selects required data. Interferograms can be selected either completely or in half (the central part) giving reduced resolution. Modules (absolute values) of spectra can be selected in terms of spectral intervals (reduced range).

There are defined 15 data transmission modes, some modes provide interferograms and some modes provide spectra (the numbering is inheritance of mars 96 project):

- **MODE 0** – It is a special mode of transmission of Autonomous test data. 20 Kwords
- **MODE 2** - full LW interferograms. 4096 MEASUREMENTS, 65 536 BITS. 4 Kwords
- **MODE 4** - reduced resolution interferograms (2048 points in the LW channel and 8192 in the SW channel). 163 840 BITS. Only the central part of the interferogram is transmitted neglecting the outer parts. 10 Kwords.
- **MODE 5** - reduced resolution LW interferograms. 32 768 BITS. 2 Kwords.
- **MODE 6** - reduced resolution SW interferograms. 131 072 BITS. 8 Kwords.
- **MODE 7** – In this mode the lw interferogram is transmitted complete,while the sw interferogram is cut in the following way : 2000 words around the zopd are identified, then the interferogram is completed only on right side. 13 Kwords =26 K Bytes.= 208 000 bits.
- **MODE 8** – similar to mode 7 but for both channels on the right side: 12 Kwords = 24 K bytes.=192 000 bits.
- **MODE 9** - modules of LW and SW spectra (8192 spectral points in the SW channel and 2048 points in the LW channel).
- **MODE 10** - modules of LW spectra. 29 568 bits per measurement.
- **MODE 15** - modules of SW spectra with reduced range, with the LW complete (2000 points in the LW channel and 2000 points in the SW channel). Total 4000 measurements, 64000 bits. This is the night sidemode.
- **MODE 16** - modules of SW spectra (6144 points), 98 304 bits.
- **MODE 17** - full interferograms (4096 points in the LW channel and 16384 points in the SW channel)
- **MODE 18** - full SW interferograms (and 16384 points in the SW channel)
- **MODE 27** – In this mode the lw interferogram is transmitted complete,while the sw interferogram is cut in the following way : 2000 words around the zopd are identified, then the interferogram is completed only on left side. 13 Kwords =26 K Bytes.= 208 000 bits. the night sidemode.

- **MODE 28** – similar to mode 27 but for both channels on the left side: 12 Kwords = 24 K bytes.=192 000 bits.

**IT SHOULD BE CLEAR THAT INTERFEROGRAM MODES ARE PREFERRED OVER THE MODES WITH FFT (9- 10- 15- 16).**

First we ask how many bits we take in the 15 modes.  
Repetition time has been assumed to be 10 sec.

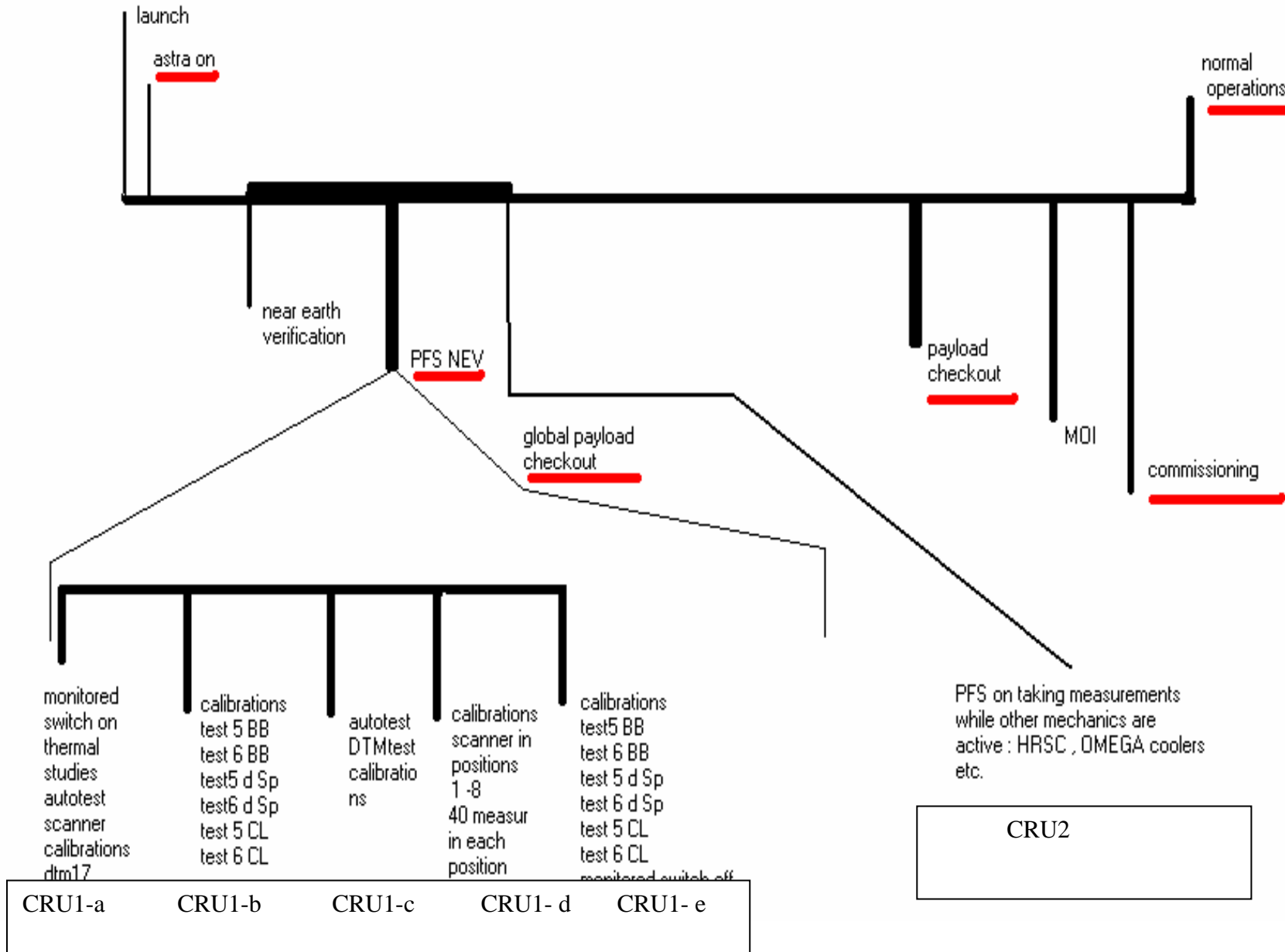
Working below 4000 km altitude we have 90 minutes, if each measurement takes 10 sec, we have 540 measurements per orbit to which we have to add 60 calibration measurements (more in commissioning phase) and two autotest data set:

NUMBER	MODE	Number Kwords	Bits per measure	bits per s	Megabits per orbit	Megabits per day
0	AUTOTEST	20	327 680	32 768	2x= 0.655	1.965
2	INTERF LW	4	65 536	6 554	35.389	106.167
4	INTERF (S+L)/2	10	163 840	16 384	88.473	265.419
5	INTERF LW/2	2	32 768	3 277	17.694	53.082
6	INTERF SW/2	8	131 072	13 107	70.779	212,337
7	INT L+1SIDE S	13	212 992	21 299	115.015	345.045
8	1 SIDE L+S	12	196 608	19 661	106.168	318.504
17	FULL INT L+S	20	327 680	32 768	176.947	530.841
18	FULL INT S	16	262 144	26 214	141.557	424,671
27	INT L+1 SIDE S	13	212 992	21 299	115.015	345.045
28	1 SIDE L+S	12	196 608	19 661	106.168	318.504
9	SPECTRLW+SW	8	131 072	13107	70.779	212,337
10	SPECTR LW	2	32 768	3276	17.694	53.082
15	SPECTR PARTS	4	65 536	6553	35.389	106.167
16	SPECTR PARTS	6	98 304	9830	53.083	159.249

## 12 - CALIBRATIONS IN SPACE

In June 2003, there will be the Near Earth Verification. In this phase we shall perform a number of calibrations of the LW and of the SW channel. The general plan is given below :









T0+1556 m - Scanner su BB  
T0+1557 m - Test 5, N=10  
T0+1587m - N=10, Test 6  
T0+1627 m Scanner su deepspace  
T0+1628 m - Test 5, N=10  
T0+1658 m - N=10, Test 6  
T0+1698 m Scanner su Internal Calibration Lamp  
T0+1699 m - Test 5, N=10  
T0+1729 m - N=10, Test 6  
T0+1769 m [go to sleep](#)  
----- end CRU 1 - b -----  
..... CRU 1 - c .....DAY 3.....

T0+2880 - PFS wakeup  
T0+2881m - N=1: perform autonomous test. DTM=0  
T0+2882 m - Scanner su Internal Calibration Lamp  
T0+2883 m - set DTM=2, N= 10, test 9  
T0+2885 m - set DTM=4, N= 10, test 9  
T0+2887 m - set DTM=5, N= 10, test 9  
T0+2889 m - set DTM=6, N= 10, test 9  
T0+2891 m - set DTM=7, N= 10, test 9  
T0+2893 m - set DTM=8, N= 10, test 9  
T0+2895 m - set DTM=17, N= 10, test 9  
T0+2897 m - set DTM=18, N= 10, test 9  
T0+2899 m - set DTM=27, N= 10, test 9  
T0+2901 m - set DTM=28, N= 10, test 9  
T0+2903 m - set DTM=9, N= 10, test 9  
T0+2905 m - set DTM=10, N= 10, test 9  
T0+2907 m - set DTM=15, N= 10, test 9  
T0+2909 m - set DTM=16, N= 10, test 9  
T0+2911 m - go to sleep

-----start pericenter pass simulation -----

T0+2945 m - wakeup  
T0+2949 m - test2, N=2  
T0+2955 m - DTM=0, N=1, autotest  
T0+2956 m - N=10, Test 4  
T0+2962 m - DTM 17, N=500  
T0+2963 m - Scanner su BB, Test 9  
T0+3055 m - N=10, Test 4  
T0+3061 m - DTM=0, N=1, autotest  
T0+3062 m- go to sleep

-----stop pericenter pass simulation -----

T0+3073 m- PFS wakeup  
T0+3074 m - set temper. SW detec. = 250 K  
T0+3114 m - Test 4, DTM 17, N=200  
T0+3234 m - go to sleep

----- end CRU 1 - c -----

..... CRU 1 - d .....DAY 4.....

		<b>PFS for Mars Express</b> December 2002	<b>PFS</b> INTERNAL NOTE CALIBRATION II Page 124	<b>P.I. Vittorio Formisano</b> <b>CNR IFSI</b>
---	--	--	---	---

T0+4340 - PFS wakeup  
T0+4340 - set temper. SW detec. = 250 K  
T0+4341m – Scanner over BB – N=200 – dtm 17 – gain 1,3- Test 9  
T0+4381m – Scanner deep space – N=200 – dtm 17 –gain 1,3 -Test 9.  
T0+4421 m – Scanner Cl.Lamp – N=200 –dtm 17 – gain 1,3 -Test 9.  
T0+4461 m- scanner position 1, N=40, gain 1,3 – Test 9  
T0+4469 m - scanner position 2, N=40, gain 1,3 – Test 9  
T0+4477 m – scanner position 3, N=40, gain 1,3 – Test 9  
T0+4485 m – scanner position 4, N=40, gain 1,3 – Test 9  
T0+4493 m – scanner position 5, N=40, gain 1,3 – Test 9  
T0+4501 m – scanner position 6, N=40, gain 1,3 – Test 9  
T0+4509 m – scanner position 7, N=40, gain 1,3 – Test 9  
T0+4517 m – scanner position 8, N=40, gain 1,3 – Test 9  
T0+4525 m [go to sleep](#)

----- end CRU 1 - d -----  
..... CRU 1 - e .....DAY 5 .....

T0+5760 - PFS wakeup  
  
T0+5761 m -Test 4, DTM 17, N=200, gain 1,3  
T0+5876 m - Scanner su BB  
T0+5877 m – Test 5, N=10  
T0+5907 m – N=10, Test 6  
T0+5947 m Scanner su deepspace  
T0+5948 m – Test 5, N=10  
T0+5978 m – N=10, Test 6  
T0+6018 m Scanner su Internal Calibration Lamp  
T0+6019 m – Test 5, N=10  
T0+6049 m – N=10, Test 6  
T0+6089 m scanner on BB  
T0+6090 m [block double pendulum](#)  
T0+6120 m [test 1](#)  
T0+6125 m [PFS off](#)

----- end CRU 1 - e -----  
-----end near earth verification -----

With this data we can study :

- The thermal behaviour of PFS.
- The internal and external communication.
- The optical alignment in space.
- The mechanical behaviour .
- The calibration sources status.
- Responsivity and NER in space.
- The best laser diode working temperature.
- The best gain factors for SW and LW channel.
- The effect of the SW filter thermal reduction.

		<b>PFS for Mars Express</b> December 2002	<b>PFS</b> INTERNAL NOTE CALIBRATION II Page 125	<b>P.I. Vittorio Formisano</b> <b>CNR IFSI</b>
---	---	--	---	---

## 13 – CONCLUSIONS

The LW channel behaves normally, but has a NER which is rather high. Conditions in space may improve the situation, and indeed we shall repeat the calibrations in space several times, in different conditions, to be sure of the performance of the instrument .

The present NER, in any case, seems to be good enough to provide a temperature profile retrieved with enough accuracy.

In any case the high NER induces us to average spectra, we shall take as many measurements as possible.

The SW channel behaves in a very complex way :

The detector is non linear.

SNR increases with gain up to 3 (5 times higher) .

Non linearity does not change with gain.

By cooling the detector the output signal increases: responsivity is higher, but non linearity is obtained earlier.

The internal calibration lamp may provide useless saturated interferograms with a cold detector. For this reason in NEV activity we shall try to heat the detector when looking at the calibration lamp.

In any case the best operating conditions for the experiment seems to be with the SW detector as cold as possible (200 K), and gain factors should be LWC = 1, and SWC = 3. Gain factors are LW : 0,1,2,3 ; and SW : 0,1,2,3,4,5,6,7.

In these conditions the SW channel appears to be very good and very powerful.

In the following figures 97 and 98 synthetic spectra with the measured NER are shown. The SW detector is assumed to be at 200 K, so the figures give an idea of the PFS results at Mars on a single measurement basis.

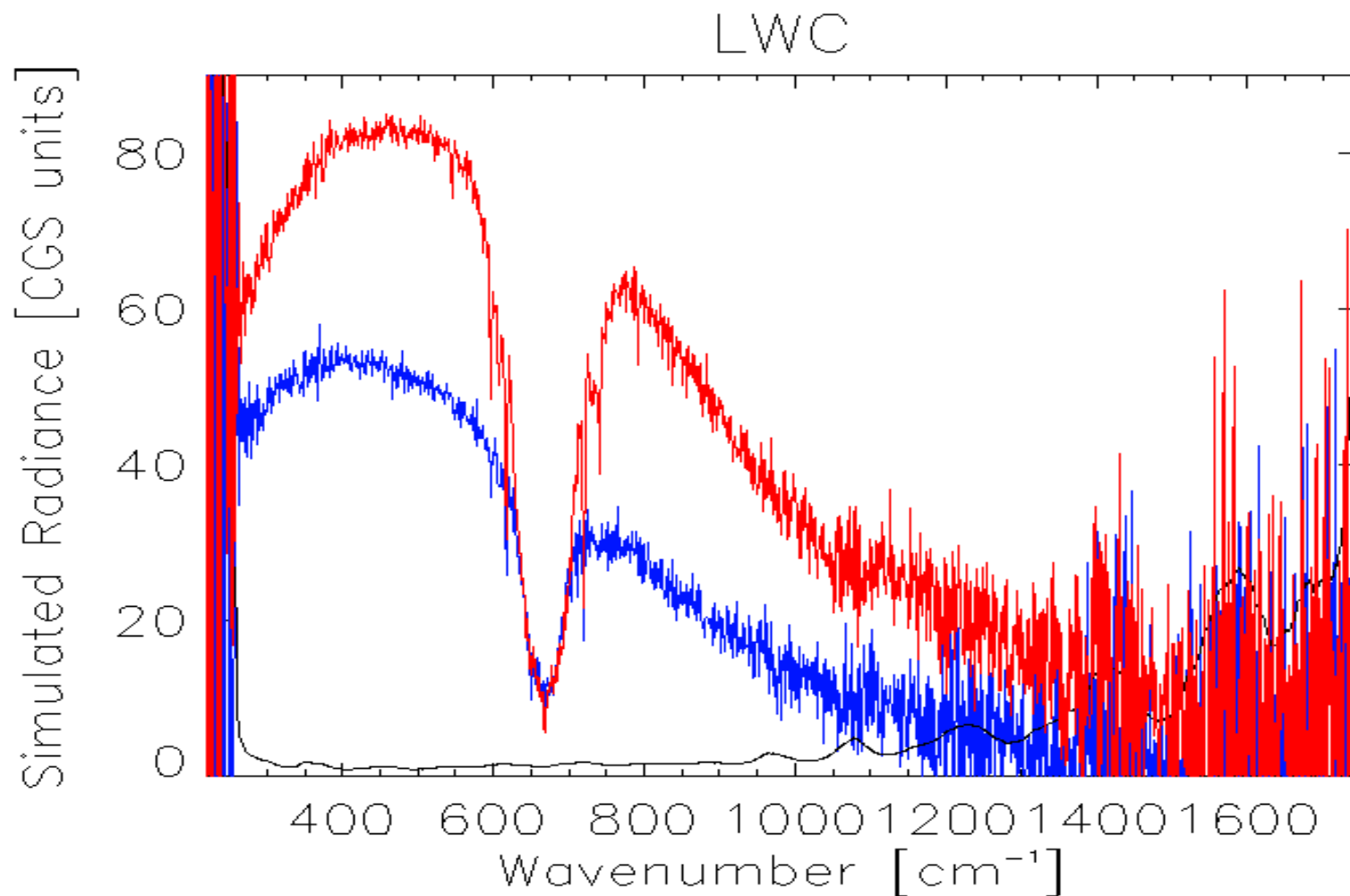


**Figure 97** – Simulated Martian spectra with noise added : average low albedo and low temperature conditions.

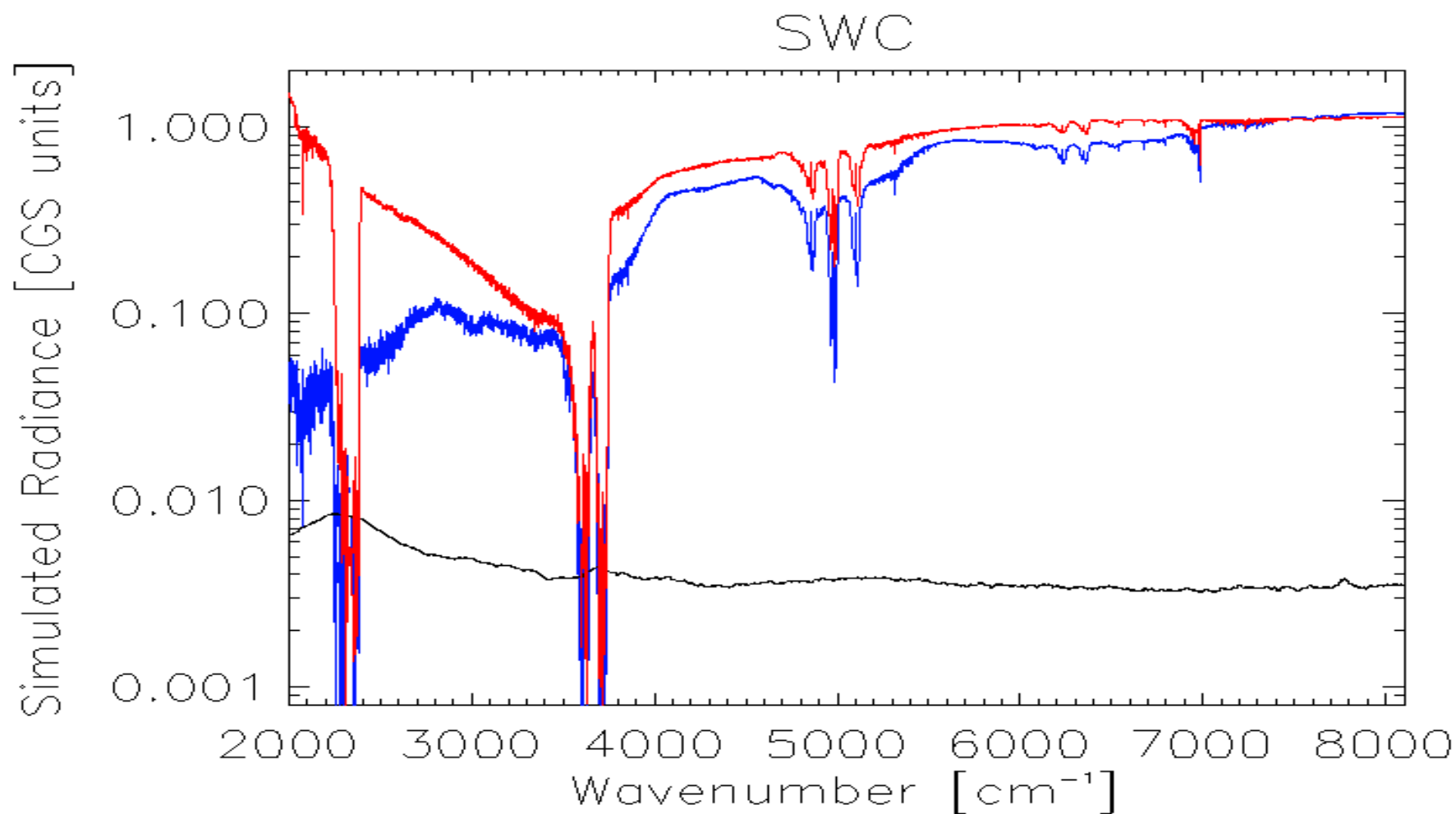


**Figure 98** – Simulated Martian spectra with real noise added: conditions are for SW detector cooled at 200 K and gain 3. Red equator, albedo 0.2, bleu polar over ice cup.